An investigation of residual stresses induced by elevated temperature post-curing of glass reinforced plastic structures

by

JOHANN FREDERICK OOSTHUIZEN

Thesis submitted in compliance with the requirements for the degree

Doctor Technologiae: Engineering: Mechanical

in the

FACULTY OF ENGINEERING

Department of Mechanical Engineering

at the

TECHNIKON FREE STATE

March 2000

Promoter: Dr M A Stone (AEA Technology)

Co-promoter: Dr J A Strauss (Technikon Free State)

DECLARATION OF INDEPENDENT WORK

I, JOHANN FREDERICK OOSTHUIZEN, do hereby declare that this research project submitted for the degree DOCTOR TECHNOLOGIAE: ENGINEERING: MECHANICAL, is my own independent work and that it has not previously been submitted to any institution by me or anyone else as part of any qualification.

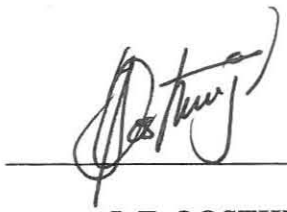

2000/03/08

J. F. OOSTHUIZEN **DATE**

This work I dedicate to my darling wife, Annelie, who supported and encouraged me through the years during which I spent so much time in the study. Also to our three sons, Robert, Herman and Johann, who had to endure my various moods and lack of attention.

I also thank our Lord for providing me with the strength and perseverance to complete this work.

ACKNOWLEDGEMENTS

I wish to acknowledge some persons and institutions for their contributions (financial, academic, emotional support) whilst I was working on this project:

- Dr Mark A. Stone, promoter and mentor – for his guidance and encouragement that I truly needed during the course of this project, also for his input in the papers that were produced resulting from the research conducted in this project.
- NATIONAL RESEARCH FOUNDATION - the NRF was the major financial contributor to this project. This work would in all likeness not have been completed without the funding that was awarded to this project. Part of the funding was applied to attend conferences and courses in Durban, Australia, USA and also the annual Wits R/P Conference where I was able to part with some of the work that was done and discuss certain problems that I had at times. The consumables and travelling required for this project were also costly.
- TECHNIKON FREE STATE – the Technikon was the second major contributor to this project. Software upgrades were of extreme importance to this project. This ensured that continuous contact with the software developers was available, although I only had need for this on few occasions. Part contribution to the conferences and courses are greatly appreciated. The most important period during the course of this study was the six months granted as study leave, this is greatly appreciated.
- FIBREWOUND CC. – one of the leading companies in South Africa with regards to the manufacture of GRP vessels and components. The supply of test pieces and resin is greatly appreciated.
- NCS Resins – for the sponsoring of the DION 9100 vinyl ester resin.

- OWENS CORNING – for the sponsoring of the glass mat required for the in-house manufacture of test pieces.
- AECI Engineering Department, in particular the Pressure Vessel & Piping Section – this is where my interest in this subject began while working on vessel designs where prescribed post-cure procedures were often thought to be problematic causing lengthy discussions on this topic.
- My colleagues at the Faculty of Engineering, Technikon Free State. I appreciate the support that I had from my colleagues, especially those that showed interest in my work and progress. The interest shown acted as fuel to keep me going to the end.
- My family – I believe that the most important people of all for the duration of this project were my family. My wife Annelie gave strong emotional support and, I hope, understood the mood swings that I experienced. My sons, Robert, Herman and Johann, who often did not understand these various moods but with eventual recognition supported me with this endeavour. My parents and parents-in-law whom showed their constant support whilst I was busy with this study.

SUMMARY

Performing an elevated temperature post-cure procedure on glass reinforced plastic vessels and components that are subjected to aggressive chemical environments enhances the mechanical and chemical resistant properties of a laminate. This is a result of the completion of the cross-link polymerisation reaction at an elevated temperature. The post-cure process is however the cause of matrix embrittlement and possibly also contributes to crazing on the inner surface of the vessels or similar components.

To determine the cause of crazing at the inner surface this work investigates the stress and strain development, resulting from post-cure, in chopped strand mat reinforced laminates in the form of small bore tubes, small bore full face flanges and small diameter vessels. The investigation consists of experimental measurements during post-cure procedures and numerical simulations of these procedures on specified test specimens.

The numerical simulations consist of finite element analyses of models using commercially available finite element analysis software. Material properties for the analyses are determined using two different, but well-known approaches. The post-cure simulations are conducted by applying laminate shrinkages, by analogy, as coefficients of thermal expansion with a unit temperature difference in the finite element models.

Initially only the structural layers of the laminates were considered and analysed for post-cure shrinkage. However, the results obtained did not show any cause for crazing occurring on the inner surfaces. The resin rich corrosion barrier, that is usually applied as a first layer when manufacturing a vessel component, was added to the finite element

models and analysed for post-cure stresses and strains. These results clearly indicate that the corrosion barrier causes stress conditions at the inner surfaces that should be unacceptable for the GRP vessel industry.

The experimental and predicted results are compared to determine the accuracy of the finite element analyses.

Factors influencing the accuracy of strain gauge measurements on laminates constructed of CSM are presented. The study investigates issues to be considered when finite element analyses are required on composite material components to determine the residual manufacturing stresses.

The study's relevance to industry is discussed and topics for further and additional studies are recommended.

OPSOMMING

Die toepassing van 'n verhewe temperatuur na-kuur prosedure op glasvesel versterkte plastiek vate en komponente, wat aan aggresiewe chemiese toestande onderwerp word, verhoog die chemiese weerstands- en meganiese eienskappe van die lamel. Die verhoging van hierdie eienskappe is as gevolg van die voltooiing van die oorkruispolimeriserings-reaksie by die verhewe temperatuur. Die na-kuur proses is egter die oorsaak van matriksverbrokkeling en dra moontlik by tot barsvorming op die binne-oppervlak van vate of soortgelyke komponente.

Om die oorsaak van barsvorming op die binne-oppervlak te bepaal, ondersoek die studie die spannings- en vervormingsontwikkeling, as gevolg van na-kuurkrimping, in kort-glasvesel versterkte lamelle in die vorm van klein-diameter buise, klein-diameter vol-vlak flense en klein-diameter vate. Die ondersoek bestaan uit eksperimentele metings gedurende na-kuur prosesse en numeriese simulasies van die prosesse op spesifieke toetsstukke.

Die numeriese simulasies bestaan uit eindige element analises van modelle deur gebruik te maak van kommersieel beskikbare eindige element analise sagteware. Die materiaal eienskappe, vir aanwending in die analises, is bepaal deur gebruik te maak van twee verskillende, tog bekende naderingswerke. Die na-kuur simulasies word uitgevoer deur die toepassing van na-kuur lamelkrimpings, in ooreenstemming met die gebruik van termiese uitsettingskoëffisiënte, tesame met 'n eenheidstemperatuurverandering in die eindige element modelle.

Die stuktuurlae van die lamelle was allereers beskou en vir na-kuurkrimping geanaliseer. Die resultate het egter nie enige oorsaak van barsvorming by die binne-oppervlaktes getoon nie. Die harsryke korrosie skutlaag, wat gewoonlik as 'n eerste laag in die vervaardiging van vate opgelê word, was tot die eindige element modelle toegevoeg en vir spanning en vervorming geanaliseer. Die resultate van die analises toon duidelik dat die korrosie skutlaag die oorsaak van binne-oppervlakspanninginstoestande is wat onaanvaarbaar vir die glasveselversterkte platiek industrie behoort te wees.

Die eksperimentele en voorspelde resultate word vergelyk om die akkuraatheid van die eindige element analises te bepaal.

Faktore wat die akkuraatheid van die vervormingsmetings op kort-glasvesel versterkte platiek lamelle beïnvloed word voorgestel. Die studie ondersoek faktore wat in ag geneem moet word as eindige element analises op saamgestelde materiaal komponente vereis word vir die bepaling van residuele vervaardigingsspannings.

Die studie se industriële toepaslikheid word bespreek en onderwerpe vir verdere en addisionele studies word aanbeveel.

TABLE OF CONTENT

LIST OF TABLES

LIST OF FIGURES

1. INTRODUCTION

1.1 Problem statement

There remain many problems with regard to the design of fibre reinforced parts and components that are unsolved and worthy of further investigation. Cure and post-cure kinetics of the resin and the stresses that are induced by these kinetics can be listed under these problems.

During the design of glass reinforced plastic (GRP) vessels it is often required to specify that a particular vessel be post-cured at an elevated temperature after manufacture. The main reasons for this procedure are to reduce the quantity of volatiles present in the resin, to enhance the mechanical properties of the laminate and improve the chemical resistance of the surface, the chemical barrier, that would be exposed to the aggressive mediums contained or processed in the vessel. The chemical barrier surface is usually the inner surface of the vessel. However, the post-cure process could cause embrittlement of the resin matrix if excessive post-cure temperature is applied. The post-cure process could also initiate matrix cracks (crazing) at the surface of the chemical barrier due to high shrinkage strains and induced stresses. The process induced stresses could eventually be detrimental to the total integrity of the vessel and, instead of enhancing the required mechanical properties, promote stress conditions that would lead to a shorter than required lifetime of the vessel.

Shrinkage and warpage are directly related to residual stresses, which result from locally varying strain fields that occur during the consolidation and the post-cure stage of the manufacturing process [1]. Nonuniform thermo-chemical and thermo-mechanical actions,

such as consolidation and post-cure shrinkage, and temperature variations during the manufacturing process coupled with the fibre orientation and fibre volume fraction are the cause of these strain gradients.

Modelling and simulation of the manufacturing process has become an important issue as it enables the designer to predict shrinkage, warpage and the associated stresses and strains. It also helps researchers to understand the physics and phenomena that take place during the manufacturing process.

It is also the designer's responsibility to ensure that stress conditions, during manufacture and operation, in any component do not exceed the allowable values set by the design and manufacturing codes of practice given that the operational conditions remain as specified in the process design. This would only be achieved if the designer is aware of all the factors that need to be considered that are the cause of stress development during manufacture and operation.

1.2 Aim of the study

The objective of this work is to investigate the mechanics in the laminate during post-cure of glass reinforced plastic (GRP) vessels and similar components and hence to determine the magnitude of the strains and stresses associated with this process. This will be done through strain gauge recordings during experimental post-curing of composite components and innovative modelling, analysis and simulation of the thermo-chemical and thermo-mechanical behaviour during the total manufacturing process.

This should present guidance to the designer as to what the order of the residual manufacturing stresses and strains might be prior to the manufacture, installation and

commissioning of the specific component. This study will also present issues to be considered when predicting residual manufacturing stresses and strains by finite element analyses on GRP components, in particular components constructed of chopped strand mat (CSM) bound with a resin matrix.

1.3 Hypothesis

The stresses and strains developed during the post-cure process, on GRP vessels and components, can be predicted to an acceptable accuracy by making use of commercially available finite element analysis software. The material properties required in the finite element models can be calculated by using the properties of the resin matrix and the glass fibres. However, the laminate post-cure shrinkage can be used, by analogy, as a coefficient of thermal expansion with the application of 1°C as nodal temperature difference. The laminate shrinkage is calculated by substituting the matrix coefficient of thermal expansion (CTE), α_m, with a measured strain value of the resin post-cure shrinkage, S_m and applying a zero value for the fibre CTE (α_f) in the well known methods for laminate CTE predictions.

1.4 Scope of the study

Due to the wide field of composite materials and the vast number for items and components manufactured in GRP it is required to limit the scope of the study. The study will be limited to products consisting of chopped strand mat reinforced resin laminates in the shape of small bore tubes, small bore full face flanges and small diameter vessels with ellipsoidal dished ends. The resin utilised will be of the vinyl ester type. Also, since chopped strand mat is used as reinforcement material, it will be assumed that the in-plane elastic properties of the laminate remain essentially isotropic.

2. LITERATURE SURVEY

2.1 Traditional Materials versus Fibrous Composite Materials

Metallic, or traditional material, vessels are conveniently designed by calculating the permissible stresses, based on measured tensile and ductility properties. Being made from traditional materials, which are normally isotropic and essentially homogeneous, their mechanical and physical properties do not depend on the direction in which they are measured and do not vary from point to point in a given volume. Fibrous composite materials are different, [2], and it is essential to consider all the aspects of design, including manufacture, together if an efficient, safe and cost-effective product is to be produced. The designer must be aware of these different considerations for several reasons, namely:

- the composite material and structure are usually manufactured at the same time and little or no modification to the final product is possible after manufacture;
- the materials may be highly anisotropic and are heterogeneous. This is a consequence of their fibrous structure and of the comparatively large size of the fibres. The strength and stiffness properties of polymer composites reflect the reinforcing properties of the fibres only in the direction parallel to them;
- for any combination of polymers and fibres there is a large number of possible materials which can be made, depending on the relative proportions of the components and the orientation of the fibres. Further variability is due to the effect of the fibre length in short fibre composites, the mixing of fibres and the use of core materials.

There are various design implications due to these differences:

- property data are relatively scarce and it is not always apparent how to use the information available to estimate the properties of other fibre/resin combinations;

- there is a need to understand how composite properties relate to those of the components;
- it is necessary to understand how composite properties change with fibre volume fraction and fibre orientation;
- it is necessary to understand how composite properties change during manufacture and with structural loading;
- care must be exercised to allow for the low transverse (through-thickness) and shear properties of the materials.

2.2 Design and Manufacturing Codes

2.2.1 British Standards

BS 4994 [3] is the British Standard Specification for design and construction of vessels and tanks in reinforced plastics. Although the manufacture of vessels and tanks in reinforced plastics is a wide field, this standard only covers part of the field, namely, the use of polyester, epoxy and furane resins in wet lay-up systems.

Laminar constructions are usually heterogeneous and the design method in BS 4994, being based on unit loading, is particularly suited to the design of composites of reinforced plastics. The calculation of an appropriate laminate construction is based on the allowable unit loading and unit modulus for the type of composite proposed. In addition, the allowable strain in the laminate is limited to ensure that breakdown of the resin-reinforcement bond does not occur in any part of the structure.

The strain limit is set to the lower of 0.2 % (2000$\mu\varepsilon$) or a value determined from the allowable unit loading and unit modulus of the material under consideration. The allowable unit loading is determined by dividing the ultimate tensile unit strength by a design factor. The design factor is the product of five individual factors relating to the method of manufacture, the chemical environment, the operating temperature, cyclic loading conditions and the curing procedure. All the individual factors are greater than one, therefore the allowable unit loading will be smaller than the ultimate unit loading. The factor relating to the curing procedure is the smallest when full post-cure is specified, namely 1.1, while the greatest when the vessel operates at temperatures higher than 45°C and no post-curing is specified, namely 1.5. From this it can be seen that the allowable unit loading will be the greater should full post-curing be specified and the calculated laminate thickness will be smaller, for the same operating conditions, than for non post-cured vessels.

BS 4994 does not specify any specific post-curing procedure but refers the designer to the resin supplier's instructions. It does however note:

> *"The post-curing temperature should be chosen to ensure that the laminate will comply with the mechanical, temperature and chemical performance required by the design. High performance resins generally require a post-cure temperature of at least 80°C to develop their optimum properties and, wherever possible, the tank or vessel should be post-cured at the design temperature."*

BS 4994 also specifies that the heat distortion temperature (HDT) of a fully cured resin system shall be not less than 20°C higher than the design temperature.

2.2.2 American Standards

In contrast to BS 4994, ASME X, [4], bases the design of fibre reinforced plastic (FRP) vessels on permissible stresses as determined by the designer. The calculations, as suggested in ASME X, constitute only a tentative determination that the design, as shown on the drawings, complies with the requirements of Section X of ASME for the design conditions set forth in the Design Specification. It is consequently the fabricator's responsibility to prove that a vessel so designed will safely withstand the service conditions set forth in the Design Specification. As proof, one or more prototype vessels shall be subjected to destructive tests.

ASME X does not give specific instructions for the post-curing procedure but does give the following requirement:

> *"**Cure***
>
> *If other than ambient temperature cure is employed, the design and operation of the curing equipment shall provide uniform heating over the entire surface of the vessel. Heating may be done from the inside or the outside of the pressure vessel or from both inside and outside. The cure times and temperatures shall conform to those stipulated in the qualified Procedure Specification (see Form Q-107 for Class I vessels and Form Q-120 for Class II vessels)".*

Referring to the form quoted in ASME X, the post-curing schedule must be determined by the designer or manufacturer and qualified by the inspector. The post-curing procedure must therefore be obtained from the resin supplier's instructions.

Resin supplier's instructions, in general, do not indicate whether the designer should consider the laminate shape and/or thickness in order to formulate a post-curing procedure. They merely indicate that, should the chemical medium contained or processed in the vessel be at a temperature (operating temperature) that is sufficiently high to cause chemical attack of the vessel inner surface, post curing should be applied. As an example, Dow Chemical Company give the post-curing procedure for DERAKANE™, vinyl ester resins as [5]:

> *"To achieve the optimum chemical and mechanical properties from the resin, and minimise the residual styrene content, it is often necessary to post-cure, typically for two to three hours at 85° to 100°C, especially when resin is cured at room temperature. Temperature increase and decrease should be gradual to avoid thermal shock."*

2.3 Curing Mechanisms and Stresses

With the almost infinite number of cure components available, including accelerators, promoters, catalysts and inhibitors, the designers and fabricators frequently have difficulty in formulating a cure system for a specific process. In addition, designers and fabricators, who are primarily interested in the final properties of the resin rather than the complexities of the curing systems, rarely have the staff or facilities for cure component evaluation. Thus they depend on resin manufacturers, catalyst manufacturers and other specialists for guidance. The field of cure system development and evaluation is indeed large and, as in any case where a large number of people are involved, a diversity of confusing options exist [6].

2.3.1 The curing mechanism of an unsaturated polyester resin.

The unsaturation points in a polyester resin are the reactive sites that participate in the curing mechanism. The polyester molecule is composed predominantly of stable unreactive single bonds, with the reactive double bonds, with the reactive bonds distributed along the backbone. Each styrene molecule also contains a reactive double bond. The reactivity, however, is not so great as to occur spontaneously at ambient temperatures. The function of the cure system is to assist in the initiation of the reactions.

In the case of unsaturated polyesters the cure system, in particular the catalyst, initiates the crosslinking reaction. When the catalyst, which is normally a peroxide, breaks down, it forms highly unstable free radicals. These radicals subsequently attack at the reactive sites (carbon-carbon double bonds) of the unsaturated polyester and styrene molecules, thus initiating the crosslinking reaction. Accelerators and promoters do just what their names suggest, namely accelerate the rate of crosslinking reaction by promoting faster catalyst breakdown.

The reactants, styrene and unsaturated polyester, contain a certain amount of energy and the product, cured resin, contains somewhat less energy; the difference in these energy levels is the reason for the heat given off as the resin cures. In order to get the reactants to form products though, it is necessary to first put a certain amount of energy into the system. The function of the catalyst is then to increase the potential energy and thus cause the reaction to occur. Accelerators and promoters increase the rate of formation of catalyst radicals and thus make the curing reaction proceed at a rate fast enough to be of practical importance.

Another significant factor in polyester curing is heat or temperature. Chemical reactions tend to proceed faster at higher temperatures and this curing reaction is no exception. The heat does not normally cure the resin as such, but makes the catalyst breakdown more rapid. Additional heat is also used for post curing, which essentially completes the reaction [6]. As a thermosetting resin cures its material characteristics change dramatically, transitioning from the behaviour of a viscous fluid (low shear stiffness), in its uncured state, to a viscoelastic or elastic solid (high shear stiffness), in its fully cured state.

Significant reduction in specific volume (cure shrinkage) associated with the cross-link polymerisation reaction also occurs during cure. These changes in resin directly influence the effective mechanical properties and cure shrinkage strains of the composite during cure [7].

2.3.2 Curing residual stresses

Glass fibre reinforced composite laminates consist of two different materials: glass and resin, therefore they are essentially anisotropic solids. These two materials are combined in many different ways such as short fibre mats, long fibre woven roving and unidirectional filament windings.

Due to the heterogeneous layer construction and the material anisotropy of GRP laminates, the internal mutual constraints and the thermal incompatibility between the layers complicate the induced thermal stresses. The self-equilibrating stresses can cause damage in the laminate structure and alter its structural functionality.

A number of studies considering the thermal and transient thermal stresses in thick laminated composite shells, tubes and plates have been published, and a variety of approaches proposed for the prediction of stresses induced by thermal or thermo-mechanical loading [8-14]. In general they have all shown that thermal stresses are associated with thermal strain incompatibility and that these stresses can exist without the action of external forces. In isotropic solid bodies, they arise from either non-uniform temperature gradients or external constrained boundaries. In generally anisotropic solids, the stresses can occur even under uniform temperature change due to the thermal incompatibility.

An important mechanism contributing to stress development, which is seldom considered in the literature, even in many references not cited, is the volumetric shrinkage of the thermosetting resin associated with the cross-link polymerisation reaction. The residual stress development in thick laminates could be potentially worse than thermal-induced stresses. Various studies have been conducted on the process-induced stresses attempting to formulate procedures and models to predict these stresses [7,15-19]

Bogetti and Gillespie [7] proposed a methodology for predicting the evolution of residual stress development during the curing process. A one-dimensional cure simulation analysis is coupled to an incremental laminated plate theory model to study the relationships between complex gradients in temperature and degree of cure. These material models are incorporated into a micromechanics model to predict the effective mechanical properties and process-induced strains of the composite during cure. The cure simulation analysis takes two material models into account that describes the mechanical property changes and volumetric cure shrinkage associated with the cross-linked polymerisation. The property

changes and cure shrinkage of the resin directly influence the homogeneous mechanical properties and process-induced strains in the composite. The two material models describe the modulus development and the volumetric chemical shrinkage of the resin during cure. These models are then used to compute the effective homogeneous unidirectional mechanical properties of the individual layers at each increment of the cure simulation. From this the composite chemical and thermal shrinkage strains are computed to determine the total process-induced composite strains. The process-induced stresses are then calculated using the classical laminated plate theory as theoretical basis employing an incremental Hooke's law formulation.

Guemes [15] presented a model to predict the residual stress due to curing in thick or thin laminated cylinders, decoupling the stress analysis from the cure kinetics. The method employs a 3D elasticity solution, calculating in-plane and normal stresses. Guemes found that the main factor for influencing the stress state within the laminate is the temperature change, due to exotherm and post-curing at elevated temperatures, and not the tensioning of the filaments during winding nor the fibre motion. Differences in thermal expansion among the mandrel and the uncured laminate create a tensile stress state during the heating phase. Mainly the fibres of the inner layers support this tensile stress. Guemes also found that it is the final temperature and not the cure cycle history which will define these stresses. During the analysis of the cooling period, Guemes found that curing residual stresses remain permanently in the laminate and for failure predictions, these stresses need to be added to those resulting from operational loads.

Guemes, however, did not consider an important mechanism contributing to stress development, i.e. the volumetric shrinkage of the thermosetting resin associated with the

cross-link polymerisation. The effects of chemical shrinkage on residual stress development in thick laminates could be potentially worse, for example, if shrinkage were to occur within the interior region of a laminate that is constrained by a fully cured exterior region. A similar situation occurs on the micromechanics level where resin shrinkage during cure is constrained by the reinforcement phase [7].

Guemes [15] determined that a high cooling rate will promote an uneven distribution of temperatures through the laminate, and consequently, a transient stress state will be superimposed over the residual stress field developing in the laminate. It was found that these transient stresses are one order of magnitude lower than the residual stresses and do not represent a real threat under normal processing conditions.

From the above Guemes concluded that the anisotropic expansion of the individual layers of the laminate is the main source of residual stresses and consequently the stress analysis can be decoupled from the cure kinetics and the fibre motion. Guemes also concluded that, for thick cylinders, high residual transverse tensile stresses are found, confirming that a risk of spontaneous delamination exists.

Eduljee and Gillespie [18] have studied the curing strains developed during the lay-up of composite tubes and devoted some work to developing a methodology for predicting the thermoelastic response during the cure and post-cure process whilst the tube is being manufactured. This model was then used to understand the interactions of various process parameters on their residual stress development. As with many other researchers they considered tubes manufactured by the filament winding technique, which makes for convenient mathematical modelling. The model presented considers the sequential

addition of layers during the build-up of tubes and calculates the incremental stresses and strains due to the addition of the layer by considering the winding tension at a processing temperature. It also considers stresses due to thermal loads but it does not consider the chemical shrinkage that the resin under goes during consolidation and post-cure. The effect of this shrinkage is therefore not accounted for in their work.

Stone *et al.* [19] studied the effect of matrix shrinkage during post-cure on tubes and presented results of a theoretical investigation of the associated stresses. They showed that inner-wall tensile residual stresses of sufficient magnitude to promote environmentally assisted cracking could readily be induced by the post-cure process. The stress calculation utilised the resin post-cure shrinkage by analogy to a matrix coefficient of thermal expansion to determine the laminate shrinkages. Tube shrinkage stresses were then determined by making use of the Rayleigh-Ritz method involving the minimising the total potential energy with respect to the displacement functions chosen.

2.4 Discussion of the literature

As can be seen that, from the literature presented, research has been concentrated on the stresses and strains produced by either mechanical or thermal loading and by usually only considering the laminate thermal properties. It is also shown that some work has been conducted on the stress development resulting from resin shrinkage during cure and post-cure. However, the majority of the work has been done on laminated tubes and for obvious reasons does not take variations of shape into account. The work presented in the current literature concentrates on laminates with unidirectional material properties since the mathematical modelling should be accurate. Very little work appears to have been done on laminate constructed of randomly oriented fibres. This could be due to the manufacturing

method of the mat not guaranteeing consistent mat thickness and in-plane laminate elastic material properties. However, the methods and theories available can be applied to random oriented fibre laminates if consideration is given to fibre contribution factors applied in some cases.

Previously published work presented therefore serves as a starting point for the stress and strain prediction resulting from the thermo-chemical loads such as the chemical shrinkage of the matrix.

3. STRESS CALCULATION OF PLATES AND SHELLS

3.1 Introduction

It is often required, and preferable, to estimate the stresses and strains developed during post-cure prior to the manufacture of the vessel component. Methods described in the work, such as the finite element method, are not always practicable since the majority of the manufacturers do not have access to the software for specialised analysis required on problematic vessel configurations. Manufacturers also tend to address problem areas on the vessels by the addition of layers to "strengthen" the laminate and hence, unknowingly, potentially create areas that could assist the mechanisms thought to cause cracking or failure in laminates.

For the purpose of this work the method of stress and strain calculation in plates and shells, using the laminate and circular cylindrical composite theory, will be described although the methods are well known in the field of composite design.

3.2 Elastic constants of a layer

Prior to performing stress and strain calculations the elastic constants of the layer under consideration need to be determined. Micromechanics equations have been developed to predict layer properties from the properties of fibre, matrix and their respective volume fractions. Except for the prediction of the longitudinal modulus (E_1) and the major Poisson ratio (ν_{12}), equations for other constants are based on empirical constants, which vary from one material system to another. These values so calculated will be used as guides and will be experimentally determined as verification for the purpose of this work.

3.2.1 Elastic constants in the fibre direction, the rule of mixture

Young's modulus along fibre direction (E_1) and the major Poisson ratio (ν_{12}) are calculated by using the rule of mixture. This is based on the volume fraction (V) of the fibres (f) and the matrix (m) in a laminate. E_1 and ν_{12} are given by

$$E_1 = E_f V_f + E_m V_m \qquad \text{Eq. 3.1}$$

and

$$\nu_{12} = \nu_f V_f + \nu_m V_m \qquad \text{Eq. 3.2}$$

3.2.2 Elastic constants, transverse to the fibre direction and shear constants

3.2.2.1 The modified rule of mixture

Young's modulus transverse to the fibre direction (E_2) is commonly determined by the modified rule of mixture [20].

$$\frac{1}{E_2} = \frac{1}{V_f + \eta_2 V_m}\left(\frac{V_f}{E_f} + \eta_2 \frac{V_m}{E_m}\right) \qquad \text{Eq. 3.3}$$

where η_2 is the transverse contribution factor from the matrix into the stiffness of the layer. The value of η_2 is usually assumed to be around 0.5.

The in-plane shear modulus (G_{12}) follows a similar procedure as the calculation of E_2.

$$\frac{1}{G_{12}} = \frac{1}{V_f + \eta_{12} V_m}\left(\frac{V_f}{G_f} + \eta_{12} \frac{V_m}{G_m}\right) \qquad \text{Eq. 3.4}$$

where η_{12} is the shear contribution factor from the matrix into the stiffness of the layer. The value of η_{12} is usually also assumed to be around 0.5.

3.2.2.2 Halpin-Tsai Equations for laminate moduli

Composite laminates constructed of random oriented fibres do not present formulae formulated by micromechanics to determine the laminate elastic properties. These properties, due to the construction method of the reinforcement mat, need to be determined by making use for proven empirical formulae. Halpin and Tsai [21] have developed such formulae using simple and generalised equations to approximate the in-plane and transverse moduli of aligned short fibre composites. These equations are simple and can readily be used in the design process. Moreover, the predictions of these equations are quite accurate if the fibre volume fraction does not approach the value of 1[22].

The Halpin-Tsai equation for the in-plane modulus is written as

$$\frac{E_1}{E_m} = \frac{1+(2l/d)\eta_1 V_f}{1-\eta_1 V_f} \qquad \text{Eq. 3.5}$$

where

$$\eta_1 = \frac{(E_f/E_m)-1}{(E_f/E_m)+2l/d} \qquad \text{Eq. 3.6}$$

with (l/d) being the fibre aspect ratio, l and d being the fibre length and diameter respectively.

The transverse composite modulus can be written as

$$\frac{E_2}{E_m} = \frac{1+\xi_1\eta_2 V_f}{1-\eta_2 V_f} \qquad \text{Eq. 3.7}$$

where

$$\eta_2 = \frac{(E_f/E_m)-1}{(E_f/E_m)+\xi_1} \qquad \text{Eq. 3.8}$$

in which ξ_1 is a measure of reinforcement and depends on the fibre geometry, packing geometry, and loading conditions. The values of ξ_1 are obtained by comparing Eq. 3.7 and Eq. 3.8 with exact elasticity solutions through curve-fitting techniques. Halpin and Tsai have suggested that a value for ξ_1 between 1 and 2 may be used for fibres with circular or square cross sections. For rectangular cross-section fibres, ξ_1 may be calculated as

$$\xi_1 = 2\frac{a}{b} \qquad \text{Eq. 3.9}$$

where a/b is the rectangular cross-section aspect ratio with the dimension a taken in the direction of the loading. Predictions of the Halpin-Tsai equation for transverse composite modulus have been shown as a function of fibre volume fraction in Fig. 3.1 for different constituent modulus ratios.

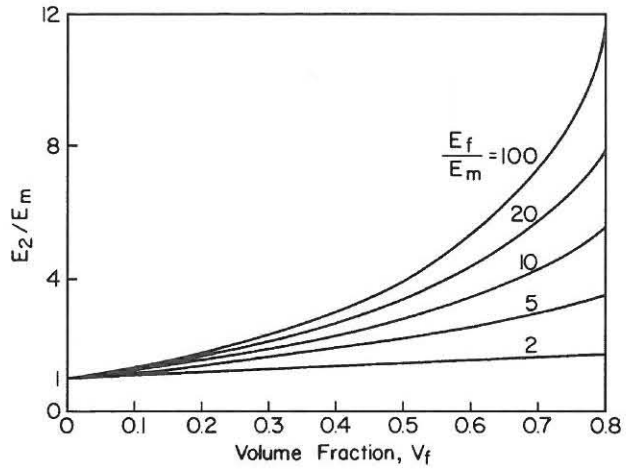

Fig. 3.1 Predictions of Halpin-Tsai equation [Eq. 3.7] for transverse composite modulus.

Halpin and Tsai have demonstrated the applicability of these equations by showing that the predictions of Eq. 3.7 agree very well with some of the more exact solutions. A more thorough discussion on the comparison of the Halpin-Tsai equations and the exact elasticity solution has been presented in the original reference [21]. Also given in this

reference are similar simple relations for other composite properties. It is suggested that the Halpin-Tsai equations are quite adequate to satisfy the practical requirements for the predictions of transverse composite modulus, particularly as the variations in composite materials manufacturing processes always cause a variation in the composite moduli. Therefore, one cannot hope to precisely predict composite moduli.

Similarly, the shear modulus (G_{12}) can be determined by the Halpin-Tsai equation as follows

$$G_{12} = G_m \frac{1+\xi_2 \eta_{12} V_f}{1-\eta_{12} V_f} \qquad \text{Eq. 3.10}$$

where

$$\eta_{12} = \frac{(G_f/G_m)-1}{(G_f/G_m)+\xi_2} \qquad \text{Eq. 3.11}$$

The values of ξ_2 =1 for the calculation of G_{12} seem to give good results [20]. For ξ_2 =1, the relation in Eq. 3.10 becomes

$$G_{12} = G_m \frac{(G_f + G_m)+V_f(G_f - G_m)}{(G_f + G_m)-V_f(G_f - G_m)} \qquad \text{Eq. 3.12}$$

3.2.2.3 Poisson's ratio in the through-thickness (or transverse) direction with in-plane loading

The Poisson's ratio in the through-thickness, or transverse to the fibre direction, is possibly the most difficult to determine accurately. The mixture rule is generally used but it tends to underestimate this particular Poisson's ratio since it ignores the constraints that the stiffer fibres place on the tendency of the softer matrix material to contract in the fibre direction when stretched normal to the fibres [23]. Foye [23] presents Eq. 3.13, with an

effective Poisson's ratio of the matrix material in place of the conventional one, to predict the through-thickness Poisson' ratio, ν_{13}, for composite layers that contain stiff, circular, isotropic fibres bonded to a soft matrix material such as being used in this study.

$$\nu_{13} = V_f \nu_f + V_m \nu_m \left\{ \frac{1+\nu_m - \nu_{12}(E_m/E_1)}{1-\nu_m{}^2 + \nu_m \nu_{12}(E_m/E_1)} \right\} \qquad \text{Eq. 3.13}$$

3.2.2.4 Poisson's ratio in the in-plane direction with through-thickness (or transverse) loading

The Poisson's ratio in the in-plane direction, due to loading in the through-thickness direction, ν_{31}, will not be the same as ν_{13} since the fibres are obviously expected to apply a greater degree of restraint in the in-plane direction. The calculation of ν_{31} can be done by using the following relation

$$\frac{\nu_{13}}{E_1} = \frac{\nu_{31}}{E_3} \qquad \text{Eq. 3.14}$$

3.2.2.5 Averaged elastic constants for randomly orientated discontinuous fibres

If the fibre orientation in a composite is truly random in a three-dimensional sense, the composite exhibits three-dimensional isotropy. Such a situation is likely to exist when the fibre length, L, is much less than the thickness (t) of the part. Composites with low aspect ratio reinforcement such as whiskers or microfibres generally fall into this category. However, in many short-fibre composite parts (e.g., GRP vessel components made from chopped strand mat) the fibre length is much greater than the thickness of the part or laminate. In this case fibre orientation in the thickness direction is not possible and the material exhibits two-dimensional isotropy, or planar isotropy [24].

One major aspect is that fibre orientation is more important than fibre length in the determination of off-axis elastic constants of unidirectional composites. Further support for this conclusion is provided by the observation that continuous fibre models give reasonably accurate predictions of elastic properties of randomly oriented fibre-reinforced composites.

The concept of averaging the elastic constants over all possible orientations by integration was apparently introduced by Cox [25], who modelled paper, for two-dimensional and three-dimensional cases, as a planar mat of continuous fibres without matrix material. The Cox formulas for the averaged isotropic elastic constants of random arrays of fibres are given here, but they are not considered accurate enough for design use. For the two-dimensional case

$$\tilde{E} = \frac{E_f \nu_f}{3}$$

$$\tilde{G} = \frac{E_f \nu_f}{8}$$

$$\tilde{\nu} = \frac{1}{3} \qquad \text{Eq. 3.15}$$

where $\tilde{E}$ = averaged Young's modulus for randomly oriented fibre composite,

$\tilde{G}$ = averaged shear modulus for randomly oriented fibre composite, and

$\tilde{\nu}$ = averaged Poisson's ratio for randomly oriented fibre composite.

Tsai and Pagano [26] also developed the expressions for the averaged elastic constants for laminates containing random oriented fibres. These expressions are for the Young's and shear moduli respectively and are presented as

$$\tilde{E} = \frac{3}{8}E_1 + \frac{5}{8}E_2 \qquad \text{Eq. 3.16}$$

and

$$\tilde{G} = \frac{1}{8}E_1 + \frac{1}{4}E_2 \qquad \text{Eq. 3.17}$$

where E_1 and E_2 are respectively the longitudinal and transverse moduli of an aligned short-fibre composite having the same fibre aspect ratio and fibre volume fraction as the composite under consideration. The moduli E_1 and E_2 can be calculated by using the Halpin-Tsai equations, Eq. 3.5 and Eq. 3.7, or can be determined experimentally.

Christensen and Waals [27] also used the averaging approach to find the isotropic elastic constants for continuous fibre composites with two-dimensional and three-dimensional random fibre orientation. For the two-dimensional case they obtained

$$\tilde{E} = \frac{1}{u_1}(u_1^2 - u_2^2)$$

$$\tilde{\nu} = \frac{u_2}{u_1} \qquad \text{Eq. 3.18}$$

where

$$u_1 = \frac{3}{8}E_1 + \frac{G_{12}}{2} + \frac{(3 + 2\nu_{12} + 3\nu_{12}^2)G_{23}K_{23}}{2(G_{23} + K_{23})} \qquad \text{Eq. 3.19}$$

and

$$u_2 = \frac{1}{8}E_1 - \frac{G_{12}}{2} + \frac{(1 + 6\nu_{12} + \nu_{12}^2)G_{23}K_{23}}{2(G_{23} + K_{23})} \qquad \text{Eq. 3.20}$$

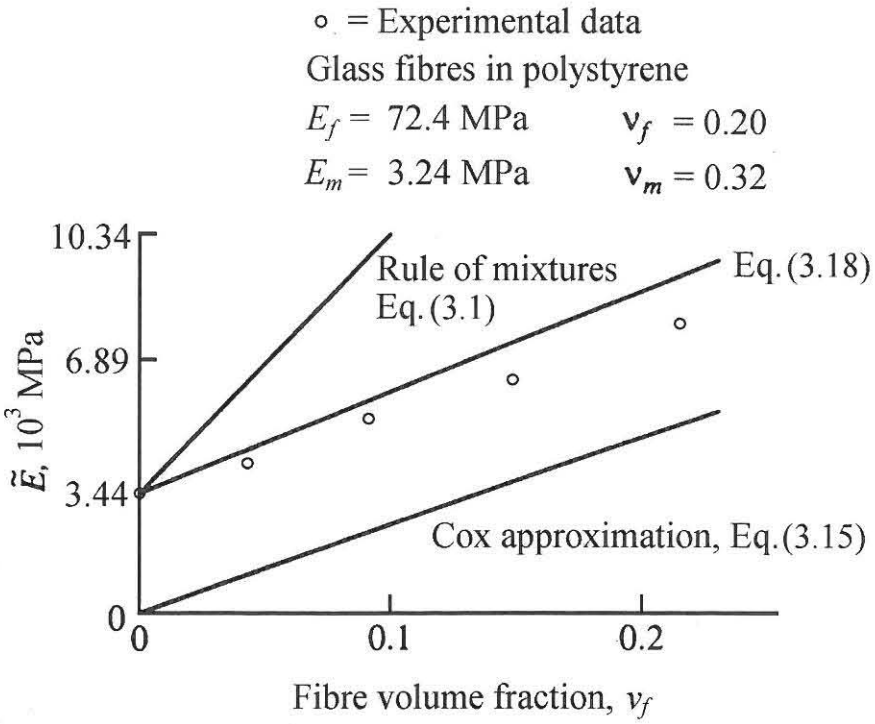

Fig. 3.2 Comparison of Christensen-Waals two-dimensional analysis for Young's modulus of randomly oriented fibre with rule of mixtures and Cox approximation for a glass/polystyrene composite.

Christensen and Waals used previously developed micromechanics equations by Hashin [28, 29] and Hill [30] to calculate the five independent engineering constants E_1, ν_{12}, G_{12}, G_{23}, and K_{23}, where K_{23} is the plain strain bulk modulus for dilation in the 2-3 plane. The results from Eq. 3.18 for a glass/polystyrene composite are shown in Fig. 3.2. The Christensen and Waals model is seen to give much better agreement with measurements than either the Cox model or the rule of mixtures.

3.3 Coefficients of thermal expansion of a layer

3.3.1 Coefficients of thermal expansion using Shapery's equations

The thermal behaviour of a unidirectional layer is characterised in terms of two principal thermal coefficients of thermal expansion (CTE), α_1 and α_2. These coefficients can be related to the geometric and material properties of the constituents. Approximate micromechanical relations for the coefficients of thermal expansion were given by Schapery [31] for isotropic constituents. Although these relations have been developed for unidirectional layers they are generally also applied to random oriented fibre composites.

The longitudinal coefficient for a continuous fibre composite is given by [31]

$$\alpha_1 = \frac{E_f \alpha_f V_f + E_m \alpha_m V_m}{E_f V_f + E_m V_m} \qquad \text{Eq. 3.21}$$

where

E_f, E_m = Fibre and matrix moduli, respectively

α_f, α_m = Fibre and matrix coefficients of thermal expansion, respectively

V_f, V_m = Fibre and matrix volume ratios, respectively

The relation is similar to the rule of mixtures for longitudinal modulus and gives fairly accurate results. The relation for the transverse coefficient of expansion, which is based on energy principles, is

$$\alpha_2 = \alpha_f V_f (1+\nu_f) + \alpha_m V_m (1+\nu_m) - \alpha_1 (\nu_f V_f + \nu_m V_m) \qquad \text{Eq. 3.22}$$

where

ν_f, ν_m = Poisson's ratios of fibre and matrix, respectively

α_1 = Longitudinal CTE of the layer from Eq. 3.21.

Once the principal coefficients α_1 and α_2 are known, the coefficients can be referred to the reference axes (x, y) by applying the following transformation relations

$$\alpha_x = \alpha_1 m^2 + \alpha_2 n^2$$

$$\alpha_y = \alpha_1 n^2 + \alpha_2 m^2$$

$$\alpha_{xy} = \alpha_s = 2(\alpha_1 - \alpha_2)mn \qquad \text{Eq. 3.23}$$

with $m = \cos\theta$ and $n = \sin\theta$

and θ being the fibre orientation relative to the x-axis.

3.3.2 Coefficients of thermal expansion using the Halpin-Pagano method

Eq. 3.21 and Eq. 3.22 primarily give the CTE values for a unidirectional fibre reinforced laminate. Halpin and Pagano [32] demonstrated that the isotropic thermal expansion coefficients can be predicted by

$$\alpha_x = \frac{\alpha_1 + \alpha_2}{2} + \frac{Q_{11} - Q_{22}}{Q_{11} + Q_{22} + 2Q_{12}} \frac{\alpha_1 - \alpha_2}{2} \qquad \text{Eq. 3.24}$$

where the elastic constants in the stiffnesses Q_{11}, Q_{22} and Q_{12} are calculated by Eq. 3.5 and Eq. 3.7 and the CTE values for α_1 and α_2 are calculated by Eq. 3.21 and Eq. 3.22. The stiffnesses Q_{11}, Q_{22} and Q_{12} are given in Eq. 3.25 in the next section.

3.4 Laminate stiffness

When predicting the coefficients of thermal expansion of multi-directional laminates it is required to determine the laminate stiffness in terms of geometry, material properties and stacking sequence [33, 34, 35].

3.4.1 Reduced ply stiffness

Using the elastic constants, determined by using the appropriate method as shown before, the ply stiffness along the principal material axes, $[Q]_{1,2}$, is determined by four reduced stiffnesses Q_{11}, Q_{22}, Q_{12} and G_{66} using the following relations:

$$Q_{11} = \frac{E_1}{1-\nu_{12}\nu_{21}}$$

$$Q_{22} = \frac{E_2}{1-\nu_{12}\nu_{21}}$$

$$Q_{12} = \frac{\nu_{21}E_1}{1-\nu_{12}\nu_{21}} = \frac{\nu_{12}E_2}{1-\nu_{12}\nu_{21}}$$

$$Q_{66} = G_{12} \qquad \text{Eq. 3.25}$$

where

$$[Q]_{1,2} = \begin{bmatrix} Q_{11} & Q_{12} & 0 \\ Q_{21} & Q_{22} & 0 \\ 0 & 0 & Q_{66} \end{bmatrix} \qquad \text{Eq. 3.26}$$

3.4.2 Transformed reduced ply stiffness

Normally, the layer principal axes (1, 2) do not coincide with the loading of reference axes (x, y). A transformation matrix $[T]$ is employed to transform the reduced stiffness from the principal axes to the reference axes giving a transformed reduced stiffness matrix $[Q]_{x,y}$ for each of the plies k

$$[Q]_{x,y} = [T^{-1}]_k \begin{bmatrix} Q_{11} & Q_{12} & 0 \\ Q_{21} & Q_{22} & 0 \\ 0 & 0 & Q_{66} \end{bmatrix} [T]_k = \begin{bmatrix} Q_{xx} & Q_{xy} & Q_{xs} \\ Q_{yx} & Q_{yy} & Q_{ys} \\ Q_{sx} & Q_{sy} & Q_{ss} \end{bmatrix}_k \qquad \text{Eq. 3.27}$$

where

$$[T]_k = \begin{bmatrix} m^2 & n^2 & 2mn \\ n^2 & m^2 & -2mn \\ -mn & mn & m^2 - n^2 \end{bmatrix}_k \qquad \text{Eq. 3.28}$$

with $m = \cos\theta$ and $n = \sin\theta$

The six transformed reduced stiffnesses can be expressed as

$$Q_{xx_k} = m_k^4 Q_{11} + n_k^4 Q_{22} + 2m_k^2 n_k^2 Q_{12} + 4m_k^2 n_k^2 Q_{66}$$

$$Q_{yy_k} = n_k^4 Q_{11} + m_k^4 Q_{22} + 2m_k^2 n_k^2 Q_{12} + 4m_k^2 n_k^2 Q_{66}$$

$$Q_{xy_k} = m_k^2 n_k^2 Q_{11} + m_k^2 n_k^2 Q_{22} + (m_k^4 + n_k^4) Q_{12} - 4m_k^2 n_k^2 Q_{66}$$

$$Q_{xs_k} = m_k^3 n_k Q_{11} + m_k n_k^3 Q_{22} + (m_k n_k^3 - m_k^3 n_k) Q_{12} - 2(m_k n_k^3 - m_k^3 n_k) Q_{66}$$

$$Q_{ys_k} = m_k n_k^3 Q_{11} + m_k^3 n_k Q_{22} + (m_k n_k^3 - m_k^3 n_k) Q_{12} - 2(m_k n_k^3 - m_k^3 n_k) Q_{66}$$

$$Q_{ss_k} = m_k^2 n_k^2 Q_{11} + m_k^2 n_k^2 Q_{22} - 2m_k^2 n_k^2 Q_{12} + (m_k^2 - n_k^2)^2 Q_{66} \qquad \text{Eq. 3.29}$$

3.4.3 Laminate stiffnesses

The laminate stiffness can be expressed in terms of three laminate stiffness matrices, $[A]$, $[B]$ and $[D]$, which are functions of geometry, material properties and stacking sequence of the individual plies $k = 1,2..n$.

$$[A] = \begin{bmatrix} A_{xx} & A_{xy} & A_{xs} \\ A_{yx} & A_{yy} & A_{ys} \\ A_{sx} & A_{sy} & A_{ss} \end{bmatrix}$$

where

$$[T]_k = \begin{bmatrix} m^2 & n^2 & 2mn \\ n^2 & m^2 & -2mn \\ -mn & mn & m^2 - n^2 \end{bmatrix}_k \qquad \text{Eq. 3.28}$$

with $m = \cos\theta$ and $n = \sin\theta$

The six transformed reduced stiffnesses can be expressed as

$$Q_{xx_k} = m_k^4 Q_{11} + n_k^4 Q_{22} + 2m_k^2 n_k^2 Q_{12} + 4m_k^2 n_k^2 Q_{66}$$

$$Q_{yy_k} = n_k^4 Q_{11} + m_k^4 Q_{22} + 2m_k^2 n_k^2 Q_{12} + 4m_k^2 n_k^2 Q_{66}$$

$$Q_{xy_k} = m_k^2 n_k^2 Q_{11} + m_k^2 n_k^2 Q_{22} + (m_k^4 + n_k^4) Q_{12} - 4m_k^2 n_k^2 Q_{66}$$

$$Q_{xs_k} = m_k^3 n_k Q_{11} + m_k n_k^3 Q_{22} + (m_k n_k^3 - m_k^3 n_k) Q_{12} - 2(m_k n_k^3 - m_k^3 n_k) Q_{66}$$

$$Q_{ys_k} = m_k n_k^3 Q_{11} + m_k^3 n_k Q_{22} + (m_k n_k^3 - m_k^3 n_k) Q_{12} - 2(m_k n_k^3 - m_k^3 n_k) Q_{66}$$

$$Q_{ss_k} = m_k^2 n_k^2 Q_{11} + m_k^2 n_k^2 Q_{22} - 2m_k^2 n_k^2 Q_{12} + (m_k^2 - n_k^2)^2 Q_{66} \qquad \text{Eq. 3.29}$$

3.4.3 Laminate stiffnesses

The laminate stiffness can be expressed in terms of three laminate stiffness matrices, $[A]$, $[B]$ and $[D]$, which are functions of geometry, material properties and stacking sequence of the individual plies $k = 1,2..n$.

$$[A] = \begin{bmatrix} A_{xx} & A_{xy} & A_{xs} \\ A_{yx} & A_{yy} & A_{ys} \\ A_{sx} & A_{sy} & A_{ss} \end{bmatrix}$$

$$[B]=\begin{bmatrix} B_{xx} & B_{xy} & B_{xs} \\ B_{yx} & B_{yy} & B_{ys} \\ B_{sx} & B_{sy} & B_{ss} \end{bmatrix}$$

$$[D]=\begin{bmatrix} D_{xx} & D_{xy} & D_{xs} \\ D_{yx} & D_{yy} & D_{ys} \\ D_{sx} & D_{sy} & D_{ss} \end{bmatrix} \qquad \text{Eq. 3.30}$$

where

$$A_{ij} = \sum_{k=1}^{n} t_k (Q_{ij})_k$$

$$B_{ij} = \sum_{k=1}^{n} -t_k z_k (Q_{ij})_k$$

$$D_{ij} = \sum_{k=1}^{n} \left(t_k z_k^2 + \frac{t_k^3}{12} \right) (Q_{ij})_k \qquad \text{Eq. 3.31}$$

with $i, j = x, y, s$.

where t_k is the ply thickness of individual layers k=1,2..3, and z_k is the centroidal co-ordinate of layer k from the laminate neutral axis and calculated by

$$z_k = h_o - \left(\frac{t_k}{2} + h_{k-1} \right) \qquad \text{Eq. 3.32}$$

with $h_o = \frac{1}{2}\left(\sum_k t_k \right)$ and $h_k = \sum_{k=1}^{k} t_k$

These matrices are the average elastic parameters of the multidirectional laminate with the following significance:

A_{ij} are the extensional stiffnesses, or in-plane laminate moduli, relating in-plane loads to in-plane strains.

B_{ij} are the coupling stiffnesses, or in-plane/flexure coupling laminate moduli, relating in-plane loads to curvatures and moments to in-plane strains.

D_{ij} are bending or flexural laminate stiffnesses relating moments to curvatures.

3.5 Thermal effects in unidirectional layers

The laminate, or combination of layers, undergoes hygrothermal deformation when subjected to a uniform change in temperature. In this study it is rather considered to undergo thermo-chemical deformation since the manufacturing process, i.e. the cure and post-cure phases, are studied. However, the same procedure as for hygrothermal strain calculation is employed with the only difference being the type of thermal expansion employed in the calculations, which will be explained later in this work. Also, for the purpose of this study it is assumed that there is no moisture deformation induced, although moisture could play a role during the post-cure where the test specimens are heated to effect post-cure. Hence in the calculations, no reference will be made to moisture expansion coefficients.

3.5.1 Thermal strains

Thermal strains referred to the principal material directions are given by

$$e_1 = \alpha_1 \Delta T$$

$$e_2 = \alpha_2 \Delta T$$

$$e_6 = 0 \qquad \text{Eq. 3.33}$$

The transformed thermal strains referred to the reference axes (x, y) are

$$e_x = e_1 m^2 + e_2 n^2$$

$$e_y = e_1 n^2 + e_2 m^2$$

$$e_{xy} = e_s = 2(e_1 - e_2)mn \qquad \text{Eq. 3.34}$$

with $m = \cos\theta$ and $n = \sin\theta$

3.5.2 Thermal force and moment resultants

The deformations resulting from a change in temperature, i.e. the thermal strains induced in the laminate, cause thermal force and moment resultants, which are defined as

$$\begin{bmatrix} N_x^T \\ N_y^T \\ N_s^T \end{bmatrix} = \sum_{k=1}^{n} \begin{bmatrix} Q_{xx} & Q_{xy} & Q_{xs} \\ Q_{yx} & Q_{yy} & Q_{ys} \\ Q_{sx} & Q_{sy} & Q_{ss} \end{bmatrix}_k \begin{bmatrix} e_x \\ e_y \\ e_s \end{bmatrix}_k t_k \qquad \text{Eq. 3.35}$$

$$\begin{bmatrix} M_x^T \\ M_y^T \\ M_s^T \end{bmatrix} = \sum_{k=1}^{n} \begin{bmatrix} Q_{xx} & Q_{xy} & Q_{xs} \\ Q_{yx} & Q_{yy} & Q_{ys} \\ Q_{sx} & Q_{sy} & Q_{ss} \end{bmatrix}_k \begin{bmatrix} e_x \\ e_y \\ e_s \end{bmatrix}_k z_k t_k \qquad \text{Eq. 3.36}$$

where

t_k = the thickness of the layer k,

$[N^T]_{x,y}$ = thermal force resultant

$[M^T]_{x,y}$ = thermal moment resultant

For this work it is assumed that there are no mechanical forces or moments applied to the laminate, hence, the thermal force and moments are taken as the total force and moment resultants.

3.5.3 Coefficients of thermal expansion of multidirectional laminates

Once the thermal force and moment resultants are known, the coefficients of expansion of multidirectional laminates can be determined with the following

$$\begin{bmatrix} \bar{\alpha}_x \\ \bar{\alpha}_y \\ \bar{\alpha}_s \end{bmatrix} = \begin{bmatrix} a_{xx} & a_{xy} & a_{xs} \\ a_{yx} & a_{yy} & a_{ys} \\ a_{sx} & a_{sy} & a_{ss} \end{bmatrix} \begin{bmatrix} N_x^T \\ N_y^T \\ N_s^T \end{bmatrix} + \begin{bmatrix} b_{xx} & b_{xy} & b_{xs} \\ b_{yx} & b_{yy} & b_{ys} \\ b_{sx} & b_{sy} & b_{ss} \end{bmatrix} \begin{bmatrix} M_x^T \\ M_y^T \\ M_s^T \end{bmatrix} \quad \text{Eq. 3.37}$$

3.6 Laminate strains and stresses

3.6.1 Reference plane strains

By using the thermal force and moment resultants, the reference plane strains and curvatures can be calculated by

$$\begin{bmatrix} \varepsilon_x^o \\ \varepsilon_y^o \\ \gamma_s^o \\ \kappa_x \\ \kappa_y \\ \kappa_s \end{bmatrix} = \begin{bmatrix} a_{xx} & a_{xy} & a_{xs} & b_{xx} & b_{xy} & b_{xs} \\ a_{yx} & a_{yy} & a_{ys} & b_{yx} & b_{yy} & b_{ys} \\ a_{sx} & a_{sy} & a_{ss} & b_{sx} & b_{sy} & b_{ss} \\ c_{xx} & c_{xy} & c_{xs} & d_{xx} & d_{xy} & d_{xs} \\ c_{yx} & c_{yy} & c_{ys} & d_{yx} & d_{yy} & d_{ys} \\ c_{sx} & c_{sy} & c_{ss} & d_{sx} & d_{sy} & d_{ss} \end{bmatrix} \begin{bmatrix} N_x^T \\ N_y^T \\ N_s^T \\ M_x^T \\ M_y^T \\ M_s^T \end{bmatrix} \quad \text{Eq. 3.38}$$

where

$[\varepsilon^o]_{x,y}$ = reference plane strain, and

$[\kappa]_{x,y}$ = laminate curvature.

$$[a] = [A^{-1}] - \{[B^*][D^{*-1}]\}[C^*]$$

$$[b] = [B^*][D^{*-1}]$$

$$[c] = -[D^{*-1}][C^*]$$

$$[d] = [D^{-1}]$$

with

$$[A^{-1}] = \text{inverse of matrix } [A]$$

$$[B^*] = -[A^{-1}][B]$$

$$[C^*] = [B][A^{-1}]$$

$$[D] = [D] - \{[B][A^{-1}]\}[B]$$

3.6.2 Net strains

The net strains at any point in the laminate can be related to the reference plane strains and laminate curvatures as follows

$$\begin{bmatrix} \varepsilon_x \\ \varepsilon_y \\ \gamma_s \end{bmatrix}_k = \begin{bmatrix} \varepsilon_x^o \\ \varepsilon_y^o \\ \gamma_s^o \end{bmatrix} + z_k \begin{bmatrix} \kappa_x \\ \kappa_y \\ \kappa_s \end{bmatrix} \qquad \text{Eq. 3.39}$$

The net layer strains are then given by

$$\begin{bmatrix} \varepsilon_{xe} \\ \varepsilon_{ye} \\ \gamma_{se} \end{bmatrix}_k = \begin{bmatrix} \varepsilon_x \\ \varepsilon_y \\ \gamma_s \end{bmatrix}_k - \begin{bmatrix} e_x \\ e_y \\ e_s \end{bmatrix}_k \qquad \text{Eq. 3.40}$$

The net layer principal strains are then calculated by employing the transformation matrix given in Eq. 3.28 and hence

$$\begin{bmatrix} \varepsilon_{1e} \\ \varepsilon_{2e} \\ \gamma_{6e} \end{bmatrix}_k = [T]_k \begin{bmatrix} \varepsilon_{xe} \\ \varepsilon_{ye} \\ \gamma_{se} \end{bmatrix}_k \qquad \text{Eq. 3.41}$$

3.7 Laminate hygrothermal stresses

By applying the layer stiffness given by Eq. 3.26 the principal hygrothermal stresses, in this case the thermal stresses, are

$$\begin{bmatrix} \sigma_1 \\ \sigma_2 \\ \tau_k \end{bmatrix}_k = [Q]_{1,2_k} \begin{bmatrix} \varepsilon_{1e} \\ \varepsilon_{2e} \\ \gamma_{6e} \end{bmatrix}_k \qquad \text{Eq. 3.42}$$

As an alternative the thermal stresses can be calculated in the laminate co-ordinate system

$$\begin{bmatrix} \sigma_x \\ \sigma_y \\ \tau_s \end{bmatrix}_k = [Q]_{x,y_k} \begin{bmatrix} \varepsilon_{xe} \\ \varepsilon_{ye} \\ \gamma_{se} \end{bmatrix}_k \qquad \text{Eq. 3.43}$$

4. MATERIAL PROPERTIES FOR STRESS AND STRAIN PREDICTION

4.1 Introduction

Accurate mechanical and thermal engineering material properties are required for the prediction of stresses and strains, induced by thermo-mechanical loading, in composite components. Apart from experimental testing, there are various methods for predicting these properties as is described in Chapter 3. The methods presented in Chapter 3 will now be used to create a table of material properties for application in the stress prediction by FEA. Experimentally determined properties will also be presented and tabulated for use in the stress predictions with the aim of comparing the stress results to the models in which predicted material properties were used.

For the purpose of this work experimental material properties are defined as values obtained for specified material properties by means of experimental testing and predicted material properties are defined as specified material properties obtained by means of calculation procedures. Experimentally determined material property values are often required in the calculation of subsequent material properties. These subsequent material properties will also be classified as predicted values.

4.2 Base materials elastic properties

Elastic material properties of the glass fibres and resin matrix, used in this study, have been determined and published in various references. These properties are the primary source for the calculation or prediction of the laminate material properties. The Young's moduli,

Poisson's ratios and coefficients of thermal expansion of the glass fibres, E-glass, and resin matrix are presented in Table 4.1 as is obtained from Hancox and Mayer [2] and [36]. The experimental determination of the fibres shear modulus is extremely difficult. For practical purposes of the shear modulus of the fibres and the matrix can be calculated by using the Young's modulus and Poisson's ratio of the respective materials in the relation:

$$G_{12} = \frac{E}{2(1+\nu_{12})} \qquad \text{Eq. 4.1}$$

The shear moduli so determined are also given in Table 4.1.

Table 4.1 Material properties of E-glass and Vinyl Ester resin

	Material	
Property	**E-glass**	**Vinyl Ester resin**
E	72.5×10^3 MPa [2]	3.2×10^3 MPa [36]
ν	0.2 [2]	0.35 [2]
α	5×10^{-6}/°C [2]	60×10^{-6}/°C [2]
G_{12}	30.21×10^3 MPa	1.185×10^3 MPa

Fibre and matrix volume fractions are also required for the determination of the laminate elastic properties as is shown in the rules of mixture formulae, therefore burn-off tests are required to determine the mass fractions and eventually the volume fractions. The volume fractions shown in Table 4.2 were obtained from burning the cut-outs of a vessel and cut-offs from the tubes and flange that were manufactured for the experiments presented in Chapter 5. Experienced GRP laminators manufactured the vessel using CSM and CoRezyn VE8300 vinyl ester resin. The tubes and the flange were manufactured using CSM and DION 9100 vinyl ester resin. The calculation followed the procedure given in Gibson [34, pp. 64-67] but did not take any void fraction into account. The Young's modulus, Poisson's ratio and the coefficient of thermal expansion are represented by E, ν

and α and the mass fraction and volume fraction are represented by M and V with the subscripts (f, m) referring to the unrestrained bulk fibre and matrix properties respectively.

Table 4.2 Mass and Volume fractions of CSM/vinyl ester resin laminates

Laminate	Property			
	Fibre mass fraction M_f	Matrix mass fraction M_m	Fibre volume fraction V_f	Matrix volume fraction V_m
DION 9100 tube	0.284	0.716	0.149	0.851
DION 9100 flange	0.309	0.691	0.165	0.835
CoRezyn VE8300	0.33	0.67	0.18	0.82

4.3 Laminate elastic material properties

4.3.1 Experimentally determined properties

Kitching, *et al.* [37], did extensive experimental testing to determine material properties for E-glass chopped strand mat / polyester resin laminates using compression, tension, bending, torsion and hydrostatic pressure tests. These test results are of particular importance since they present results of elastic moduli and Poisson's ratios in the in-plane and the through-thickness directions. The tests were carried out on three laminates of similar construction, of which one was used to determine the majority of the elastic properties. A summary of the averaged elastic material properties obtained from this one laminate in compression and torsion tests are shown Table 4.3 with the subscripts x, y and z indicating the property directions as shown in Fig. 4.1.

Table 4.3 Summary material properties of a CSM / polyester laminate

	Test Method	
Property	**Compression**	**Torsion**
E_x	10 780 MPa	
E_y	10 780 MPa	
E_z	6 028 MPa	
G_{xy}	-	1 430 MPa
$\nu_{xy} = \nu_{yx}$	0.315	
$\nu_{xz} = \nu_{yz}$	0.250	
$\nu_{zx} = \nu_{zy}$	0.340	

These properties are also presented in Table 4.5 – Property 1.

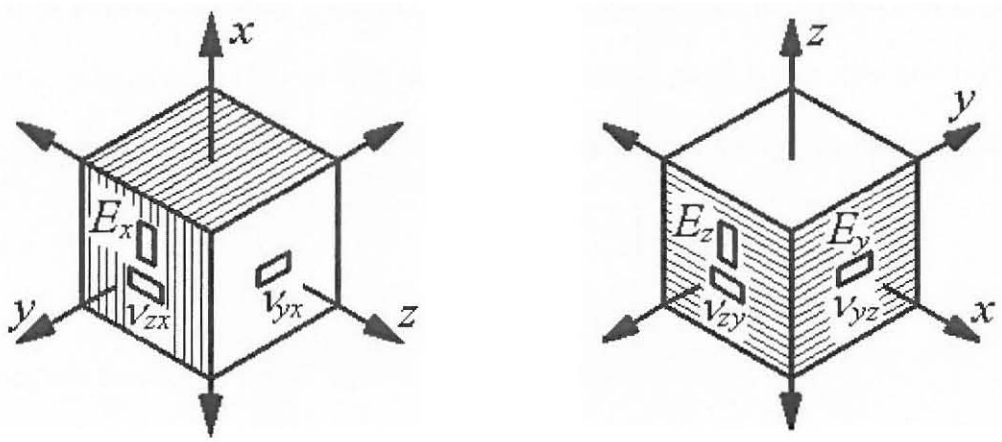

(a) *(b)*

Fig. 4.1 Elastic properties – notation for loading in the: (a) in-plane direction: (b) transverse (through-thickness) direction

4.3.2 Calculated elastic properties CoRezyn VE8300 structural laminates

The theories and formulae shown in Chapter 3 have been derived, mainly, to calculate or predict elastic properties for unidirectional fibre composites. The majority do not give accurate predictions of the properties of randomly oriented fibres. This is to be expected since the method of manufacture of this type of reinforcement cannot guarantee uniform

fibre orientations and density. As can be seen in the modified rule of mixture, Eq. 3.3, and the Halpin-Tsai equations, Eq. 3.5 and Eq. 3.7, a factor is incorporated in the formulae which approximates the contribution of the fibres to the stiffness of the laminate. This factor is usually dependent on the type of reinforcement material or the type of matrix used in the laminate. The fibre volume fraction is usually also considered when deciding on the magnitude of this factor. Suggested magnitudes of these factors are usually given but limit the designer to a small selection of materials since not all fibre and resin types were tested for these factors.

When considering the material properties of a CSM laminate it can be assumed that the laminate is in-plane isotropic since the mechanical properties are the same in all in-plane directions. Considering Fig. 4.2 it is assumed that the 1-2 plane is isotropic and that, for simplification, the subscripts 1 and 2, used in the material properties, are interchangeable, i.e.,

- Young's moduli $E_1 = E_2$;
- Poisson's ratio's $\nu_{13} = \nu_{23}$, $\nu_{12} = \nu_{21}$ and $\nu_{31} = \nu_{32}$.

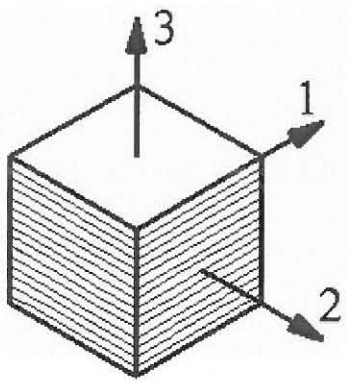

Fig. 4.2 CSM Laminate principal material directions

For the calculation of the elastic material properties of a composite with layers constructed of random oriented fibres, such as CSM, the following assumptions, with reference to Fig. 4.1, are valid:

- Young's moduli in the x,y-planes, E_x and $E_y = E_1$ which is also equal to and E_2;
- Since $E_x = E_y$, Poisson's ratio's $\nu_{xy} = \nu_{yx} = \nu_{12}$ and $\nu_{zx} = \nu_{zy} = \nu_{31}$.

4.3.2.1 Calculation of Young's moduli and Poisson's ratios for in-plane and through-thickness directions and loading using the rule of mixture

If the rule of mixtures, Eq. 3.1, is used to calculate the values of E_x with the base material properties as listed in Table 4.1 and Table 4.2, then the magnitude would be 15 678 MPa. However, this does not reflect the experimental value obtained by Kitching, *et al.* [37] as is shown in Table 4.3, i.e. 10 780 MPa for the Young's modulus with a volume fraction of 0.2. This is due to the fact that the rule of mixtures is valid unidirectional fibre composites and the fibres and the laminates tested were manufactured using a random oriented fibre mat. It can be assumed that a reinforcement reduction factor needs to be incorporated in Eq. 3.1, reflecting the reduced contribution of the random fibres in the in-plane direction. Eq. 3.1 can then be written as

$$E_1 = \psi E_f V_f + E_m V_m \qquad \text{Eq. 4.2}$$

with ψ being the reinforcement reduction factor for the fibres. To obtain a value of E_1 to reflect those in Table 4.3, it is seen that the fibres only contribute 62.5% of its unidirectional properties as random oriented fibres if the fibre volume fraction given by Kitching *et al.* [37] is used. The reinforcement reduction factor (ψ) of 0.625 then gives E_1 = 10 783 MPa. However, at the design stage the actual magnitude of E_1 is not known therefore it is suggested to assume that only 50% of the fibres contribute to the Young's

modulus and hence a value for the reduction factor be taken as 0.5. Using the base material properties listed in Table 4.1, E_1 then has a magnitude of 9 151 MPa.

By using the volume ratios and material properties in Table 4.1, Eq. 3.2 predicts the in-plane Poisson's ratios, ν_{12} and ν_{21}, to be 0.323 with the measured value in Table 4.3 being 0.315. For the calculation of the Poisson's ratio ν_{31}, Eq. 3.13 is used along with the properties given in Table 4.1 and the calculated values for E_1 and ν_{12}. The magnitude of this ratio ν_{31} is then 0.423.

The modified rule of mixture equation for the through-thickness Young's modulus E_3, Eq. 3.3, suggests a value for the transverse contribution factor from the matrix (η_2) to be assumed around 0.5, which gives E_3 to be 4 741 MPa. The values for $E_1 = E_2$, E_3, ν_{12} and ν_{31} are presented in Table 4.5 – Properties 6 and 7.

4.3.2.2 Calculation of Young's moduli for in-plane and through-thickness using the Tsai-Pagano equations

As stated previously in 3.2.2.2 these methods have been developed for unidirectional fibre laminates with some additional considerations to be made to make it applicable to random oriented fibre laminates. The empirical equations presented by Tsai and Pagano [26], Eq. 3.16 and Eq. 3.17 can be effectively used to determine the averaged in-plane Young's modulus and the shear modulus if E_1 and E_3 are calculated by Eq. 3.5 and Eq. 3.7. For practical purposes the fibre length and diameter required in Eq. 3.5 will be taken as 40 mm and 10 μm. E_1 so calculated gives a value of 15 660 MPa that resembles the value given

by Eq. 3.1, which was previously stated as being too large if compared with experimental values since it was developed for a unidirectional short fibre laminate.

If the Halpin-Tsai equation, Eq. 3.7, for the through-thickness Young's modulus is used, a value for the reinforcement contribution factor, ξ_1, needs to be assumed. This value is supposed to be dependent on the fibre and packing geometry and also the loading conditions and it is suggested that a value of 1 to 2 be used. Using the material properties in Table 4.1, it is found that $\xi_1 = 2$ gives $E_3 = 5\ 004$ MPa and with $\xi_1 = 1$ gives $E_3 = 4\ 464$ MPa. Although it is suggested that a reliable experimental value for E_3 be obtained so that ξ_1 can be determined from a combination of Eq. 3.7 and Eq. 3.8, it is not always practical since it is dependent on the fibre volume fraction, which could vary through the laminate. For this work the value $\xi_1 = 2$ will be used giving $E_3 = 5\ 004$ MPa, which will be used in future analyses where this material combination is applied.

By substituting the Halpin-Tsai equations for E_1 and E_3 in Eq. 3.16, the Tsai-Pagano equation, the magnitude of the modulus for the random fibre construction, E_r, is given as 8 999 MPa. This seems to be in more agreement with the experimental values. E_r is then taken as the modulus in the in-plane direction with E_3 as that of the through-thickness (transverse) modulus. The values for $E_r = E_1$ and E_3 are presented in Table 4.5 – Properties 14 and 15.

4.3.2.3 Calculation of shear moduli using the modified rule of mixtures, the Halpin-Tsai and the Tsai-Pagano equations

The prediction of the shear modulus seems to be more problematic. Eq. 3.4 and Eq. 3.10 also have contribution factors for the fibres or matrix. For Eq. 3.4 it is suggested that a value around 0.5 is used for η_{12}, which gives G_{12} as 4 467 MPa. For Eq. 3.10 it is suggested that a value of 1 for ξ_2 gives good results which results in G_{12} = 1 658 MPa. Although these equations have been developed for unidirectional composite laminates and present results that seem to be acceptable, consideration should be given to Eq. 3.17 that presents an averaged value for G_{12} to be applied in a random oriented fibre construction. By substituting the Halpin-Tsai equations for E_1 and E_3 in Eq. 3.17 a value of 3 208 MPa for G_r is obtained. These calculated values do not compare well to that given in Table 4.3, but Kitching, *et al.* [37] did report that the value for G_{12} was low since simple torsional theory for a homogeneous elastic material was used for the calculation of this value and that it might not be completely valid. The values for G, calculated by using the different methods, are presented in Table 4.5.

4.3.2.4 Calculation of Poisson's ratio's for in-plane and through-thickness directions and loading using the Tsai-Pagano equations

Since averaged values for E_r and G_r have been determined and a random fibre composite is considered isotropic in its plane, its in-plane Poisson's ratio can be calculated using the following isotropic relationship between E_r, G_r and ν_r

$$\nu_r = \frac{E_r}{2G_r} - 1 \qquad \text{Eq. 4.3}$$

This gives $\nu_r = \nu_{13} = 0.403$ with the value of ν_{31} determined by Eq. 3.14 to be 0.224.

The in-plane Poisson's ratios with in-plane loading, ν_{12} and ν_{21}, is determined with Eq. 3.2 to be 0.323. These values are presented in Table 4.5 – Properties 14 and 15.

4.3.3 Calculated elastic properties DION 9100 structural laminates

Some of the experiments presented in Chapter 5 were manufactured using CSM/DION 9100 vinyl ester resin system. The calculation of the laminate elastic properties were performed by applying the same methods as is given in 4.3.2 with the applicable volume fraction presented in Table 4.1. The laminate properties are presented in Table 4.5.

4.3.4 Calculated elastic properties of the inner surface layer

Whilst attempting to predict curing strains of any laminate to the highest degree of accuracy it is essential to include as many aspects and variations of the laminate construction in the analysis model. One of the components of a laminate, used in the chemical industry, which is usually ignored for the laminate mechanical properties, is the chemical barrier. This can consist of either a gel coat or a resin rich surface layer ensuring a high concentration of resin at the surface that is exposed to the chemical aggressive environment. The thickness of a surface layer on a pipe or vessel shells could be as much a 1.5 mm depending on the required specifications. This layer is generally not taken into account in the strength calculations but due to the high resin concentration it does have an effect on the post-cure stress distribution in the laminate. For the analyses presented in Chapter 6, especially where the surface layer is also considered, it was required to conduct burn-off tests of the surface layer obtained from laminate. The mass and volume fractions obtained for the surface layer is presented in Table 4.4.

Table 4.4 Mass and Volume fractions of surface layer

Mass fraction		Volume fraction	
M_f	M_m	V_f	V_m
0.059	0.941	0.027	0.973

Using the measured fibre volume fraction of the surface layer and the elastic properties in Table 4.1 the elastic properties E_1, E_2, E_3, G_{12}, ν_{12} and ν_{13} were determined using the procedures described in 4.3.2. These values are also presented in Table 4.5 – Properties 8 and 9.

4.4 Thermo-chemical properties

4.4.1 Post-cure shrinkage of the resin matrix (S_m)

During post-cure at elevated temperature the resin matrix undergoes a chemical shrinkage associated with the completion of the cross-link polymerisation reaction. If this cure shrinkage is measured as a strain it can then, by analogy, be used as a CTE for the calculation of the laminate cure shrinkage. Laboratory tests were therefore carried out on the two vinyl ester resin systems used in this study, i.e. DION 9100 and CoRezyn VE8300. The castings were prepared and cured at ambient conditions before attaching strain gauges to the sides of the castings. The castings were then placed in a drying oven and heated gradually to a maximum temperature of 96°C during which the strains due to thermal expansion and chemical shrinkage and the oven temperature were recorded. Fig. 4.3 and Fig. 4.4 represent the strains recorded during the heating and cooling cycles of the post-cure of the castings.

The measured strain values increased due to thermal expansion as the oven temperature increased to a threshold temperature in the proximity of 45-50°C at which the maximum strain value in each of the casting were attained. At this temperature the continuation of the chemical curing process, i.e. crosslinking, was activated and the castings experienced shrinkage. From Fig. 4.3 and Fig. 4.4 it seems that the majority of the curing had been

completed at 80°C since the castings presented linear expansion at higher temperatures. The gradient of the increase in strains between 80°C and 95°C were less than the first parts indicating that crosslinking were still taking place.

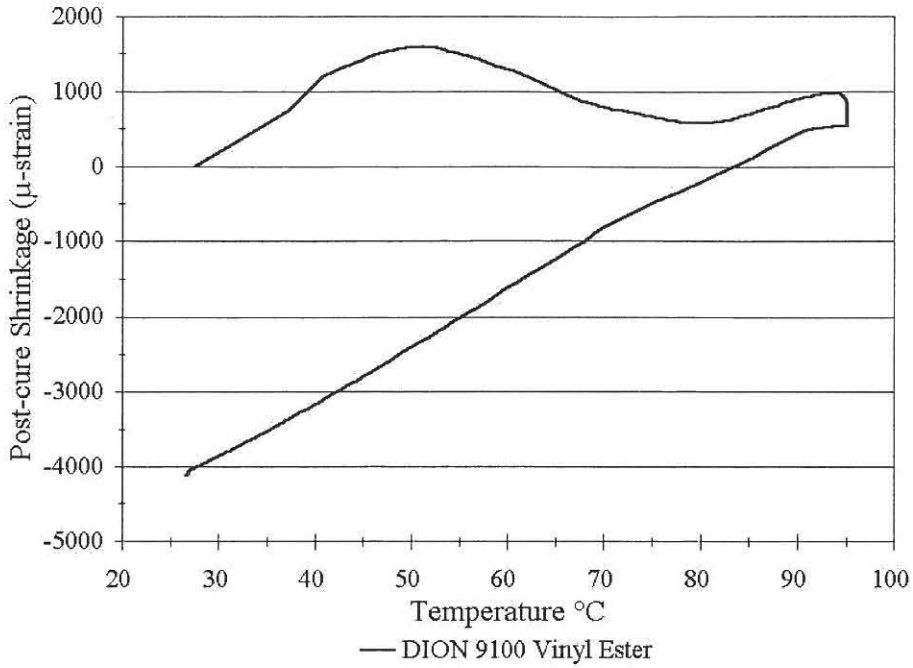

Fig. 4.3 Strain vs. Temperature for DION 9100 Vinyl Ester during post-cure

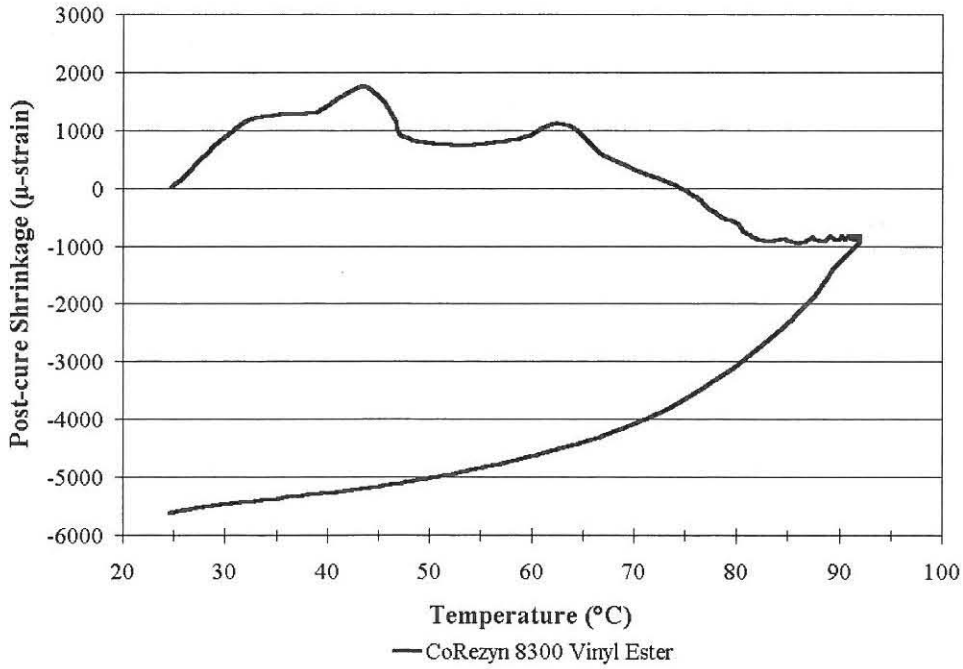

Fig. 4.4 Strain vs. Temperature for CoRezyn VE8300 Vinyl Ester during post-cure

At a constant temperature of 95°C the strain decreased to a constant value of 550$\mu\varepsilon$ for the DION and -855$\mu\varepsilon$ for the CoRezyn before the castings were cooled to room temperature. During the cooling period the strains decreased by magnitudes of 4645$\mu\varepsilon$ for the DION and 4767$\mu\varepsilon$ for the CoRezyn at room temperature to obtain final shrinkages strain of -4095$\mu\varepsilon$ and -5622$\mu\varepsilon$ respectively for the castings. These shrinkages do however not represent the shrinkage that a component, manufactured from a CSM/vinyl ester matrix, would undergo. The shrinkage of the composite would differ greatly from what is presented here, as is shown in Fig. 5.5 and Fig. 5.6. Comparing Fig. 4.3 to Fig. 5.5 and Fig. 5.6 it can be seen that if the free shrinkage of the resin is restrained, by a material such as CSM or woven roving mat or filaments (WR), high shear forces/stresses would be created along the fibre length of the reinforcement. High bulk stresses could also be induced.

4.4.2 Coefficients of thermal expansion of resin matrix (α_m) and of glass fibres (α_f)

The coefficients of thermal expansion of the resin matrix and the glass fibres are required when stress calculations and predictions need to be done. The individual values for the matrix and the fibres are used to calculate the laminate CTE's in the principal material directions. The coefficient of thermal expansion of the glass fibres (α_f) is readily available in the literature and is given as 5×10^{-6}/°C (*See* Table 4.1). The CTE of the resin system (α_m) is also available from literature but it is has been found that various factors influence the actual CTE. The actual CTE value often differs from the values given in the literature, hence it is advisable to measure the CTE of the resin system used in the specific case. The CTE of the resin system used in this study, the DION 9100 vinyl ester, can be determined from the strain recordings taken during the cooling cycle of the post-cure procedure.

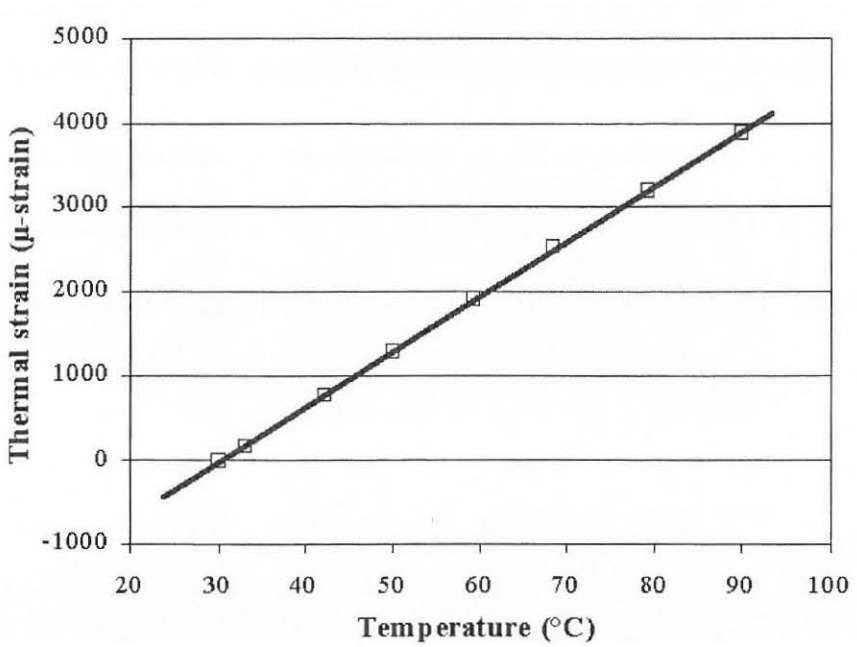

Fig. 4.5 Thermal expansion of DION 9100 vinyl ester resin

Fig. 4.5 presents the thermal strain recordings from which the CTE can be equated to the gradient of the curve and has a magnitude of 65.36×10^{-6}/°C when calculated by

$$\alpha_m = \frac{\varepsilon_{T2} - \varepsilon_{T1}}{T_2 - T_1} \qquad \text{Eq. 4.4}$$

with T_1 = temperature at first strain reading

T_2 = temperature at second strain reading

ε_{T1} = strain reading at T_1

ε_{T2} = strain reading at T_2

4.4.3 Laminate coefficients of thermal expansion

The laminate CTE's are required for the prediction of thermal stresses and strains in components when thermal loading is considered. The laminate CTE's can also be determined by assessing the gradient of strain recordings taken during elevated temperature post-cure of a CSM/vinyl ester laminate. Since the reinforcing material is

chopped strand mat, the CTE in the in-plane direction remains constant in all in-plane angles, i.e. $\alpha_1 = \alpha_2$, when the material directions are assumed to be as is given in Fig. 4.2. Fig. 4.6 presents the thermal strain recordings in the in-plane and the through-thickness directions. The experimental CTEs for the laminate are calculated by using the same method as given in (4.4.2) and are given as $\alpha_1 = \alpha_2 = 27.27 \times 10^{-6}/°C$ and $\alpha_3 = 94.18 \times 10^{-6}/°C$.

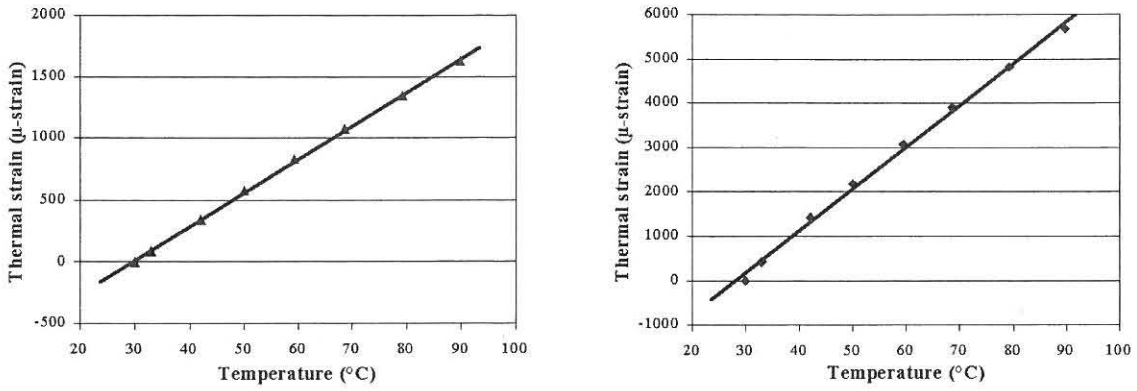

(a) *(b)*

Fig. 4.6 Thermal expansion in the (a) in-plane and (b) through-thickness directions

It is however not always possible to determine the laminate CTEs by experiment and therefore it is preferable to predict the values during the design stage. This is made possible by using the approach suggested by Halpin and Pagano [32], which is presented in 3.3.2. The CTEs so determined are presented in Table 4.5.

4.4.4 Post-cure shrinkage during of CSM laminate (*S*)

As stated in 4.4.1 the post-cure shrinkage of the matrix is required to predict the free post-cure shrinkage of a laminate. This is done according to methods laid out in Stone *et al.* [18] where the prediction of the laminate post-cure shrinkages are treated by analogy to the determination of CTEs for materials for which the fibre and matrix CTEs are different. In

Eq. 3.21 and Eq. 3.22 the matrix CTE is replaced by the matrix post-cure shrinkage strain, S_m, with the glass fibres taken to have a zero shrinkage value. By referring to the principal material directions given in Fig. 4.2, Eq. 3.21 and Eq. 3.22 are then written as

$$S_1 = S_2 = \frac{E_m S_m V_m}{E_f V_f + E_m V_m} \qquad \text{Eq. 4.5}$$

and

$$S_3 = S_m V_m (1+\nu_m) - S_1(\nu_f V_f + \nu_m V_m) \qquad \text{Eq. 4.6}$$

The shrinkages can, by analogy, be calculated by using the approach suggested by Halpin and Pagano [32], using Eq. 4.5 and Eq. 4.6, and the reduced stiffness matrix, $[Q]$, using Eq. 3.25, for a single unidirectional layer having the same fibre volume fraction as the CSM laminate are calculated. The in-plane shrinkage is then given by

$$S_x = S_y = \frac{S_1 + S_3}{2} + \frac{Q_{11} - Q_{22}}{Q_{11} + Q_{22} + 2Q_{12}} \frac{S_1 - S_3}{2} \qquad \text{Eq. 4.7}$$

where the Young's moduli required in the four reduced stiffnesses in Eq. 3.25 are given by the methods of calculation proposed in 4.3.2.

For the purpose of this work, the through-thickness shrinkage, S_z, of the CSM laminate will be taken to be equal to S_3, as determined by Eq. 4.6. Values for the post-cure shrinkage so determined for the laminates used in this study are given in Table 4.5. Note that this method is only applied to the post-cure shrinkage strain prediction. Any stresses or strains that are induced by thermo-mechanical loading after the post-cure has been completed should be predicted using true CTEs obtained by experiment or from the applicable references.

4.5 Summary of material properties to be used in analyses

Table 4.5 presents a summary of the material properties, determined by experiment and theory, which will be used for the analyses in the remainder of this work.

Table 4.5 Summary of material properties of CSM laminates for use in analyses

Property	Experimental	Theoretical values with shrinkage theory given in parenthesis					
	Property 1	Property 2	Property 3	Property 4	Property 5	Property 6	Property 7
		DION 9100 Tube, (Halpin-Pagano)	DION 9100 Tube (Schapery)	DION 9100 Flange (Halpin-Pagano)	DION 9100 Flange (Schapery)	CoRezyn VE8300 (Halpin-Pagano)	CoRezyn VE8300 (Schapery)
S_m *(CoRezyn VE8300)*	-	-	-	-	-	$-5\ 340 \times 10^{-6}$	$-5\ 340 \times 10^{-6}$
S_m *(DION 9100 tube)*	$-4\ 095 \times 10^{-6}$	$-4\ 095 \times 10^{-6}$	$-4\ 095 \times 10^{-6}$	-	-	-	-
S_m *(DION 9100 flange)*	-	-	-	$-3\ 210 \times 10^{-6}$	$-3\ 210 \times 10^{-6}$	-	-
E_1	10 780 MPa	8 125 MPa	8 125 MPa	8 649 MPa	8 649 MPa	9 151 MPa	9 151 MPa
E_2	10 780 MPa	8 125 MPa	8 125 MPa	8 649 MPa	8 649 MPa	9 151 MPa	9 151 MPa
E_3	6 028 MPa	4 434 MPa	4 434 MPa	4 587 MPa	4 587 MPa	4 741 MPa	4 741 MPa
$\nu_{12} = \nu_{21}$	0.315	0.328	0.328	0.325	0.325	0.323	0.323
$\nu_{13} = \nu_{23}$	0.340	0.424	0.424	0.424	0.424	0.423	0.423
$\nu_{31} = \nu_{32}$	0.25	0.231	0.231	0.225	0.225	0.219	0.219
G_{12}	1430 MPa	1564 MPa	1564 MPa	1 611 MPa	1 611 MPa	1 658 MPa	1 658 MPa
α_x	12.4×10^{-6}/°C	34.5×10^{-6}/°C	16.1×10^{-6}/°C	34.6×10^{-6}/°C	15.1×10^{-6}/°C	33.5×10^{-6}/°C	14.2×10^{-6}/°C
α_y	12.4×10^{-6}/°C	34.5×10^{-6}/°C	16.1×10^{-6}/°C	34.6×10^{-6}/°C	15.1×10^{-6}/°C	33.5×10^{-6}/°C	14.2×10^{-6}/°C
α_z	60.3×10^{-6}/°C	64.6×10^{-6}/°C	64.6×10^{-6}/°C	63.7×10^{-6}/°C	63.7×10^{-6}/°C	62.9×10^{-6}/°C	62.9×10^{-6}/°C
S_x	$-1\ 987 \times 10^{-6}$	$-2\ 198 \times 10^{-6}$	-824×10^{-6}	$-1\ 727 \times 10^{-6}$	-587×10^{-6}	$-2\ 775 \times 10^{-6}$	-893×10^{-6}
S_y	$-1\ 987 \times 10^{-6}$	$-2\ 198 \times 10^{-6}$	-824×10^{-6}	$-1\ 727 \times 10^{-6}$	-587×10^{-6}	$-2\ 775 \times 10^{-6}$	-893×10^{-6}
S_z	$-4\ 124 \times 10^{-6}$	$-4\ 434 \times 10^{-6}$	$-4\ 434 \times 10^{-6}$	$-3\ 428 \times 10^{-6}$	$-3\ 428 \times 10^{-6}$	$-5\ 622 \times 10^{-6}$	$-5\ 622 \times 10^{-6}$

Table 4.5 Summary of material properties of CSM laminates for use in analyses (Cont'd)

Property	Theoretical values with shrinkage theory given in parenthesis							
	Property 8	Property 9	Property 10	Property 11	Property 12	Property 13	Property 14	Property 15
	Surface tissue (Halpin-Pagano)	Surface tissue (Schapery)	DION 9100 for tube (Ave'd) (Halpin-Pagano)	DION 9100 for tube (Ave'd) (Schapery)	DION 9100 flange (Ave'd) (Halpin-Pagano)	DION 9100 flange (Ave'd) (Schapery)	CoRezyn VE8300 (Ave'd) (Halpin-Pagano)	CoRezyn VE8300 (Ave'd) (Schapery)
S_m *(CoRezyn VE8300)*	-	-	-	-	-	-	$-5\,340 \times 10^{-6}$	$-5\,340 \times 10^{-6}$
S_m *(DION 9100 tube)*	-	-	$-4\,095 \times 10^{-6}$	$-4\,095 \times 10^{-6}$	-	-	-	-
S_m *(DION 9100 flange)*	-	-	-	-	$-3\,210 \times 10^{-6}$	$-3\,210 \times 10^{-6}$	-	-
E_1	4 084 MPa	4 084 MPa	7 967 MPa	7 967 MPa	8 491 MPa	8 491 MPa	8 999MPa	8 999MPa
E_2	4 084 MPa	4 084 MPa	7 967 MPa	7 967 MPa	8 491 MPa	8 491 MPa	8 999MPa	8 999MPa
E_3	3 396 MPa	3 396 MPa	4 648 MPa	4 648 MPa	4 826 MPa	4 826 MPa	5 004 MPa	5 004 MPa
$\nu_{12} = \nu_{21}$	0.346	0.346	0.328	0.328	0.325	0.325	0.323	0.323
$\nu_{13} = \nu_{23}$	0.383	0.383	0.398	0.398	0.401	0.401	0.403	0.403
$\nu_{31} = \nu_{32}$	0.319	0.319	0.232	0.232	0.228	0.228	0.224	0.224
G_{12}	1 254 MPa	1 254 MPa	2 849 MPa	2 849 MPa	3 031 MPa	3 031 MPa	3 208 MPa	3 208 MPa
α_x	51.3×10^{-6}/°C	38.9×10^{-6}/°C	35.4×10^{-6}/°C	16.1×10^{-6}/°C	34.2×10^{-6}/°C	15.1×10^{-6}/°C	33.6×10^{-6}/°C	14.2×10^{-6}/°C
α_y	51.3×10^{-6}/°C	38.9×10^{-6}/°C	35.4×10^{-6}/°C	16.1×10^{-6}/°C	34.2×10^{-6}/°C	15.1×10^{-6}/°C	33.6×10^{-6}/°C	14.2×10^{-6}/°C
α_z	65.5×10^{-6}/°C	65.5×10^{-6}/°C	64.6×10^{-6}/°C	64.6×10^{-6}/°C	63.7×10^{-6}/°C	63.7×10^{-6}/°C	62.9×10^{-6}/°C	62.9×10^{-6}/°C
S_x	$-4\,500 \times 10^{-6}$	$-3\,290 \times 10^{-6}$	$-2\,262 \times 10^{-6}$	-824×10^{-6}	$-1\,704 \times 10^{-6}$	-586×10^{-6}	$-2\,734 \times 10^{-6}$	-893×10^{-6}
S_y	$-4\,500 \times 10^{-6}$	$-3\,290 \times 10^{-6}$	$-2\,262 \times 10^{-6}$	-824×10^{-6}	$-1\,704 \times 10^{-6}$	-586×10^{-6}	$-2\,734 \times 10^{-6}$	-893×10^{-6}
S_z	$-5\,877 \times 10^{-6}$	$-5\,877 \times 10^{-6}$	$-4\,434 \times 10^{-6}$	$-4\,434 \times 10^{-6}$	$-3\,428 \times 10^{-6}$	$-3\,428 \times 10^{-6}$	$-5\,622 \times 10^{-6}$	$-5\,622 \times 10^{-6}$

5. COMPONENT LAY-UP, CURE AND POST-CURE

5.1 Introduction

To investigate the mechanics of post-cure shrinkage in components with complex geometries is it necessary to first study the mechanics of simple geometries to obtain a full understanding of the mechanisms involved. The curing and post-cure shrinkage of the matrix must be known and also what the effect of these shrinkages, on the strain and stress condition of the pipe, will be.

It is well known, and has also been shown in 4.4, that polyester and vinyl ester resin systems undergo chemical shrinkage during polymerisation. This shrinkage, if restrained by elements such as fibres or other reinforcement, induces strains in the component that could exceed strain and stress limits set by the various design- and manufacturing codes [38, 39]. The strains and stresses thus produced could be of sufficient magnitude to promote environmentally assisted cracking (EAC) in certain operating environments.

Consideration should also be given to the strains developed during the actual lay-up of individual layers. These strains are developed by the shrinkage of the matrix in each layer as it consolidates and induces stresses in the pipe. It is expected that, due to the shrinkage of the outer layer of the pipe, the inner diameter should be reduced and therefore place the inner surface in compression. Compression stresses are thought to be favourable to prevent EAC since the material is prone to EAC if the tensile stresses in the exposed material tend to be high. These strains are of primary importance for the determination or prediction of the residual stresses resulting from post-cure and limited experimental work appears to have been carried out on this aspect.

Complex distributions of curing strains of a high order are experienced in components with complex geometric shapes, such as nozzle-vessel connections and in flanges. It has been suggested that, to prevent or limit these high strains, the components should be post-cured individually prior to assembly. After the assembly of the components the whole vessel should then again undergo a post-curing cycle to obtain a fully post-cured state of the total vessel.

In order to determine actual strains produced during all stages of manufacture the following experimental work is required:

- measurement of the strains produced during the lay-up and consolidation of a tubular system;
- measurement of the strains induced by post-cure of this tubular system;
- measurement of the strains produced by post-cure of a full-face flange;
- measurement of the strains produced by post-cure of a nozzle-vessel connection.

5.2 Experimental analysis

5.2.1 50NB Pipe Lay-up, Cure and Post-Cure

5.2.1.1 Curing strains developed in a tube during lay-up of layers

It is generally believed that fibre reinforced tubes shrink in diameter, or circumference, due to the chemical shrinkage of the resin matrix. In order to investigate this aspect, prior to studying more complex geometries, two identical tubes with internal diameters of 50 mm and a length of 290 mm were manufactured on an expandable mandrel using DION 9100 vinyl ester resin and chopped strand mat (CSM). The experiment was designed to

determine the magnitude of the shrinkage strains in both the hoop and longitudinal directions. The mandrel employed in this operation consisted of a PVC tube with an outside diameter of 50 mm and a 3 mm wide longitudinal slot which was to enable the mandrel to contract diametrically. To obtain reasonable stability during the manufacturing process end pieces were inserted at the ends of the PVC mandrel to maintain circular form of the tube. Cellophane tape was used to cover the slot, keeping the resin matrix from entering and setting in the aperture and preventing contraction of the mandrel. To ensure that the laminate did not bond to the mandrel a release agent in the form of a paraffin wax was applied prior to the application of the initial layer. The initial layer consisted of one layer of "CHEM-MAT", a chemical grade surface tissue of 25g/m^2 [40] with a DION 9100 vinyl ester resin matrix.

After the lay-up and cure of the surface layer, two strain gauges and a thermocouple were attached to the surface tissue, using a cyano-acrilate adhesive, to measure the hoop and longitudinal strains and temperature at the inner surface during the lay-up of the body of the tubes. The strain gauges were KYOWA KFG-5-120-C1-11 type with a gauge factor of 2.1 and the adhesive was KYOWA CC-33A.

To minimise steep temperature gradients resulting from exotherm only four layers of 300g/m^2 CSM were applied by hand lay-up per day while continuously recording the strains developed during the ambient cure, with a SI3595 series data logging system [41]. To ensure that reasonable measurements were obtained from the test pieces the mandrels were removed and the paraffin wax reapplied after the second layer had cured. The mandrels were then replaced before commencing with the rest of the required layers. A wall thickness of approximately 15 mm was obtained from sixteen layers. The recorded

data was then imported into a spreadsheet and the strains were plotted to the number of applied layers.

The curves shown in Fig. 5.1 and Fig. 5.2 represent the hoop and longitudinal strains recorded during the actual lay-up of the layers of tubes 1 and 2. The peaks shown before layer 3 in both the figures indicate when the tubes were released from the mandrels. After the last, 16th, layer had cured a maximum extension hoop strain of 1629με and a longitudinal shrinkage strain of -1181με were attained during the lay-up of the layers for tube 1, and a maximum extension hoop strain of 1508με and a longitudinal shrinkage strain of -1248με for tube 2. These values are given in Table 5.1 with a correlation factor for comparison.

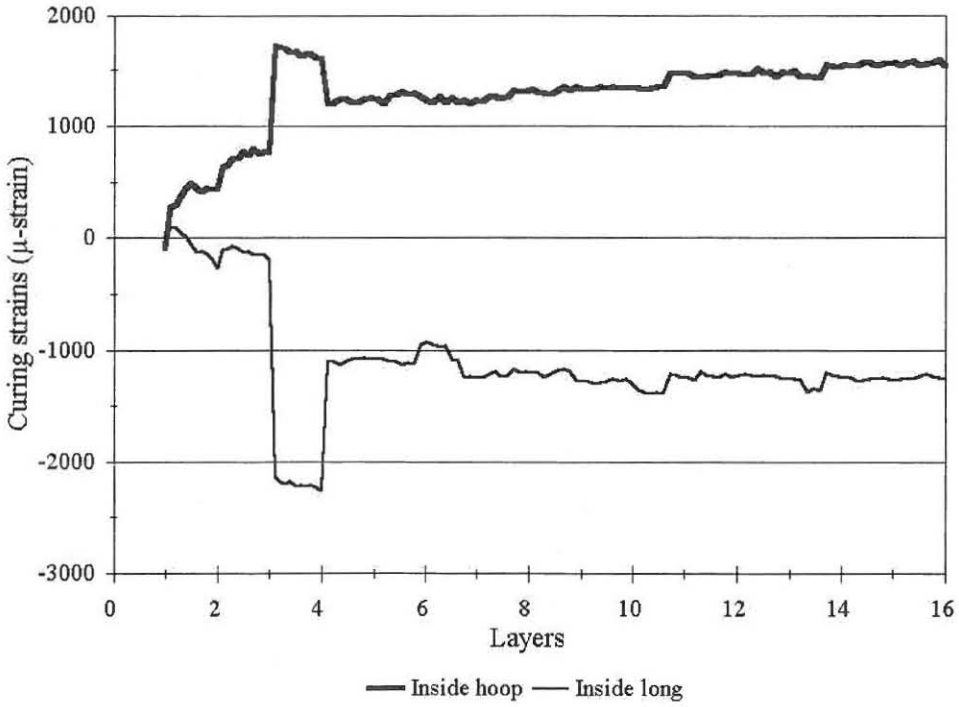

Fig. 5.1 Longitudinal & Hoop curing strains vs. layers for DION 9100/CSM tube (1) at inside surface

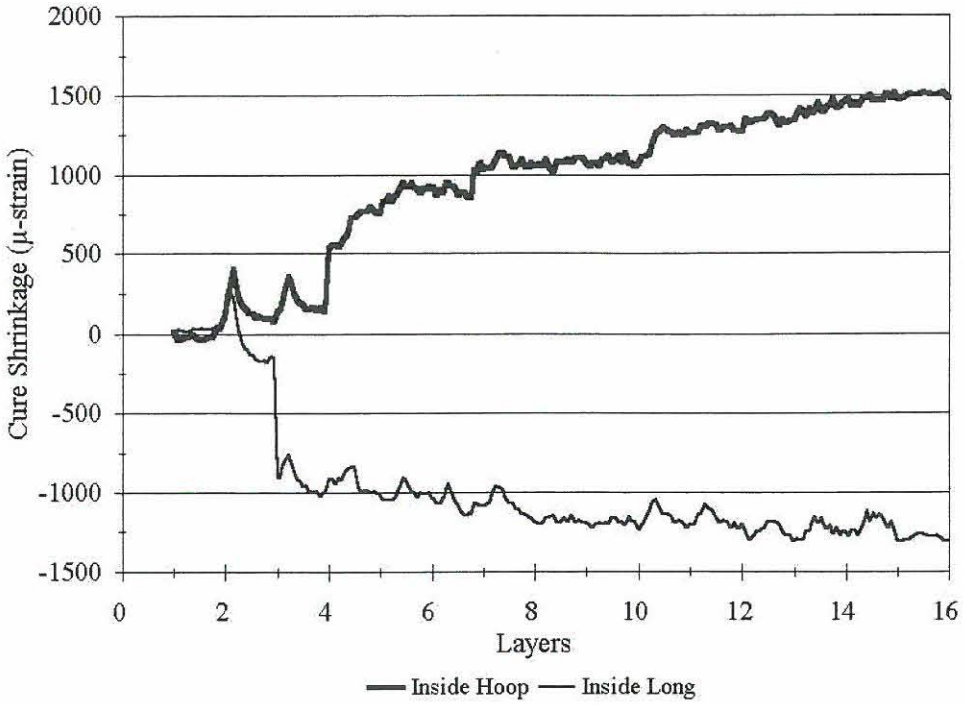

Fig. 5.2 Longitudinal & Hoop curing strains vs. layers for DION 9100/CSM tube (2) at inside surface

Table 5.1 Curing strains at the inner surface

Gauge Position & Direction	Strain Measured x 10^{-6}		Correlation
	Tube (1)	Tube (2)	%
Inside Hoop (ε_{iz})	1629	1508	92.5
Inside Longitudinal (ε_{iy})	-1181	-1248	94.3

Although the figures indicate that exotherm did play a role in the variation in strains, the zero and the maximum strain values were obtained at 18°C. Fig. 5.3 shows the temperature variation of the inner surface due to exotherm during the lay-up of the layers. It is shown that any layer for the given thickness of the tube gives a variation of approximately 4°C.

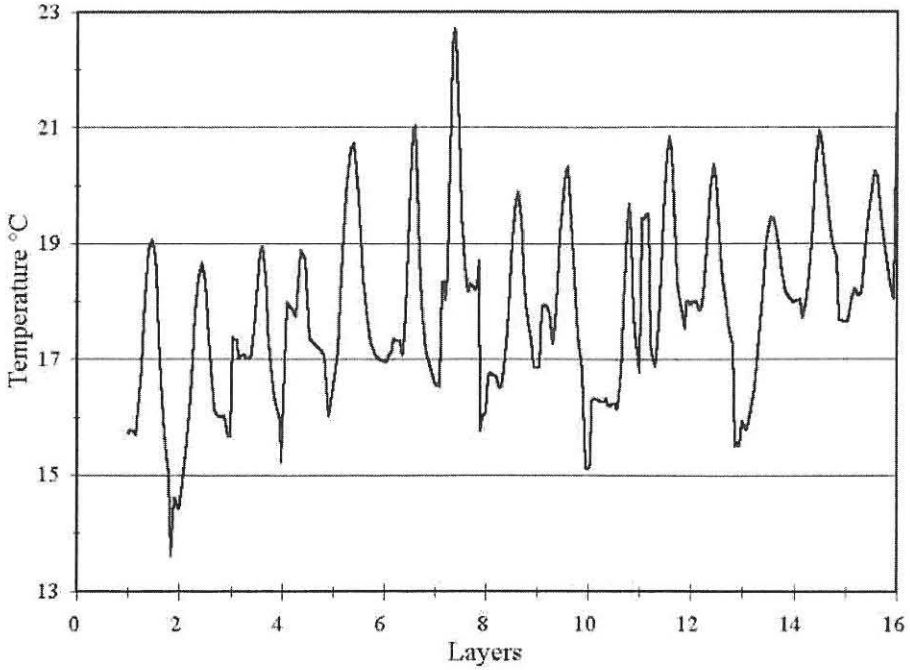

Fig. 5.3 Temperature variation of tube (1) inner surface due to exotherm

5.2.1.2 Strains resulting from cure during lay-up

Studying the strain values obtained during the lay-up of the layers, it was initially expected that strains at the inner surface would indicate a reduction in circumference as is explained in the previous section. However, the strains indicate that the inner circumference of both tubes increased by essentially the same magnitude. The inner surface did reduce in length as was expected. By interpreting the inner surface strains, the following observation is made:

- immediately after the lay-up of layer n (n = 1, 2..16), the laminate expands due to the heat generated by the exothermic reaction of layer n;
- layer n bonds to the laminate and after the exothermic reaction has been completed the whole system cools to ambient temperature;
- as the system returns to ambient temperature, layer n prevents it to return to its original size since it has cured in the expanded condition and hence a "growth" of the inner circumference is shown and residual strains are produced.

Eduljee and Gillespie [18] described this phenomenon in filament wound tubes although they considered aspects such as fibre tension and the effect of the mandrel, which is not strictly applicable in this case.

5.2.1.3 Post-cure shrinkage of CSM/vinyl ester tube

After the lay-up and ambient cure the two tubes were machined down to a wall thickness of 13.5 mm, to obtain a constant wall thickness, and prepared for post-cure by attaching two additional strain gauges, in the hoop and longitudinal directions, to the outer surface. The tubes were then placed in drying oven and heated gradually to a maximum post-curing temperature of 87°C. The tubes were maintained at maximum temperature for approximately 2½ hours and then cooled to room temperature. The post-cure temperature history is shown in Fig. 5.4. The strains resulting from thermal expansion and chemical shrinkage were recorded for the duration of the post-cure process.

Fig. 5.5 and Fig. 5.6 show the strains recorded on the tubes during the post-curing process. The figures clearly indicate the expansion of the tubes as a result of the increase in oven temperature to 45°C. Post-cure shrinkage continued at approximately 45°C where the magnitude of the chemical shrinkage was greater than the thermal expansion, hence the change in slope of the curves. The shrinkage strains measured during post-cure are given in Table 5.2. It must be kept in mind that the initial strains prior to commencing with the post-curing cycle were assumed to be zero, therefore the strains presented in Fig. 5.5 and Fig. 5.6 are real values for the post-curing process and do not include the strains developed during the lay-up phase. To obtain the residual strains induced during the total manufacturing process it is necessary to combine the post-curing strains to those obtained during lay-up. The sums of these strains for both pipes are represented in Fig. 5.7 and Fig. 5.8.

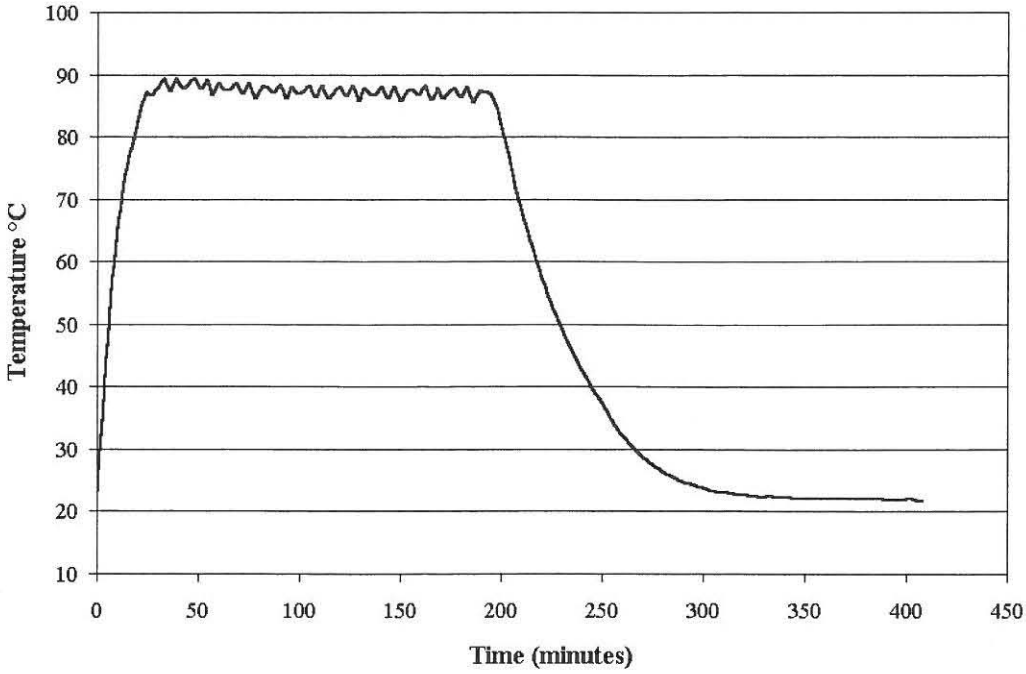

Fig. 5.4 Tube post-cure temperature history

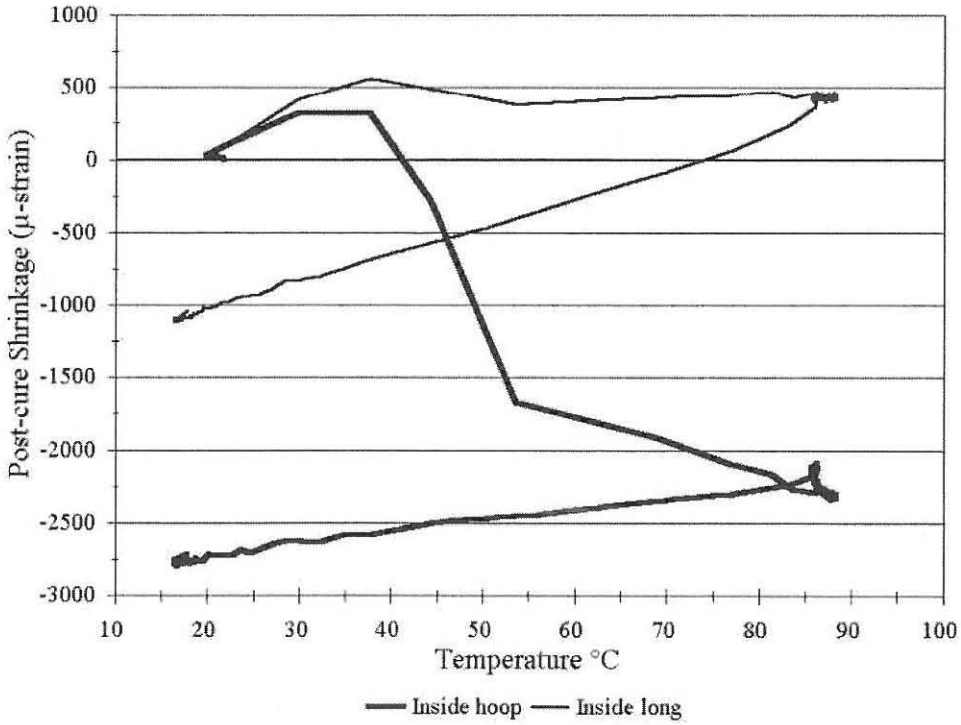

Fig. 5.5 Longitudinal & Hoop post-cure strains vs. temperature for DION 9100/CSM tube (1) on inside surface

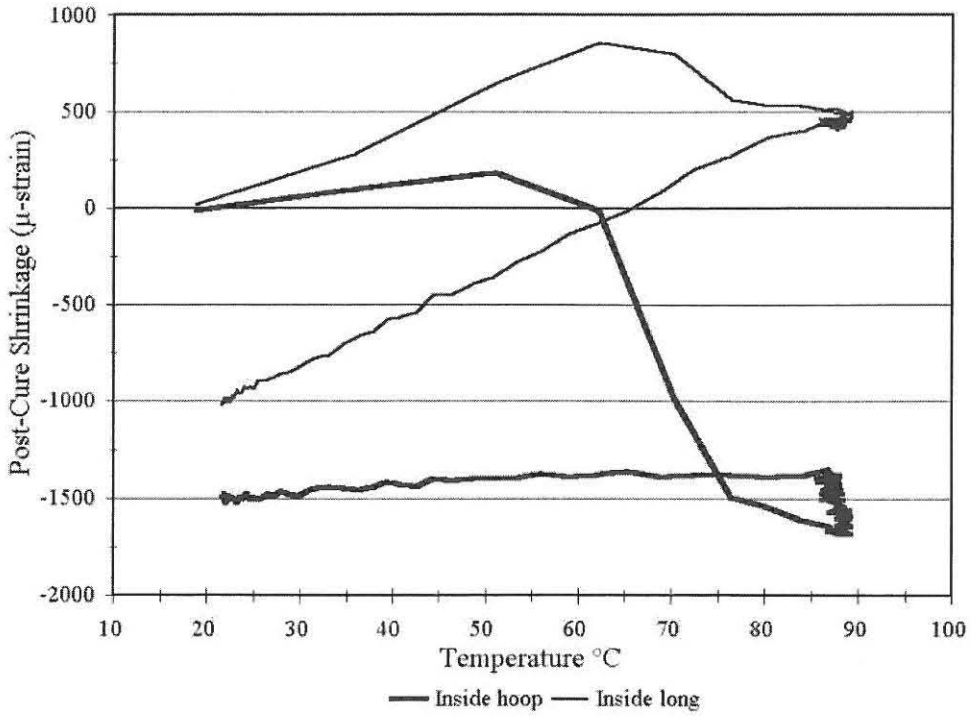

Fig. 5.6 Longitudinal & Hoop post-cure strains vs. temperature for DION 9100/CSM tube (2) on inside surface

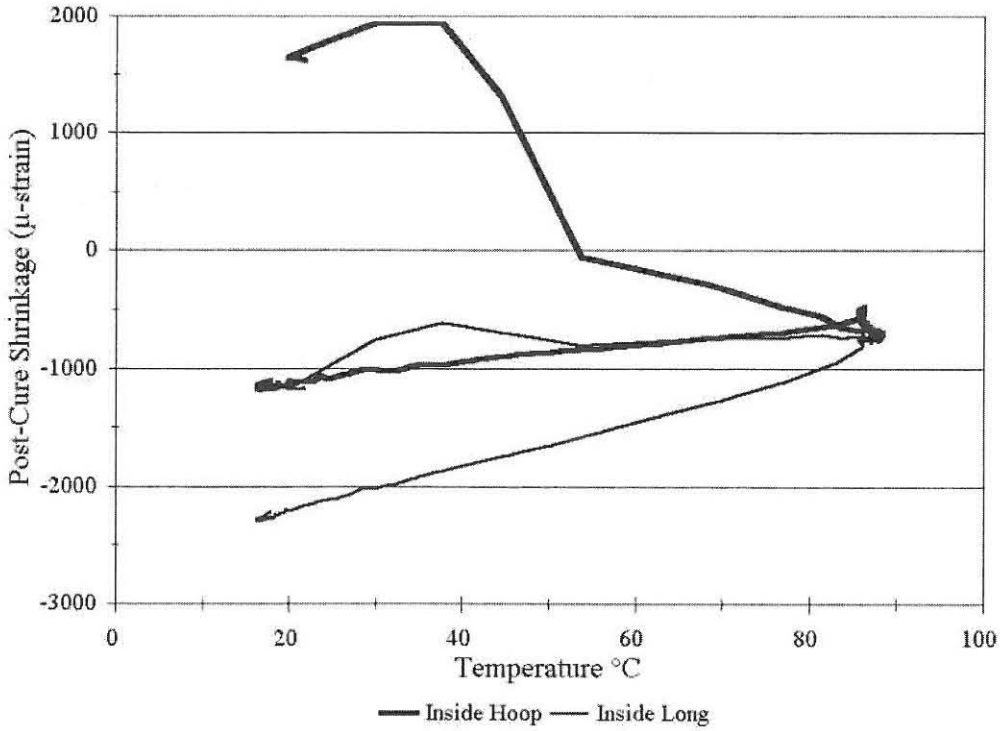

Fig. 5.7 Actual Post-cure Longitudinal & Hoop Strains vs. Temperature for DION 9100/CSM tube (1) on inside surface

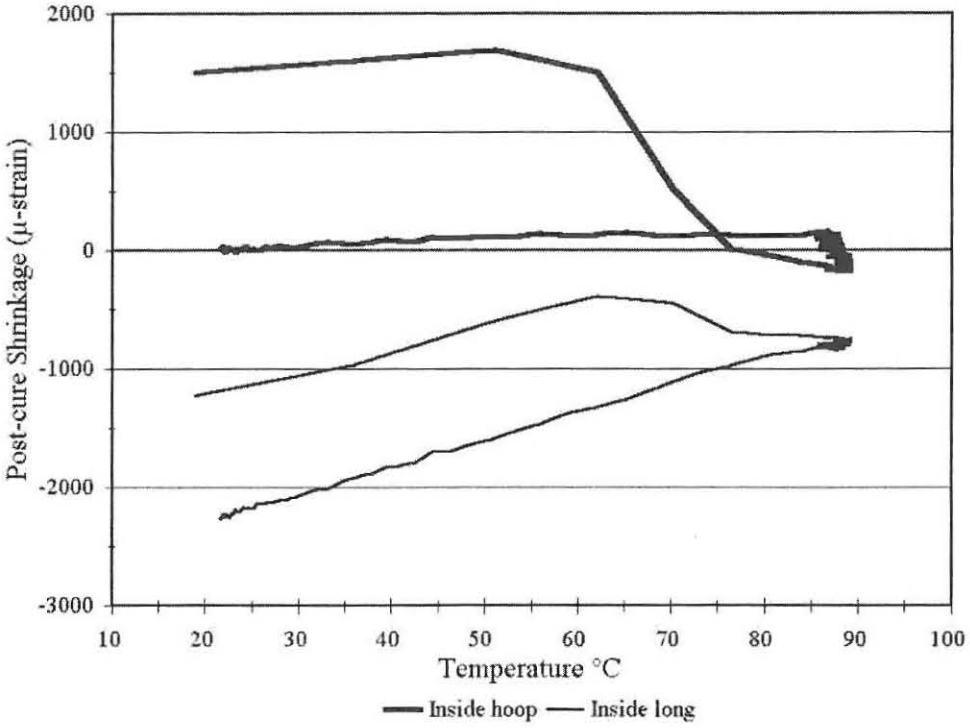

Fig. 5.8 Actual Post-cure Longitudinal & Hoop Strains vs. Temperature for DION 9100/CSM tube (2) on inside surface

Table 5.2 Post-cure shrinkage strains of the DION 9100/CSM tubes

Gauge Position & Direction	Strain Measured x 10^{-6}		Correlation
	Tube (1)	Tube (2)	%
Inside Hoop (ε_{iz})	-2729	-1495	54.8
Inside Longitudinal (ε_{iy})	-979	-1020	96

Table 5.3 presents the final strains after the combination of the cure and post-cure strains.

Table 5.3 Final shrinkage strains at inner surface of the DION 9100/CSM tubes

Gauge Position & Direction	Strain Measured x 10^{-6}		Correlation
	Tube (1)	Tube (2)	%
Inside Hoop (ε_{iz})	-1090	-13	1.2
Inside Longitudinal (ε_{iy})	-2218	-2268	97.8

From these values a good correlation is found between the longitudinal strains. The hoop strains, however, do not compare well. This could be as a result of the large variation found in the strains produced during the post-curing process. The inner surface is richer in resin and the position of the strain gauges could have been such that the quantities of resin at these positions were not the same.

The post-cure shrinkage strains at the outer surface of each of the tubes are shown in Fig. 5.9 and Fig. 5.10. The shrinkage strains measured during post-cure are given in Table 5.4. These strains are assumed to be the residual post-cure strains since no contributions could be made by additional layers. The differences in strains from the two tubes are significant although the correlations are approximately the same for the hoop and longitudinal strains.

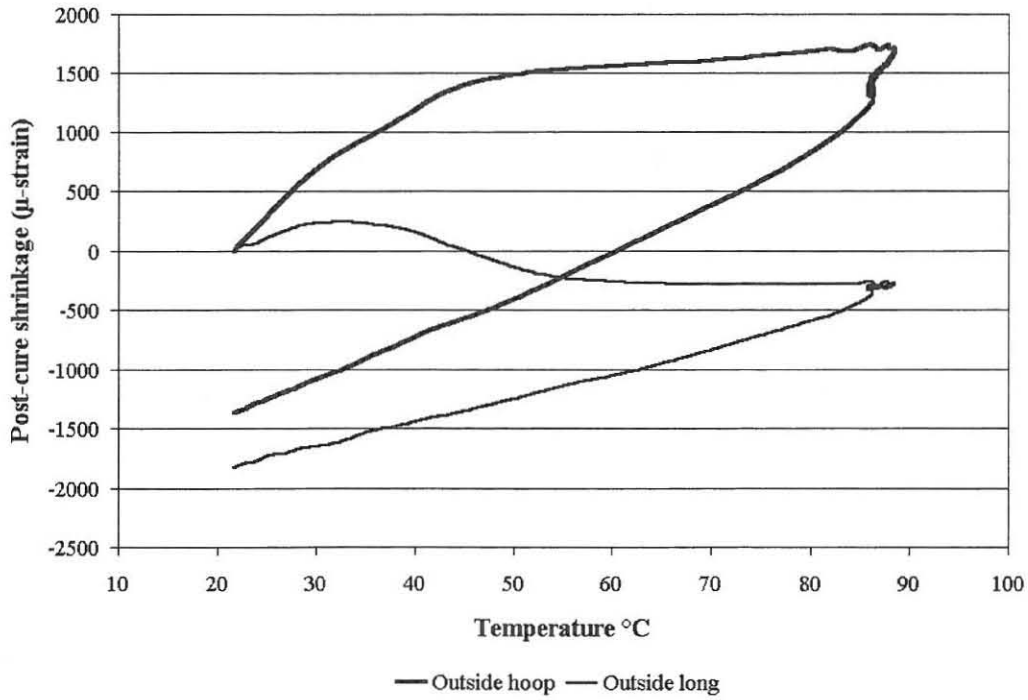

Fig. 5.9 Longitudinal & Hoop post-cure strains vs. temperature for DION 9100/CSM tube (1) on outside surface

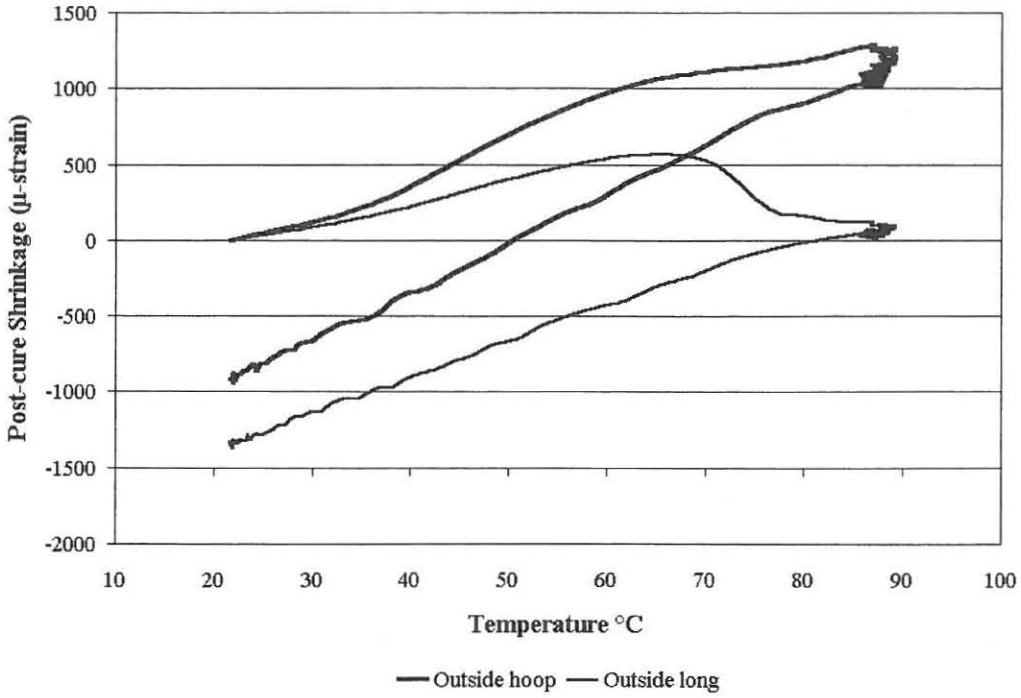

Fig. 5.10 Longitudinal & Hoop post-cure strains vs. temperature for DION 9100/CSM tube (2) on outside surface

Table 5.4 Post-cure shrinkage strains at outside surface of the DION 9100/CSM tubes

Gauge Position & Direction	Strain Measured x 10^{-6}		Correlation
	Tube (1)	Tube (2)	%
Outside Hoop (ε_{oz})	-1366	-885	64.8
Outside Longitudinal (ε_{oy})	-1833	-1306	71.3

5.2.2 50NB hubbed full face flange post-cure shrinkage

Full face and stub flanges for the use on GRP vessels and piping are usually manufactured by hand lay-up due to the complexity of the shape. It is usually accomplished by using a skin as an initial mould or shape in which the matrix and reinforcement is applied. The reinforcement and matrix is applied to the specified thickness as is required by the various design and manufacturing codes. During the lay-up of the various layers, strains are produced as a result of the curing shrinkage of the matrix. It is believed that, if a post-cure

cycle is applied to the nozzle-flange combination, the curing strains will be alleviated to acceptable levels, as is required by the various codes. This will enhance the chemical resistance of the nozzle-flange inner surface.

5.2.2.1 Manufacture of test piece

In order to determine the magnitude and nature of these post-cure shrinkage strains, a 50NB full-face flange was manufactured by hand. The mould on which the flange was constructed consisted of a PVC tube with an outside diameter of 50 mm and a flat end plate with a diameter of 151 mm. The materials used were DION 9100-vinyl ester resin as a matrix and chopped strand mat (CSM) as reinforcement. The flange was manufactured by applying a sufficient number of layers to obtain a thickness marginally greater than those given by BS 4994 [3]. A release agent in the form of a paraffin wax was applied to the mandrel prior to the application of the initial layer. The initial layer consisted of one layer of "CHEM-MAT", a chemical grade surface tissue of 25g/m^2 [40] with a DION 9100 vinyl ester resin matrix. Four layers of 300 g/m^2 CSM were applied by hand lay-up per day to minimise steep temperature gradients resulting from exotherm. During the lay-up of the individual layers, strain gauge rosettes and thermocouples were attached to the test piece at positions that was thought to be of importance. The rosettes were oriented to measure hoop, longitudinal and radial strains. The strain gauge rosettes were KYOWA KFG-2-120-D16-11 type with a gauge factor of 2.13. The adhesive was KYOWA CC-33A. The flange was then machined to the exact dimensions given by BS 4994. Fig. 5.11 shows the dimensions to which the flange was manufactured and indicates the positions of the strain gauges for measuring the post-cure shrinkage. Picture 5.1 shows the strain gauges and cabling on the actual test piece.

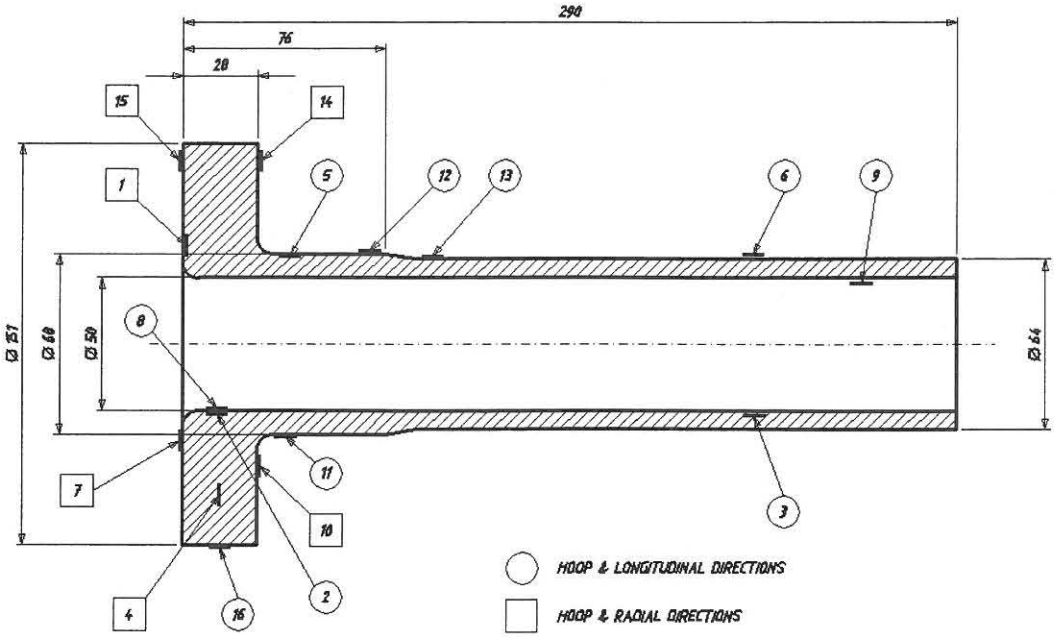

Fig. 5.11 Strain Gauges Positions on 50 NB Flange

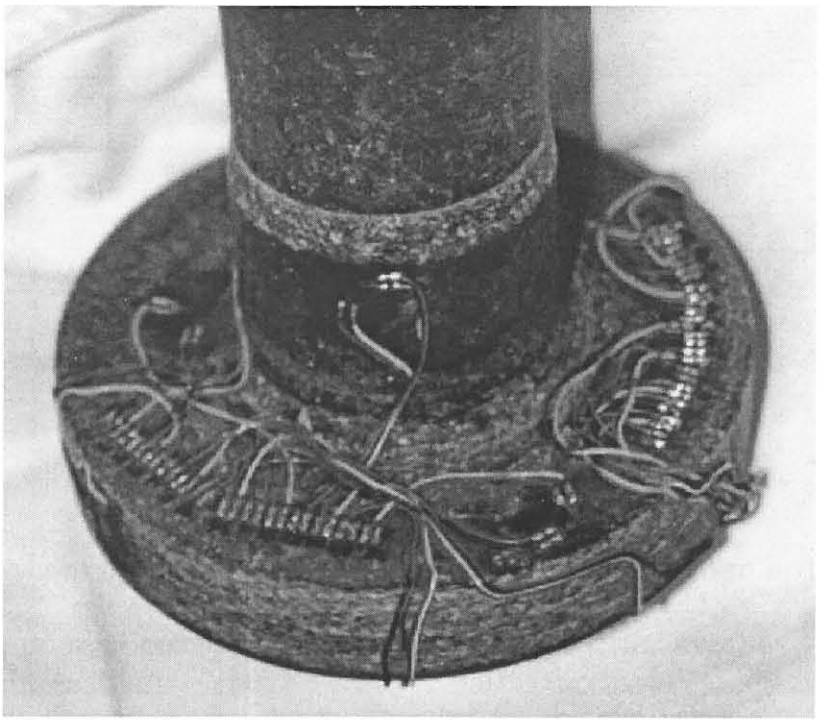

Picture 5.1 Strain gauges and cabling on 50 NB Flange

5.2.2.2 Post-cure shrinkage of hubbed flange

The shrinkage strains and temperatures at the various positions were recorded with a SI3595 series data logging system [41] while the test piece was post-cured in a drying

oven. An increase in oven temperature was applied at a gradient of 0.5°C/minute from 25°C to a maximum of 92°C, which was maintained for approximately 5 hours. Thereafter the test piece was cooled to room temperature, 24°C. Fig. 5.12 shows the temperature history of the post-cure cycle. Typical strain curves recorded during the heating, post-cure and cooling cycles are shown in Fig. 5.13 and Fig. 5.14. The recorded strain curves, for each measurement position, are given in APPENDIX A.

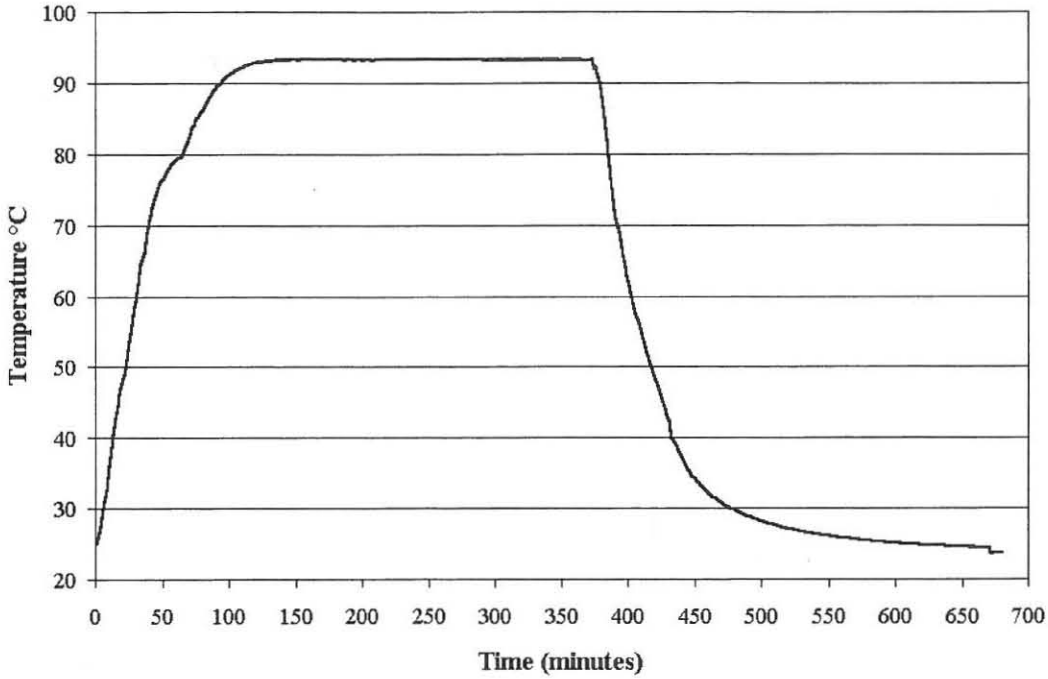

Fig. 5.12 Temperature history of test piece

The recorded shrinkage strains at all measurement positions are given in Table 5.5. The initial strains prior to commencing with the post-cure cycle were, as with the tubes, assumed to be zero, hence the strains presented are the real values for the post-curing process and do not include the strains developed during the lay-up phase. To obtain the residual strains induced during the total manufacturing process would however be a laborious and intricate action since during the manufacture of the test piece it requires to be rotated and handled many times, with a large possibility of causing breakage in the cabling.

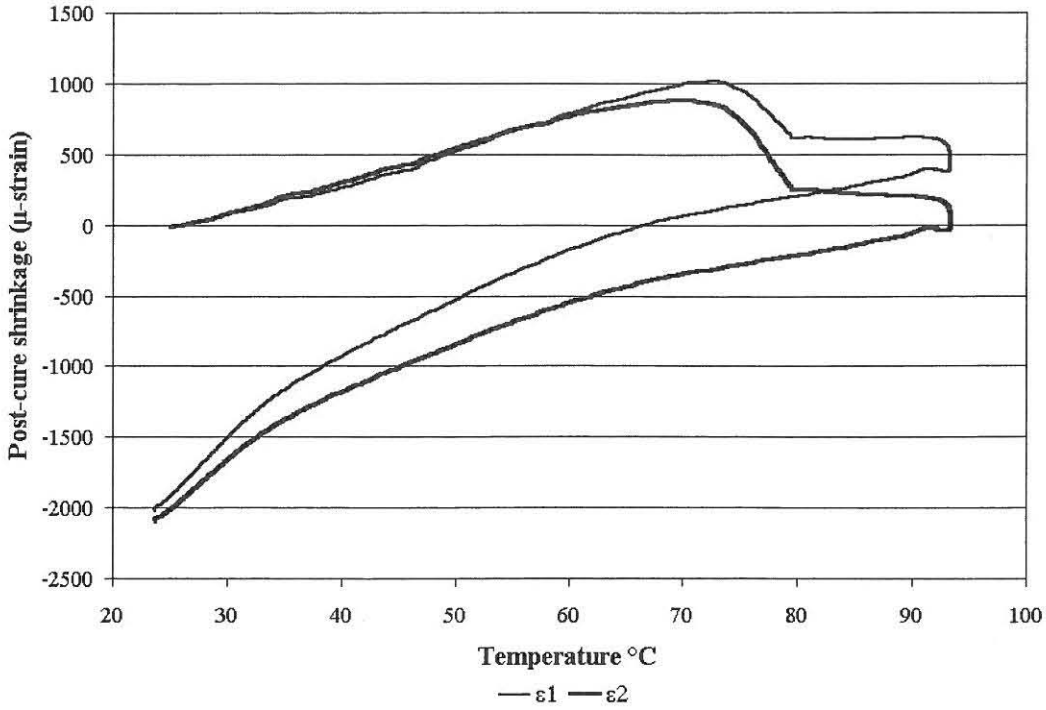

Fig. 5.13 Post-cure shrinkage at Position 1.

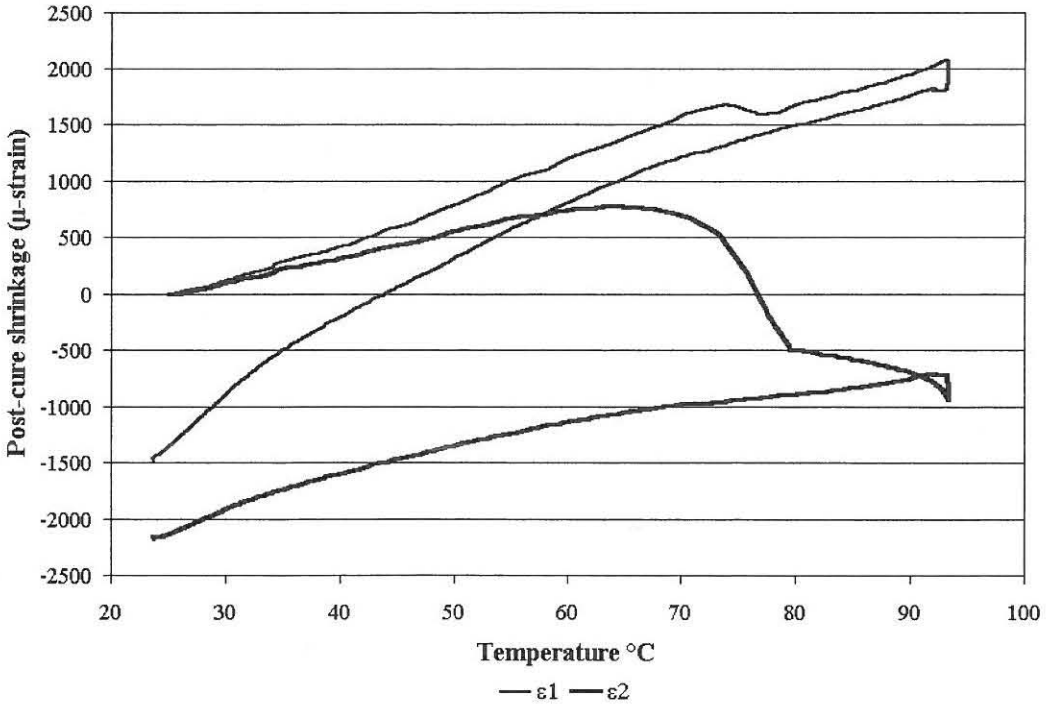

Fig. 5.14 Post-cure shrinkage at Position 2.

Table 5.5 Measured post-cure strains in full face flange

Gauge Position	Measured strain ($x10^{-6}$)		
	Hoop Strain	Longitudinal Strain	Radial Strain
1	-2098		-2025
2	-2175	-1482	
3	-1730	-1468	
4	-1316		-2810
5	-1780	-2195	
6	-1699	-2194	
7	-1756		-2446
8	-892	-3000	
9	-1721	-1822	
10	-1308		-1380
11	-995	-1672	
12	-1439	-1968	
13	-1456	-2130	
14	-1501		-1317
15	-2210		-1774
16	-1431	-3653	

5.2.2.3 Pullback of flange resulting from post-cure shrinkage

This test piece exhibited visible pullback during the manufacturing stage. This was as a result of the individual layers on the flange being allowed to cure before applying the next layer, and hence an accumulative in-plane tensile load being applied to the back of the flange. Since the material of construction was a vinyl ester resin with 6% cobalt naphthanate, the magnitude of the pull-back was not as great should the flange have been constructed of a polyester resin [42]. No effort was made to prevent the pullback and was also not measured since the objective of the experiment was to determine the shrinkage strains resulting from post-cure. Since the flange face was machined flat after the

completion of the lay-up of the layers it was possible to measure the pullback caused by the post-cure shrinkage. The pullback was measured to be 0.023 mm.

5.2.3 Nozzle to vessel connection post-cure shrinkage

Large vessels are often manufactured using the filament winding method with the nozzle manufactured separately by hand lay-up using CSM as reinforcement. The nozzle positions are then marked on the vessel, the cut-outs made and the nozzles fixed by making use of CSM overlays as reinforcement. Smaller vessels are however usually manufactured by only making use of CSM as reinforcement. Due to the combination of the different manufacturing techniques in vessels manufactured from filament winding and CSM, mechanical property variations would be expected in the region of the nozzle, this complicating the prediction of post-cure strains. For practical reasons a vessel manufactured solely from CSM is considered so that iso-planar properties can be assumed and calculated for the in-plane material properties. Furthermore, an axisymmetric vessel is considered since three-dimensional finite element modelling is time-consuming and presents difficulties in the assignment of element principle material directions. Therefore, the test piece consisted of a circular shell and a dished-end with a nozzle and reinforcement pad situated centrally in the dished-end.

5.2.3.1 Manufacture of test piece

A 100 NB full face flange and nozzle was inserted into a 508 mm diameter 2:1 semi-ellipsoidal dished end which was attached to a 508 mm diameter shell. The connection of the nozzle to the dished end complied to the specifications given in BS 4994 [3]. The specified dimensions and lay-ups required for the test are shown in Fig. 5.15.

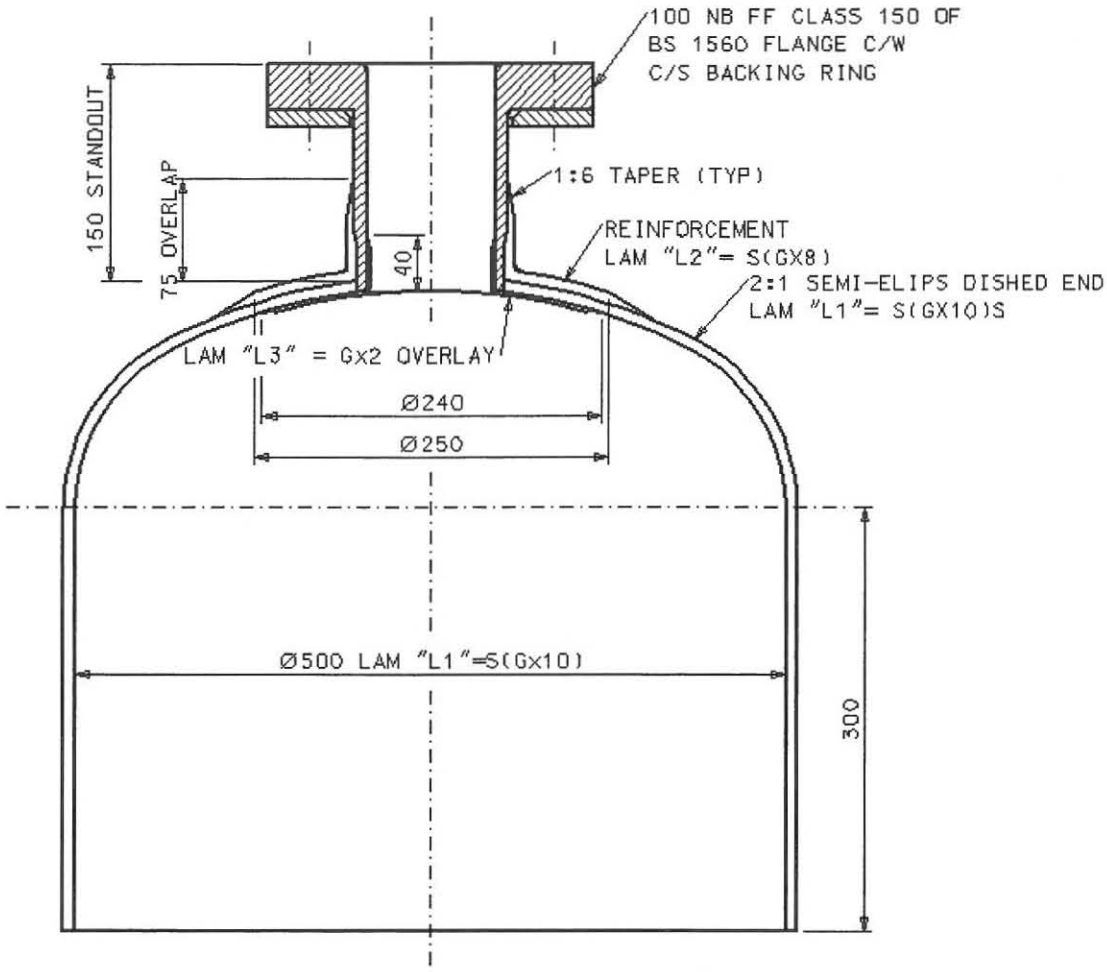

Fig. 5.15 Vessel dimensional requirements

where S = Surface tissue + 28 g/m^2 resin

G = 450 g/m^2 CSM + 900 g/m^2 resin

The materials used for the nozzle, dished end and shell were CoRezyn VE8300-vinyl ester resin as a matrix and CSM as reinforcement. KYOWA strain gauges and rosettes were attached with KYOWA CC-33A cement in positions that were determined to be of critical importance (*See Fig. 5.16*). Picture 5.2 shows strain gauges and cabling at positions 6, 7,8 and 9 prior to the reinforcement lay-up. Table 5.6 indicates the type of gauge and the gauge factor for each measurement position.

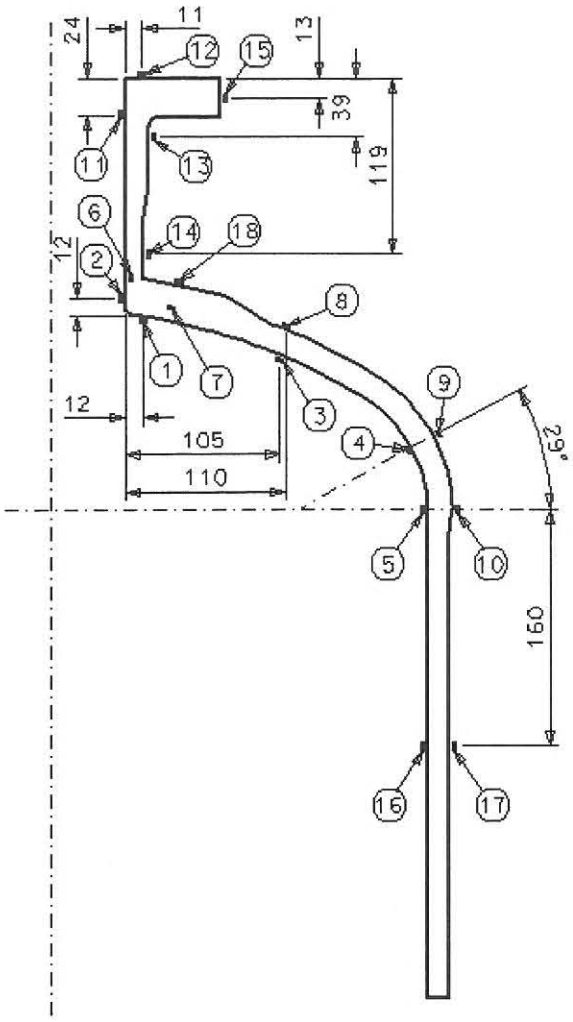

Fig. 5.16 Strain Gauge Positions on Nozzle-Dished end connection

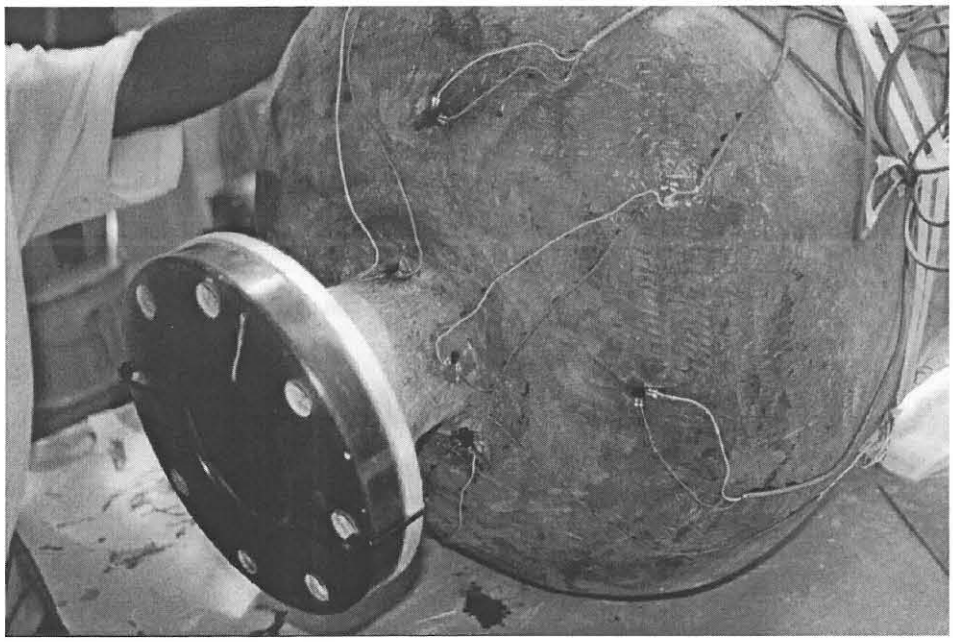

Picture 5.2 Strain Gauge Positions on Nozzle-Dished end connection

5.2.3.2 *Post-cure shrinkage of nozzle to vessel connection*

The shrinkage strains and temperatures at the various positions were recorded with a SI3595 series data logging system [41] while the test piece was post-cured in a drying oven. An increase in oven temperature was applied at an initial gradient of 1.5°C/minute from 24.6°C to a maximum of 94°C. The temperature of the oven was maintained above 90°C for approximately 3 hours. Thereafter the test piece was cooled to room temperature, 24.6°C. Fig. 5.17 shows the temperature history of the post-cure cycle. Typical strain curves recorded during the heating, post-cure and cooling cycles are shown in Fig. 5.18 and Fig. 5.19. The recorded strain curves, for each measurement position, are given in APPENDIX C.

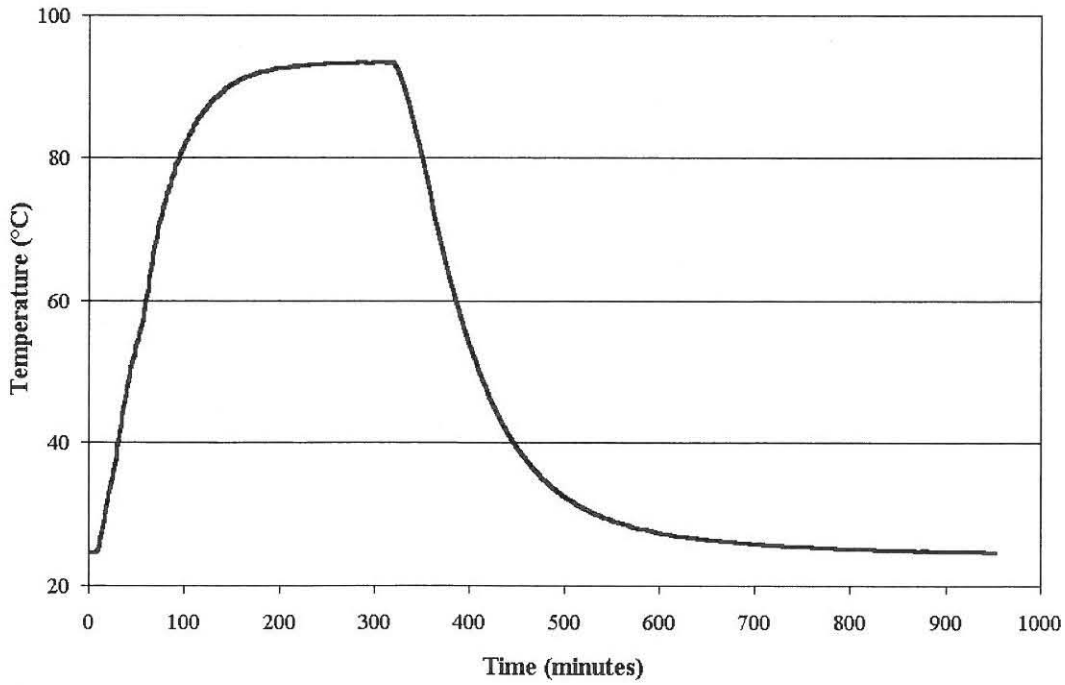

Fig. 5.17 Temperature history of nozzle-dished end post-cure cycle

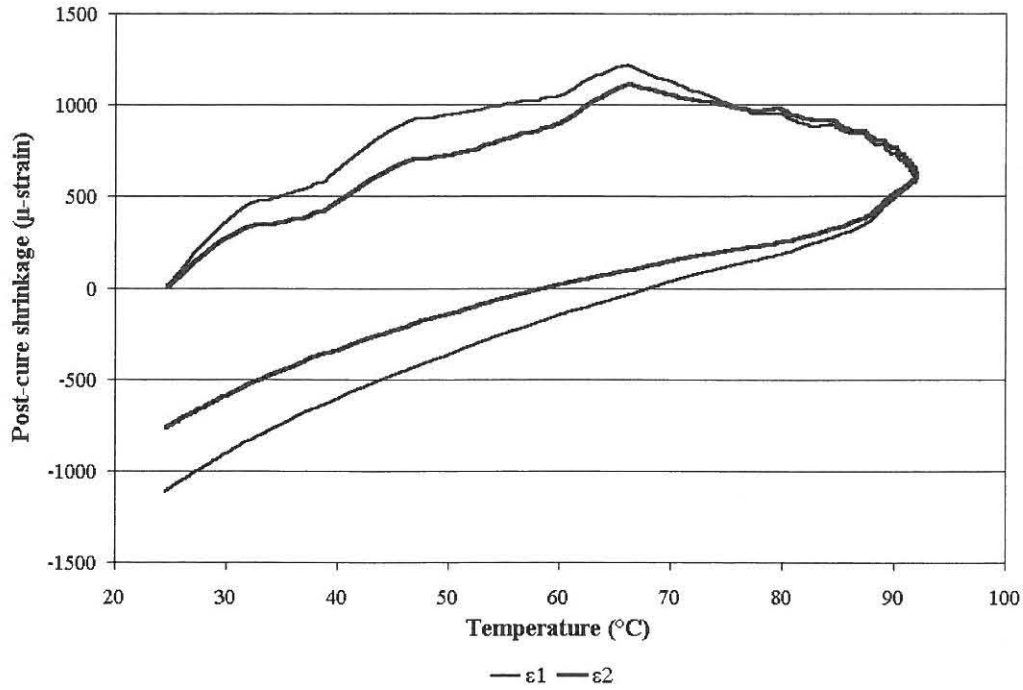

Fig. 5.18 Post-cure shrinkage at Position 3 on nozzle-dished end

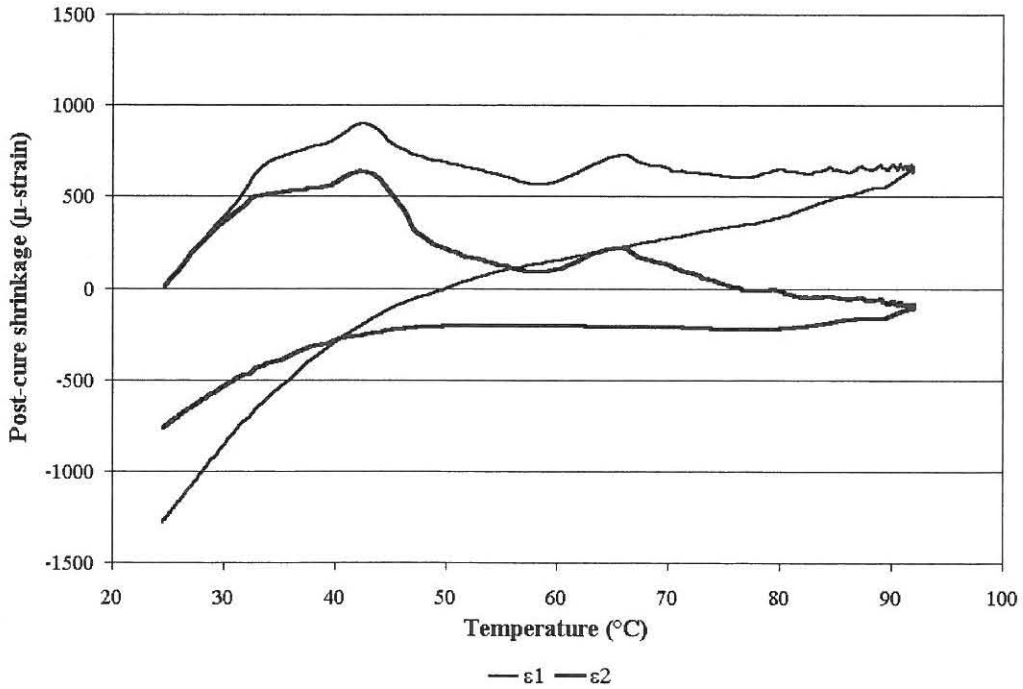

Fig. 5.19 Post-cure shrinkage at Position 12 on nozzle-dished end

The recorded shrinkage strains at all measurement positions are given in Table 5.6. These strains are presented as hoop strains and in-plane strains. Measurement position 15 does

not present the in-plane strains ε_1 since a through-thickness measurement was recorded on the edge of the flange giving ε_2 and ε_3. The initial strains prior to commencing with the post-cure cycle were, as with the tubes, assumed to be zero. Hence, the strains presented are the real values for the post-curing process and do not include the strains developed during the lay-up phase. To obtain the residual strains induced during the total manufacturing process would however be a laborious and intricate action since during the manufacture of the test piece it requires to be rotated and handled many times, with a large possibility of causing breakage in the cabling.

Table 5.6 Measured post-cure strains at nozzle-dished end connection

Gauge Position	Gauge type	Measured strain ($x10^{-6}$)		
		In-plane (longitudinal) strain (ε_1)	Hoop strain (ε_2)	Through-thickness strain (ε_3)
1	D16	-1448	-543	
2	D16	-2557	-394	
3	D16	-1128	-770	
4	D16	-811	-715	
5	D16	-1209	-913	
6	D16	-335	-508	
7	D16	-386	-422	
8	D16	-334	-804	
9	D16	-703	-633	
10	D16	-776	-946	
11	D16	-1523	-381	
12	D16	-1287	-774	
13	C1	270	-1204	
14	D16	-1574	-835	
15	D16		-1196	-1710
16	D16	-830	-1177	
17	C1	-557	-987	
18	D16	-1296	-1243	

with D16 = KYOWA KFG-2-120-D16-11 type strain gauge rosette with a gauge factor of 2.13, and C1 = KYOWA KFG-5-120-C1-11 type gauge with a gauge factor of 2.15.

6. CURE SHRINKAGE STRESS AND STRAIN PREDICTIONS BY MAKING USE OF FINITE ELEMENT MODELING AND ANALYSIS

6.1 Introduction

The finite element method is commonly used for the prediction of stresses and strains in components with complicated geometry. This method is applied by making use of commercially available finite element analysis software such as ALGOR® [43] and COSMOS/M™ [44] or other similar software with orthotropic element capabilities. One concern with using the software or any other method of analysis is that the results obtained are predicted values. These can only be found sufficiently accurate and representative if the material properties employed accurately represent that of the actual material and the geometric model created accurately resembles the actual product. In many instances none of the above can be guaranteed at the design stage and hence assumptions have to be made within reasonable limits.

To present accurate FEA procedures that could be used in industry it is important to use results obtained from experimental testing and measurements as benchmarks for comparison. For this purpose the experimental tests presented in Chapter 5 together with the material elastic properties determined in Chapter 4 will be modelled and analysed to obtain theoretical results that can be compared to the experimental results. Hence the analysis presented in this chapter will consist of:

- strains induced by post-cure of a tubular system;
- strains produced by post-cure of a full-face flange;

- strains produced by post-cure of a nozzle-vessel connection.

In most cases, such as tubular sections, flanges and nozzle to dished end connections, it is sufficient to use axisymmetric models with orthotropic material properties. However, for models where axisymmetry can not be applied, 3-dimensional models with orthotropic brick elements or composite plate elements need to be used. The 3-D models are more complex to create and computational time increases.

In most analyses problems it is usually sufficient to make use of linear static analyses for the prediction of stresses and strains. Non-linear static analyses might be required if the loading conditions should vary with time or if the material characteristics should vary with respect to the loading conditions.

6.1.1 Considerations required for the finite element models

6.1.1.1 Assumptions to be made for linear static analysis

For the linear static finite element models presented in this chapter some assumptions need to be stated. These assumptions are:

- all layers are at the same degree of cure prior to the post-cure process;
- no in-plane out-of-plane couplings occur in the CSM layers;
- no additional modulus development occurs during the post-cure process;
- the temperature application is such that full post-cure is effected.

For general purposes these assumptions can be assumed to be valid, however, for more intricate and complex work the assumptions need to be clarified and the effect thereof considered in great detail. As an example, the assumption that all layers are at the same degree of cure prior to the post-cure process is not necessarily true. The components are usually made over a period of time and hence the initial layers should be at a more

advanced state of cure than the final layers when the component is placed in the curing oven or autoclave for the post-cure process. Also, small in-plane out-of-plane couplings should occur in CSM laminates since due to the nature of the CSM material, the fibres do lay at various angles to the in-plane direction although the angles could be negligibly small. These examples should be considered to determine if significant variation in the predicted results would be obtained if an effort were made to include these effects in the analysis. For the purpose of this study the assumptions initially stated will be considered to be valid.

6.1.1.2 Elastic property assignments

When creating the model additional aspects with regard to the modelling procedure and the assignment of the material properties need to be considered. For instance, it must be clear to the designer as to what type of loading is to be applied to the model and which of the Poisson's ratios are required for the type of loading. The specified principal material direction and the type of applied loading govern the assignment of the Young's moduli and Poisson's ratios in the finite element model. Circular vessels subject to internal or external pressures should in the majority of cases only have in-plane loading applied which require the in-plane Young's moduli and the Poisson's ratios determined for in-plane loading. In cases such as flanges a through-thickness loading is applied by the bolting and hence the through-thickness moduli and Poisson's ratios for through-thickness loading need to be applied. During post-cure the magnitudes of the shrinkage strains are governed by the 3-dimensional properties of the material, therefore the moduli and Poisson's ratios in all three material directions need to be specified.

The assignment of these properties are obviously also governed by the requirements and the operation of the software that is used for the analyses. It is therefore also important to

be aware of the features and limitations of the particular software that is being used. Since ALGOR® [43] is employed in this study its requirements and operation will be will be explained. These explanations might also be directly applicable to any of the other software since the principle of solution is basically the same.

Although the Young's moduli in the laminate principal material directions are calculated as E_1, E_2 and E_3 with E_1 and E_2 being the in-plane moduli and E_3 the through-thickness modulus, the software allows these values to be applied as the designer wishes in the form of E_n, E_s and E_t. The material direction of E_n is to be specified, anti-clockwise, with respect to the model global y-direction and E_s being perpendicular to E_n. The direction of E_t is then determined by the completion of the right-hand rule. The software requires the Poisson's ratios to be entered as ν_{ns}, ν_{nt} and ν_{st}. The CTEs are also entered as α_n, α_s and α_t corresponding with the Young's moduli. It is therefore suggested that, depending on the expected model loading conditions, the moduli, Poisson's ratios and shrinkages, as is shown in Table 4.5, be applied as is indicated in Table 6.1.

Although the material properties remain the same for the different loading conditions, the emphasis on the model primary material direction changes. For mechanical and hydrostatic loading conditions the emphasis is placed on the in-plane properties and for thermal and transverse loading the emphasis is placed on the through-thickness material properties. Hence, for the prediction and analysis of post-cure strains it is suggested that the material assignments for the thermal loading conditions be used.

Table 6.1 Finite element model elastic material property assignment

Elastic property in the software	Loading condition	
	Mechanical in-plane and hydrostatic	Thermal and mechanical through-thickness
E_n	E_1	E_3
E_s	E_3	E_1
E_t	E_2	E_2
ν_{ns}	ν_{13}	ν_{31}
ν_{nt}	ν_{12}	ν_{32}
ν_{st}	ν_{32}	ν_{12}
s_n or α_n	s_x or α_x	s_z or α_z
s_s or α_s	s_z or α_z	s_x or α_x
s_t or α_t	s_y or α_y	s_y or α_y

6.2 Strains induced by post-cure of a tubular system

To predict the post-cure shrinkage in a relatively small bore tube, with the experimental test results given in 5.2.1 on p. 55, six axisymmetric models, T_1, T_2, T_3, T_4, T_5 and T_6, with 4-noded orthotropic elements were created. The models have inside diameters of 50 mm and wall thicknesses of 13.5 mm and lengths of 290 mm. The material properties for each of the models are obtained from Table 4.5. For models T_2, T_4 and T_6 an inner resin rich surface of 1 mm in thickness was incorporated to determine what the effect of a resin rich surface would have on the analysis results. Table 6.2 differentiates the six models with respect to the material assignments. At this stage only the thermal loading material directions given in Table 6.1 are considered.

Table 6.2 Material properties for tubular analyses

Model	Structural properties	Surface layer properties
T_1	Property 1	None
T_2	Property 1	Property 8
T_3	Property 2	None
T_4	Property 2	Property 8
T_5	Property 3	None
T_6	Property 3	Property 9

Since the post-cure shrinkage (S) of the laminate is used, by analogy, as a coefficient of thermal expansion a temperature change of 1°C was applied to all the nodes in the model and analysed to obtain the stresses, strains and displacements resulting from the shrinkage of the resin matrix. The predicted post-cure hoop strain distribution for the various models are shown in Fig. 6.1 to Fig. 6.4 with the predicted post-cure through-thickness strains for the various models shown in Fig. 6.7 to Fig. 6.12. These figures clearly indicate that substantial residual strains are created by the post-cure shrinkage of the tube. It is also shown that the inner circumference is placed in a tensile strain state while the outer surface is in a compressive state. It can be seen that if the inner surface is considered to be resin rich, as is obtained by a gel coat or a resin rich surface tissue, the strains can be expected to vary by some margin. Comparative strain values at the respective gauge positions for the four models are presented in Table 6.3.

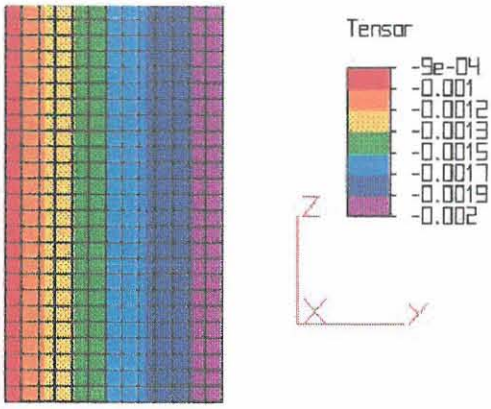

Fig. 6.1 Predicted hoop strains (Model T_1)

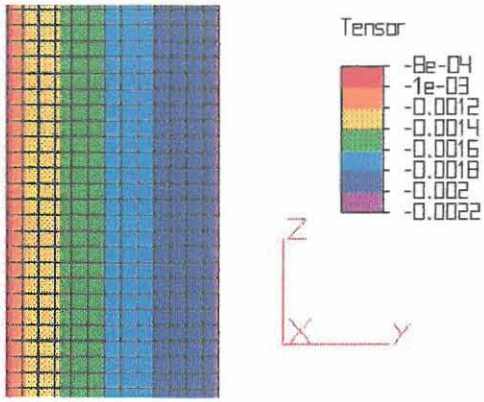

Fig. 6.2 Predicted hoop strains (Model T_2)

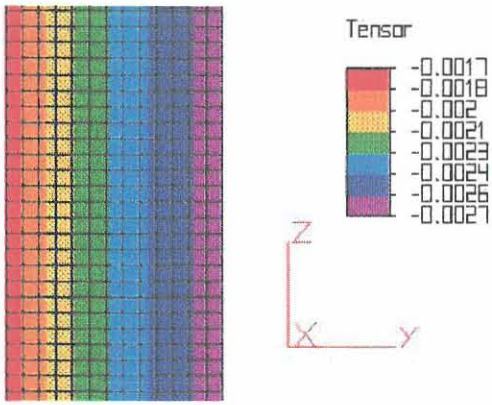

Fig. 6.3 Predicted hoop strains (Model T_3)

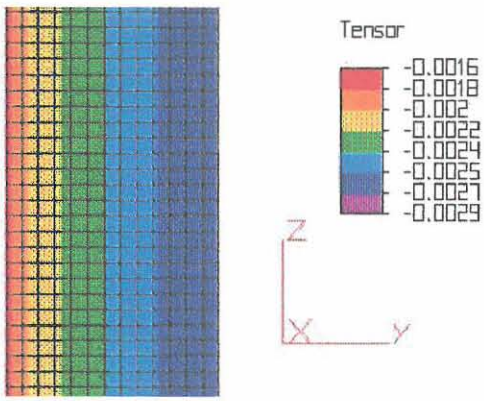

Fig. 6.4 Predicted hoop strains (Model T_4)

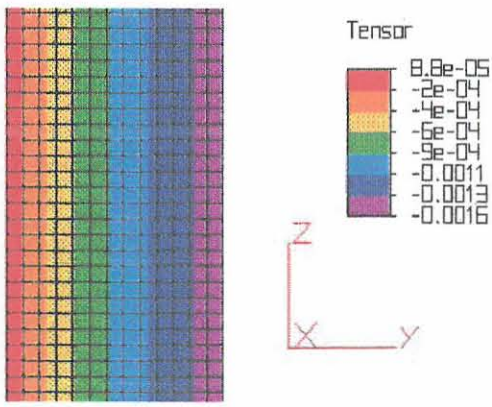

Fig. 6.5 Predicted hoop strains (Model T_5)

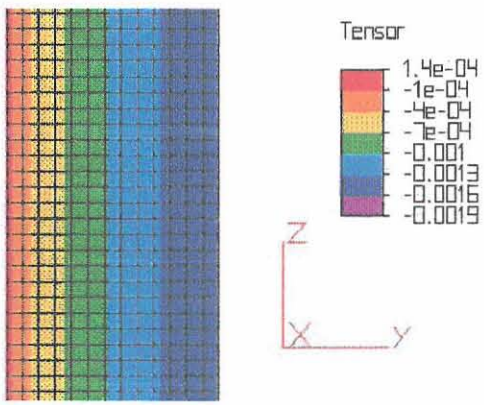

Fig. 6.6 Predicted hoop strains (Model T_6)

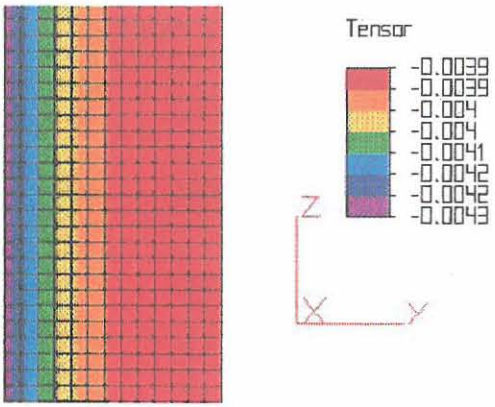

Fig. 6.7 Predicted through-thickness strains (Model T_1)

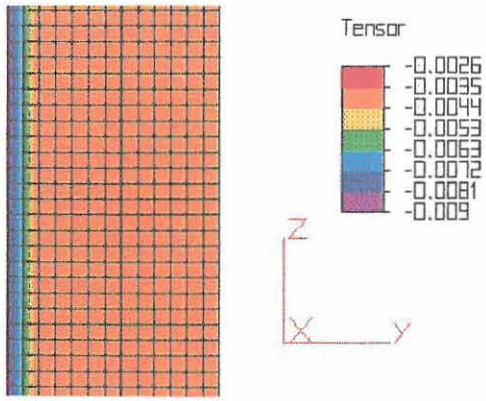

Fig. 6.8 Predicted through-thickness strains (Model T_2)

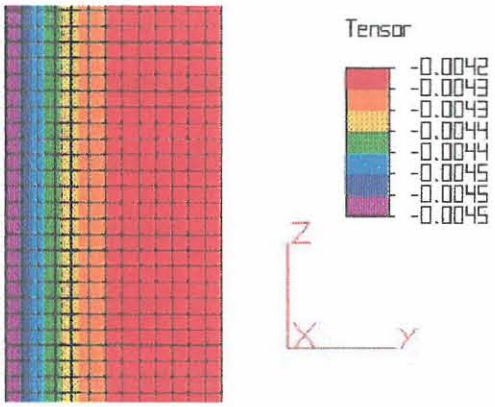

Fig. 6.9 Predicted through-thickness strains (Model T_3)

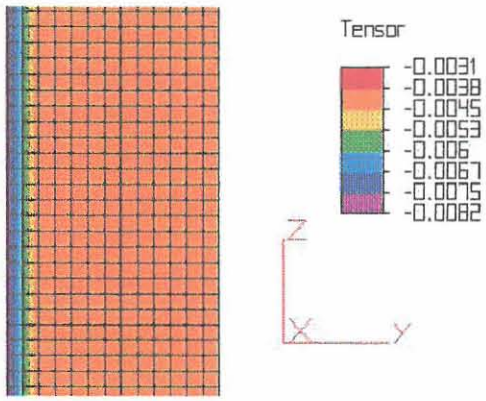

Fig. 6.10 Predicted through-thickness strains (Model T_4)

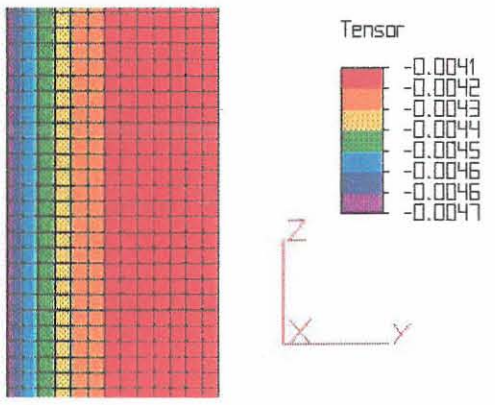

Fig. 6.11 Predicted through-thickness strains (Model T_5)

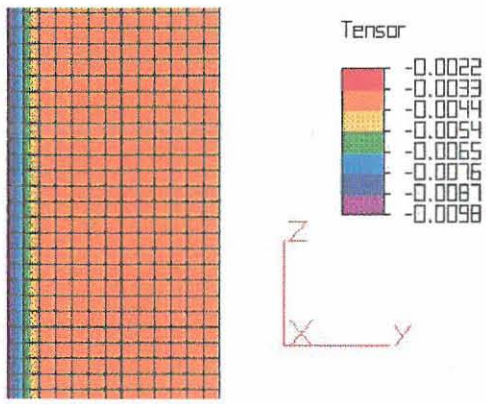

Fig. 6.12 Predicted through-thickness strains (Model T_6)

Table 6.3 Predicted post-cure shrinkage strains 50NB tubes

Direction	Post-cure strain ($\times 10^{-6}$) at gauge positions					
	Inner surface			Outer surface		
	Hoop	Long	Through-thickness	Hoop	Long	Through-thickness
T_1	-1035	-1525	-4231	-1997	-1525	-3924
T_2	-1158	-1597	-6416	-2051	-1597	-3942
T_3	-1874	-2284	-4542	-2679	-2284	-4323
T_4	-2004	-2352	-6187	-2737	-2352	-4280
T_5	-1328	-818	-4616	-1485	-818	-4190
T_6	-345	-932	-6908	-1580	-932	-4119

Direct comparisons of the predicted hoop post-cure strains, obtained at the gauge positions, to the measured strain values for each of the two tubes are presented in Fig. 6.13 and Fig. 6.14. The comparisons for the longitudinal strains are shown in Fig. 6.15 and Fig. 6.16. From these figures it is necessary to determine which of the four finite element models is the most accurate but due to the inconsistent results obtained from the tubes it is not possible to do so with confidence. All the finite element analyses indicate that the inner hoop shrinkage to be smaller in magnitude than the outer hoop shrinkage, whilst the experimental values indicate the contrary. As a measure of accuracy the deviations, of the analysis results from the experimental, were determined and are presented in Fig. 6.17 to Fig. 6.20. A mean deviation was obtained by averaging the absolute deviations at the inner and outer surfaces. These averaged deviations are shown in Fig. 6.21 and Fig. 6.22.

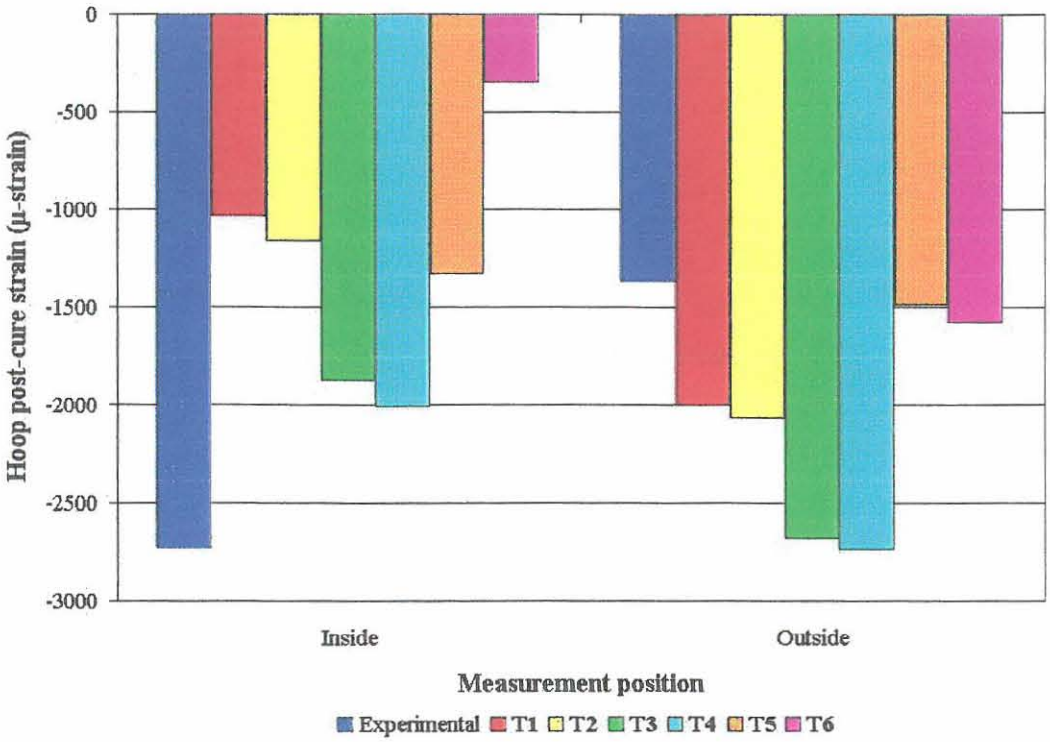

Fig. 6.13 Predicted hoop post-cure strain comparison for tube 1

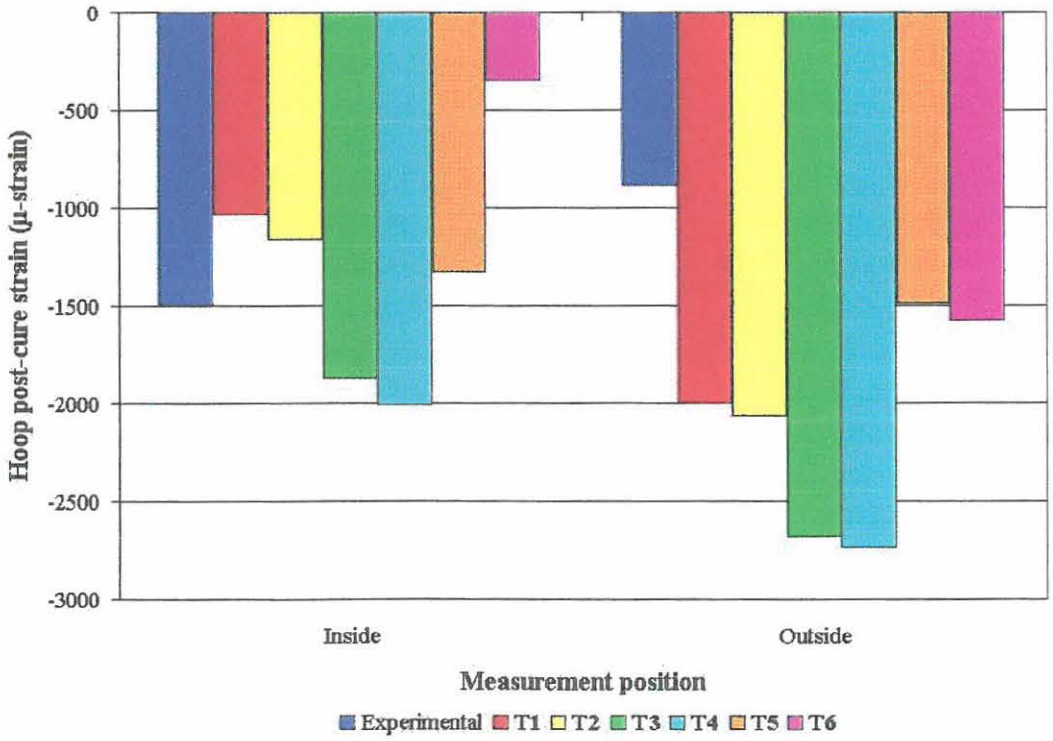

Fig. 6.14 Predicted hoop post-cure strain comparison for tube 2

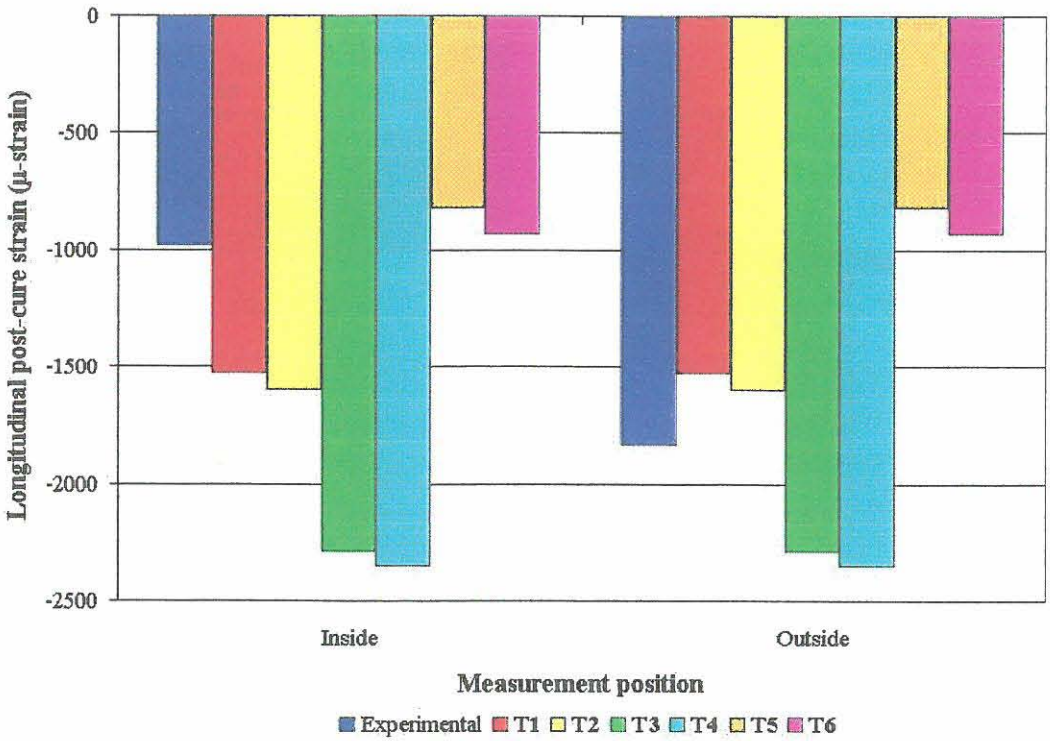

Fig. 6.15 Predicted longitudinal post-cure strain comparison for tube 1

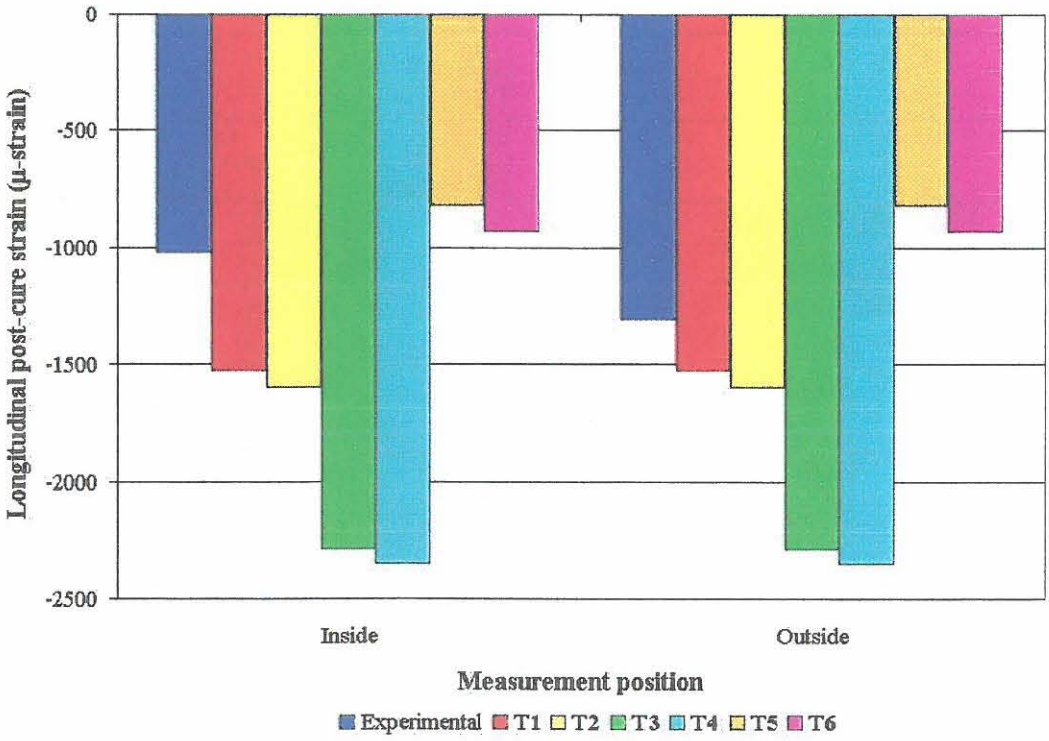

Fig. 6.16 Predicted longitudinal post-cure strain comparison for tube 2

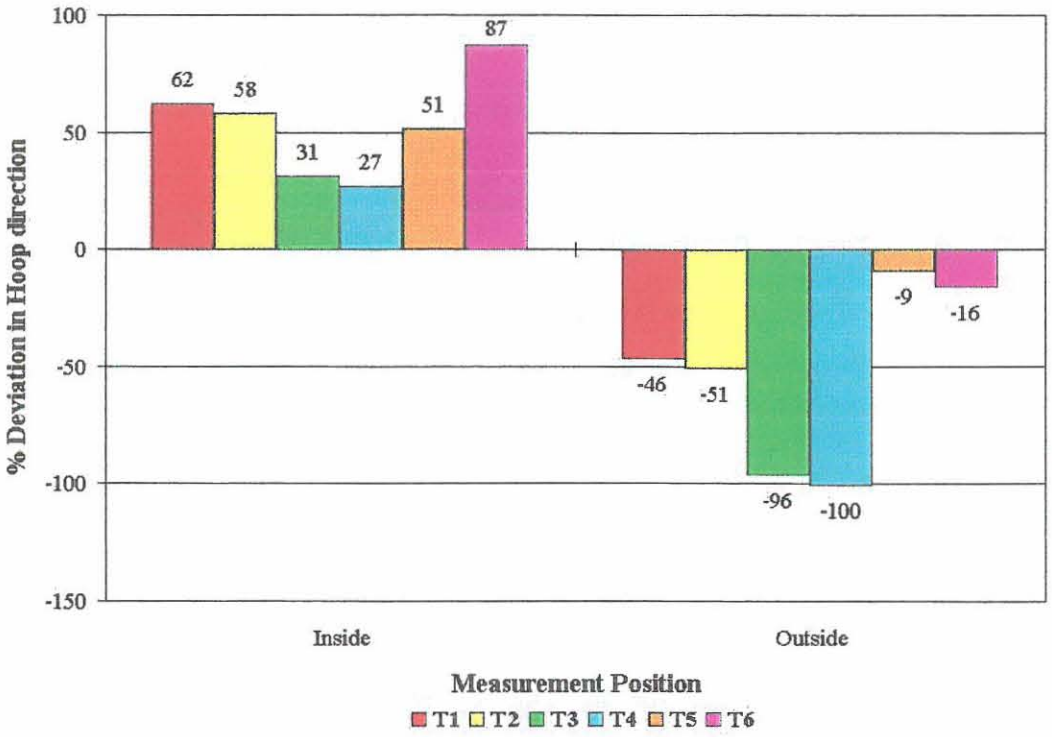

Fig. 6.17 Deviation of predicted hoop strains from experiment for tube 1

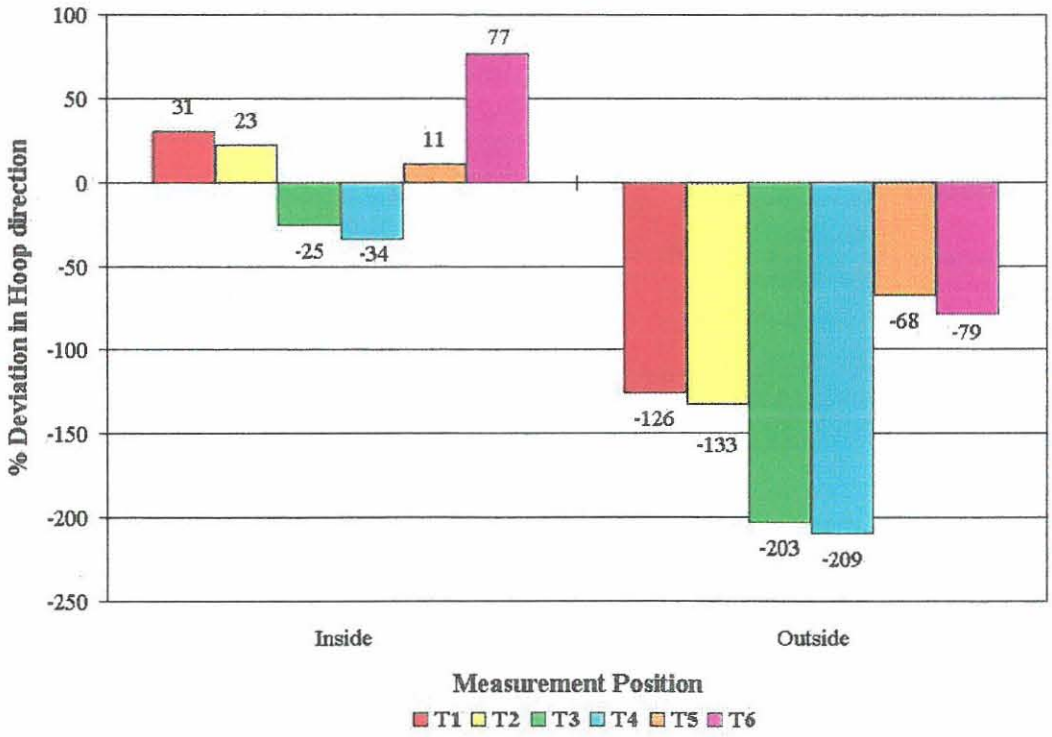

Fig. 6.18 Deviation of predicted hoop strains from experiment for tube 2

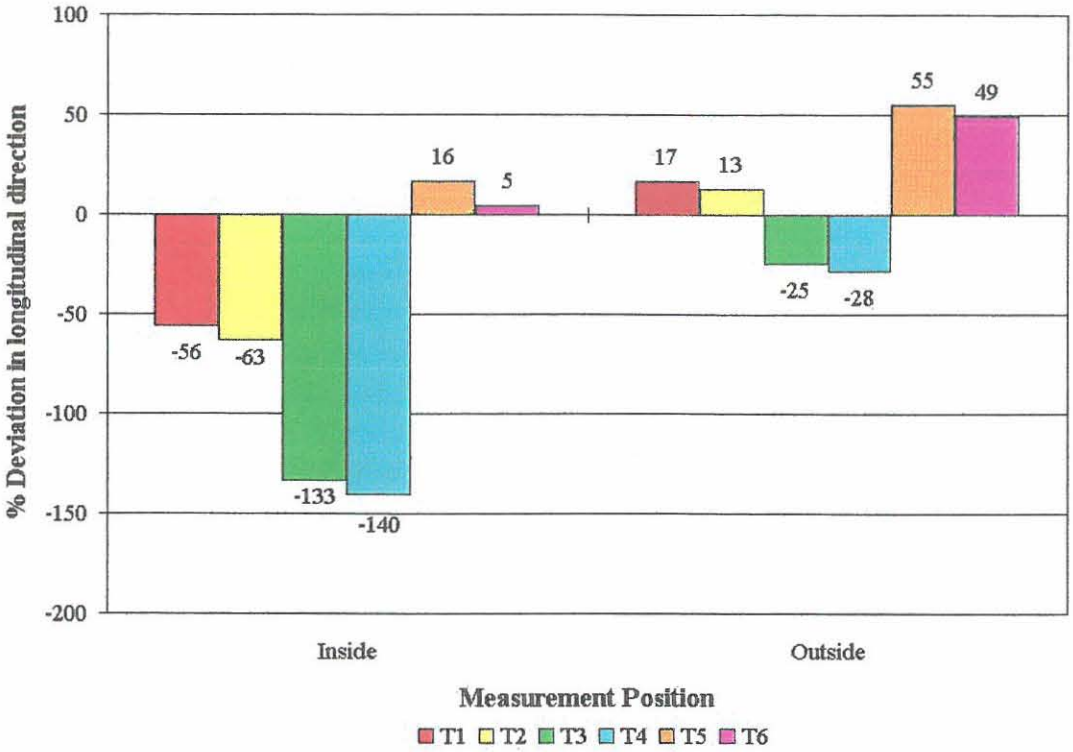

Fig. 6.19 Deviation of predicted longitudinal strains from experiment for tube 1

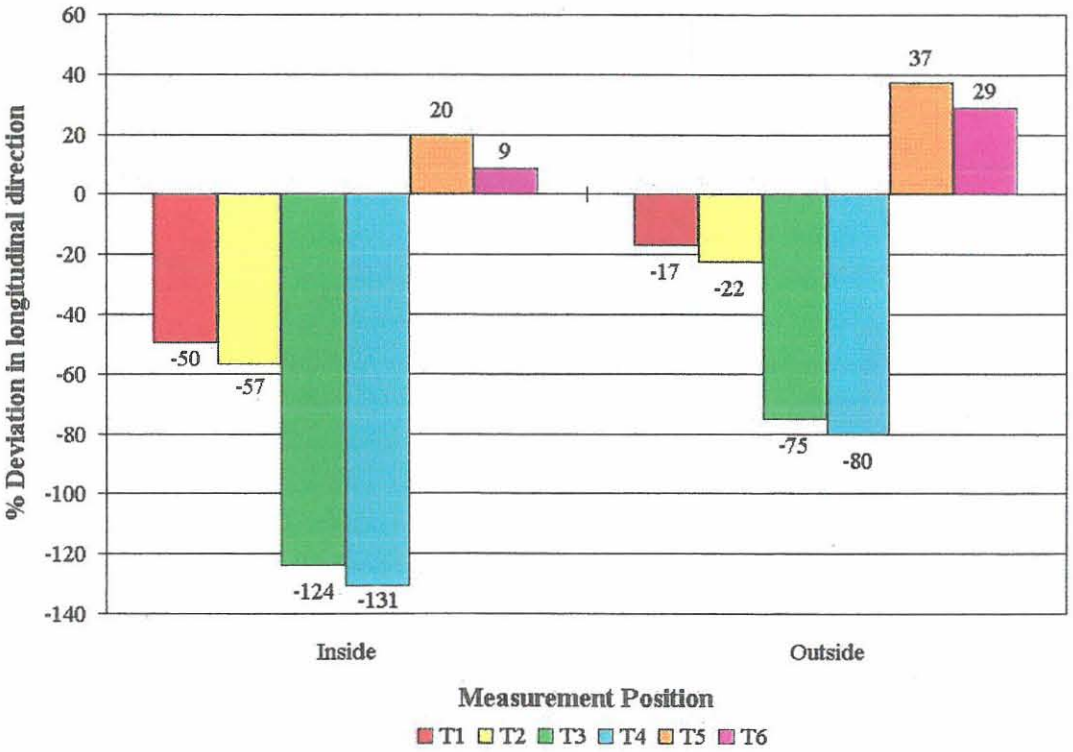

Fig. 6.20 Deviation of predicted longitudinal strains from experiment for tube 2

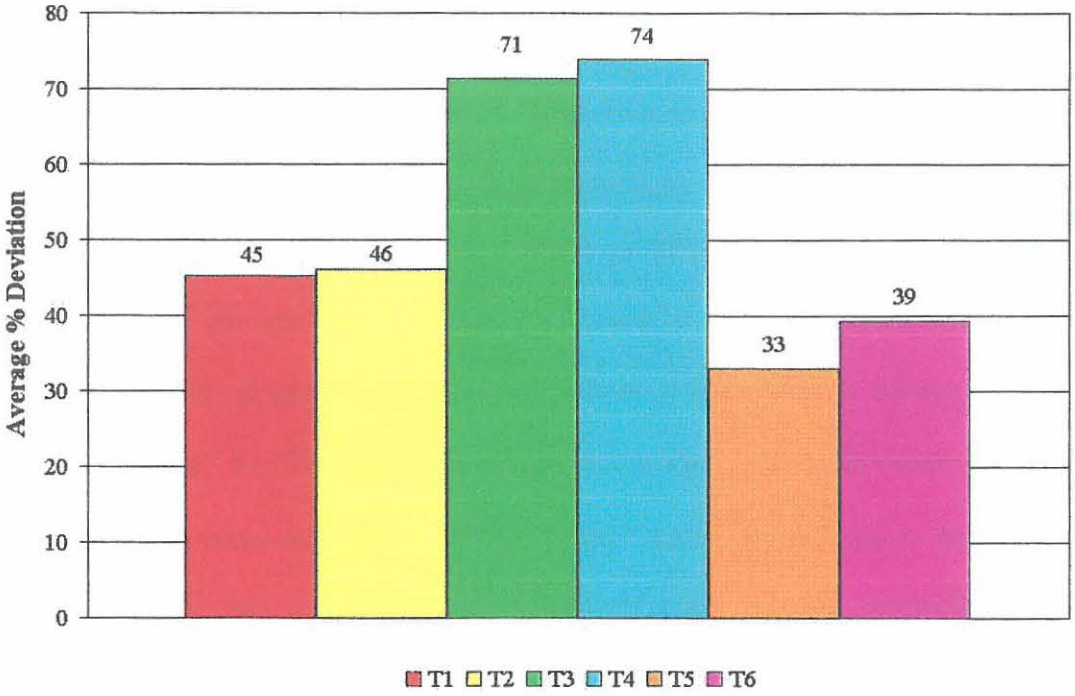

Fig. 6.21 Average deviation of hoop strains for tube 1

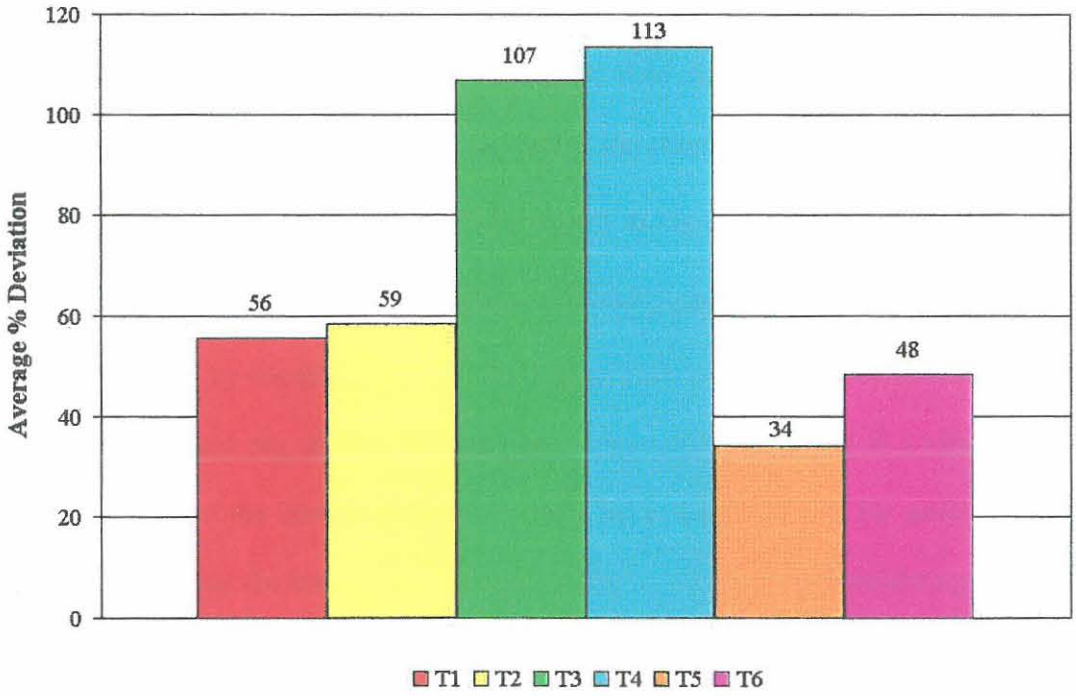

Fig. 6.22 Average deviation of hoop strains for tube 2

The averaging of these deviations, especially the average of the values obtained at the inner and outer surfaces, as a means of determining the most accurate analysis might not be entirely correct for an experiment with little variation in geometry. When considering Fig. 6.21 and Fig. 6.22 it should be remembered that large differences in the measured strains were obtained for the two tubes. It should be better to only consider the hoop strain deviations since this is normally the strain that causes complications in tubular sections. However, Fig. 6.21 and Fig. 6.22 both indicate that model T_5 presents results with the smallest deviation when compared to the experimental values. By referring to Table 6.2 it is confirmed that this model used the calculated elastic material properties for a CSM/DION 9100 vinyl ester resin laminate, using Schapery's method for the calculation of the laminate shrinkage values [31], and using the post-cure shrinkage of a DION 9100 vinyl ester resin casting to determine the laminate post-cure shrinkage.

From the analyses it is clear that the inner resin rich surface does play a role in the predicted strain values, especially in the hoop direction. By comparing the stress predictions given by model T_5 to model T_6, shown in Fig. 6.23 and Fig. 6.26, it is clear that the principal stresses at the inner surface of model T_6 is beyond the general allowable value as permitted by the design codes. The high stresses are shown to be concentrated in the surface layer and are, in both the hoop and longitudinal directions, in a tensile state. The tensile state of the inner surface also clearly indicates the reason for surface cracks appearing and hence the being prone to EAC whilst in service. By considering the Von Mises stress distribution in model T_5, Fig. 6.27, and model T_6, Fig. 6.28, it is also clear that the high resin content of the chemical barrier at the inner surface of the tube causes residual stress conditions that could be unacceptable if compared with the allowable stresses for this material.

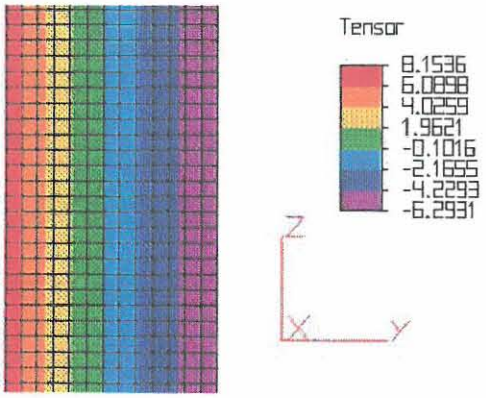

Fig. 6.23 Predicted hoop stresses (Model T_5)

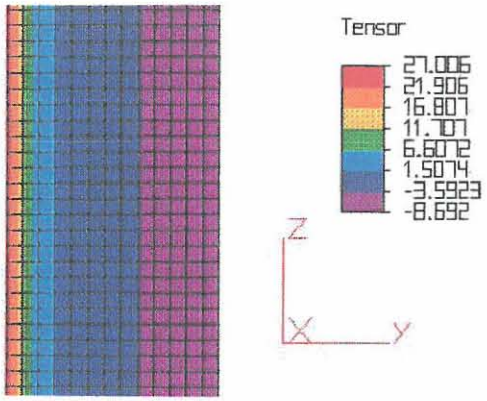

Fig. 6.24 Predicted hoop stresses (Model T_6)

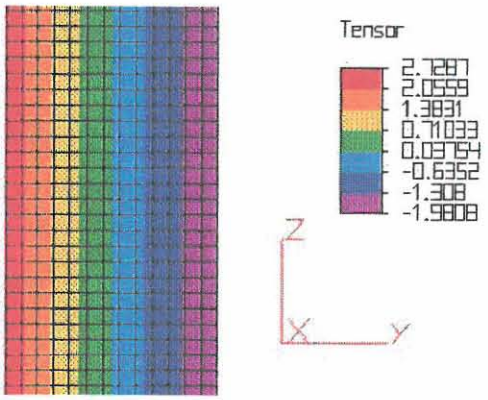

Fig. 6.25 Predicted longitudinal stresses (Model T_5)

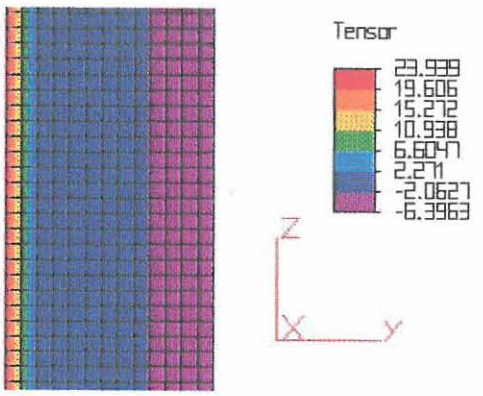

Fig. 6.26 Predicted longitudinal stresses (Model T_6)

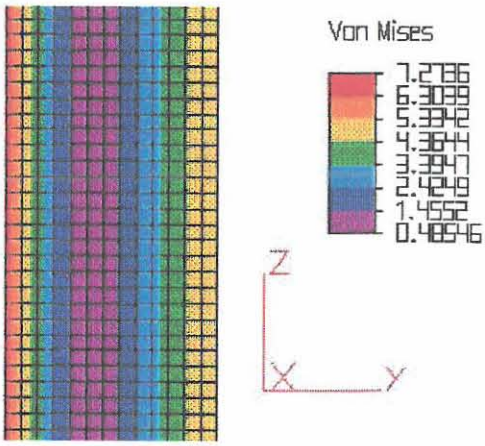

Fig. 6.27 Predicted Von Mises stress distribution (Model T_5)

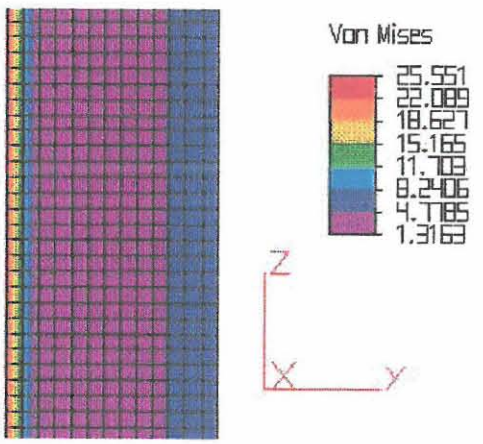

Fig. 6.28 Predicted Von Mises stress distribution (Model T_6)

6.3 Strains produced by post-cure of a full-face flange

Full face and stub flanges for the use on GRP vessels and piping are usually manufactured by hand lay-up due to the complexity of the shape. It is usually accomplished by using a skin as an initial mould or shape in which the matrix and reinforcement is applied. The reinforcement and matrix is applied to the specified thickness as is required by the various design and manufacturing codes. During the lay-up of the various layers, strains are produced as a result of the curing shrinkage of the matrix. It is believed that, if post-cure cycle is applied to the nozzle-flange combination, the curing strains will be alleviated to acceptable levels as is required by the various codes. This enhances the chemical resistance of the nozzle-flange inner surface but crazing, in areas with large variations in geometry and thickness, has been observed. The strain distribution in a typical flange, resulting from post-cure shrinkage, therefore needs to be obtained to for comparison with values recorded during an experimental post-cure.

6.3.1 The finite element model

The purpose of this section is, similar to 6.2, to determine the most accurate method to predict the post-cure strains and stresses that are developed in composite specimens with complex shapes. The experiment given in 5.2.2 is modelled using ALGOR® [43] finite element analysis software with axisymmetric orthotropic elements with the model dimensions given in Fig. 5.11. Six models were created with the material elastic properties, Young's Modulus (E) and Poisson's ratio (ν), obtained from Table 4.5 and applied as is shown in Table 6.4. Models F_2, F_4 and F_6 all have a resin rich surface of 1 mm in thickness on the tube inner surface and on the flange face, which was not considered in F_1, F_3 and F_5.

Care had to be taken to ensure that the material directions were properly represented since the flange varies in geometry and the principal material direction throughout the flange geometry does not remain constant. Photographic scans were obtained of cross-sections of the flange to determine the layer directions with respect to the model global co-ordinate system. Picture 6.1 shows the cross-section of the flange from which the directions were determined and Picture 6.2 showing a burnt-off flange section that gives a clear image of the layer directions.

Table 6.4 Material properties for flange analyses

Model	Structural properties	Surface layer properties
F_1	Property 1	No
F_2	Property 1	Yes
F_3	Property 4	No
F_4	Property 4	Yes
F_5	Property 5	No
F_6	Property 5	Yes

Fig. 6.29 shows how the photographic scan is utilised to divide the flange into regions. Fig. 6.30 and Fig. 6.31 show the assignment of the material directions, with respect to the model y-direction by considering the type of loading. These material direction assignments are assumed to represent the actual directions with sufficient accuracy.

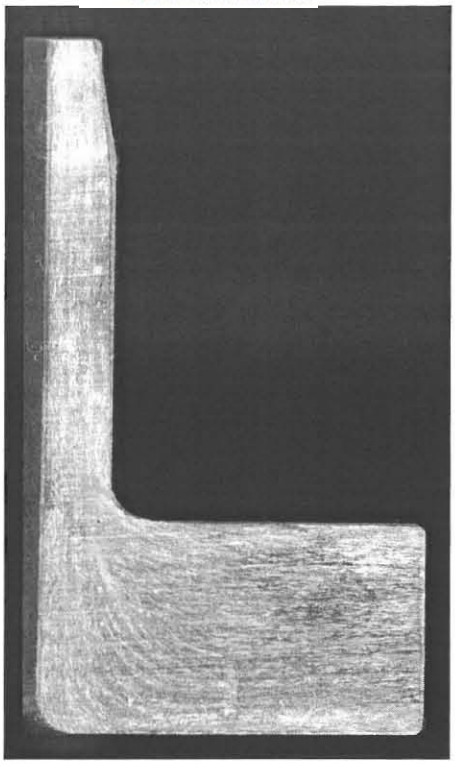

Picture 6.1 Fibre directions of full face flange

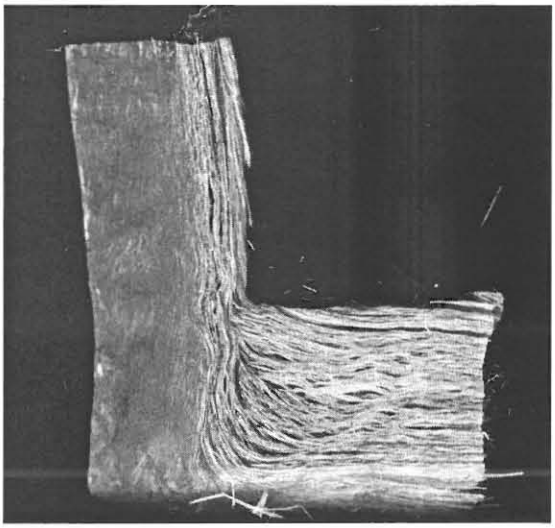

Picture 6.2 Burned out flange showing fibre directions

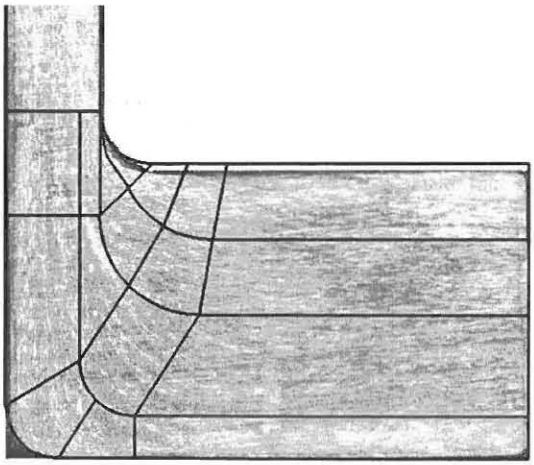

Fig. 6.29 Material direction regions of full face flange

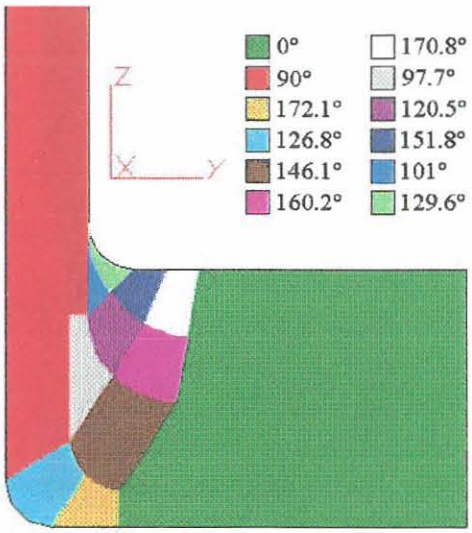

Fig. 6.30 Global material direction for E_n relative to model y-axis when considering in-plane loading

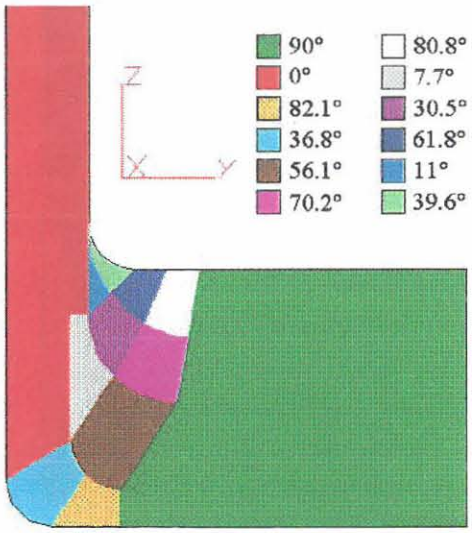

Fig. 6.31 Global material direction for E_n relative to model y-axis when considering through-thickness loading

As with the tubular model, presented in 6.2, a temperature of 1°C was applied to all nodes whilst using the post-cure shrinkage of the laminate (S) as a CTE to obtain the stresses, strains and also the pull-back developed in the flange as a result of the post-cure process. Fig. 6.32 to Fig. 6.37 show examples of the predicted strain distributions with Fig. 6.38 and Fig. 6.39 showing the strain comparisons to the experimental values. APPENDIX B presents a full compliment of the predicted strain distributions in each of the models.

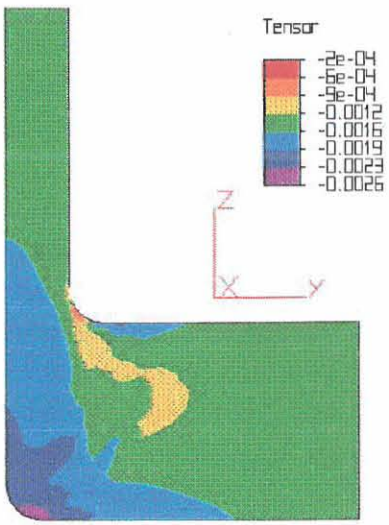

Fig. 6.32 Predicted in-plane strain (ε_1) of model F_1

Fig. 6.33 Predicted in-plane strain (ε_1) of model F_2

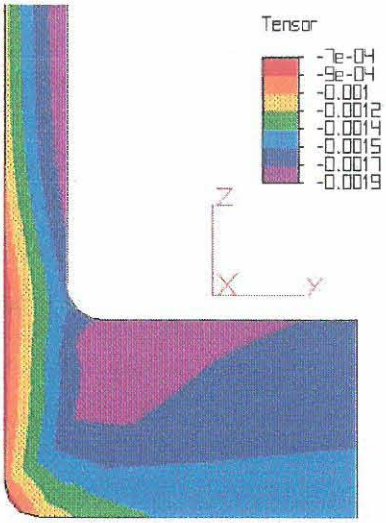

Fig. 6.34 Predicted in-plane strain (ε_2) of model F_1

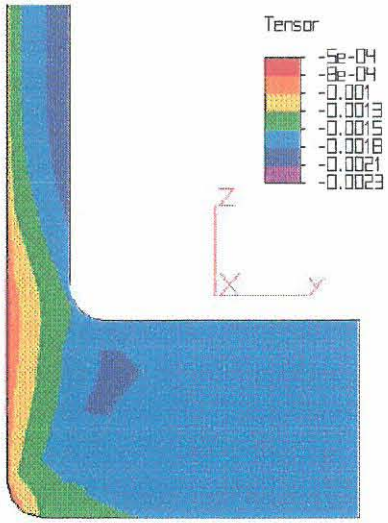

Fig. 6.35 Predicted in-plane strain (ε_2) of model F_2

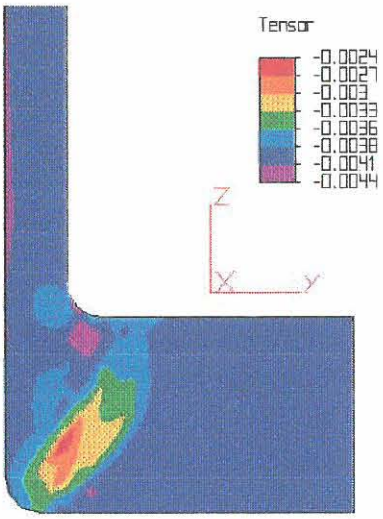

Fig. 6.36 Predicted through-thickness strain (ε_3) of model F_1

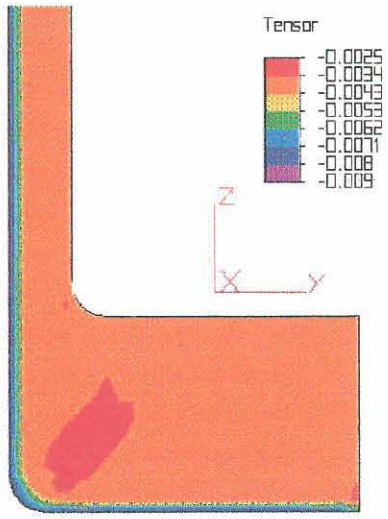

Fig. 6.37 Predicted through-thickness strain (ε_3) of model F_2

From Fig. 6.38 and Fig. 6.39 deviations can be obtained of the predicted strain values from the experimentally recorded values. The deviations are presented graphically in Fig. 6.40 and Fig. 6.41. The averaged deviations of the predicted strains in the 1st and 2nd principal material directions are shown in Fig. 6.42 and Fig. 6.43.

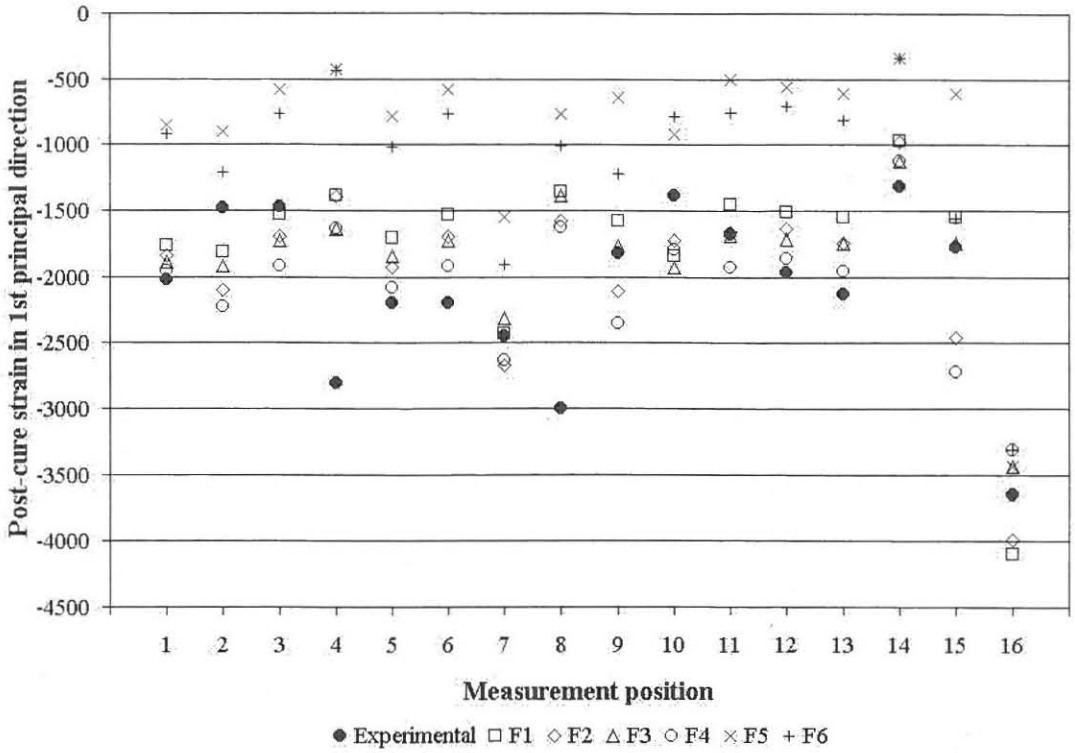

Fig. 6.38 Comparison of predicted in-plane post-cure strain (ε_1) to experiment

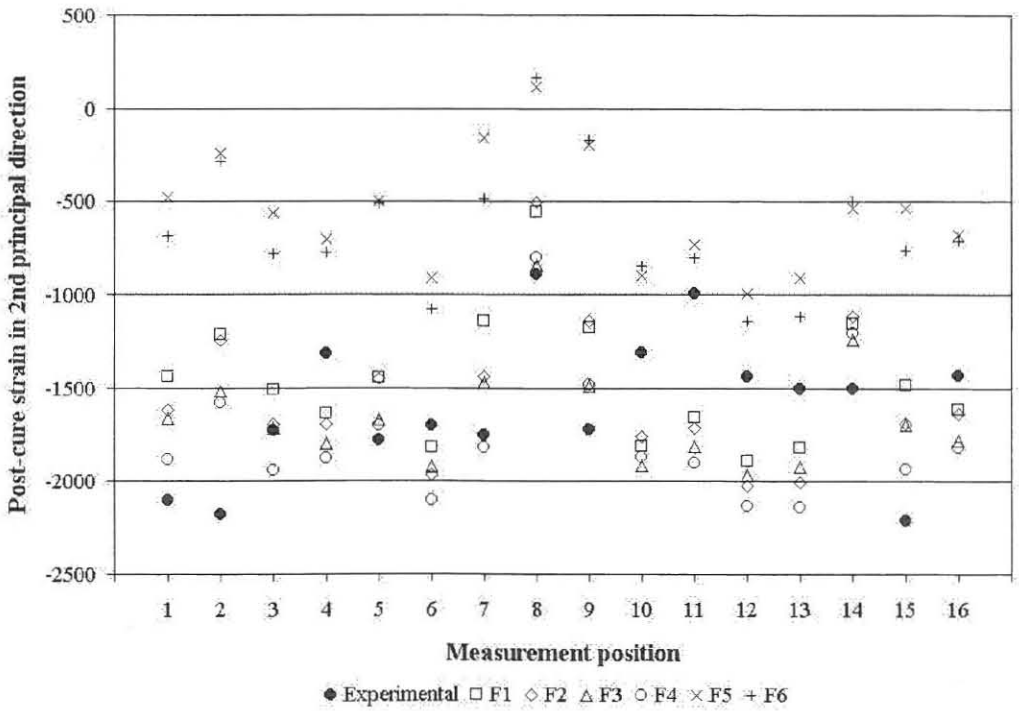

Fig. 6.39 Comparison of predicted in-plane (hoop) post-cure strain (ε_2) to experiment

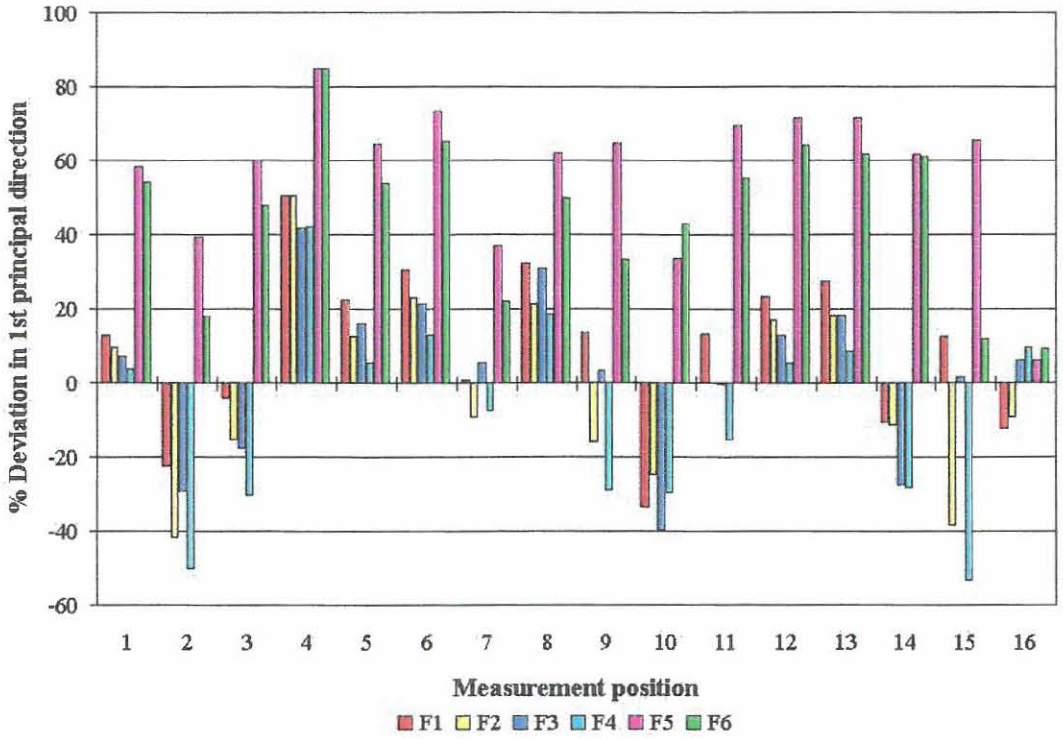

Fig. 6.40 Deviation of predicted in-plane post-cure strain (ε_1)

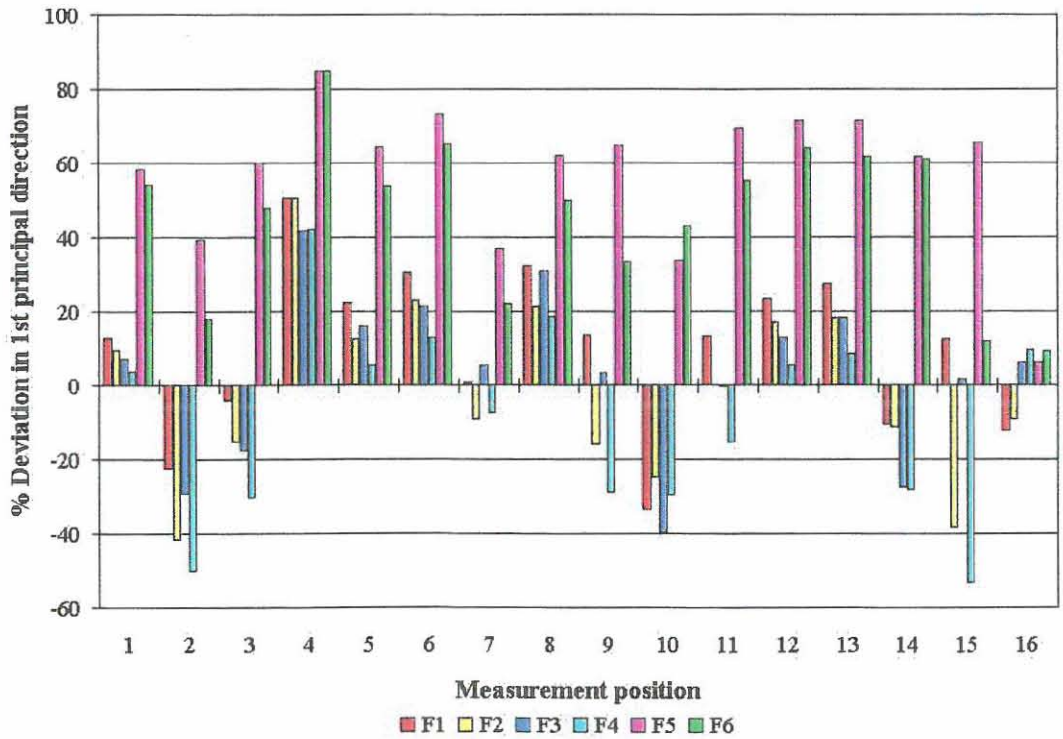

Fig. 6.41 Deviation of predicted in-plane (hoop) post-cure strain (ε_2)

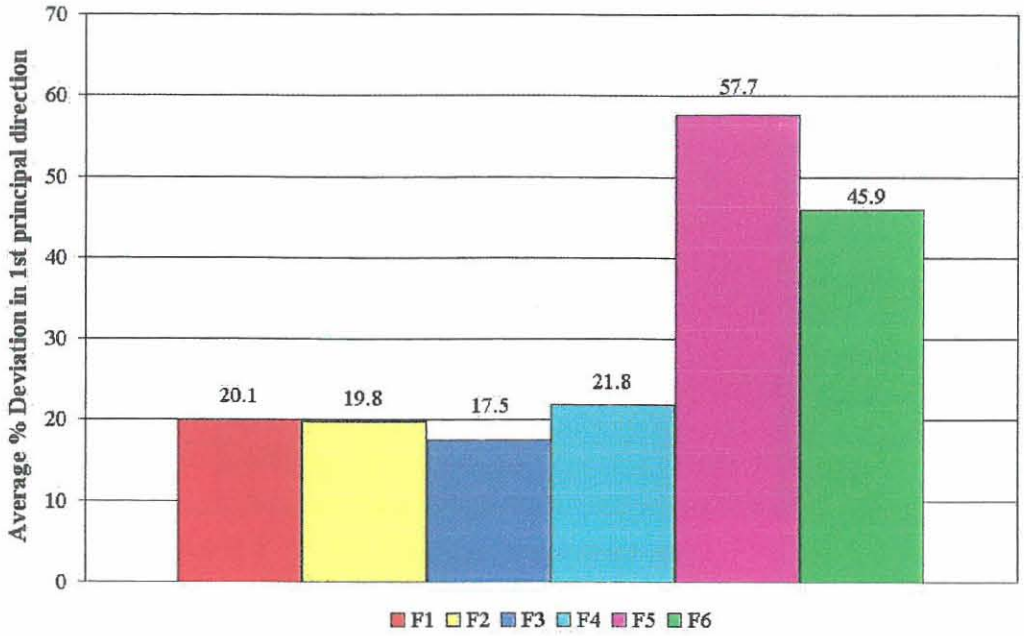

Fig. 6.42 Average deviation of predicted in-plane post-cure strain (ε_1)

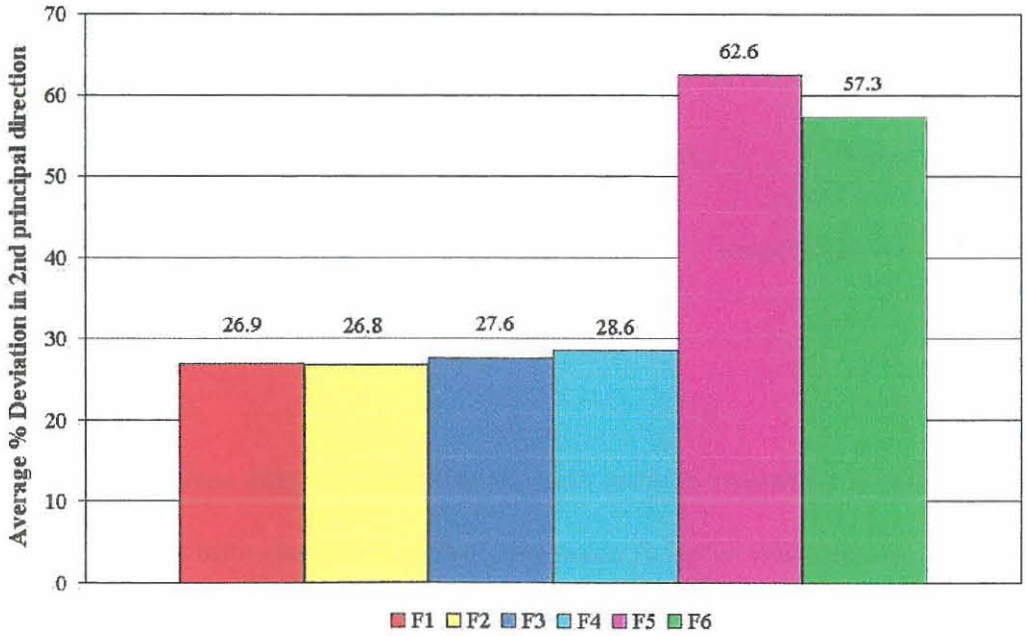

Fig. 6.43 Average deviation of predicted in-plane (hoop) post-cure strain (ε_2)

A global averaged deviation is obtained by averaging the deviations in Fig. 6.42 and Fig. 6.43 to give the values presented in Fig. 6.44.

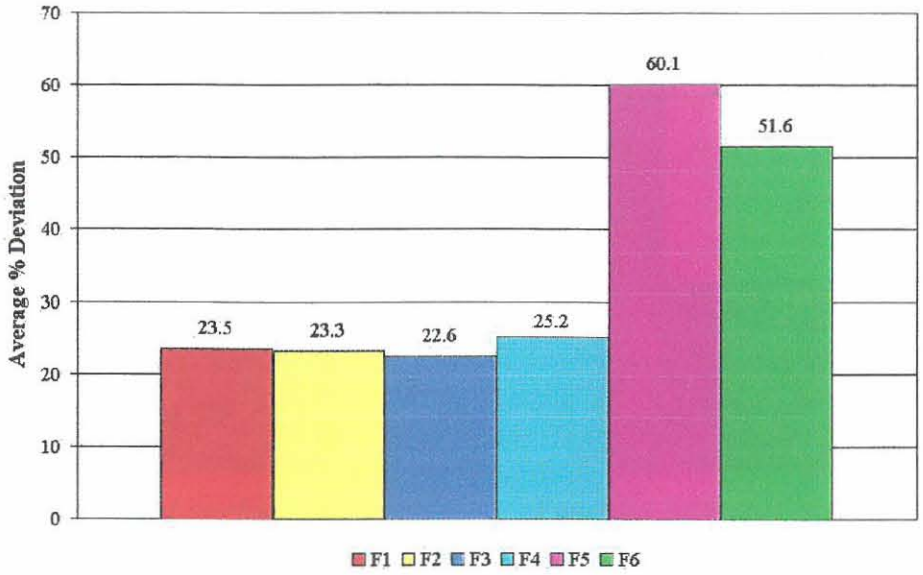

Fig. 6.44 Global averaged deviation of predicted post-cure strains

From the deviations presented in the figures it is clearly indicated that, for a component of similar geometric size and proportions which is constructed using a similar material, the most accurate prediction of the post-cure strains would be by using the methods to determine the material properties of model F_3. However, by considering the models that incorporate a resin rich surface layer, models F_2, F_4 and F_6, it is seen that the differences in the deviations when compared to models F_1, F_3 and F_5 respectively are small and that these results need to be given special attention.

The strain distributions obtained from the analyses give an indication of the magnitude of post-cure shrinkage but ultimately the designer needs to know what the stress condition in the component would be since an allowable stress value is usually prescribed be the design codes. Fig. 6.45 to Fig. 6.50 show the predicted principal stresses for models F_3 and F_4 which have the same material properties except that model F_4 has a resin rich surface included. The stress distributions obtained from the models where no resin rich surface is included show stress magnitudes that are acceptable.

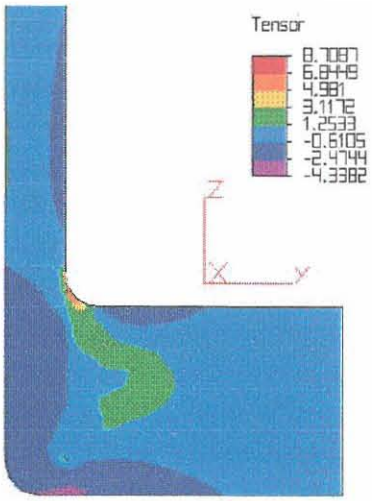

Fig. 6.45 Predicted in-plane stress (σ_1) of model F_3

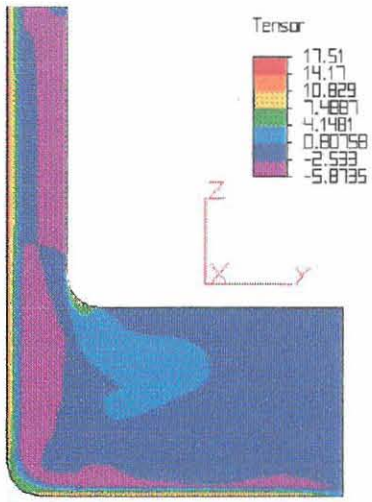

Fig. 6.46 Predicted in-plane stress (σ_1) of model F_4

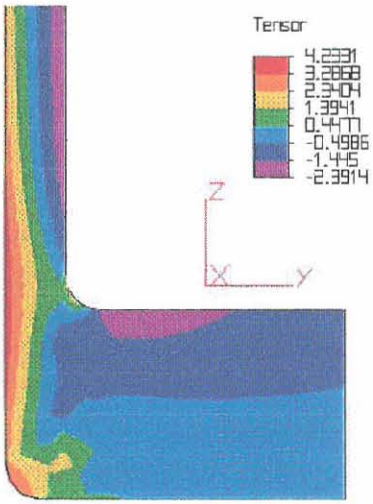

Fig. 6.47 Predicted in-plane (hoop) stress (σ_2) of model F_3

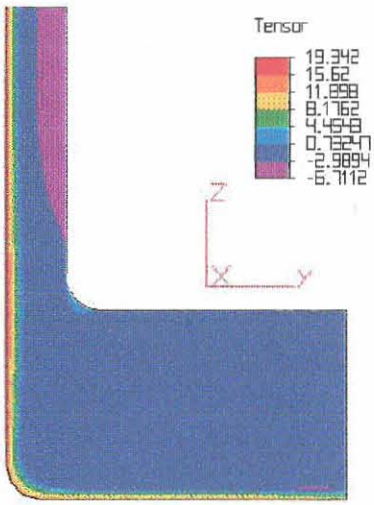

Fig. 6.48 Predicted in-plane (hoop) stress (σ_2) of model F_4

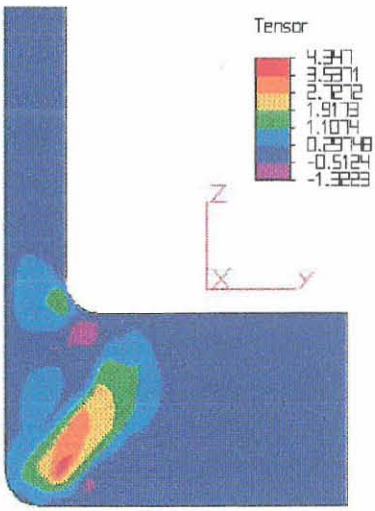

Fig. 6.49 Predicted through-thickness stress (σ_3) of model F_3

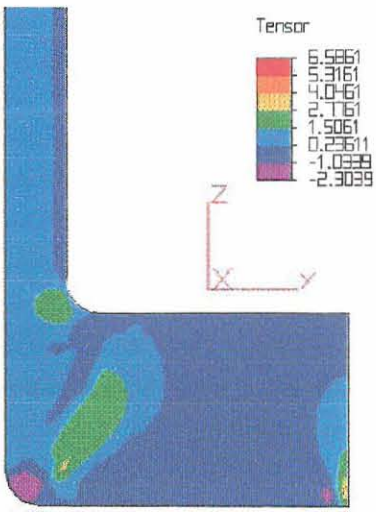

Fig. 6.50 Predicted through-thickness stress (σ_3) of model F_4

The models that have the resin rich surface show stress magnitudes, in the in-plane directions (σ_1 and σ_2), that could be unacceptably high. Fig. 6.51 and Fig. 6.52 show the Von Mises stress distribution of models F_3 and F_4. The distributions indicate clearly that the resin rich surface layer causes high residual post-cure stresses to be induced. The high stresses are concentrated at the inner surface and should be the cause for any EAC occurring.

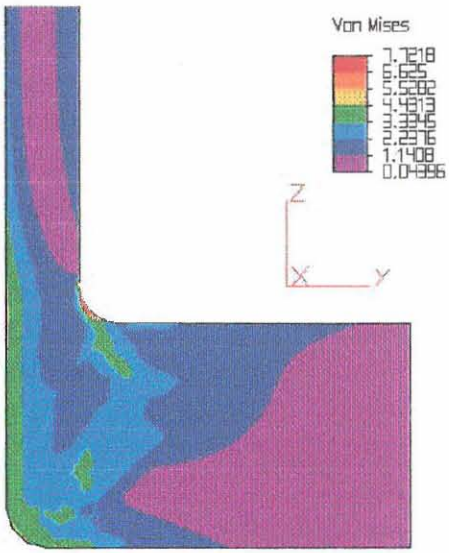

Fig. 6.51 Predicted Von Mises stress distribution of model F_3

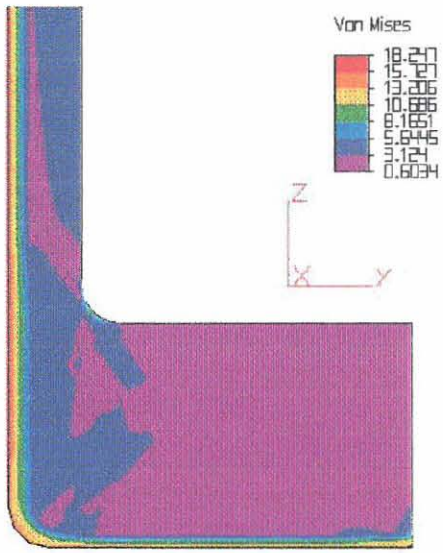

Fig. 6.52 Predicted Von Mises stress distribution of model F_4

APPENDIX B presents a full compliment of the predicted stress distributions in each of the models.

A concern that manufacturers do have is the amount of pullback that occurs during the manufacture of flanges. Although visible pullback occurs during the actual lay-up of the flange, as is reported in 5.2.2.3, the analyses show that the predicted magnitudes of pullback, during post-cure, to be in the same order as the measured value. The magnitudes of the predicted pullback, of the toe of the flange face relative to the heel, for each of the models are presented in Table 6.5.

Table 6.5 Predicted pullback of flange face

Model	Pullback (mm)
F_1	0.0384
F_2	0.0046
F_3	0.0255
F_4	-0.0111
F_5	0.0427
F_6	0.0064

It is seen that models F_2, F_4 and F_6, the models with the resin rich inner surface, predict smaller pullback magnitudes than the other models. However, it is suggested that these magnitudes, which are obtained as a result of the post-cure process, are negligibly small and that attention be given to the pullback obtained during the lay-up of the flanges.

6.4 Predicted strains produced by post-cure of a nozzle-vessel connection

During the manufacture and post-cure process strains are induced that are usually not taken into consideration during the design stage. It is however important to be aware of these strains and the prediction of these strains should be considered, especially if the laminate tends to be thick or if large variations in the geometry occur. This section will investigate the strains produced in a nozzle-vessel connection.

6.4.1 Finite element model

The purpose of this study, as stated previously, is to determine if post-cure stresses can be predicted by numerical methods with sufficient accuracy. Hence the experimental test were conducted on items with specified dimensions and mass fractions. However, considering the manufacturing methods employed in the construction of vessels, in particular for the vessel constructed for this study *(See Fig. 5.15)*, it seldom found that the specified dimensions or mass fractions are obtained. It was therefore required to obtain actual dimensions and mass fractions from the test piece. The actual dimensions used in the finite element model are shown in Fig. 6.53. As with the models in 6.2 and 6.3, six axisymmetric models with 4-noded orthotropic elements were created to the dimensions given in Fig. 6.53. Table 6.6 shows how the material properties, obtained from Table 4.5, were applied to each of the models with models D_2, D_4 and D_6 having an inner resin rich surface of 1 mm.

Since the model presented variations in geometry and also variations in the direction of the principal material directions in the knuckle and crown regions, with respect to the global

6.4 Predicted strains produced by post-cure of a nozzle-vessel connection

During the manufacture and post-cure process strains are induced that are usually not taken into consideration during the design stage. It is however important to be aware of these strains and the prediction of these strains should be considered, especially if the laminate tends to be thick or if large variations in the geometry occur. This section will investigate the strains produced in a nozzle-vessel connection.

6.4.1 Finite element model

The purpose of this study, as stated previously, is to determine if post-cure stresses can be predicted by numerical methods with sufficient accuracy. Hence the experimental test were conducted on items with specified dimensions and mass fractions. However, considering the manufacturing methods employed in the construction of vessels, in particular for the vessel constructed for this study *(See Fig. 5.15)*, it seldom found that the specified dimensions or mass fractions are obtained. It was therefore required to obtain actual dimensions and mass fractions from the test piece. The actual dimensions used in the finite element model are shown in Fig. 6.53. As with the models in 6.2 and 6.3, six axisymmetric models with 4-noded orthotropic elements were created to the dimensions given in Fig. 6.53. Table 6.6 shows how the material properties, obtained from Table 4.5, were applied to each of the models with models D_2, D_4 and D_6 having an inner resin rich surface of 1 mm.

Since the model presented variations in geometry and also variations in the direction of the principal material directions in the knuckle and crown regions, with respect to the global

co-ordinate system, care had to be taken to ensure that these directions were properly represented.

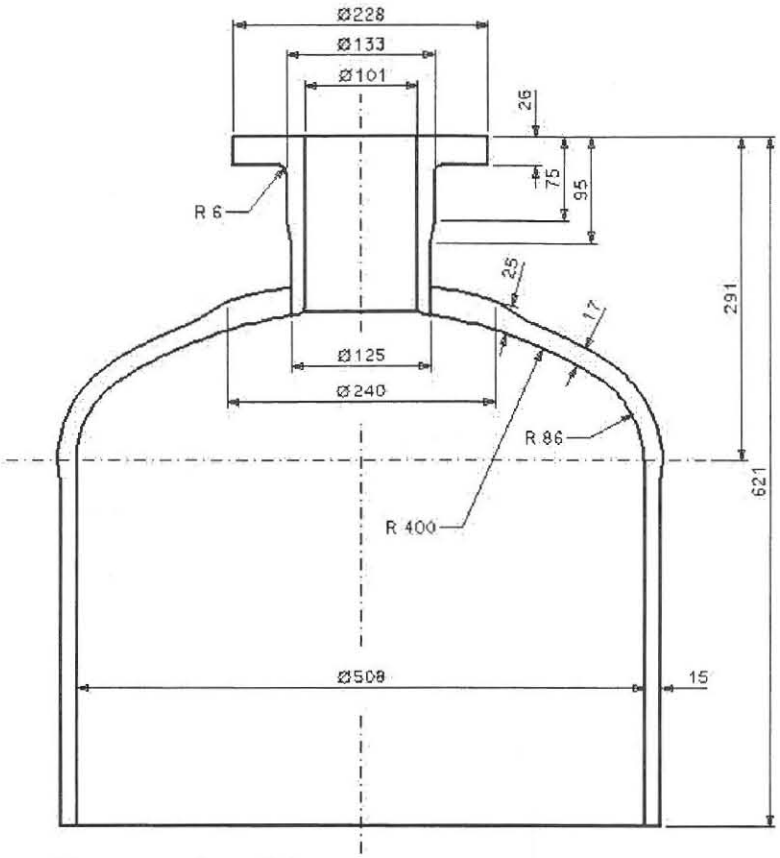

Fig. 6.53 Actual dimensions for finite element model

Table 6.6 Material properties for vessel analyses

Model	Structural properties	Surface layer properties
D_1	Property 1	None
D_2	Property 1	Property 8
D_3	Property 6	None
D_4	Property 6	Property 8
D_5	Property 7	None
D_6	Property 7	Property 9

Since it is not possible to specify the exact principal material direction for each element the model was divided into regions with specific regional principal material directions by considering the material property assignments for thermal loading given in Table 6.1.

These regions are shown in Fig. 6.54 indicating the model 1st material direction (n) with respect to the model global y-axis. The model 2nd and 3rd material directions, s and t, are determined as is described in 6.1.1.2. It must be stated that the global co-ordinate system used for these models is valid for ALGOR® [43] axisymmetric models and might differ if other FEA software is utilised.

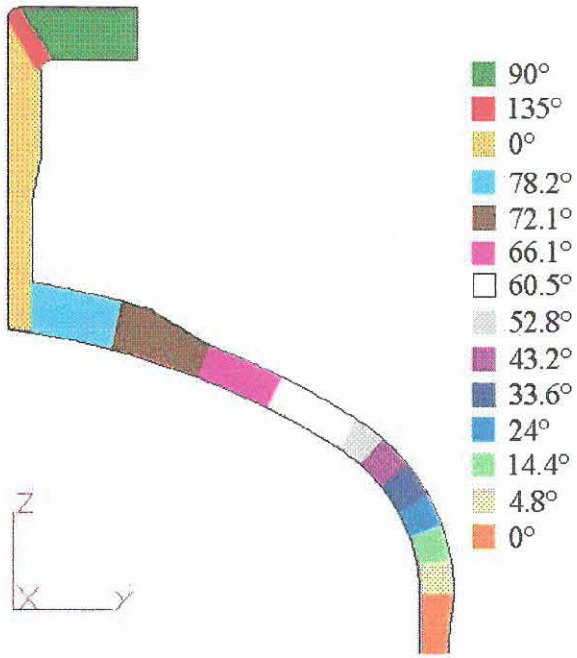

Fig. 6.54 Global 1st principal material directions relative to model y-axis

With the post-cure shrinkage (S) being used, by analogy, as a coefficient of thermal expansion a temperature change of 1 °C was applied to all the nodes and analysed to obtain the stresses, strains and displacements resulting from the shrinkage of the resin. Fig. 6.55 to Fig. 6.58 show the predicted in-plane shrinkage strains, in the 1st material direction, for models D_1, D_2, D_3, D_4, D_5 and D_6 respectively.

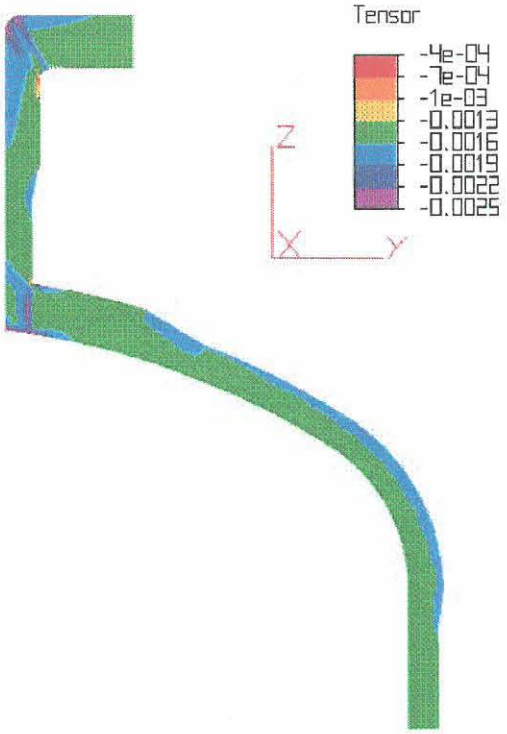

Fig. 6.55 Predicted in-plane strains (ε_1) for D_1

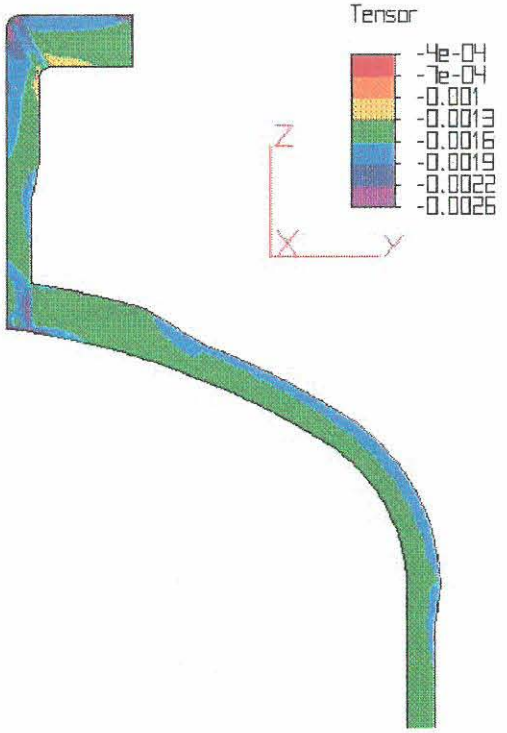

Fig. 6.56 Predicted in-plane strains (ε_1) for D_2

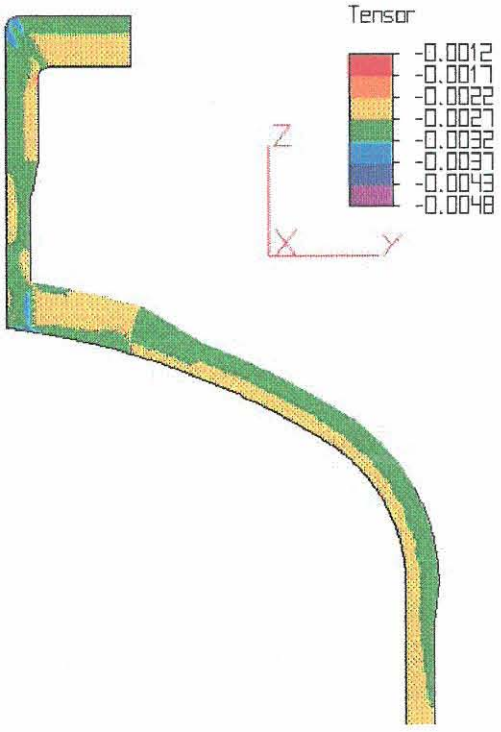

Fig. 6.57 Predicted in-plane strains (ε_1) for D_3

Fig. 6.58 Predicted in-plane strains (ε_1) for D_4

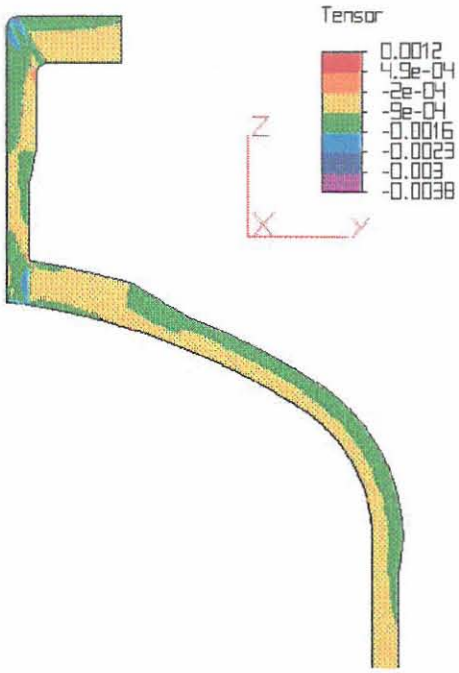

Fig. 6.59 Predicted in-plane strains (ε_1) for D_5

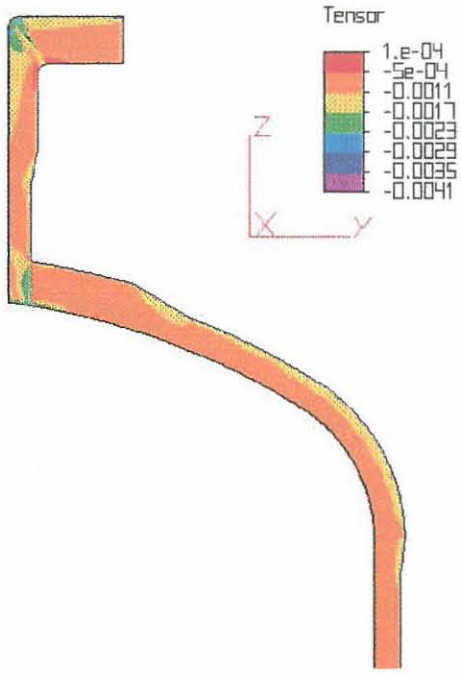

Fig. 6.60 Predicted in-plane strains (ε_1) for D_6

Fig. 6.61 to Fig. 6.66 show the predicted hoop shrinkage strains, in the 2nd, hoop, material direction, for models D_1, D_2, D_3, D_4, D_5 and D_6 respectively.

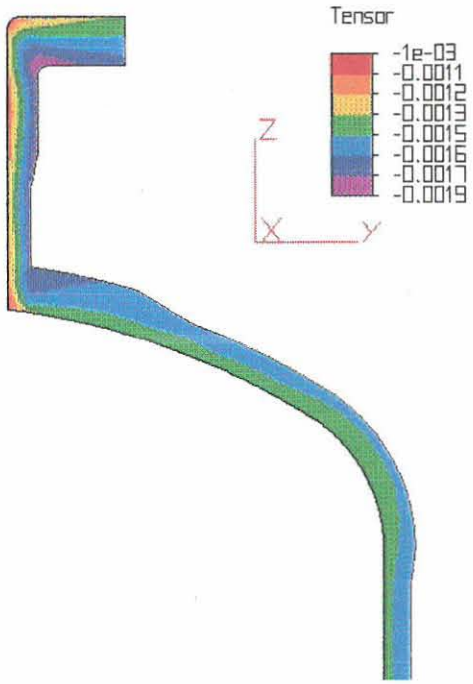

Fig. 6.61 Predicted hoop strains (ε_2) for D_1

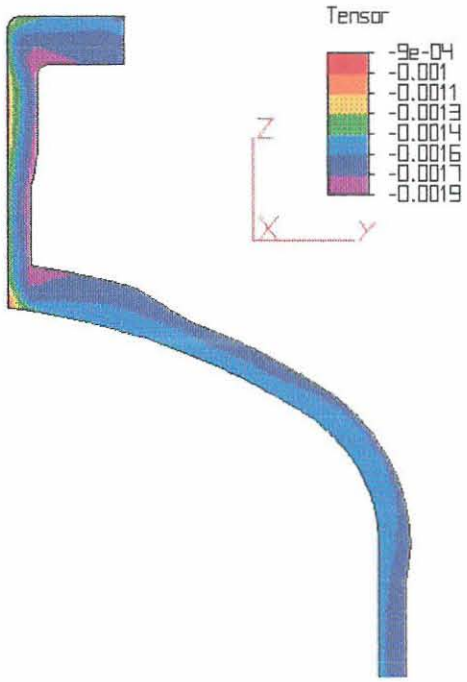

Fig. 6.62 Predicted hoop strains (ε_2) for D_2

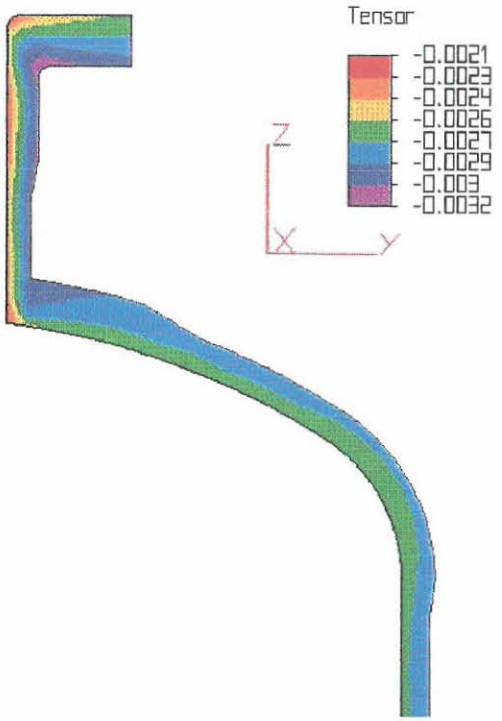

Fig. 6.63 Predicted hoop strains (ε_2) for D_3

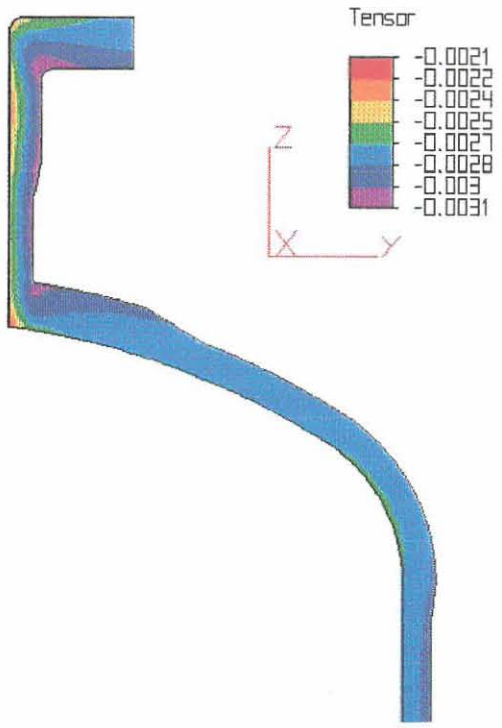

Fig. 6.64 Predicted hoop strains (ε_2) for D_4

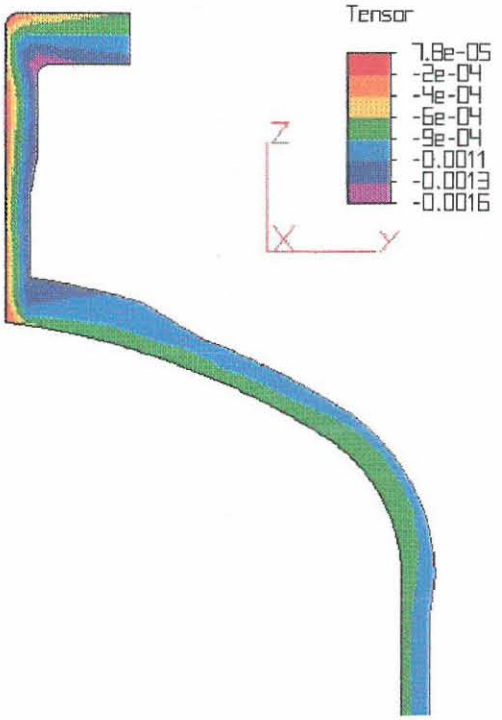

Fig. 6.65 Predicted hoop strains (ε_2) for D_5

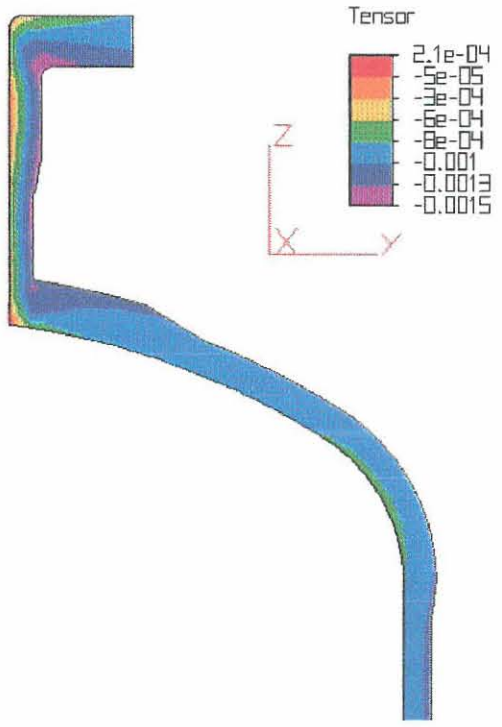

Fig. 6.66 Predicted hoop strains (ε_2) for D_6

Fig. 6.67 and Fig. 6.72 show the predicted through-thickness shrinkage strains, in the 3rd material direction, for models D_1, D_2, D_3, D_4, D_5 and D_6 respectively.

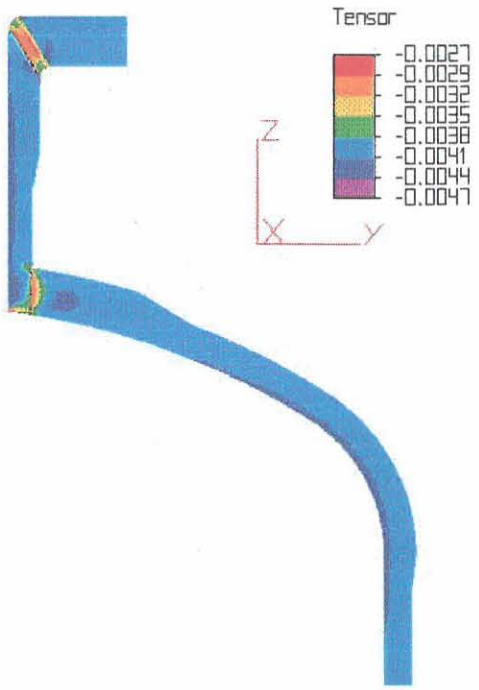

Fig. 6.67 Predicted through-thickness strains (ε_3) for D_1

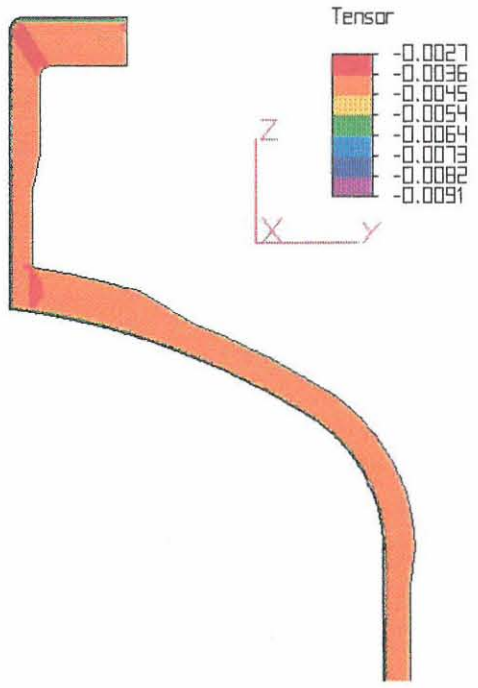

Fig. 6.68 Predicted through-thickness strains (ε_3) for D_2

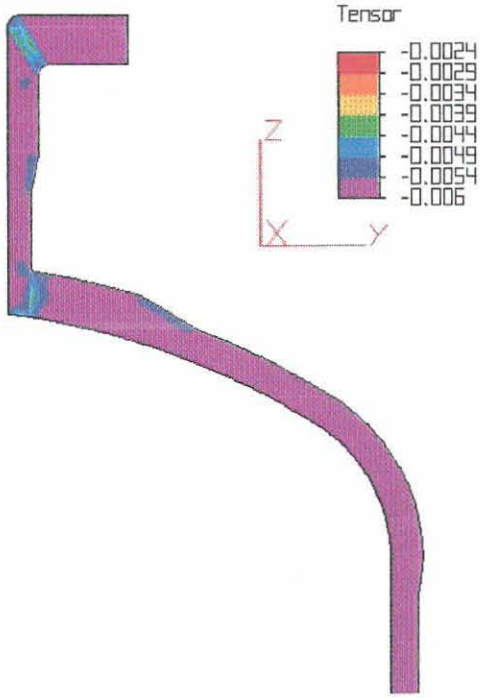

Fig. 6.69 Predicted through-thickness strains (ε_3) for D_3

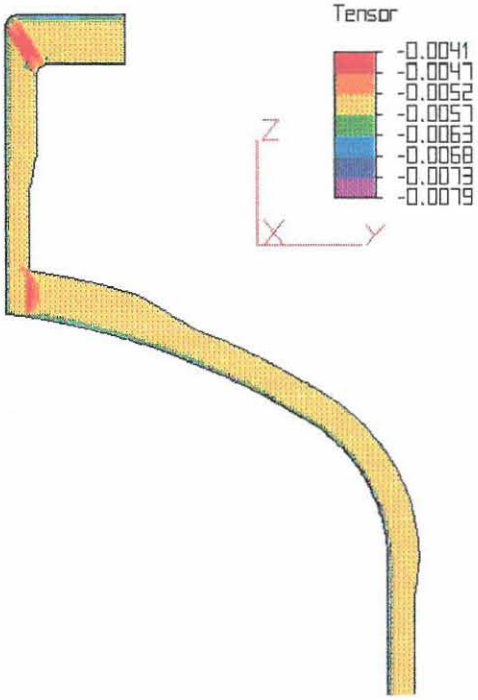

Fig. 6.70 Predicted through-thickness strains (ε_3) for D_4

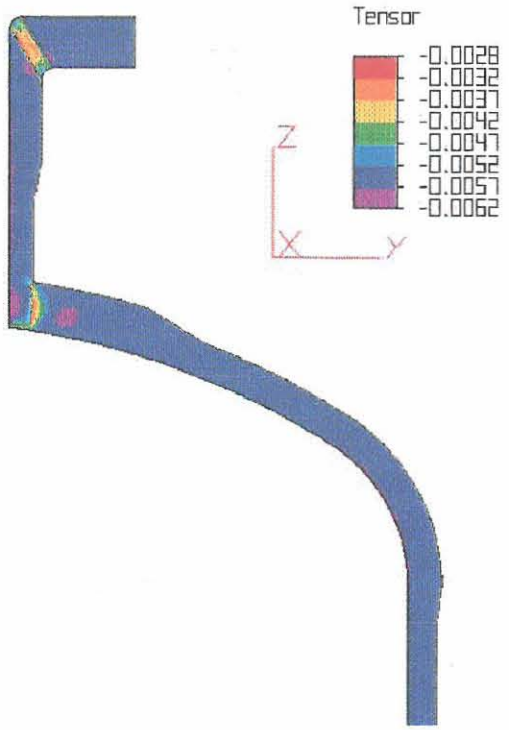

Fig. 6.71 Predicted through-thickness strains (ε_3) for D_5

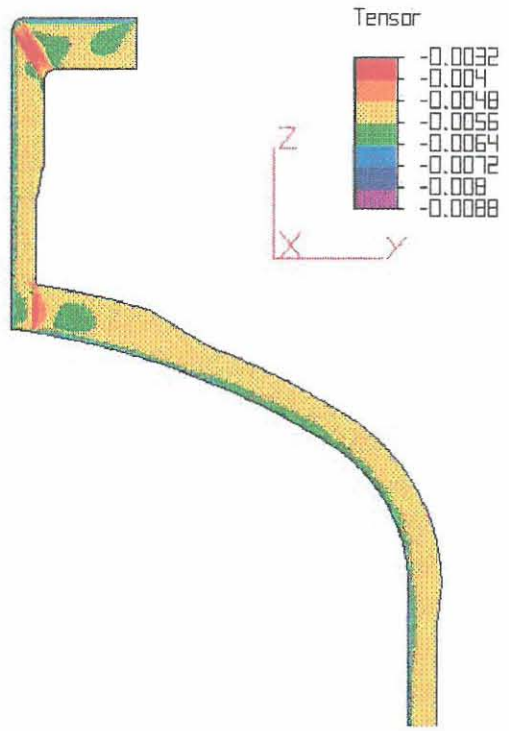

Fig. 6.72 Predicted through-thickness strains (ε_3) for D_6

The predicted strains at each of the measurement positions are given in Table 6.7. Direct comparisons of the 1st and 2nd principal post-cure strains, ε_1 and ε_2, to the experimental strain values, obtained from Table 5.6, at each of the measurement positions are presented Fig. 6.73 and Fig. 6.74.

Table 6.7 Predicted post-cure strains at nozzle-dished end connection

Strain location	Model D_1			Model D_2			Model D_3			Model D_4			Model D_5			Model D_6		
	Strain component ($\times 10^{-6}$)			Strain component ($\times 10^{-6}$)			Strain component ($\times 10^{-6}$)			Strain component ($\times 10^{-6}$)			Strain component ($\times 10^{-6}$)			Strain component ($\times 10^{-6}$)		
	ε_1	ε_2	ε_3	ε_1	ε_2	ε_3	ε_1	ε_2	ε_3	ε_1	ε_2	ε_3	ε_1	ε_2	ε_3	ε_1	ε_2	ε_3
1	-2128	-1301	-3976	-2424	-1306	-8401	-3395	-2526	-5525	-3679	-2519	-7242	-1923	-477	-5462	-2364	-460	-7716
2	-1360	-1135	-4300	-1276	-1130	-9090	-2613	-2334	-5803	-2519	-2348	-7891	-623	-161	-5977	-458	-176	-8788
3	-1463	-1475	-4132	-1498	-1539	-8776	-2703	-2717	-5660	-2724	-2763	-7584	-771	-795	-5693	-800	-858	-8271
4	-1383	-1404	-4179	-1396	-1459	-8836	-2616	-2638	-5703	-2654	-2679	-7638	-628	-664	-5767	-680	-721	-8365
5	-1413	-1436	-4163	-1479	-1494	-8788	-2650	-2674	-5688	-2687	-2716	-7613	-682	-723	-5743	-733	-782	-8324
6	-1544	-1274	-4209	-1602	-1340	-4120	-2799	-2489	-5743	-2829	-2527	-5686	-931	-419	-5822	-961	-466	-5746
7	-1500	-1530	-4146	-1578	-1580	-4084	-2746	-2777	-5686	-2802	-2808	-5644	-843	-895	-5728	-924	-937	-5668
8	-1609	-1580	-4042	-1698	-1642	-3987	-2867	-2834	-5577	-2925	-2875	-5545	-1044	-989	-5537	-1125	-1045	-5493
9	-1693	-1562	-4014	-1743	-1626	-3971	-2959	-2814	-5550	-2992	-2856	-5525	-1197	-956	-5488	-1241	-1015	-5454
10	-1624	-1600	-4028	-1663	-1667	-3988	-2882	-2856	-5564	-2907	-2900	-5541	-1069	-1026	-5512	-1103	-1087	-5480
11	-1646	-1228	-4157	-1871	-1190	-8765	-2911	-2438	-5667	-3055	-2431	-7583	-1117	-333	-5753	-1311	-321	-8294
12	-1878	-1199	-4073	-1986	-1390	-8608	-3163	-2410	-5604	-3247	-2533	-7439	-1537	-285	-5593	-1657	-452	-8044
13	-1202	-1804	-4101	-1220	-1804	-4094	-2416	-3081	-5650	-2430	-3077	-5646	-295	-1400	-5613	-316	-1391	-5608
14	-1556	-1741	-4005	-1659	-1843	-3930	-2809	-3013	-5552	-2878	-3078	-5509	-948	-1288	-5462	-1043	-1376	-5403
15	-1515	-1569	-4080	-1529	-1622	-3899	-2762	-2821	-5611	-2768	-2854	-5487	-869	-968	-5604	-878	-1013	-5432
16	-1532	-1455	-4115	-1603	-1523	-8741	-2780	-2695	-5642	-2828	-2744	-7547	-900	-759	-5667	-967	-826	-8212
17	-1523	-1598	-4068	-1617	-1677	-4005	-2771	-2854	-5603	-2834	-2906	-5566	-884	-1022	-5579	-972	-1094	-5528
18	-1493	-1712	-4044	-1484	-1762	-4028	-2742	-2978	-5582	-2736	-3009	-5574	-837	-1229	-5537	-828	-1270	-5527

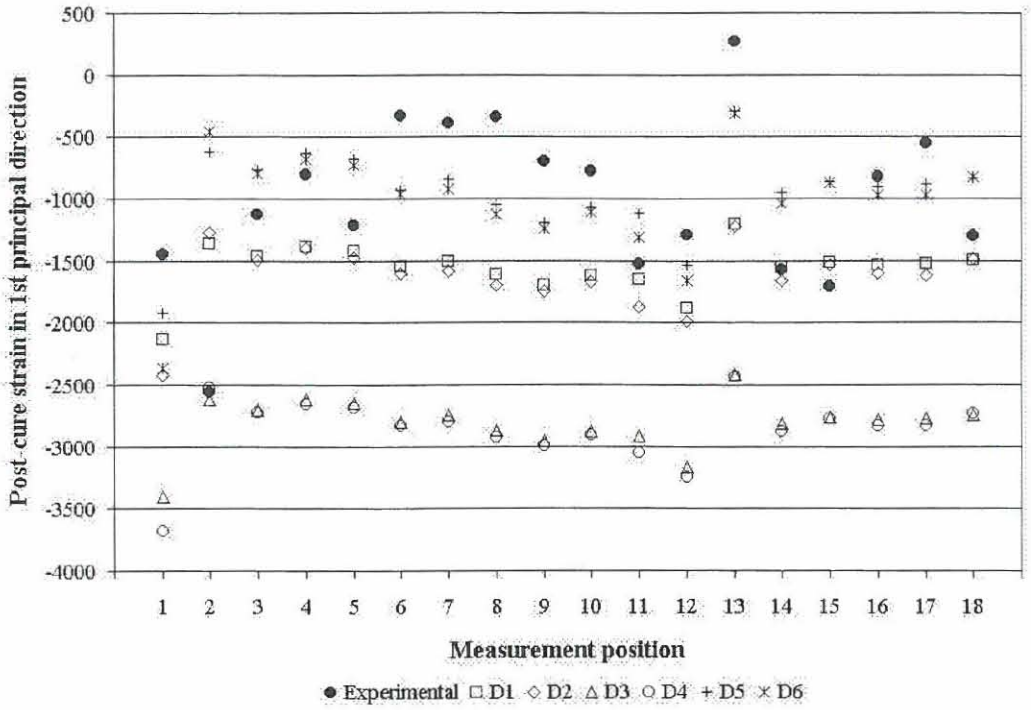

Fig. 6.73 Comparison of predicted in-plane post-cure strain (ε_1) to experiment

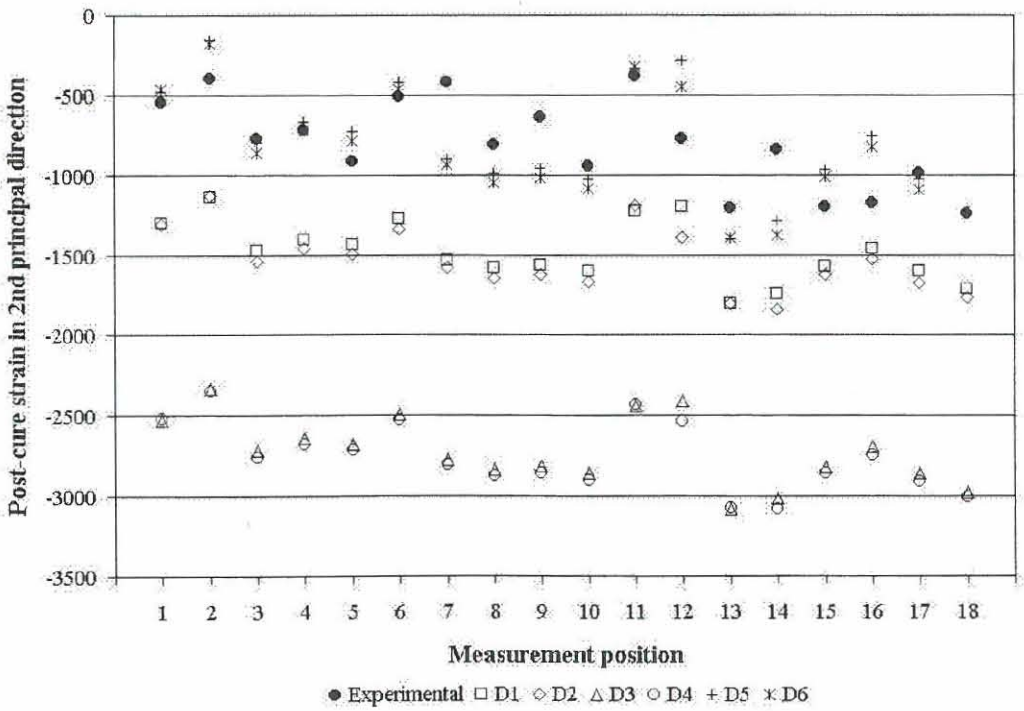

Fig. 6.74 Comparison of predicted in-plane (hoop) post-cure strain (ε_2) to experiment

From Fig. 6.73 and Fig. 6.74 it is necessary to determine which of the six finite element models is the most accurate. As a measure of accuracy the deviations, of the analysis results from the experimental, were determined and are presented graphically in Fig. 6.75 and Fig. 6.76 for the 1st and 2nd principal material directions respectively.

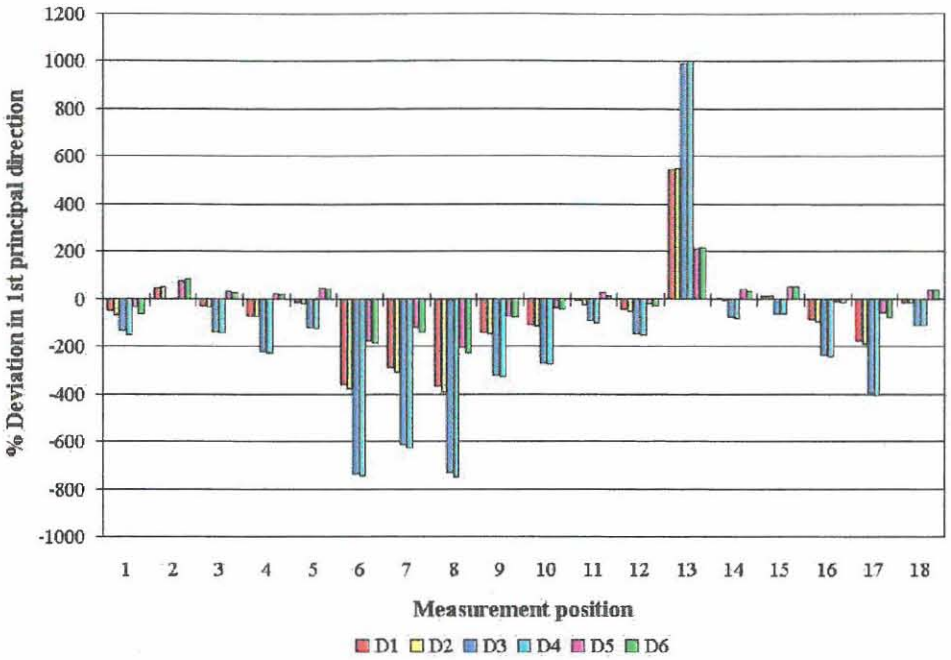

Fig. 6.75 Deviation of predicted in-plane post-cure strain (ε_1)

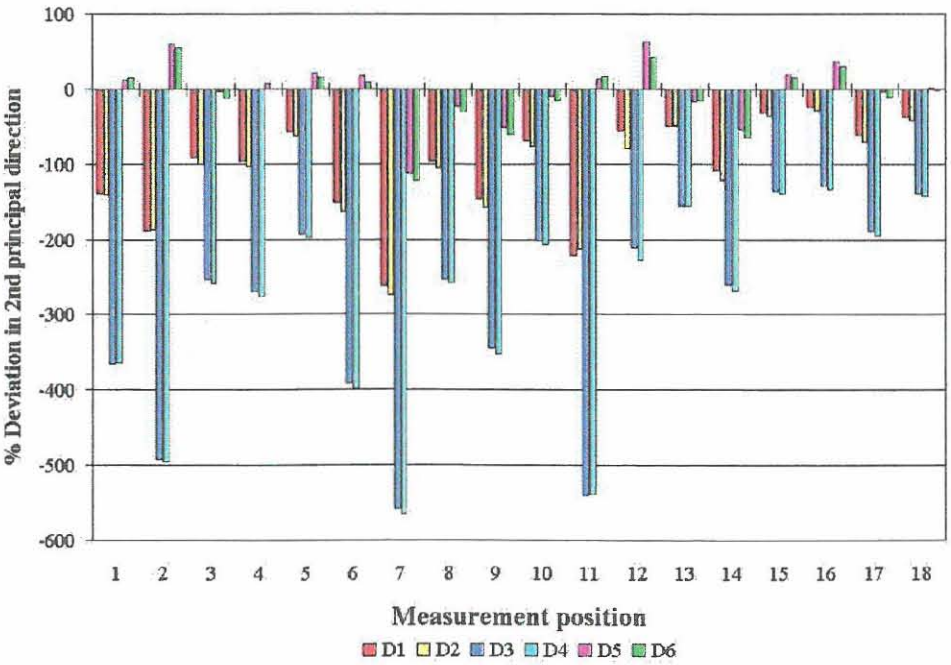

Fig. 6.76 Deviation of predicted in-plane (hoop) post-cure strain (ε_2)

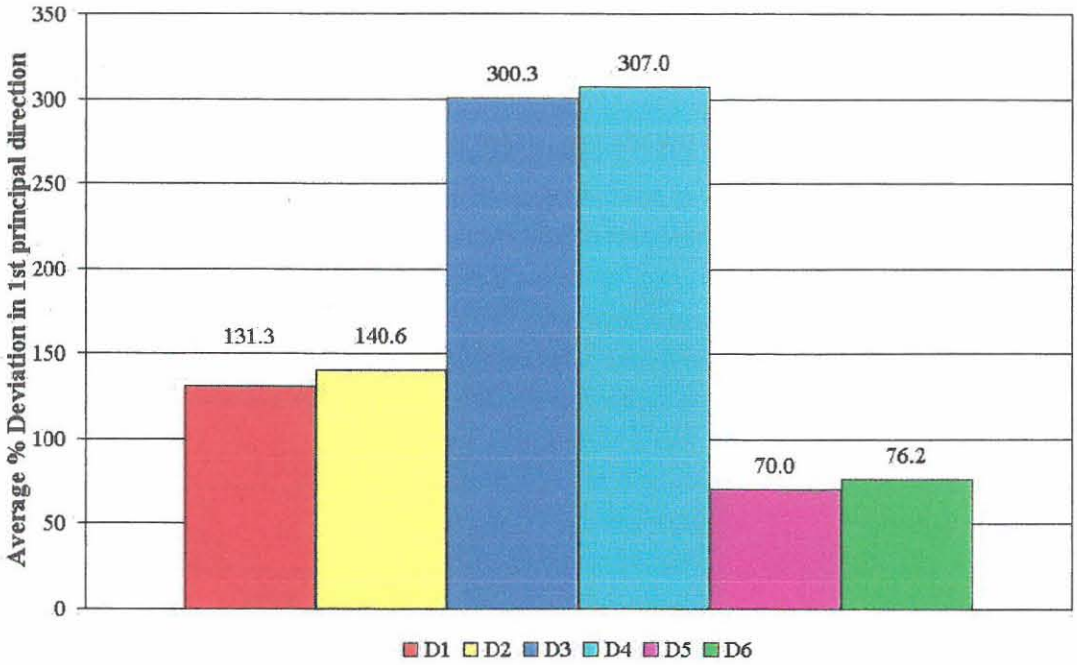

Fig. 6.77 Average deviation of predicted in-plane post-cure strain (ε_1)

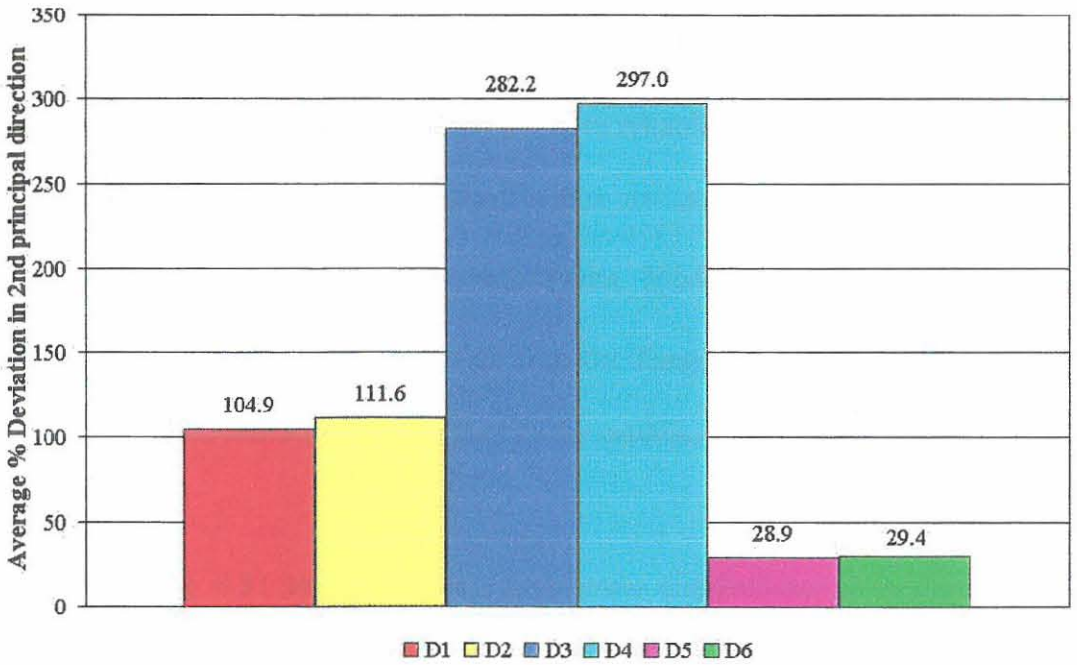

Fig. 6.78 Average deviation of predicted in-plane (hoop) post-cure strain (ε_2)

To determine the most accurate analysis, mean deviations for the whole model were obtained by averaging the deviations at all the measurement positions in Fig. 6.77 and Fig. 6.78 to give global averaged deviations, which are shown in Fig. 6.79.

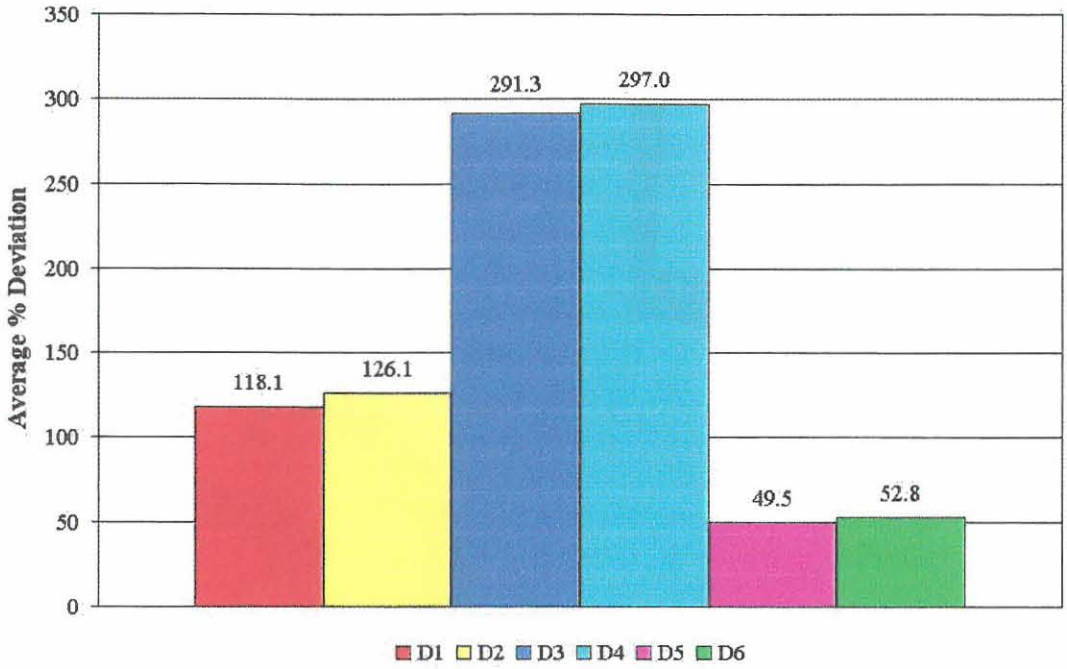

Fig. 6.79 Global averaged deviation of predicted post-cure strains

The averaging of these deviations should be more reliable than the averaging presented in 6.2 since a greater number of measurement points are considered. Fig. 6.79 indicates that model D_5 presents the most accurate overall results. Model D_6, with the resin rich surface, seems to be slightly less accurate, but as with the flange analyses presented in 6.3, it is suggested that particular attention be given to the models containing the resin rich surfaces.

Fig. 6.80 and Fig. 6.81 show the Von Mises stress distributions of models D_5 and D_6 respectively. From these figures it is clear that the general stress condition of the strength laminate is acceptable. The corrosion barrier is seen to play a dominant role in the post-cure stress development. Comparative stress magnitudes are the positions shown in the figures are presented in Table 6.8. It is clearly shown that the stress magnitudes in the

corrosion barrier, presented by model D_6, should be cause for concern. These high stresses would not affect the mechanical strength of the laminate but is so that crazing of this surface can occur.

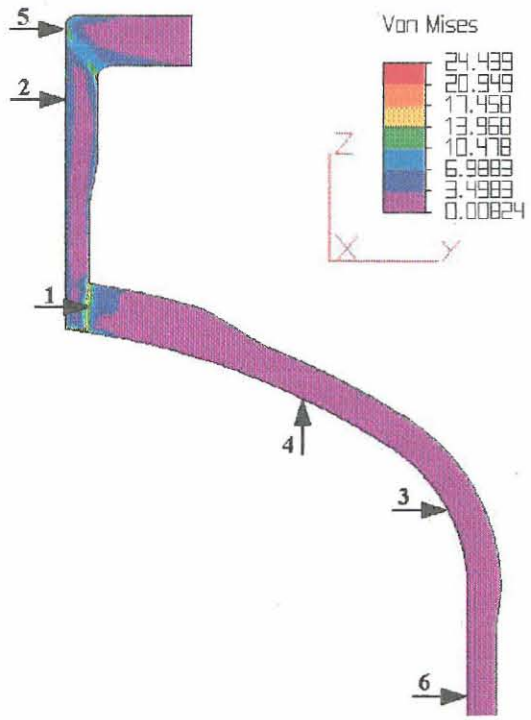

Fig. 6.80 Predicted Von Mises stresses for D_5

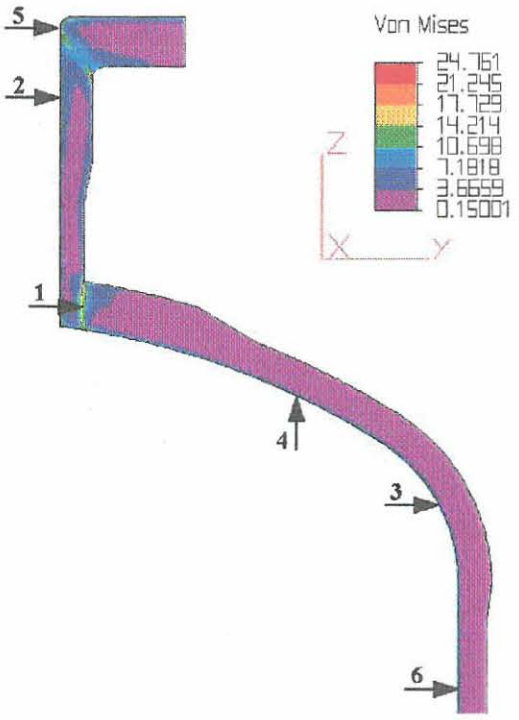

Fig. 6.81 Predicted Von Mises stresses for D_6

Table 6.8 Von Mises stresses in models D_5 and D_6

Position	Model Von Mises stress (MPa)	
	D_5	D_6
1	15.3	15.4
2	8.3	16.5
3	3.5	16.2
4	1.9	15.5
5	15.8	12.6
6	0.9	14.9

Local shear stresses are also present in the region where the nozzle had been inserted in the dished-end resulting from the abrupt change in fibre orientation. The shear stress

magnitudes, Fig. 6.82 and Fig. 6.83, can be seen as acceptable for this specific case, but should the thickness of the shell be greater, therefore presenting a larger through-thickness shrinkage, the importance of this stress could rise. High shear stresses are also evident in the flange-nozzle transition area although the magnitudes seem to be acceptable.

Fig. 6.82 Predicted shear stress distribution for D_5

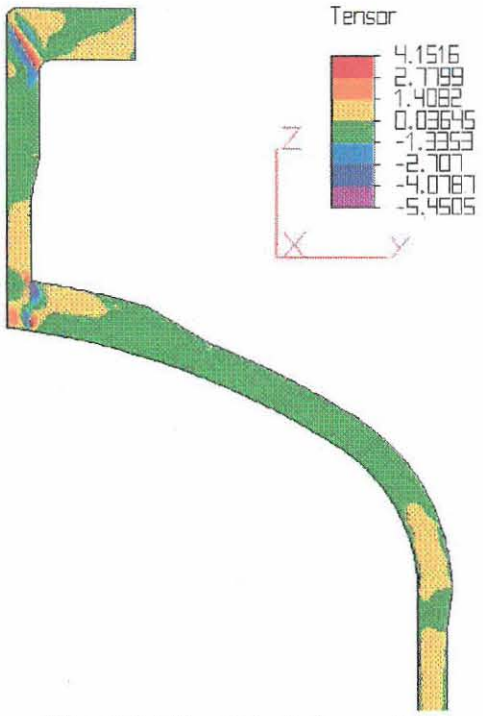

Fig. 6.83 Predicted shear stress distribution for D_6

7. DISCUSSION

7.1 Factors influencing accuracy of experimental and numerical results

7.1.1 Factors influencing material elastic properties

Various factors influence the accurate prediction of the material elastic properties of any fibre reinforced plastic material. The theories and procedures currently available for the calculation of these properties mainly consider materials that have unidirectional fibres. Various methods are available to determine the material elastic properties of random oriented fibre laminates. These methods usually include empirical factors, that must to be estimated, that allow the theories developed for unidirectional fibre laminates to be applicable in random oriented fibre laminates. The magnitudes of these factors are usually suggested to be within specified ranges that have been determined by experimentation. However, it is usually also suggested that these factors be determined experimentally for the specific system under consideration. The designer does not always have the specific factors for the system that is required and often does not have the facilities to determine them experimentally. Therefore the magnitudes of these factors are usually assumed causing the elastic properties to differ from the actual values.

Since many products are made over a period of time, especially when a component is large in its physical size or when a large number of layers need to be applied, the degree of cure could vary through the thickness of the laminate. Should specimens be tested for material properties, inaccurate results would or might be obtained if the tests were performed on laminates where the degree of cure is not the same through the material thickness.

When material elastic properties are calculated it is assumed that the laminates are in a fully cured state and that the material properties are the same at any position in the component. Properties such as Young's modulus develop as the degree of cure reaches completion, therefore the laminate properties of a laminate would differ, however slightly, from prior to the post-cure process to after the completion of the post-cure process. These slight changes would not have a significant effect on the properties used in the finite element model.

One of the major factors influencing the calculation of the laminate elastic properties is the fibre volume fraction. When designing a component it is usually specified what the volume fraction should be and it is assumed that it would be uniform throughout the construction under consideration. It is difficult to maintain a consistent volume fraction while manufacturing the component, especially when the hand lay-up method is used. The fibre volume fraction can also vary dramatically in different volumetric areas in a component. Areas with a high concentration of resin can exist in and around sharp corners of a component, e.g. in the heel and the neck of a flange. This high concentration is usually obtained due to the resistance of the fibre mat to bend or form into or around a sharp bend. The manufacturer then tends to apply more resin in that area to prevent voids occurring.

7.1.2 Factors influencing the measurements taken by the strain gauge technique during cure and post-cure

A major concern during strain gauge measurements on any system is the quality of the adhesion of any particular gauge to the specimen being tested. This concern is especially greater when gauges are attached to rough surfaces such as a composite laminate. Anomalies in the material such as voids, cracks, or even variations in bond thickness of the

cement could influence the recorded strain values. Although every effort was made to avoid these anomalies, some might have been present at or near some of the gauge positions. A specific factor that could have influenced the strain measurements in this study, which could not have been avoided, is the matrix volume fraction at the gauge positions. The volume fraction is usually determined by burn-off test of a cut-out or off-cut of a section of the laminate and is taken as an average value of the component. Small areas of matrix concentration could occur during the manufacturing stage, as explained in 7.1, and this could influence measurements taken at that position. This could be equated to a small piece of resin casting placed in the laminate at the gauge position and the strain measurement would be similar to that of the resin cure shrinkage instead of the laminate cure shrinkage.

It is assumed that components manufactured with CSM as reinforcement have iso-planar mechanical properties in the in-plane directions. This assumption is valid if a large area of the laminate is considered. However, due to the manufacturing method of the CSM, iso-planar properties can not be guaranteed when only considering a very small plane area, see Fig. 7.1.

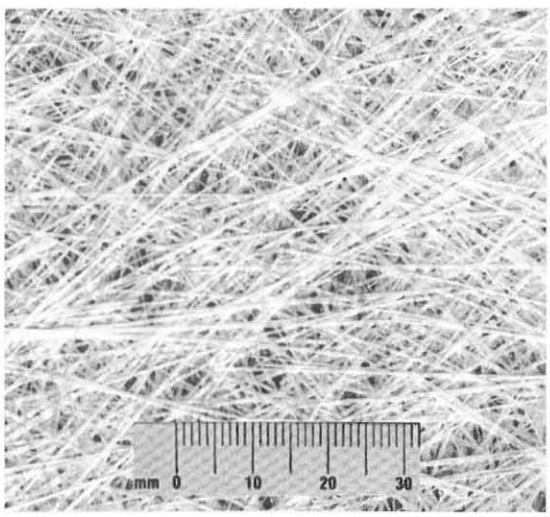

Fig. 7.1 Planar fibre directions of chopped strand mat

The stress and strain predictions are obtained from true iso-planar properties but the strain measurements could be affected by localised non-iso-planar properties. To overcome some of the problems stated above strain gauges with long gauge lengths and recordings at multiple positions with averaged results could be used on the laminates and more representative or accurate results would be obtained. The majority of the gauges used in this study had a gauge length of 2 mm, which might have been too short for the purpose that they were used.

7.1.3 Factors influencing the accuracy of the results obtained from the finite element analyses

As mentioned previously, the accuracy of the material elastic properties are of great importance when predicting the behaviour of a structure. In composite materials the fibre directions play a governing role when predicting mechanical and thermal behaviour and the consequent stress development. When composite material components are designed the fibre orientations of each layer are specified in the manufacturing specifications to ensure that the final product resembles the design so that it would behave as was predicted. However, during the manufacturing process it is not always possible to maintain the fibre directions as specified and the stresses developed under the operating conditions would the differ from those that were predicted in the design.

It is usually required to assume layer directions for material property assignments and is not always possible to use methods such as the photographic scans, shown in Picture 6.1 and Fig. 6.29, to give these directions. The assumed layer directions would largely be dependent on the designer's knowledge of and experience in the manufacturing process. Detailed knowledge of the manufacturing process and discussions with experienced manufacturers would assist in these assumptions.

Stress prediction during the design phase is also conducted on models with exact geometric sizes according to the design. The final product seldom reflects the exact dimensions as was given in the design. Unless it can be guaranteed that the dimensions of the final product would be as is specified in the design the stresses predicted in the models might only be used as guidelines.

The finite element analysis strain predictions are usually given at nodal positions and do also vary slightly at neighbouring nodes. In this study the simulated results were obtained by averaging three nodal results at the respective gauge positions.

7.1.4 General comments on the accuracy of experimental and numerical results

The most important factor influencing the material elastic properties is the fibre and matrix volume fractions. Slight variations in the fibre or matrix moduli or Poisson's ratios would not have such a significant effect when calculating the laminate elastic properties as the volume fractions. The effect of a high matrix volume fraction is clearly shown in the finite element models presented in Chapter 6 where resin rich surface layers are present, producing higher shrinkage strains than the layers with lower matrix volumes. It is therefore most important to use, or assume, volume fractions that are known to be accurate for the manufacturing method to be employed.

7.2 Discussion of experimental tests and finite element predictions

7.2.1 50NB Pipe

During the planning of this experiment it was decided to measure the strains produced by the shrinkage of the resin as each layer was added. It was expected to obtain strain readings that showed shrinkage in both the longitudinal and hoop directions as the layers

were applied. The growth in the hoop strain was not expected and thus the same experimental procedure was applied to the second tube, presenting similar results.

These experiments showed that not only are strains produced during post-cure but that strains are also produced in the laminate during lay-up, especially in the first layer, that should be considered in the design. It is believed that the magnitude of the strains developed during lay-up would depend on the ratio of the tube inner diameter and wall thickness and also ambient manufacturing conditions such as humidity and temperature. The results on the tubes show that residual manufacturing hoop strains might not be as large in magnitude if the strains developed during post-cure are considered in combination with the strains developed during lay-up.

The experimental post-cure shrinkage measured on the inner surface of the two tubes do not compare well. This is probably due to the factors influencing the measurements given in 7.1.2.

By comparing the predicted strains of the six models to the experimentally recorded strains it can be seen that, for this case, the models with the material properties determined by Schapery's method [31] were the most accurate. The hoop strains predicted on the models with only the strength laminate were within 34% of the measured values. The addition of the corrosion barrier in the analyses caused this accuracy to be less but Fig. 6.27 and Fig. 6.28 clearly show that it has a significant effect on the surface stresses. On this pure tubular case the Von Mises stress at the surface increases from 7.2 MPa to 25.5 MPa. The magnitude of the surface stress, 25.5 MPa, should be of concern as it is more than sufficient to promote EAC in certain environments.

7.2.2 50NB Hubbed full-face flange

The strains produced during lay-up were not recorded as were done with the tubes. This was purely due to the manufacturing and handling methods employed presenting risks of cable breakage. It can be assumed that the strains during lay-up would be significant at the flange face since visible pullback occurred. The post-cure process also caused additional pullback, which would have increased the radial strains at the flange face near the heel.

Some manufacturers apply additional layers with high resin (matrix) fractions as an initial layer thus providing material to be machined flat after manufacture. This might not be good practice if post-cure had to be applied since, as is shown in 6.3, high surface stresses are developed when a resin rich surface is present during post-cure. Although the machining of the flange face could assist in reducing the residual stresses at the surface, it could be possible for crazing to occur during post-cure and the thickness of material to be removed when machining not being sufficient to remove the cracks.

Whilst planning and experimenting with the finite element modelling it was found that the general assumptions made, with reference to the fibre or layer directions, did not necessarily produce results that were comparable to the experimental values. Furthermore, the initial analyses did not include a resin rich surface, which also influenced the results.

By using the photographic scan to determine the layer directions and applying the resin rich surface layer the predicted stress distributions improved and confidence in the results developed.

By comparing the predicted strains of the six models to the experimentally recorded strains it can be seen that, for this case, the models with the material properties determined by the Halpin-Pagano methods [32] were the most accurate. The average results were within 23% of the measured strains. It must be kept in mind that the accuracy of the results depends highly on the factors mentioned in 7.1.

7.2.3 Nozzle-vessel connection

As with the flange, the strains produced during lay-up were not measured. The experimentally recorded strains and the finite element analyses only consider the strains produced as a result of post-cure shrinkage. It can also be assumed that strains were developed at the inner surface during lay-up and that these strains would have some effect on the total manufacturing residual stress conditions.

The layer directions were not determined by photographic scans but were estimated and assumed to be reasonable for this case. The layer directions in the area at the heel of the flange might have been more specific, similar to that presented in Fig. 6.31.

It is shown that the resin rich surface layer does have a significant influence on the surface stress conditions. The stresses developed at the resin rich surface is such that EAC can be assisted. This is particularly evident when comparing the stress shown in Table 6.8.

By comparing the predicted strains of the six models to the experimentally recorded strains it can be seen that, for this case, the models with the material properties determined by Schapery's method [31] were the most accurate. The average results were within 50% of the measured values. This accuracy could be affected by the factors presented in 7.1.

7.2.4 General comments on the experimental tests and finite element predictions

The FEA models do not take the variation in modulus during post-cure into account. At elevated temperatures, the modulus of the matrix could be such that interfacial stress relaxation would occur. The magnitudes of the strains developed during post-cure are dependent on the temperature at which post-cure is effected. The ideal condition would be to obtain a constant through-thickness temperature as close to the glass transition temperature without damaging the fibre-matrix cohesion. The cooling after post-cure should then be applied for a period as long as practically possible to prevent steep temperature gradients within the specimen.

The accuracy of the measurements taken during the experimental testing can not be quantified due to the possible local effects of anomalies in the material at the gauge positions. If it were assumed that no local anomalies were present at the gauge positions then the accuracy of the finite element results would not be sufficient, except for the flange models F_3 and F_4. An accuracy of within 20% of the measured strains is suggested to be acceptable for the material and manufacturing methods used in this study.

7.3 Relevance to industry

The study has produced information that is directly applicable to the GRP vessel industry. GRP vessels and tubing are often manufactured, installed and commissioned without undergoing any post-cure process. The post-cure is then completed *in situ* over a lengthened time period. This period and the degree of cure will be dependent on the operating temperature of the process plants. The *in situ* post-cure of the vessels and piping

during operation could create additional problems due to the mechanical constraints applied to the vessels and piping.

Allowances for thermal expansion are usually made for any system of process piping but very seldom made for permanent shrinkage due to cure. The magnitude of the CTE of a CSM pipe is approximately 65×10^{-6} mm/mm/°C, as is shown in 4.4.2, whilst the maximum cure shrinkage of the tube is approximately 1800×10^{-6} mm/mm. From Fig. 5.9 and Fig. 5.10 it can be deduced that should a CSM pipe system be commissioned to operate to 90°C, the longitudinal strain in the pipe would change very little as the operating temperature is reached and *in situ* post-cure shrinkage is obtained. Unexpected stresses will however occur when the plant is cooled to ambient. The *in situ* post-cure shrinkage should therefore be considered when pipe stresses and support positions are determined.

When repairs are carried out on vessels new layers are usually applied in and around the repair area. The base material would have undergone a post-cure procedure prior to installation or an in-service cure period causing the laminates to shrink by some degree. The repair material undergoes cure shrinkage during lay-up and then some form of post-cure shrinkage during service or during a special post-cure procedure being applied to the component. The cure and post-cure shrinkage of the new material will then induce shear stresses at the bonding surface, tensile stresses in the new material and compressive stresses in the base material. Although, at this stage, little can be done to prevent these stresses, special consideration should be given to it and additional monitoring procedures be created for these repair areas.

8. CONCLUSION

In this study, the thermo-chemical effects of post-cure in tubular products of practical dimensions were studied. Various assumptions and considerations were made that could have influenced the results obtained from the finite element analyses and those obtained from the experimental work. These assumptions are:

- the in-plane elastic properties of the laminate remain essentially isotropic since only CSM is used as reinforcement;
- values for the contribution factors required for the calculation of the material properties were assumed;
- no moisture deformation occurred during the manufacturing and post-cure processes;
- no mechanical forces or moments were applied and that the forces and moments resulting from post-cure shrinkage are taken as the total force and moment resultants;
- the layer directions, as applied in the finite element analyses, are sufficiently accurate for this study;
- the initial strain conditions in the test specimens were zero prior to applying the post-cure procedure;
- all layers were at the same degree of cure prior to post-cure;
- no in-plane - out-of-plane couplings occur in CSM layers;
- the temperature application during post-cure is such that full post-cure is effected;
- the fibre volume fraction is uniform (constant) throughout the models;
- no local anomalies are present at the gauge positions;
- no interfacial stress relaxation occurs between the fibres and the matrix during post-cure.

From this study the following conclusions can be made:

- The use of finite element modelling and analyses on composite material products similar to those in this study should be applied with care. This study has shown that the results can not be trusted in it entirety for the materials and method of manufacture used in this study. The results should only serve as guidelines to determine possible areas where special considerations to the stress condition are required.
- The use of a resin rich surface layer causes the stress condition at the surface to be so that EAC is assisted.
- The recorded post-cure shrinkage strains might not be sufficiently accurate due to the short gauge length of the strain gauges used at the majority of the measurement positions and also due to the factors mentioned in 7.1.2. Strain gauge measurement on composite components of similar construction to those in this study, as a measure of *in situ* component evaluation, should be applied with care and the results obtained should only be used as guidelines.

It is shown that the residual stress conditions as a result of cure shrinkage of the resin can be predicted and that various factors exist that determine the accuracy of the predicted results. Cases are presented showing that the high resin content in the corrosion barrier is the cause of high surface stress development and it is suggested that other methods of applying a corrosion barrier be considered or developed.

9. RECOMMENDATIONS

- When the need arises to employ strain gauge measurements on composite material components, it must be ensured that, to improve the accuracy of the measurements, gauges with long gauge lengths are used. It is suggested that a minimum gauge length of 5 mm be used for all general measurements.
- Improved testing methods should be developed for laminates constructed with CSM as reinforcement.
- Prior to assigning fibre or layer directions to a finite element model, the designer should discuss the manufacturing procedure or methods with experienced manufacturers in order to obtain directions that would be representative of the manufactured component.
- The thickness of the specific lay-up would not always be as is indicated on the manufacturing drawing. The designer should be aware of this and information from the manufacturers would help to determine more accurate thicknesses for various lay-ups.
- The fibre and matrix volume fractions for a specific laminate construction must be as accurate as reasonably possible for calculating the laminate material properties.
- It is recommended that more extensive studies be conducted on the effect that strains produced during lay-up, in combination with post-cure strains, have on laminates.
- Research should be conducted on the stress developments of resin rich surface layers by considering the manufacturing method. This research should consider the possible application of the corrosion barrier after manufacture and post-cure of the strength laminates and what the accompanying stress conditions would be.

- It is recommended that an in-depth study be conducted on stress conditions created as a result of repairs being done on aged laminates.

APPENDIX A. Recorded post-cure strains of 50 NB full-face flange

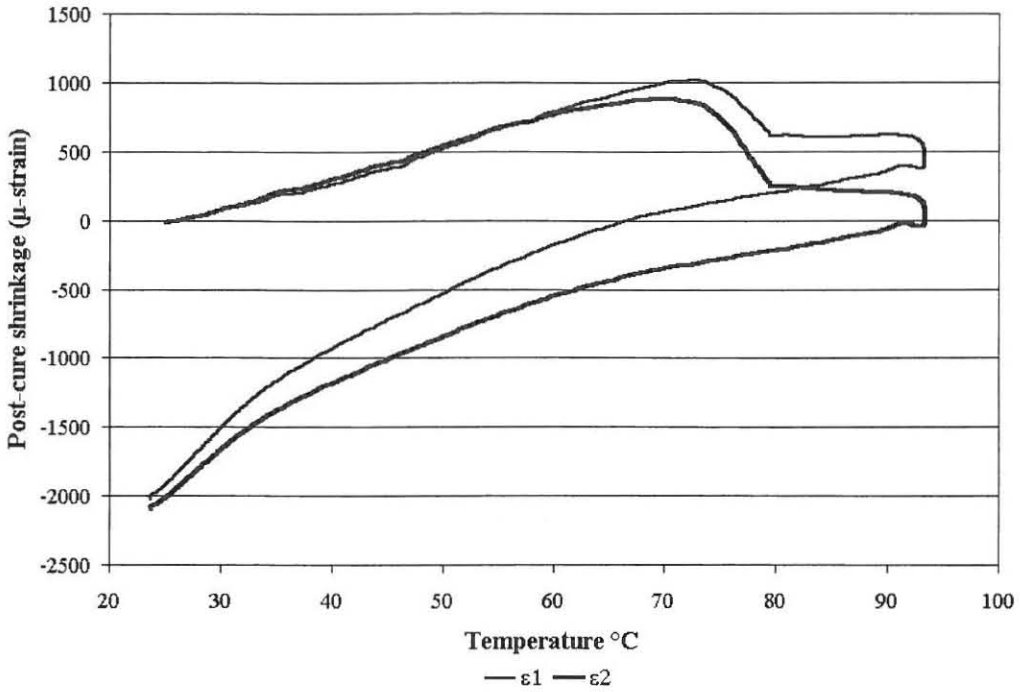

Figure A.1 Post-cure strains at position 1

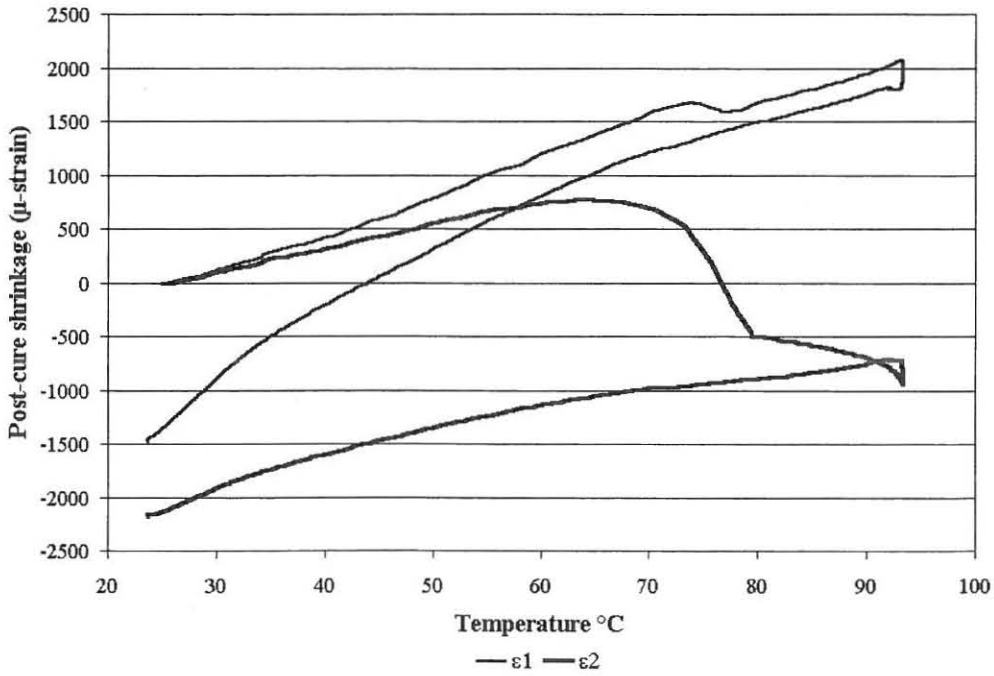

Figure A.2 Post-cure strains at position 2

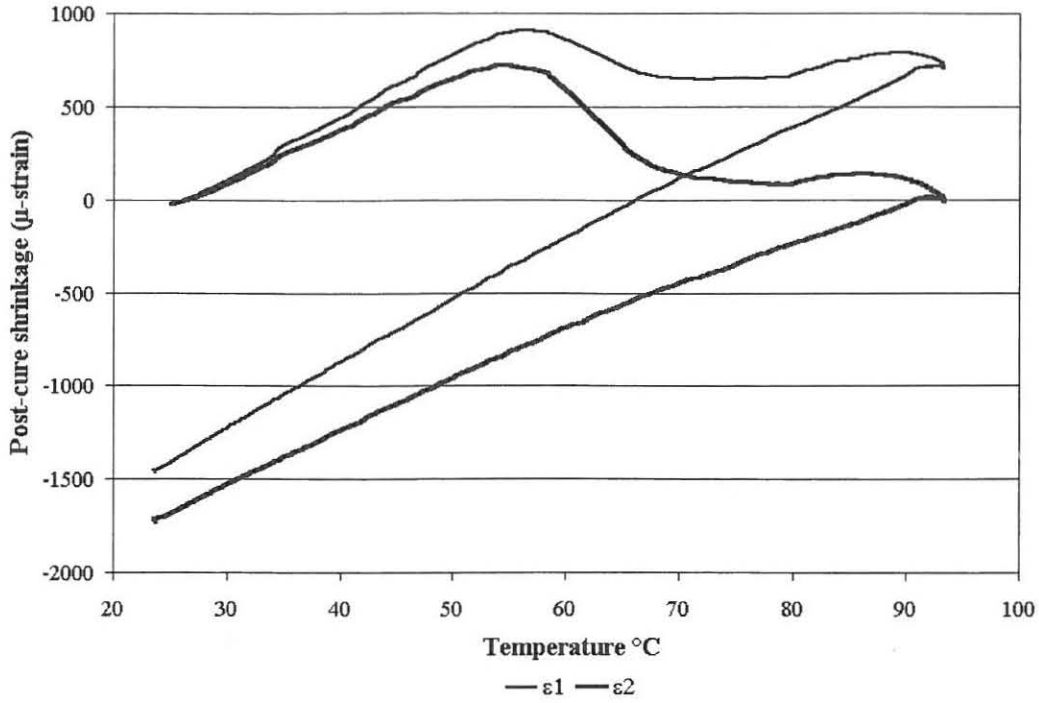

Figure A.3 Post-cure strains at position 3

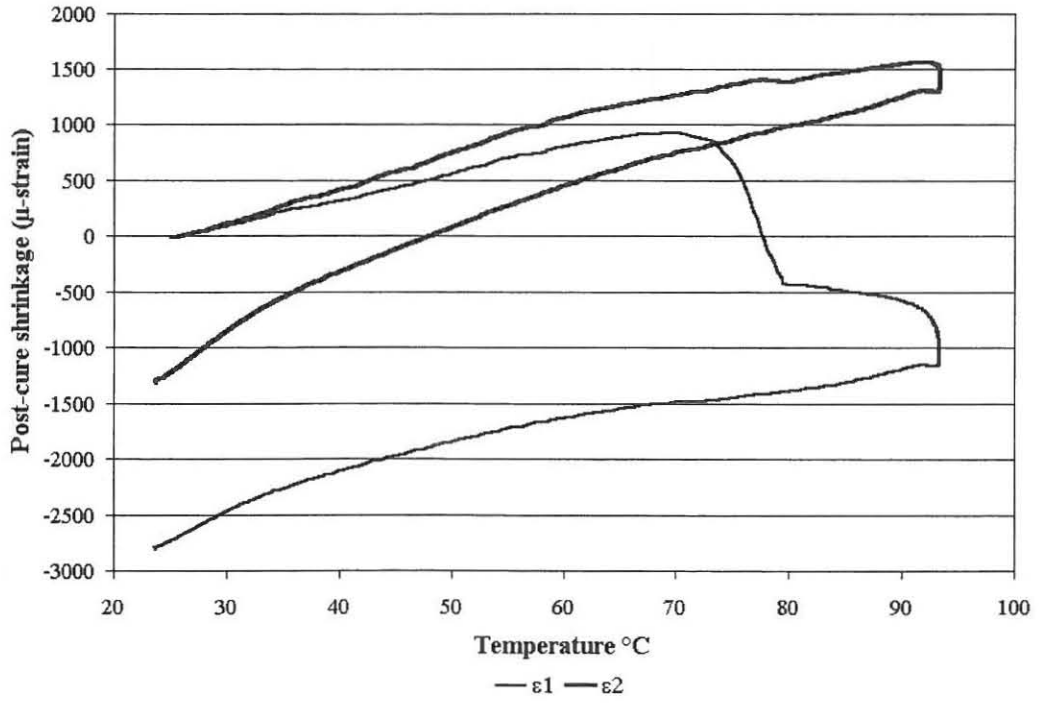

Figure A.4 Post-cure strains at position 4

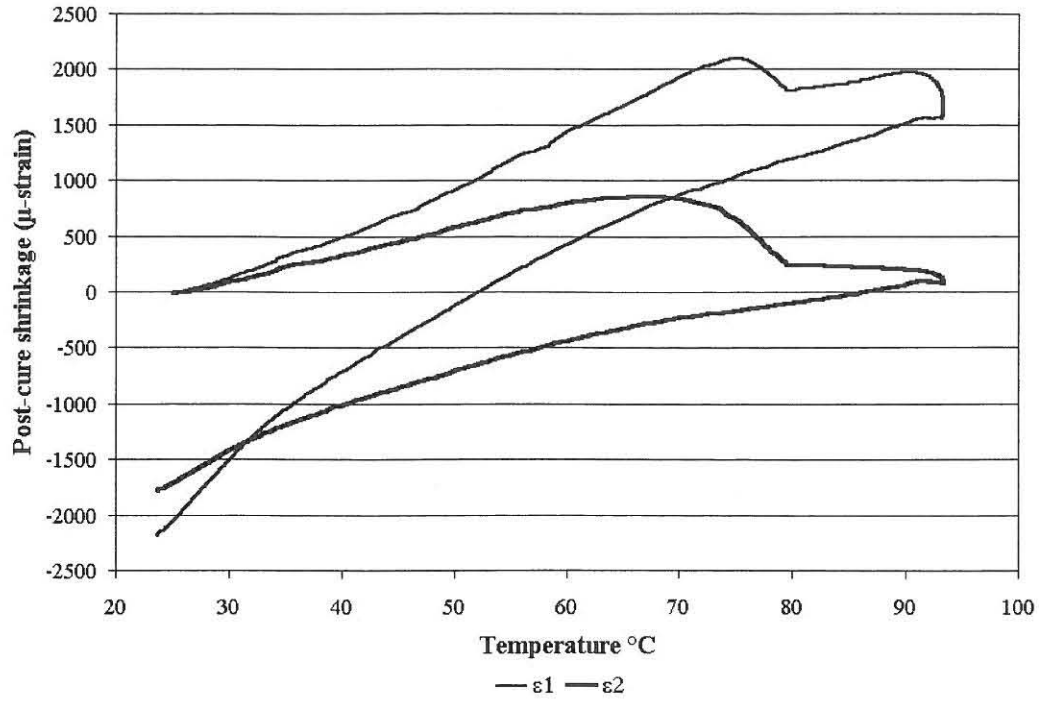

Figure A.5 Post-cure strains at position 5

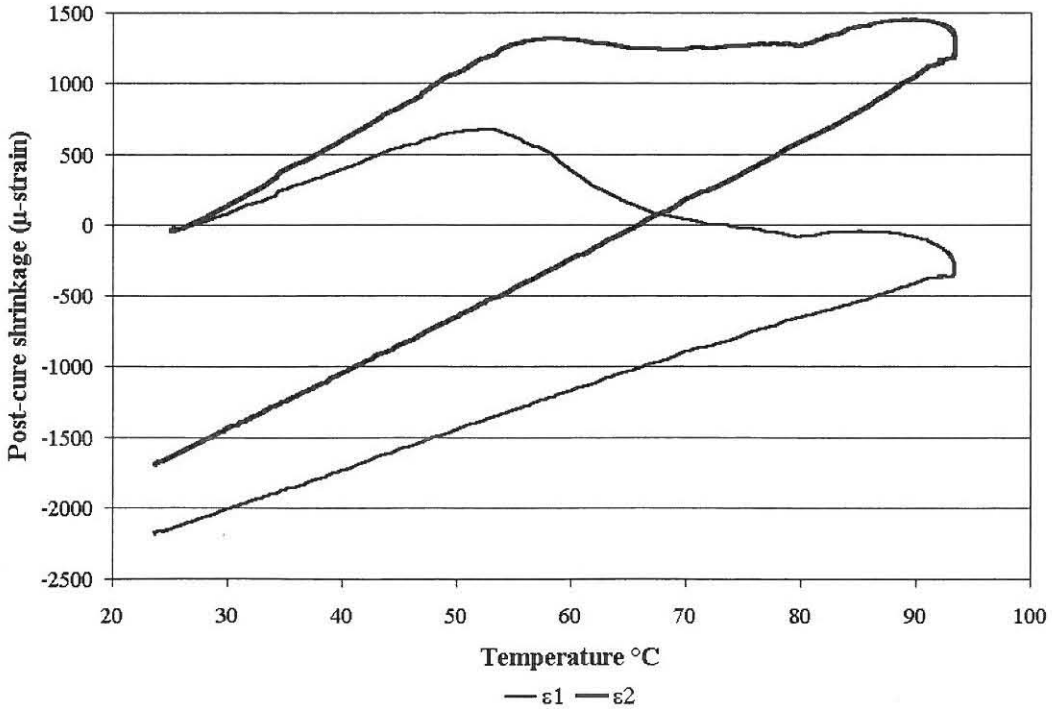

Figure A.6 Post-cure strains at position 6

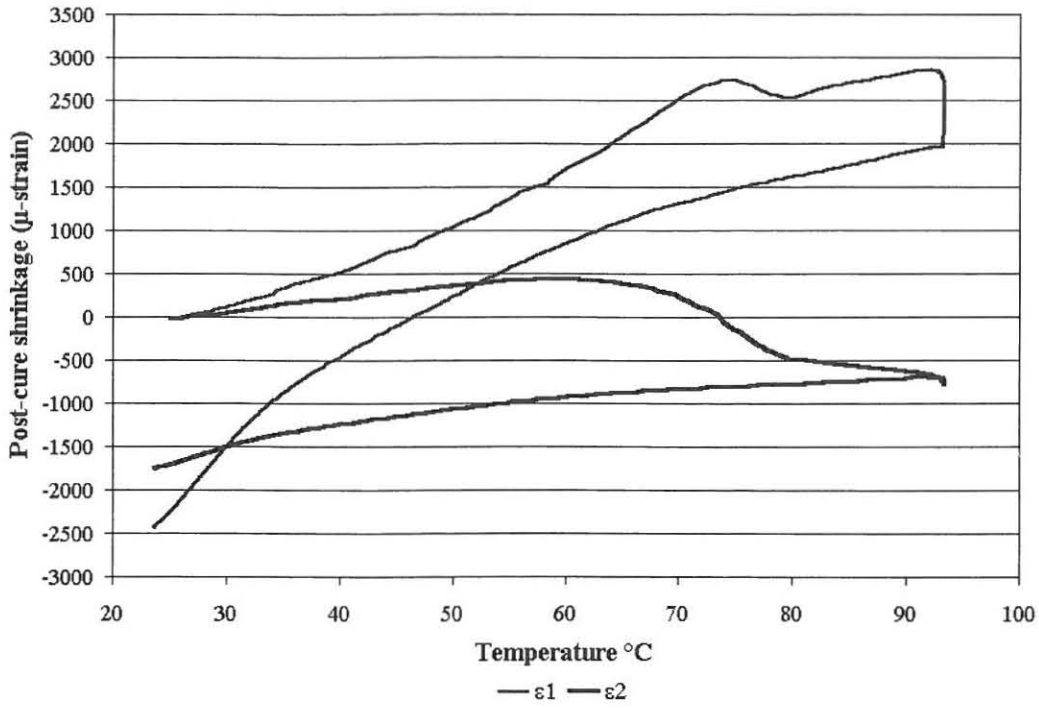

Figure A.7 Post-cure strains at position 7

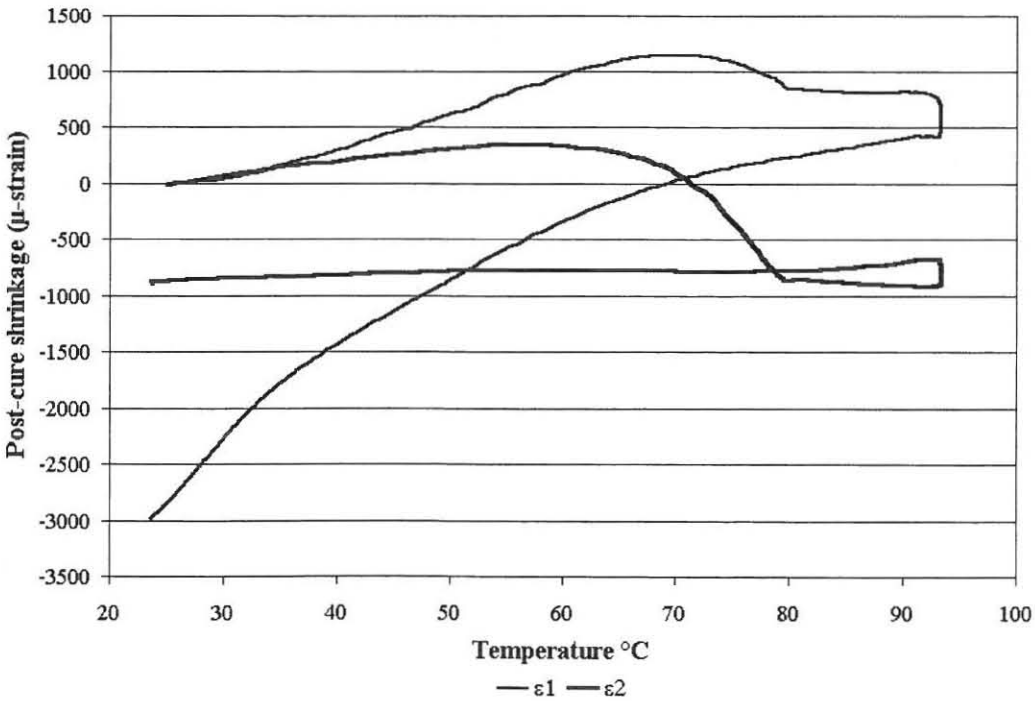

Figure A.8 Post-cure strains at position 8

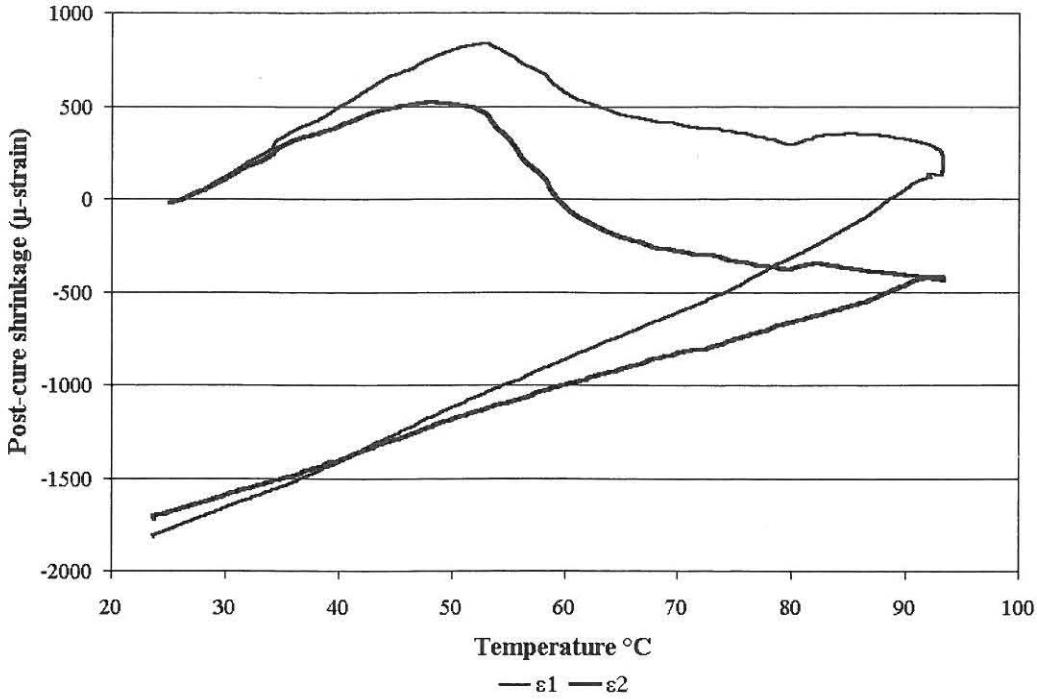

Figure A.9 Post-cure strains at position 9

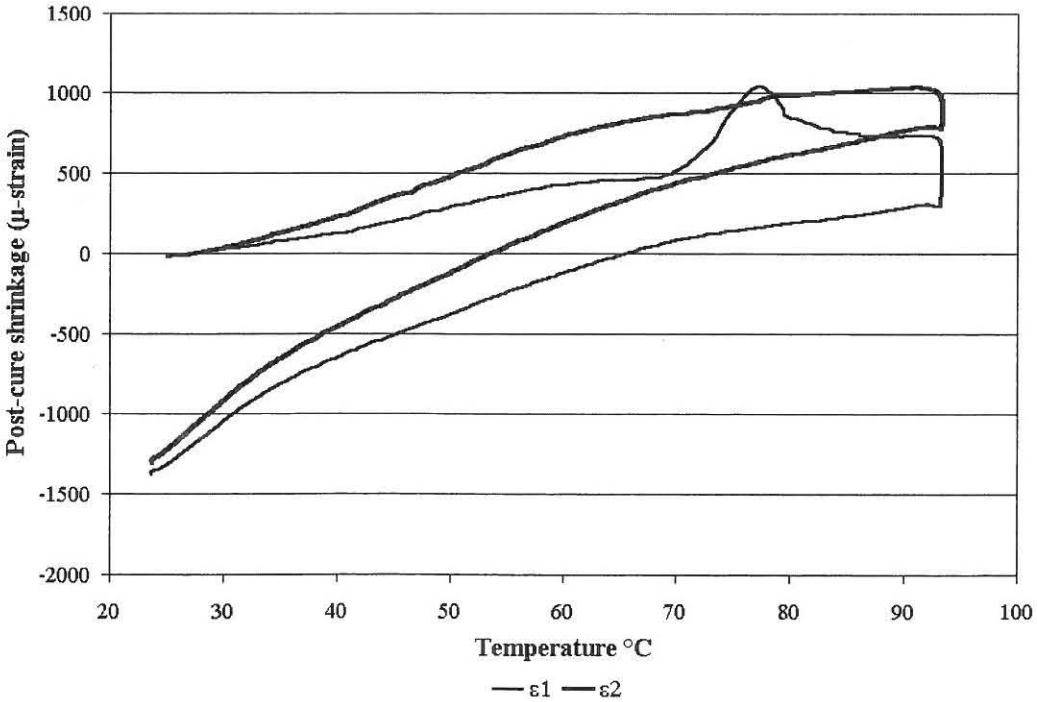

Figure A.10 Post-cure strains at position 10

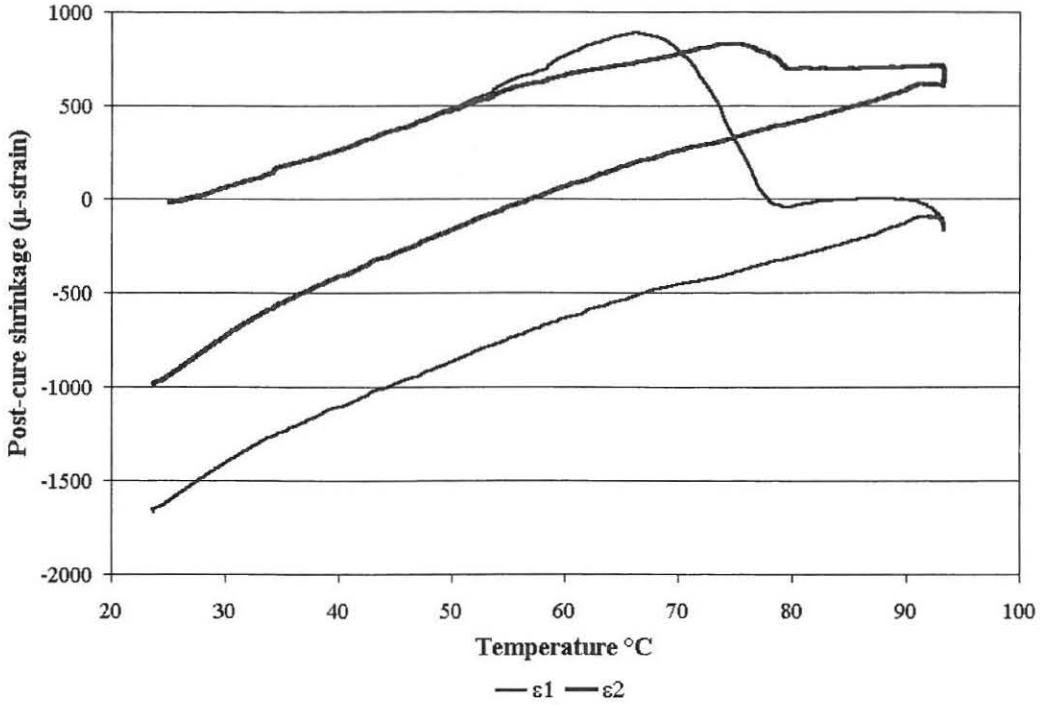

Figure A.11 Post-cure strains at position 11

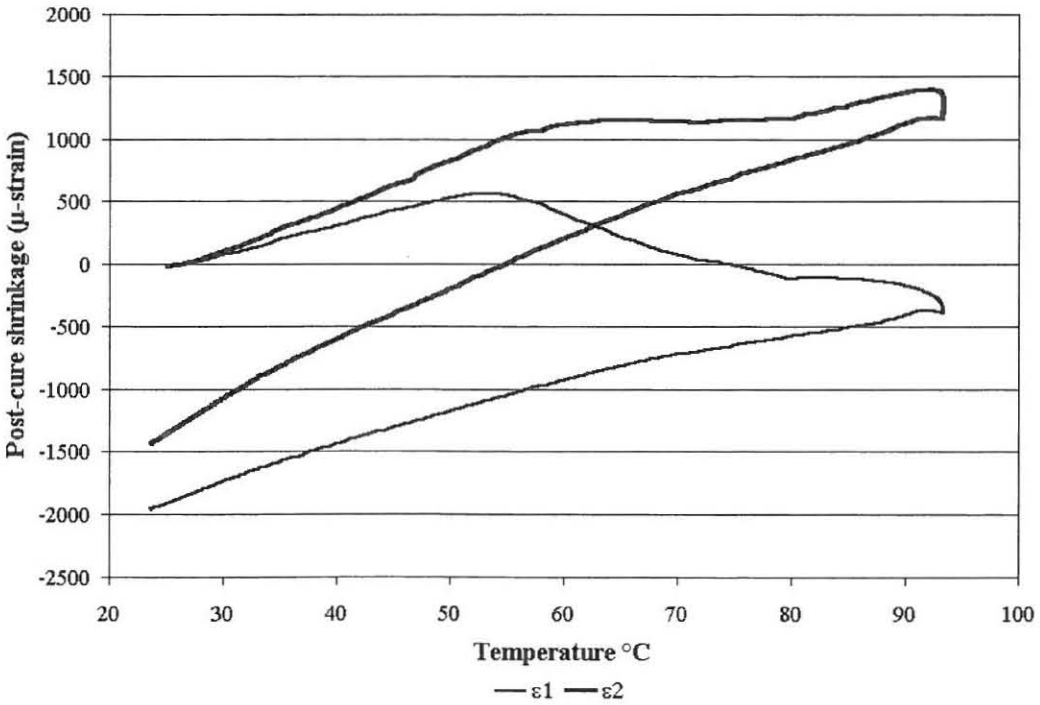

Figure A.12 Post-cure strains at position 12

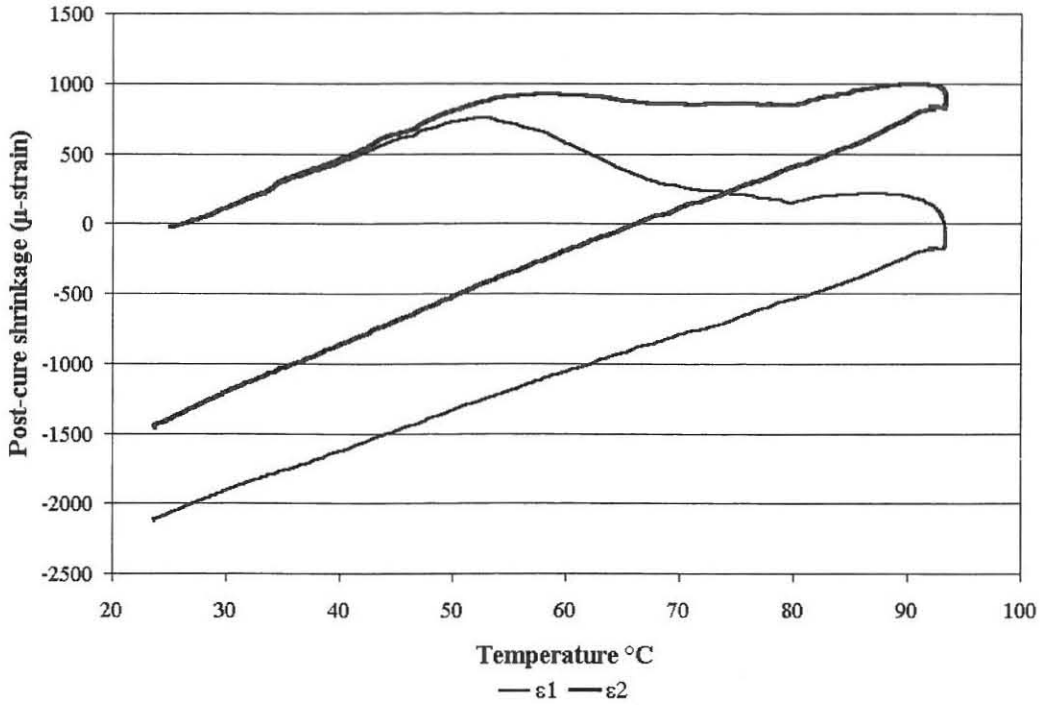

Figure A.13 Post-cure strains at position 13

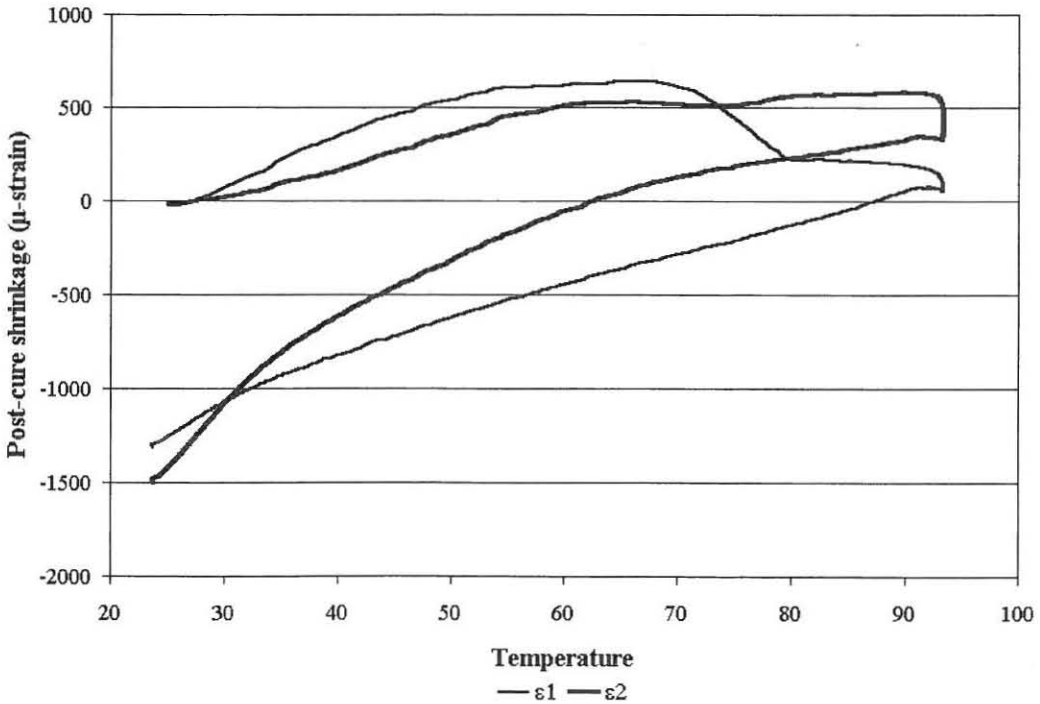

Figure A.14 Post-cure strains at position 14

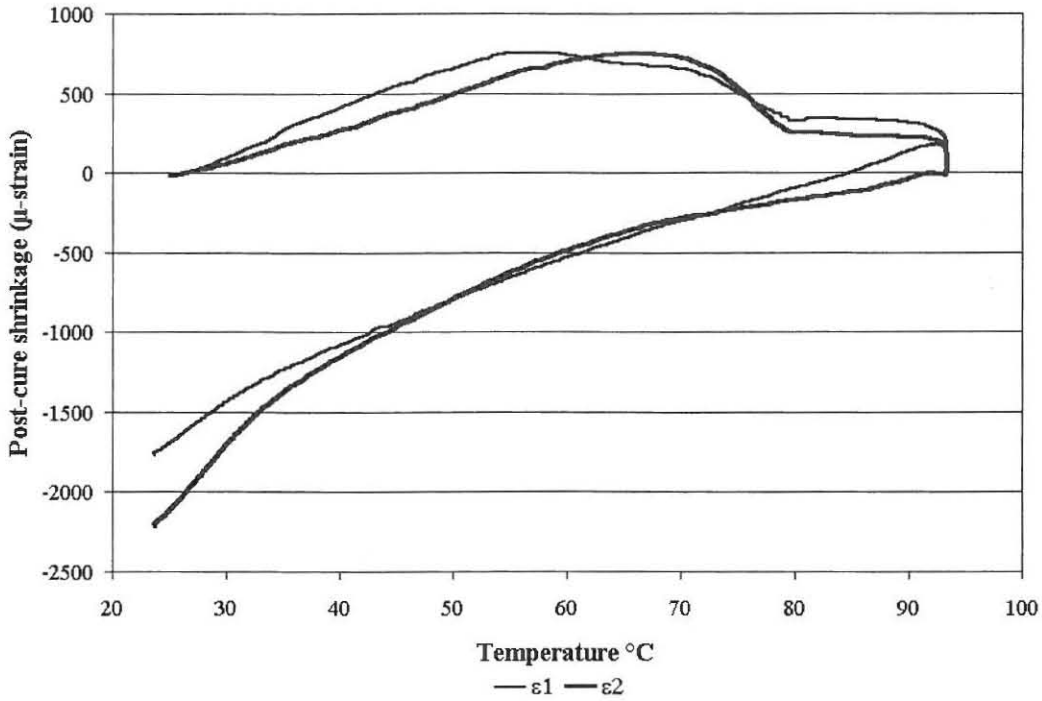

Figure A.15 Post-cure strains at position 15

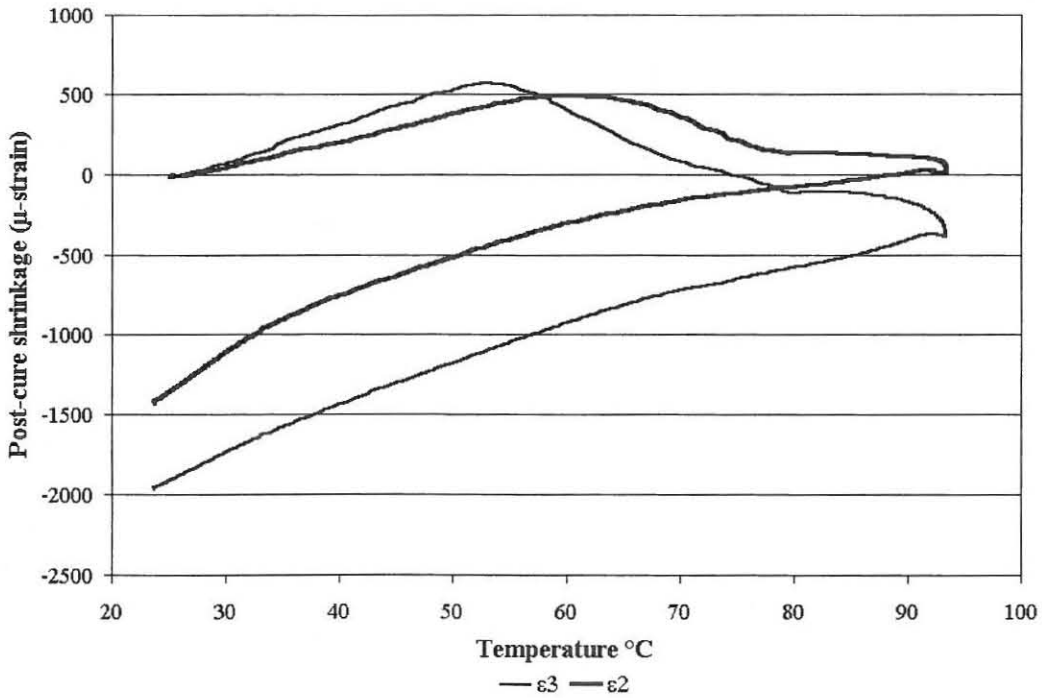

Figure A.16 Post-cure strains at position 16

APPENDIX B. Post-cure stress and strain distributions in 50 NB flange

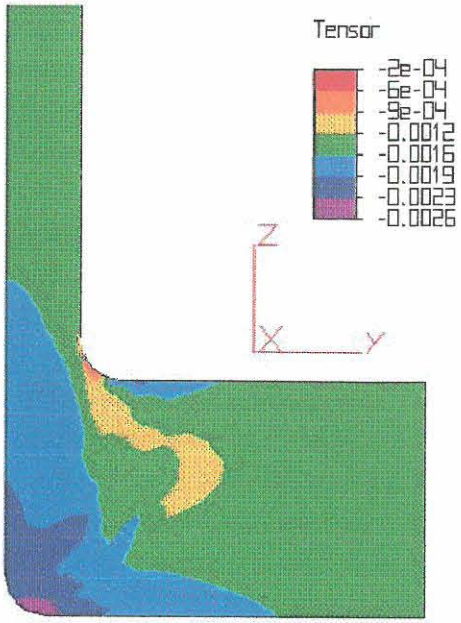

Figure B.1 Predicted in-plane strain (ε_1) of model F_1

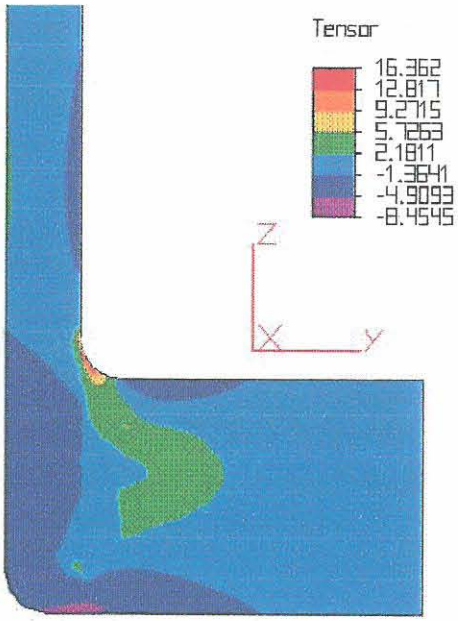

Figure B.2 Predicted in-plane stress (σ_1) of model F_1

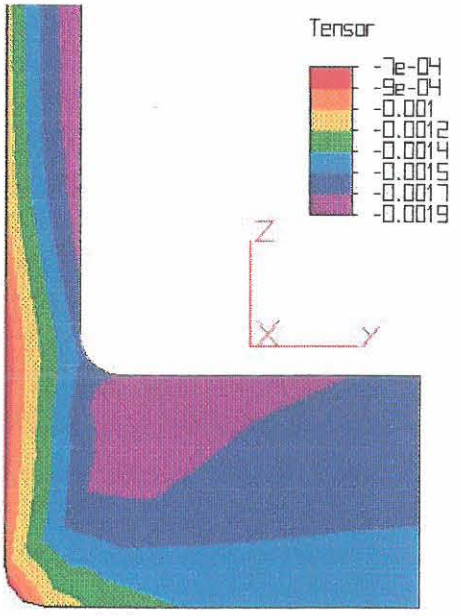

Figure B.3 Predicted in-plane strain (ε_2) of model F_1

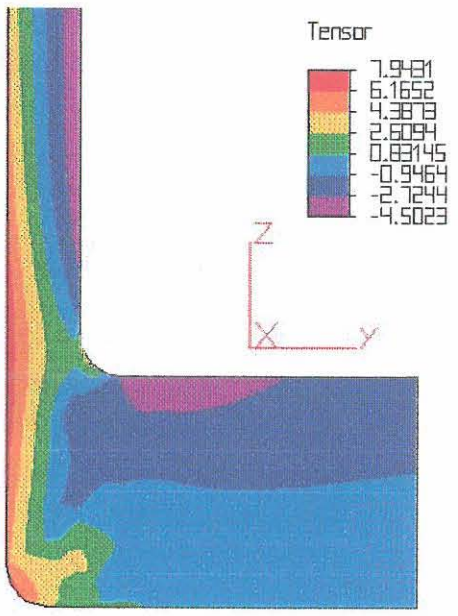

Figure B.4 Predicted in-plane stress (σ_2) of model F_1

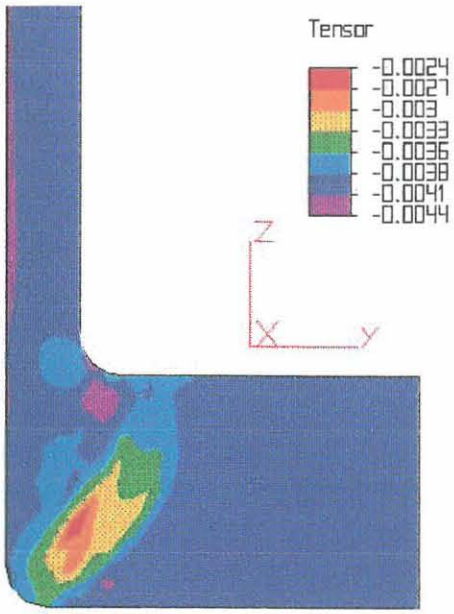

Figure B.5 Predicted through-thickness strain (ε_3) of model F_1

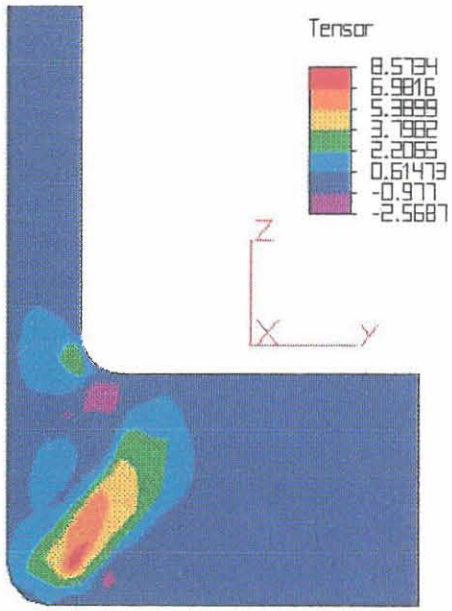

Figure B.6 Predicted through-thickness stress (σ_3) of model F_1

Figure B.7 Predicted in-plane strain (ε_1) of model F_2

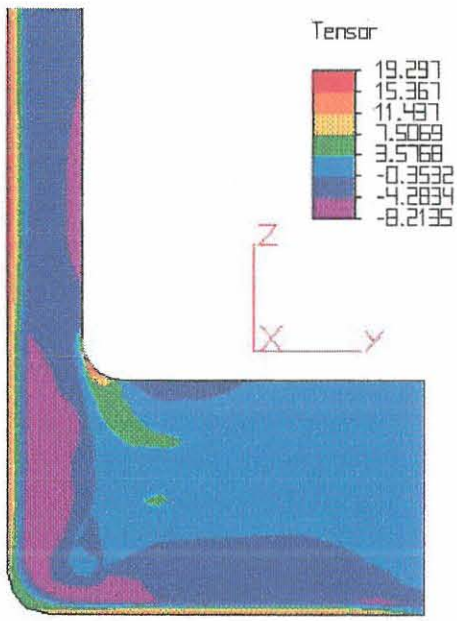

Figure B.8 Predicted in-plane stress (σ_1) of model F_2

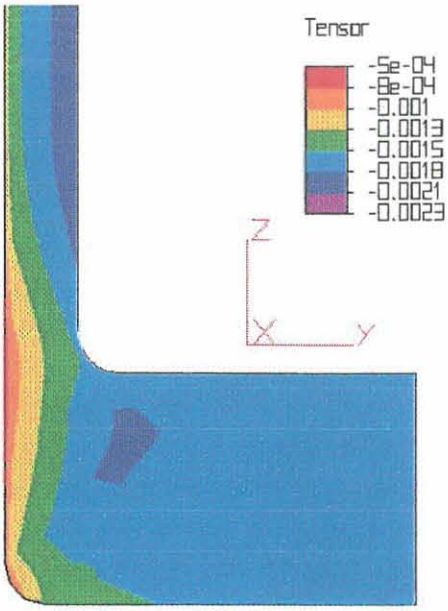

Figure B.9 Predicted in-plane strain (ε_2) of model F_2

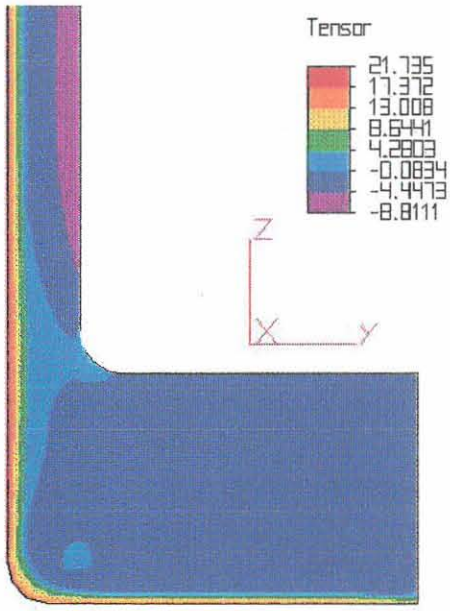

Figure B.10 Predicted in-plane stress (σ_2) of model F_2

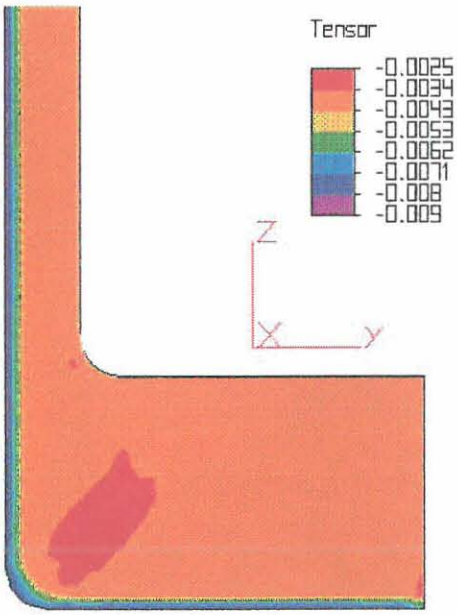

Figure B.11 Predicted through-thickness strain (ε_3) of model F_2

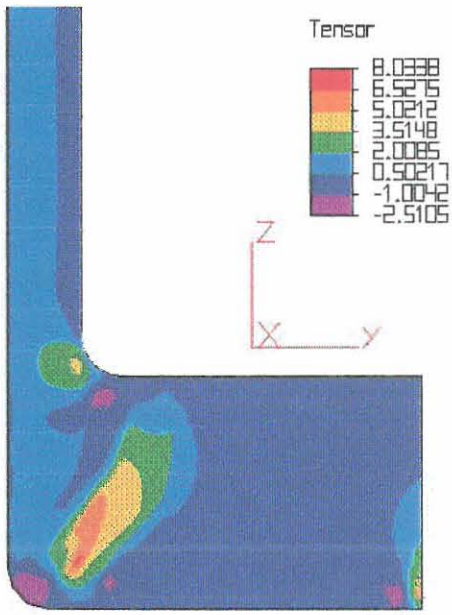

Figure B.12 Predicted through-thickness stress (σ_3) of model F_2

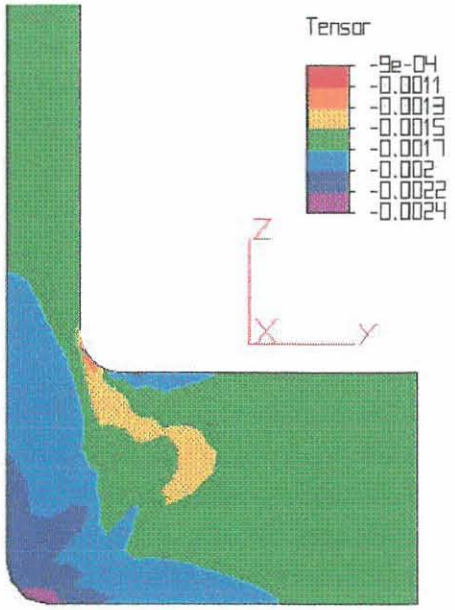

Figure B.13 Predicted in-plane strain (ε_1) of model F_3

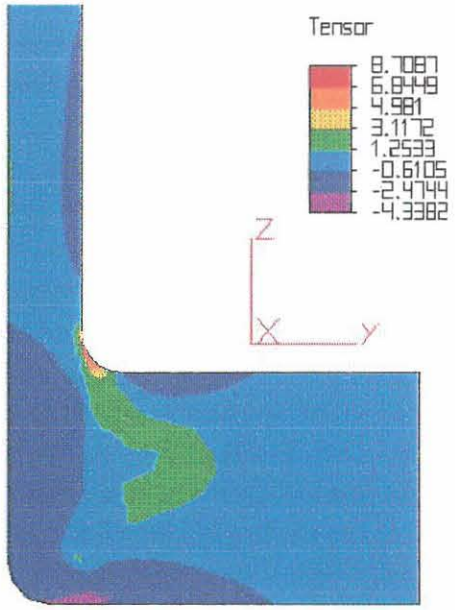

Figure B.14 Predicted in-plane stress (σ_1) of model F_3

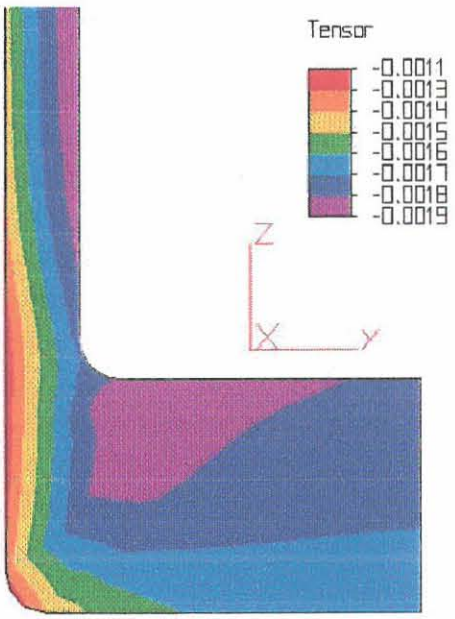

Figure B.15 Predicted in-plane strain (ε_2) of model F_3

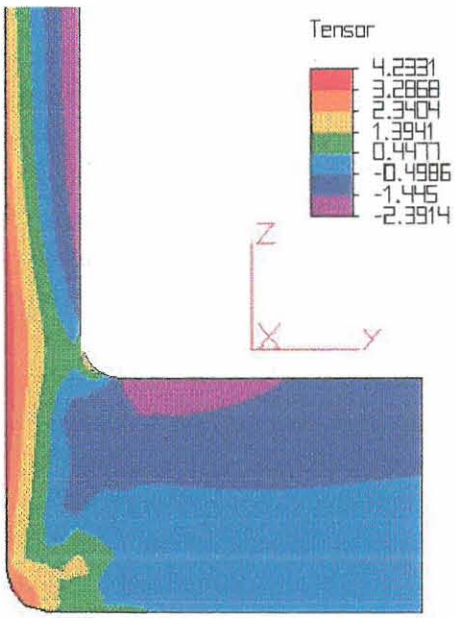

Figure B.16 Predicted in-plane stress (σ_2) of model F_3

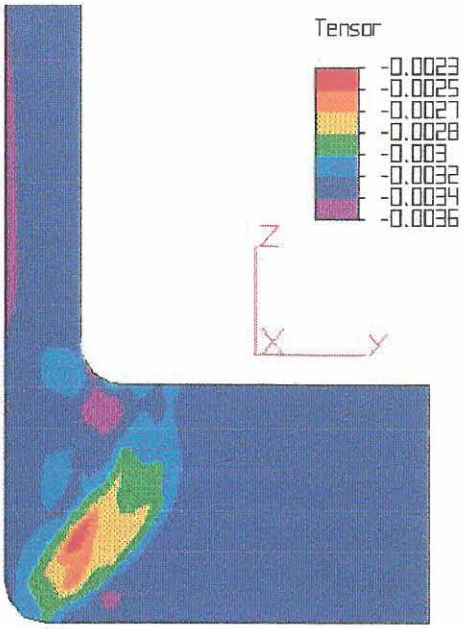

Figure B.17 Predicted through-thickness strain (ε_3) of model F_3

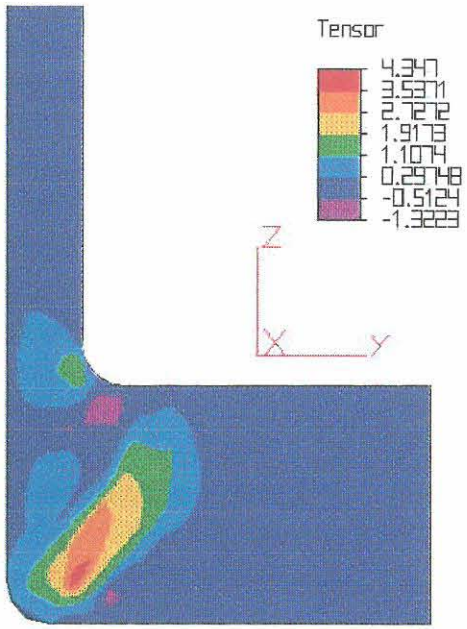

Figure B.18 Predicted through-thickness stress (σ_3) of model F_3

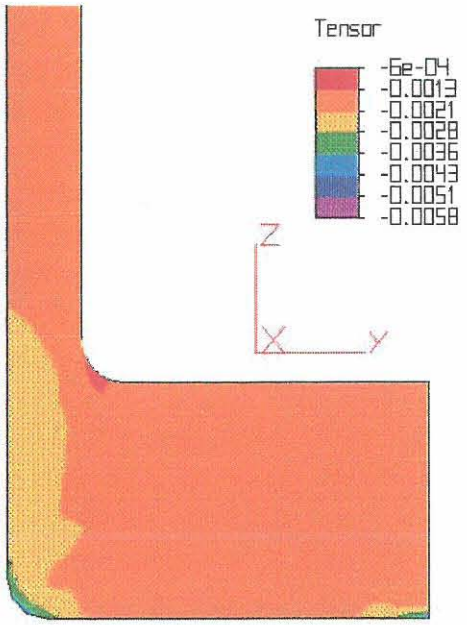

Figure B.19 Predicted in-plane strain (ε_1) of model F_4

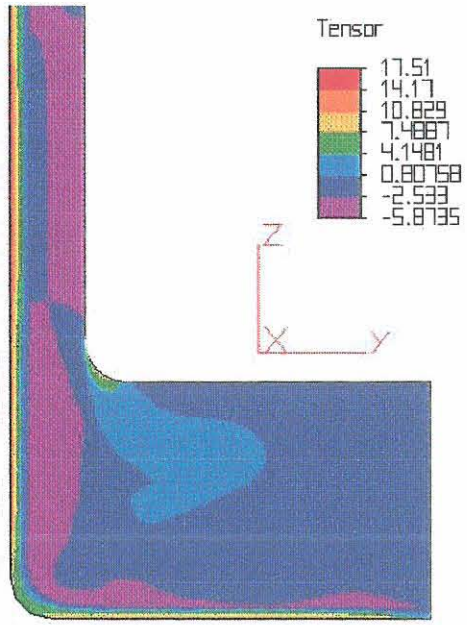

Figure B.20 Predicted in-plane stress (σ_1) of model F_4

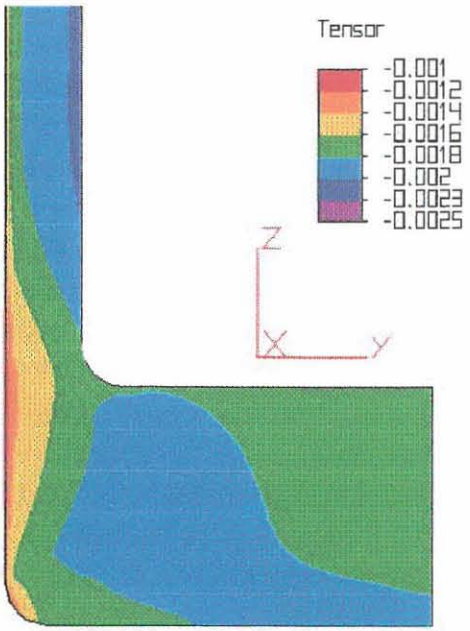

Figure B.21 Predicted in-plane strain (ε_2) of model F_4

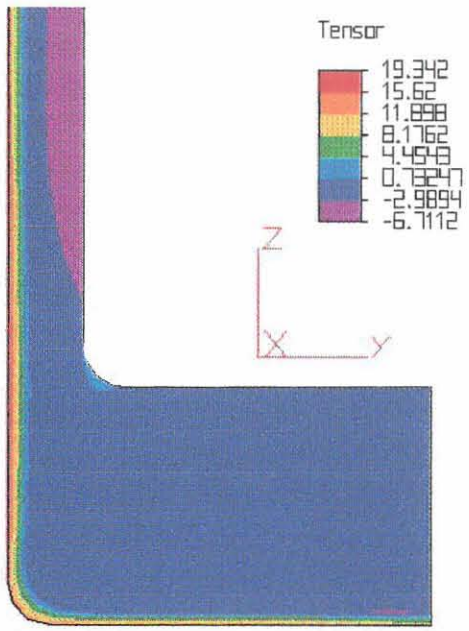

Figure B.22 Predicted in-plane stress (σ_2) of model F_4

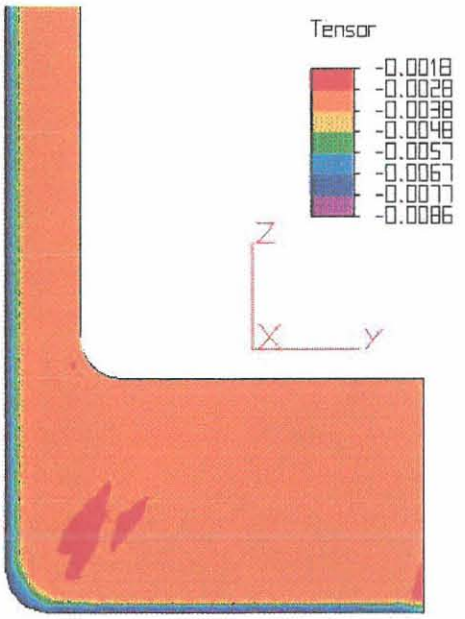

Figure B.23 Predicted through-thickness strain (ε_3) of model F_4

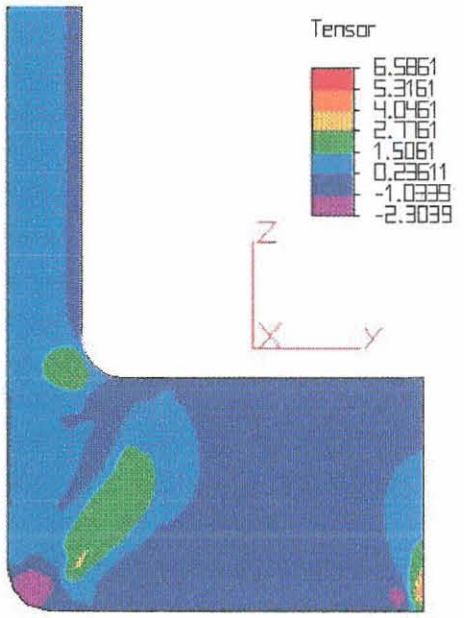

Figure B.24 Predicted through-thickness stress (σ_3) of model F_4

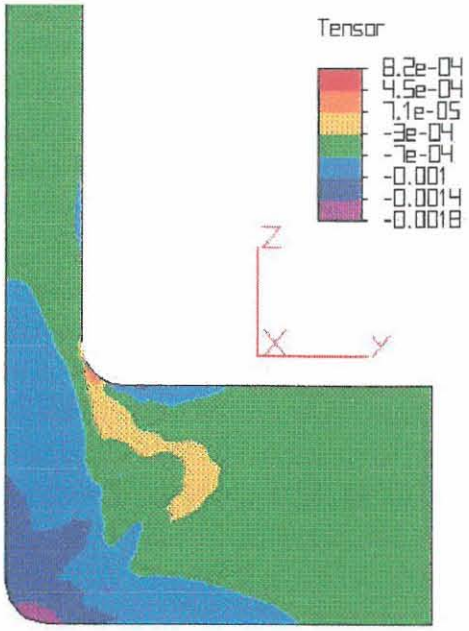

Figure B.25 Predicted in-plane strain (ε_1) of model F_5

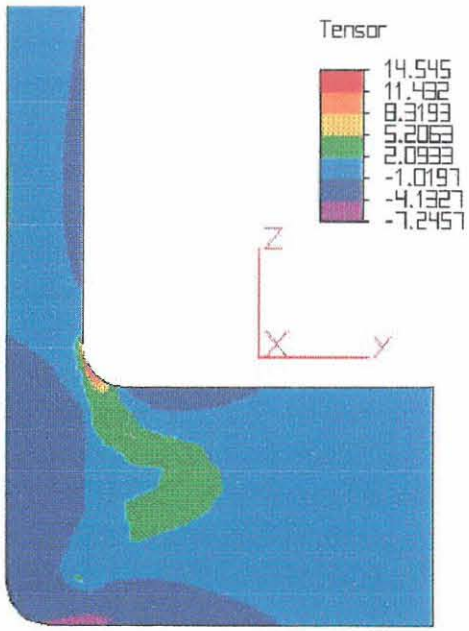

Figure B.26 Predicted in-plane stress (σ_1) of model F_5

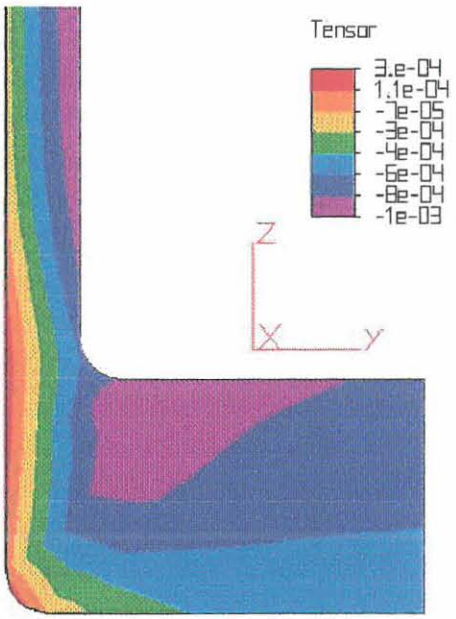

Figure B.27 Predicted in-plane strain (ε_2) of model F_5

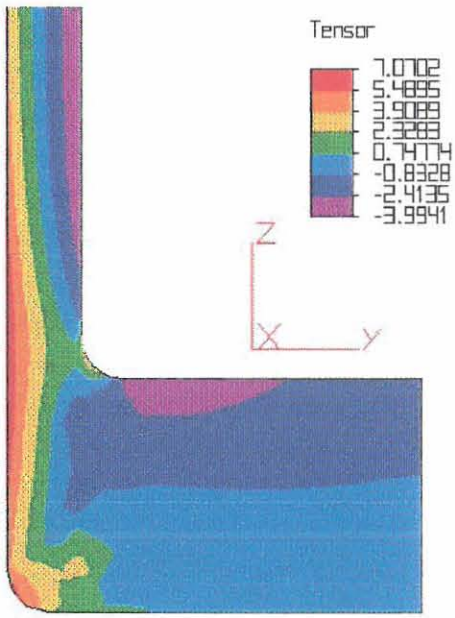

Figure B.28 Predicted in-plane stress (σ_2) of model F_5

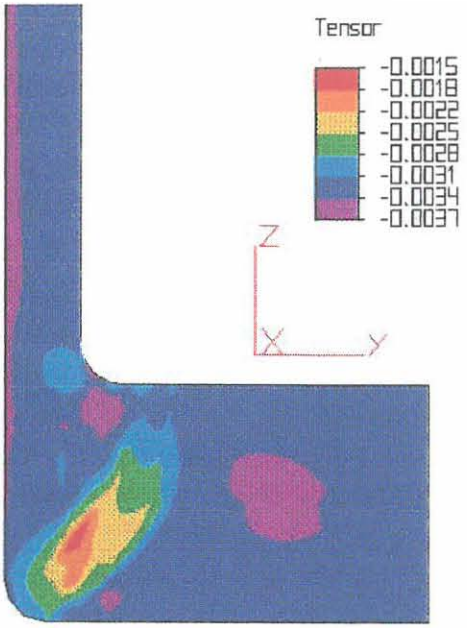

Figure B.29 Predicted through-thickness strain (ε_3) of model F_5

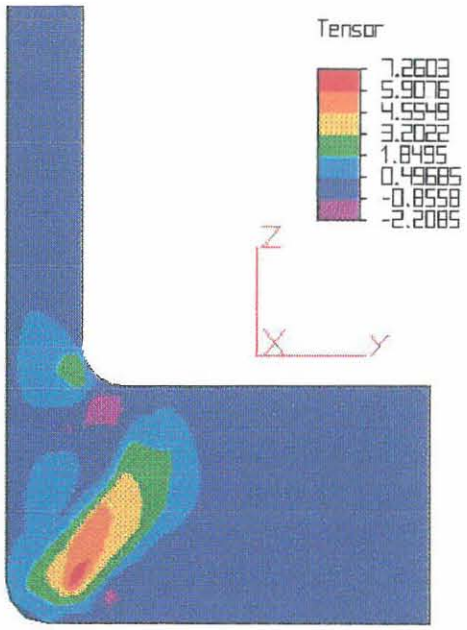

Figure B.30 Predicted through-thickness stress (σ_3) of model F_5

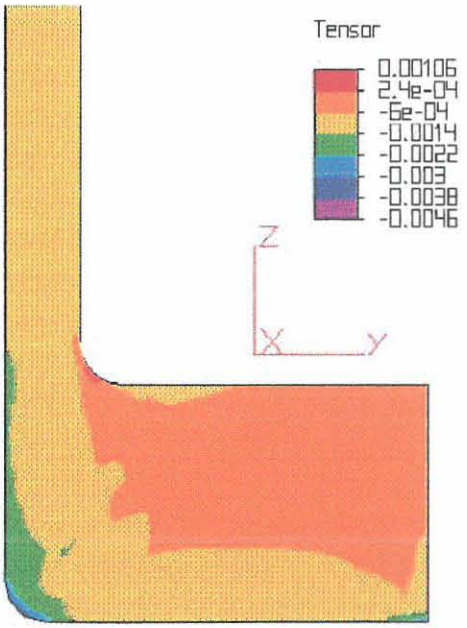

Figure B.31 Predicted in-plane strain (ε_1) of model F_6

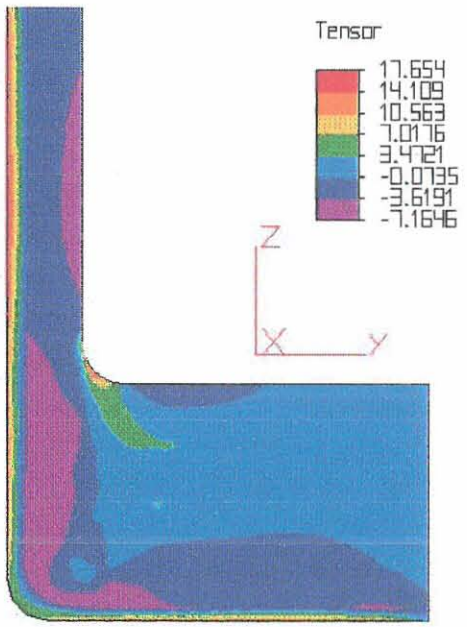

Figure B.32 Predicted in-plane stress (σ_1) of model F_6

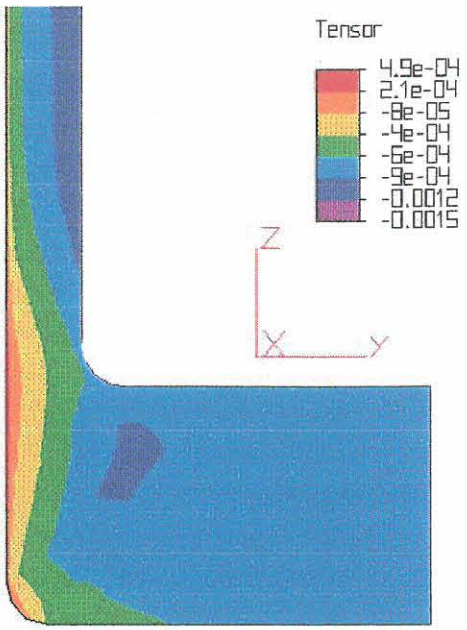

Figure B.33 Predicted in-plane strain (ε_2) of model F_6

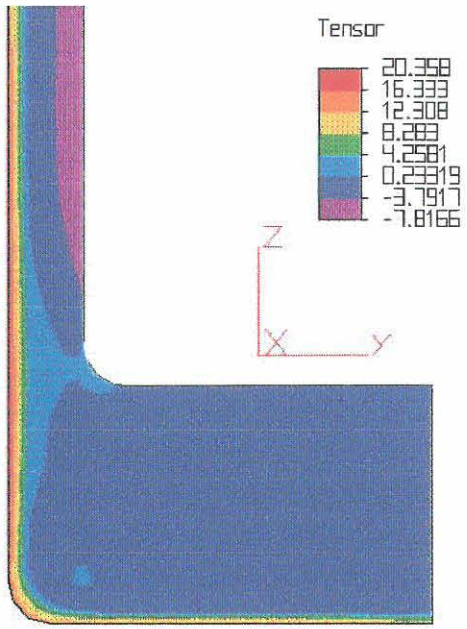

Figure B.34 Predicted in-plane stress (σ_2) of model F_6

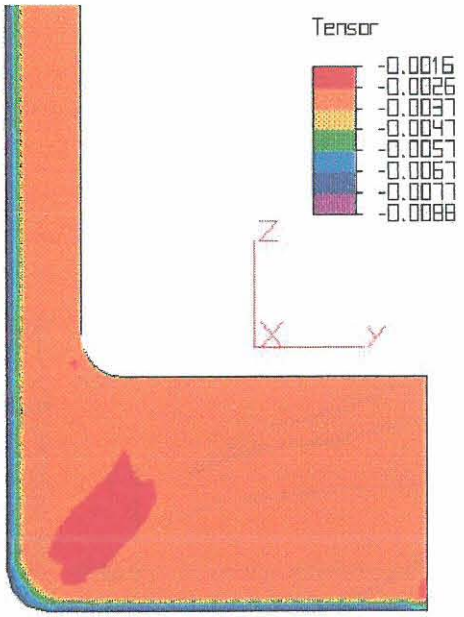

Figure B.35 Predicted through-thickness strain (ε_3) of model F_6

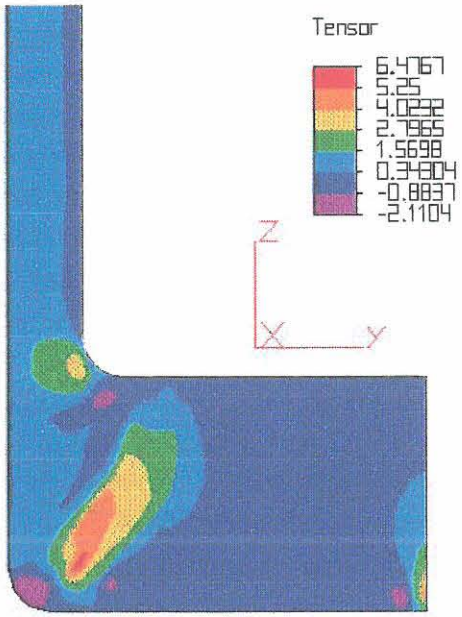

Figure B.36 Predicted through-thickness stress (σ_3) of model F_6

APPENDIX C. Recorded post-cure strains of nozzle-vessel connection

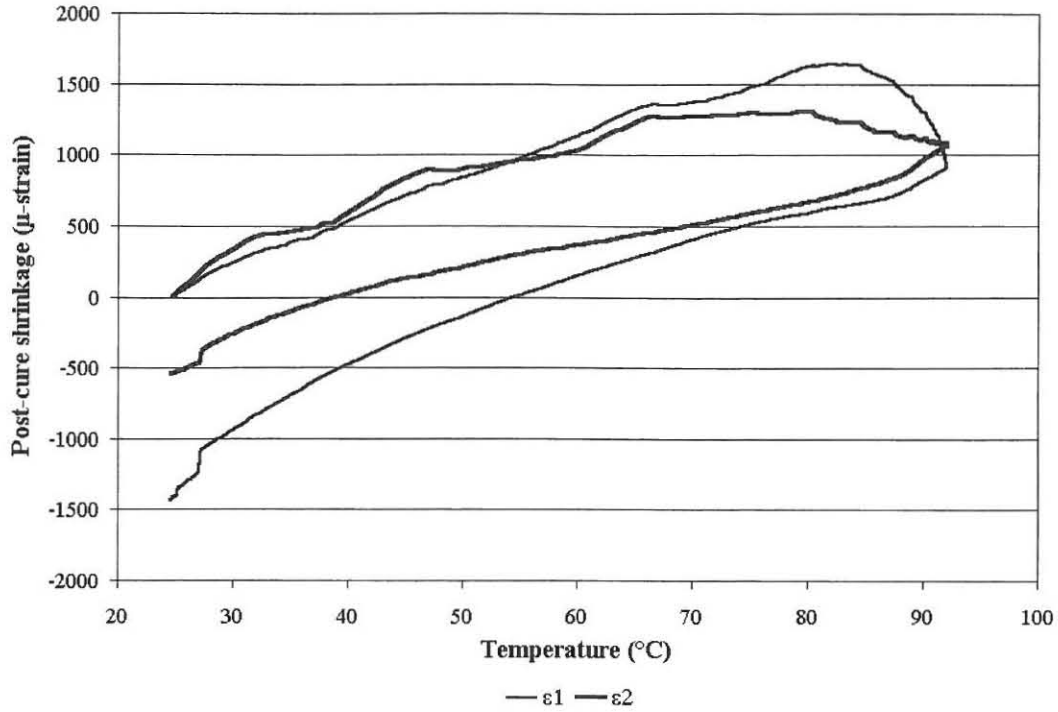

Figure C.1 Post-cure strains at position 1

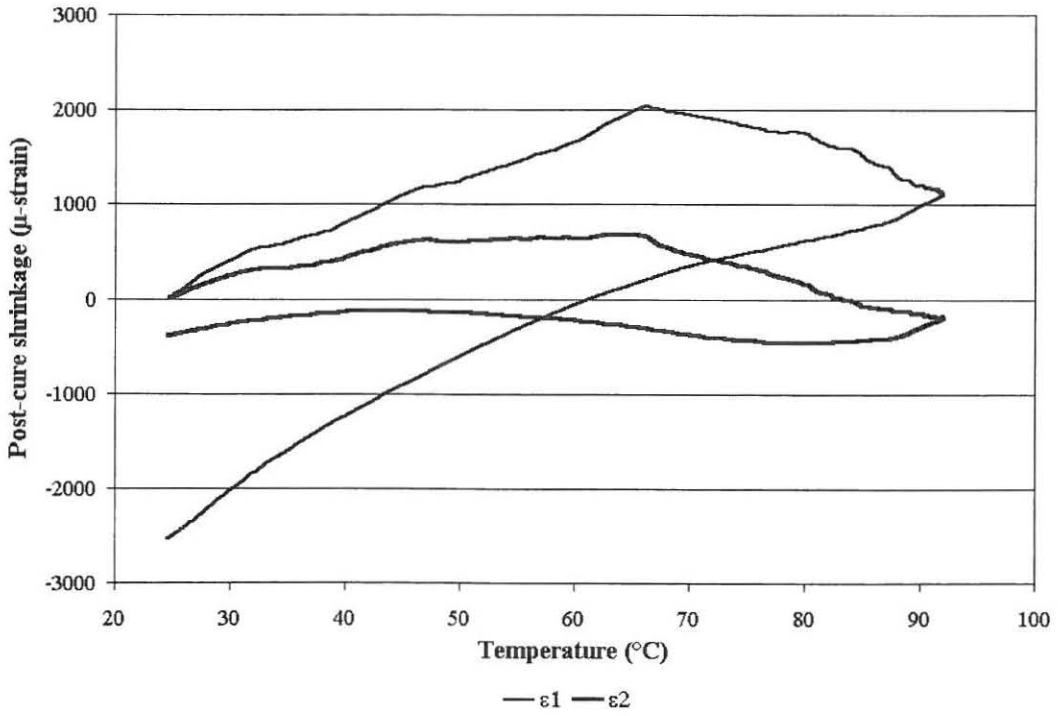

Figure C.2 Post-cure strains at position 2

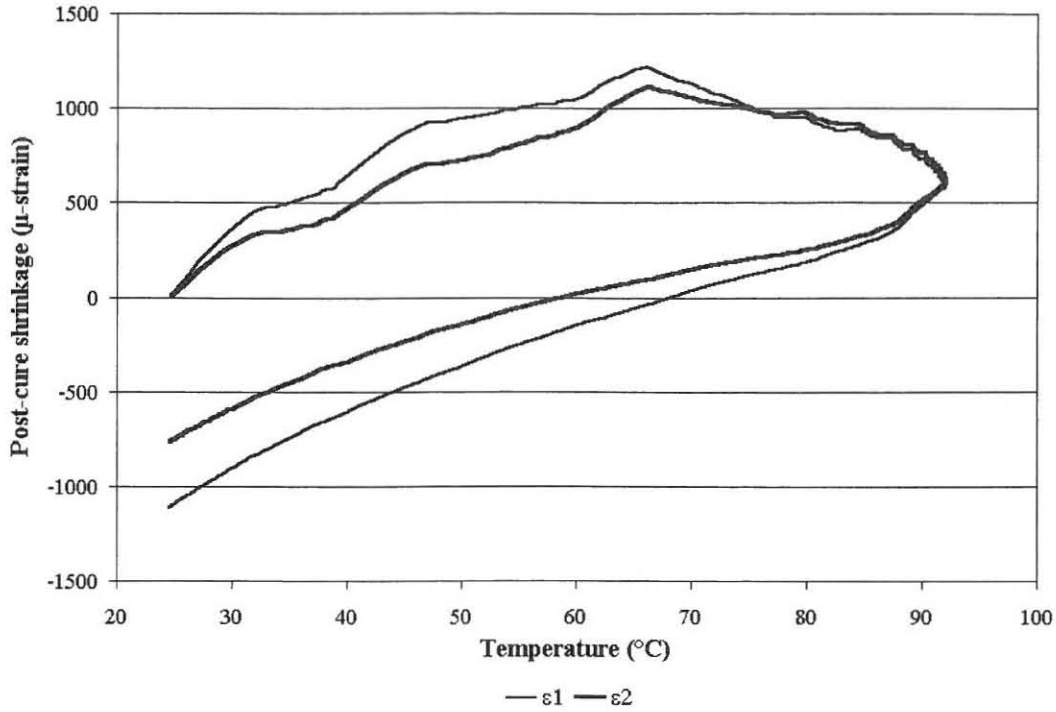

Figure C.3 Post-cure strains at position 3

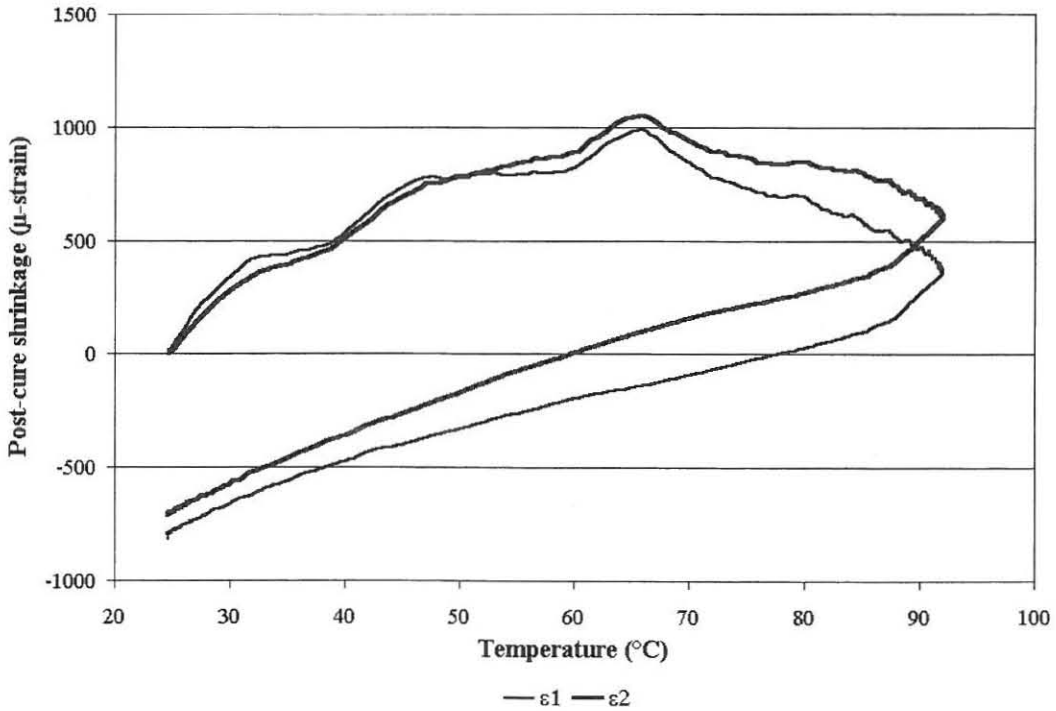

Figure C.4 Post-cure strains at position 4

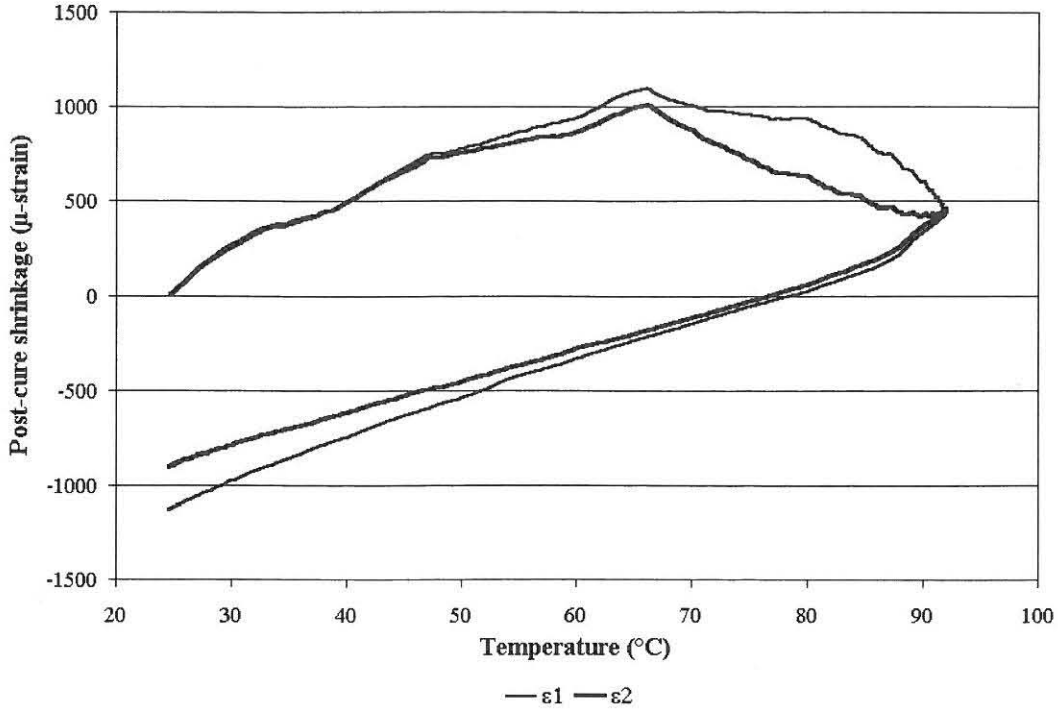

Figure C.5 Post-cure strains at position 5

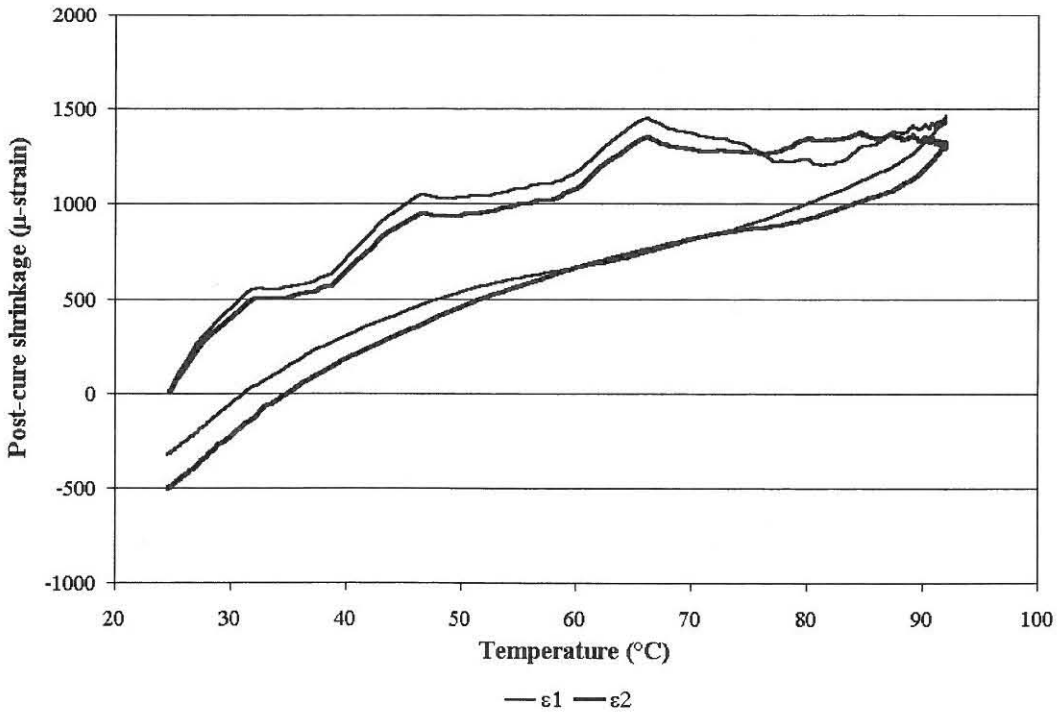

Figure C.6 Post-cure strains at position 6

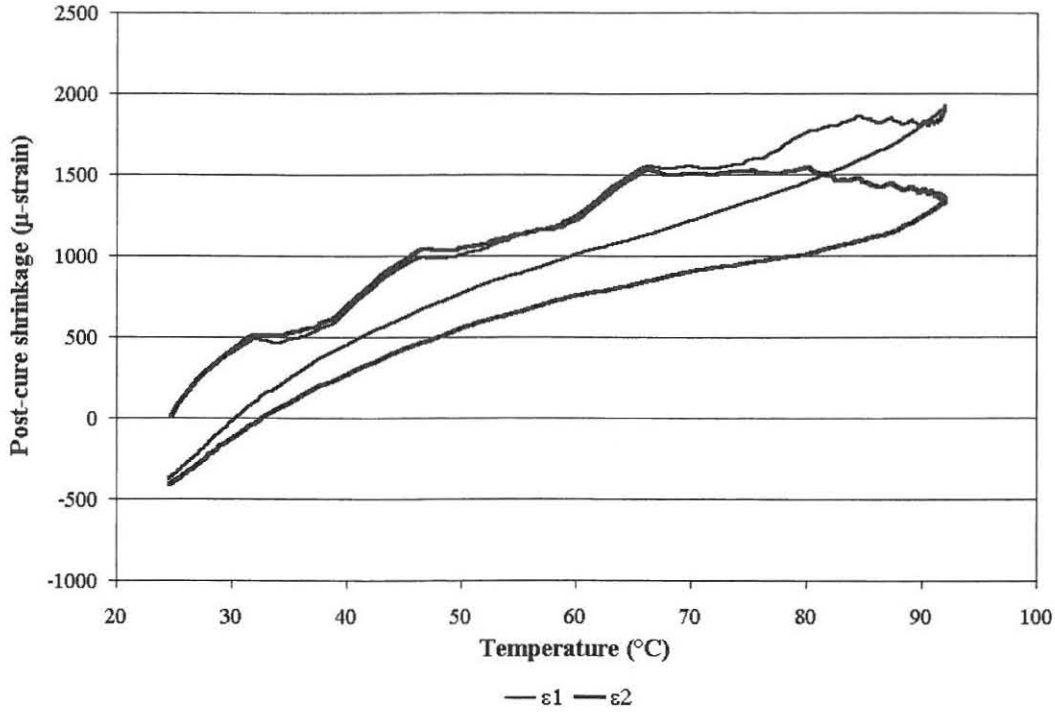

Figure C.7 Post-cure strains at position 7

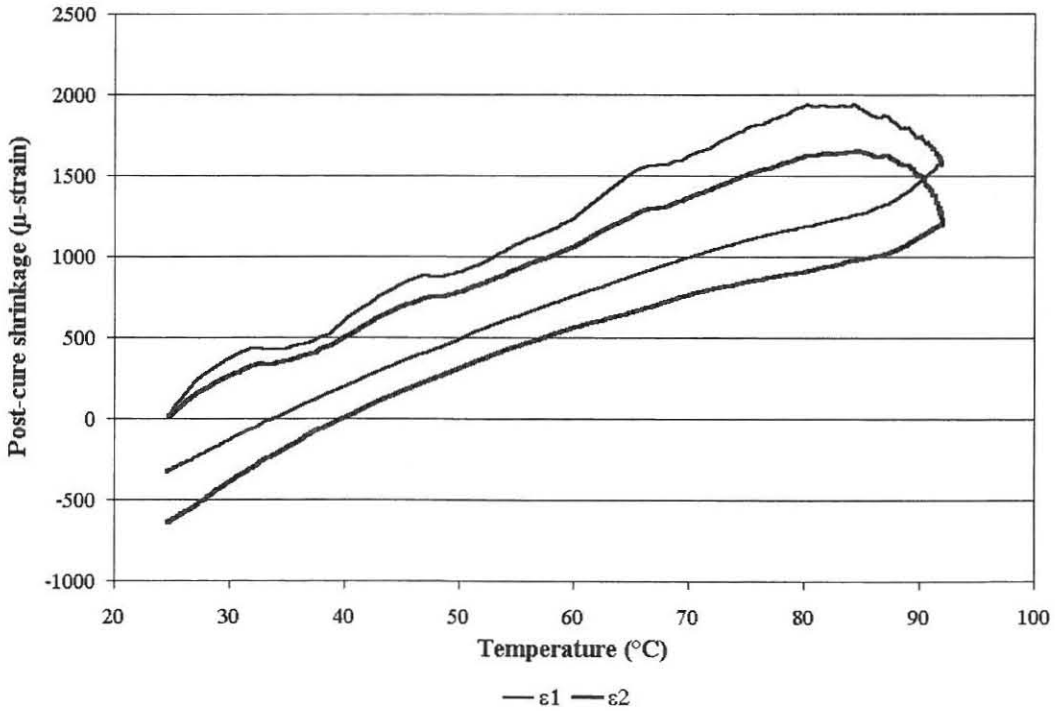

Figure C.8 Post-cure strains at position 8

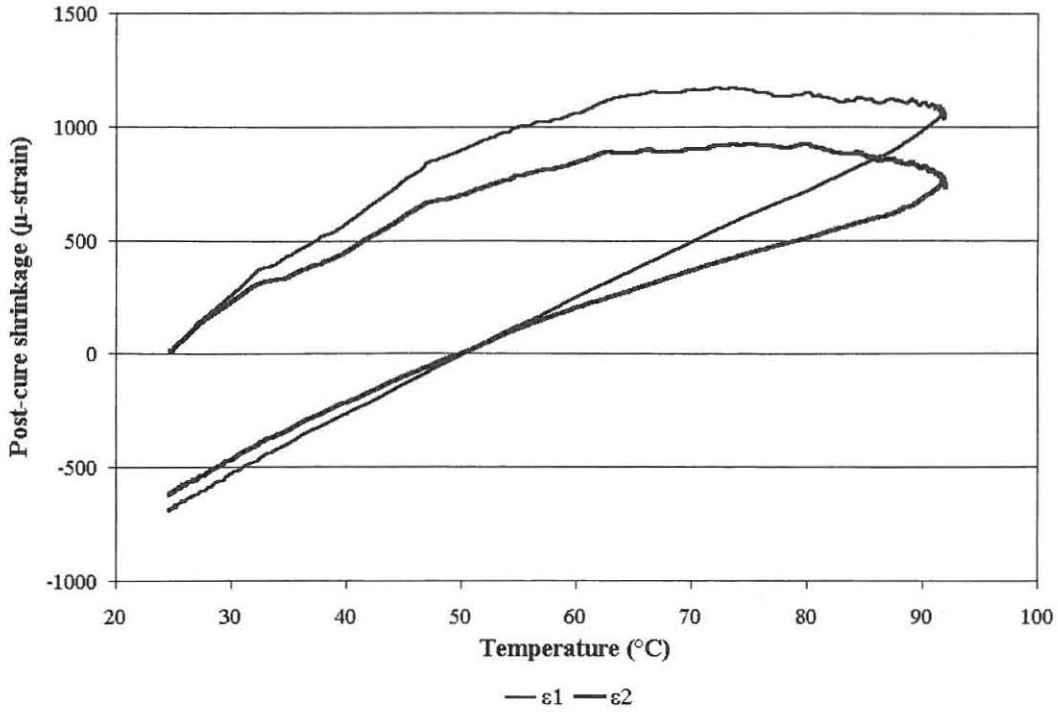

Figure C.9 Post-cure strains at position 9

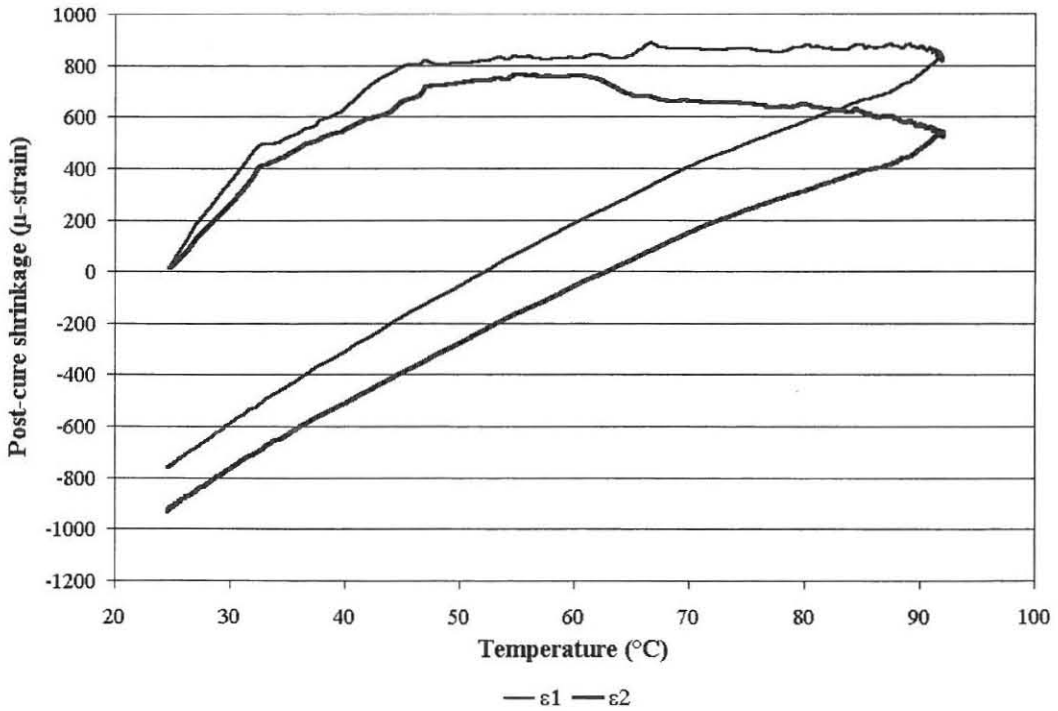

Figure C.10 Post-cure strains at position 10

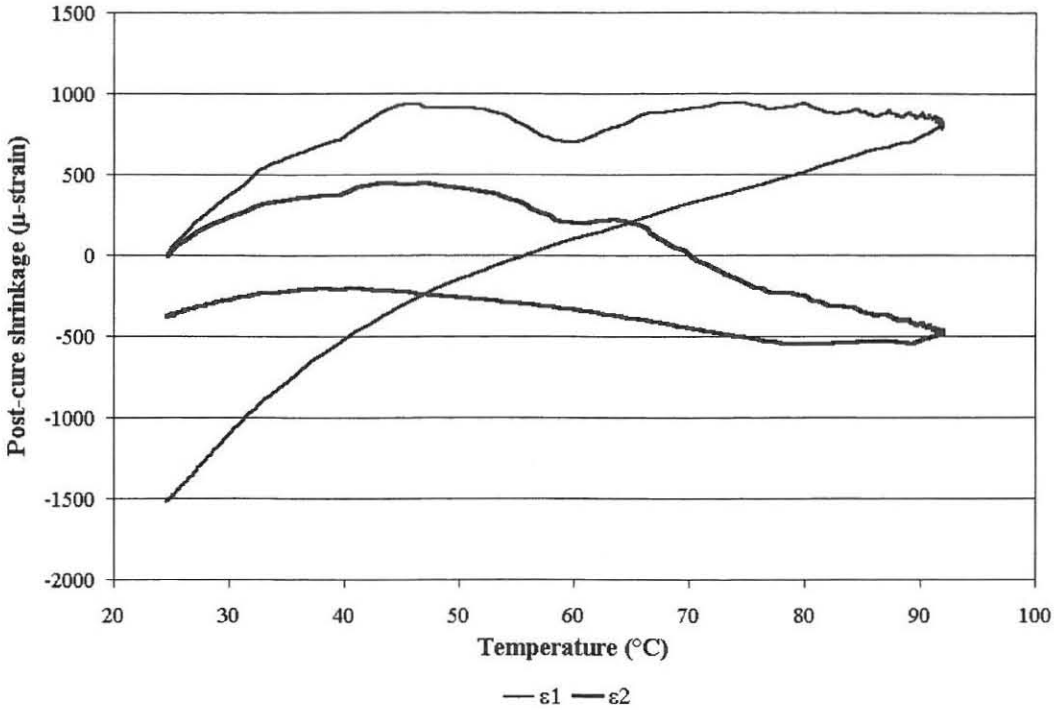

Figure C.11 Post-cure strains at position 11

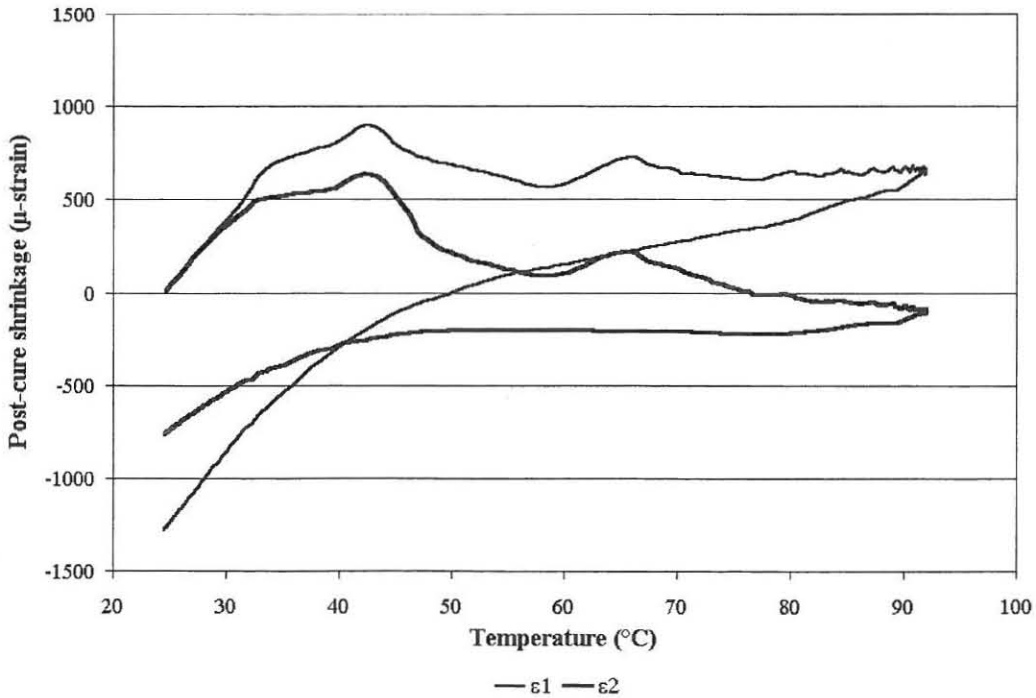

Figure C.12 Post-cure strains at position 12

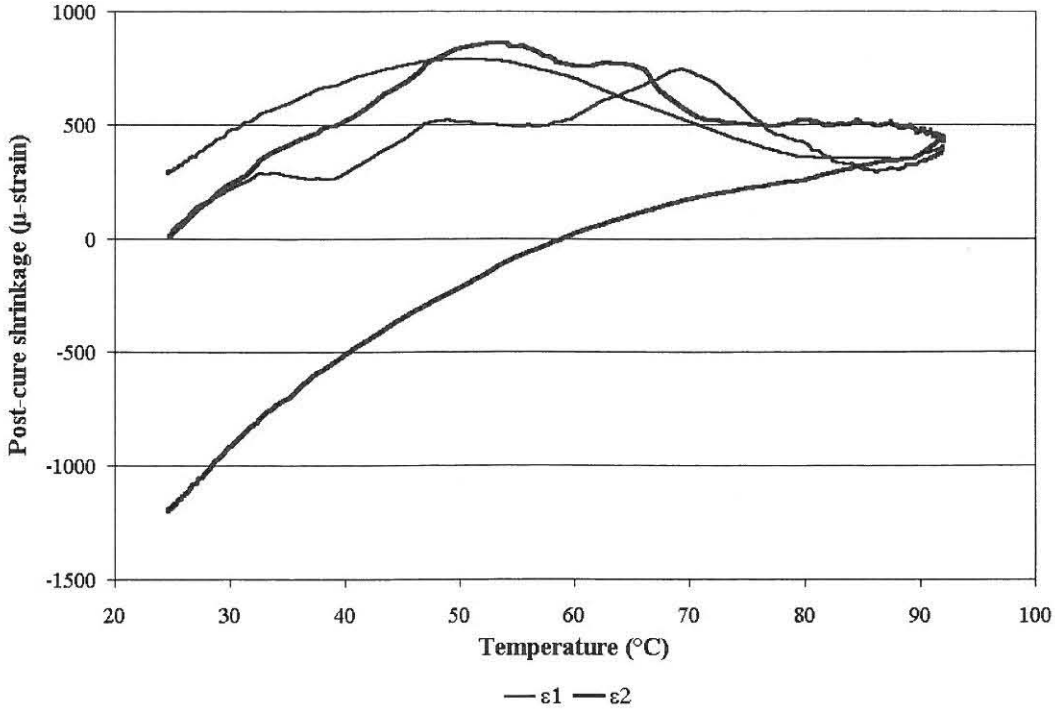

Figure C.13 Post-cure strains at position 13

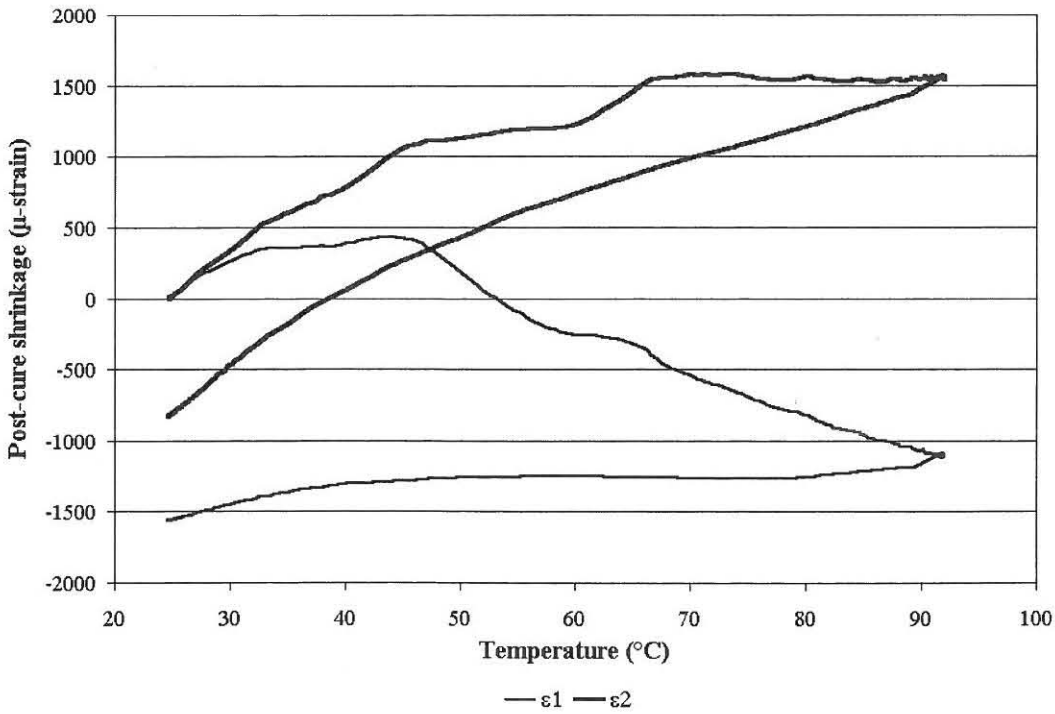

Figure C.14 Post-cure strains at position 14

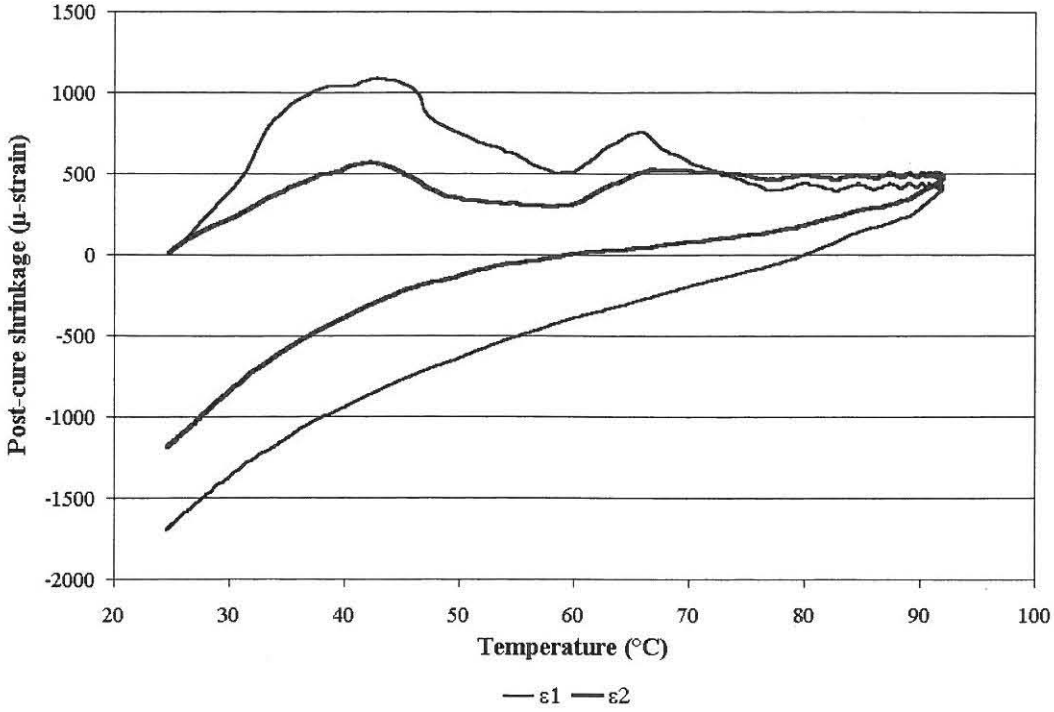

Figure C.15 Post-cure strains at position 15

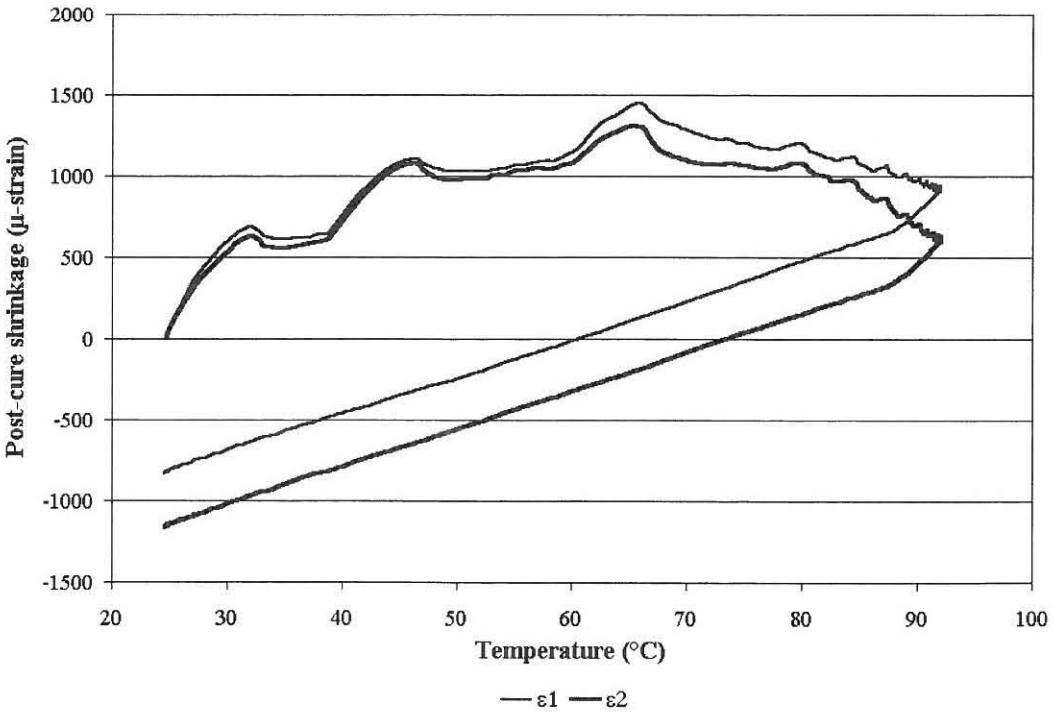

Figure C.16 Post-cure strains at position 16

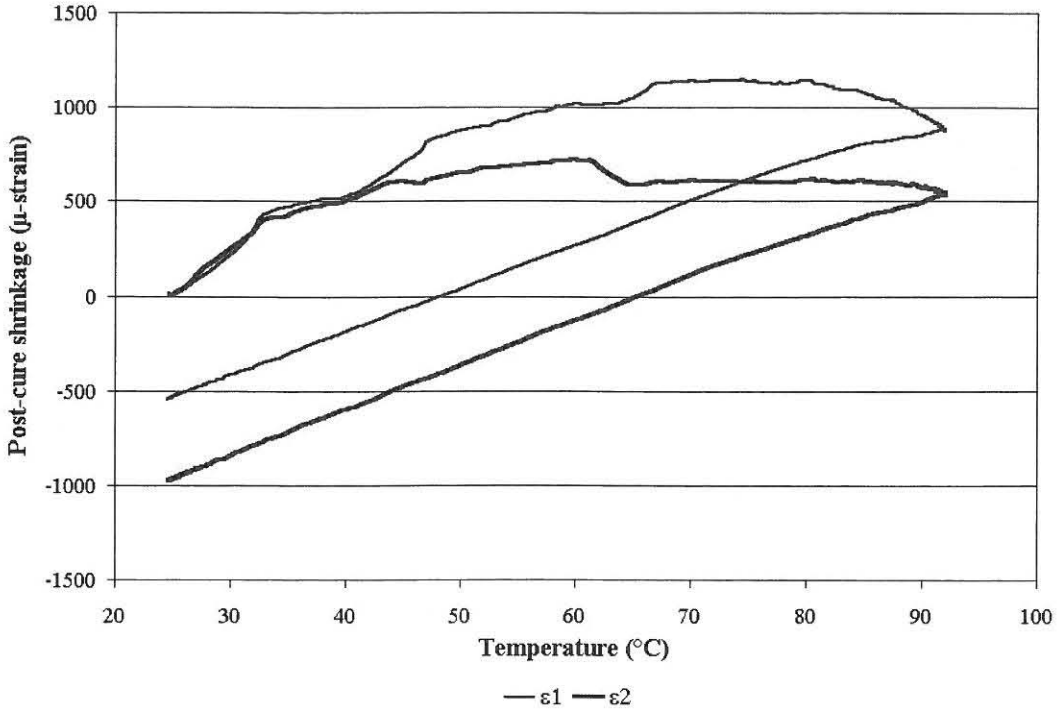

Figure C.17 Post-cure strains at position 17

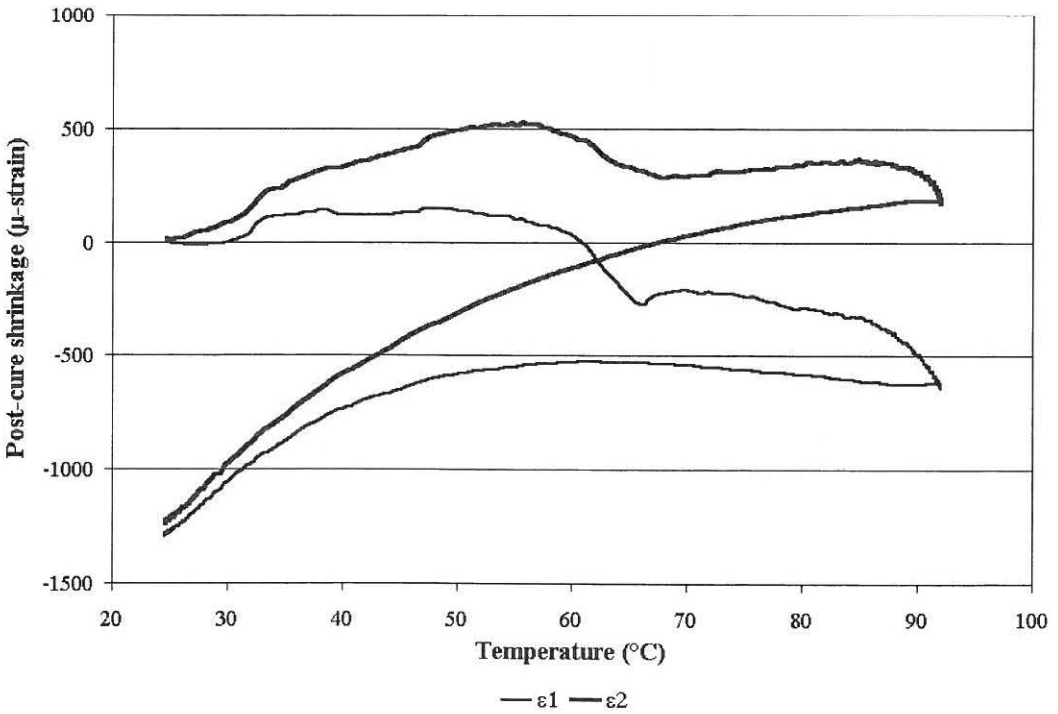

Figure C.18 Post-cure strains at position 18

APPENDIX D. Post-cure stress and strain distributions in nozzle to dished-end connection

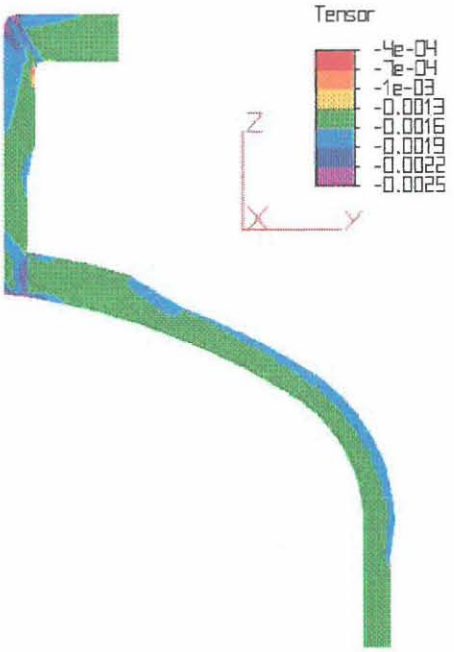

Figure D.1 Predicted in-plane strain (ε_1) of model D_1

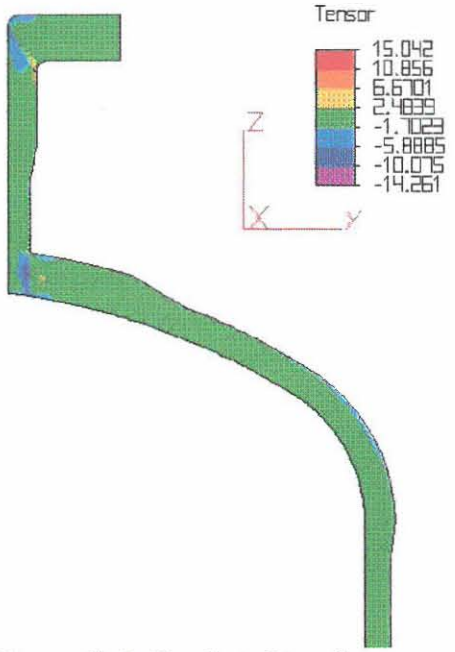

Figure D.2 Predicted in-plane stress (σ_1) of model D_1

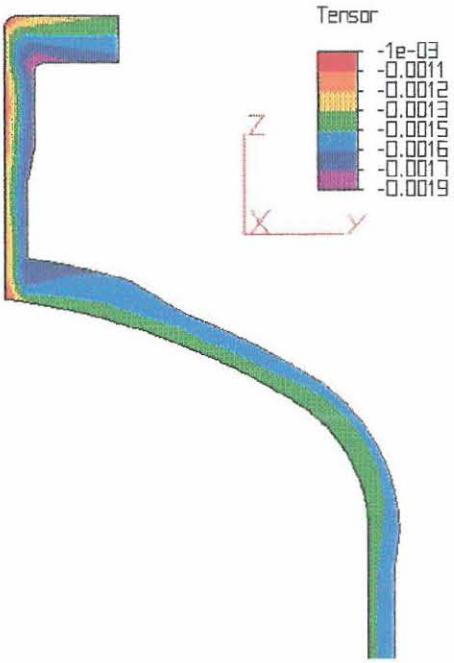

Figure D.3 Predicted in-plane strain (ε_2) of model D_1

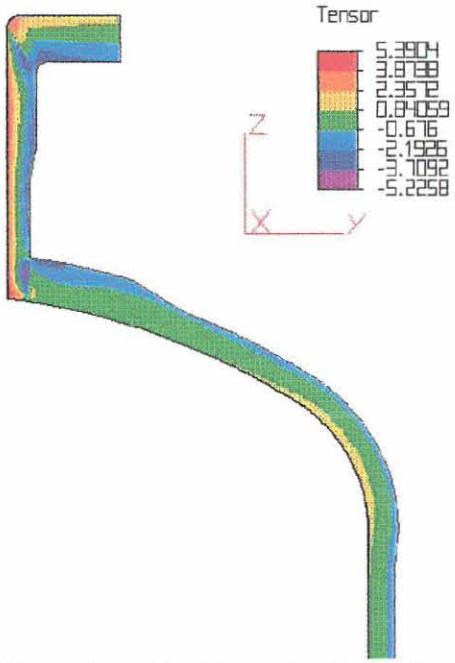

Figure D.4 Predicted in-plane stress (σ_2) of model D_1

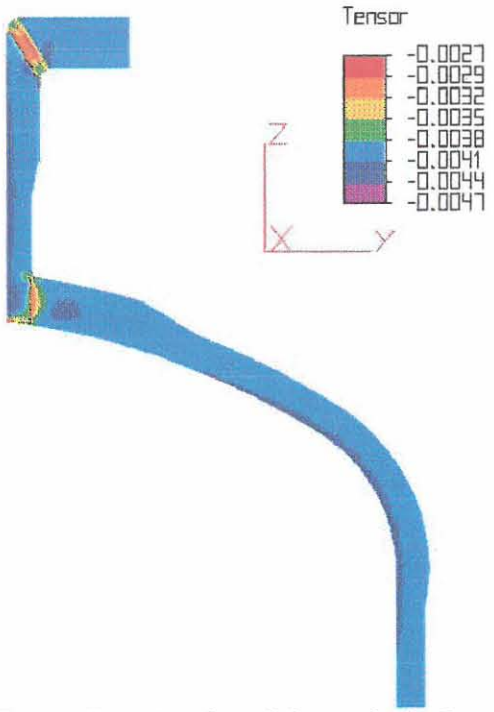

Figure D.5 Predicted through-thickness strain (ε_3) of model D_1

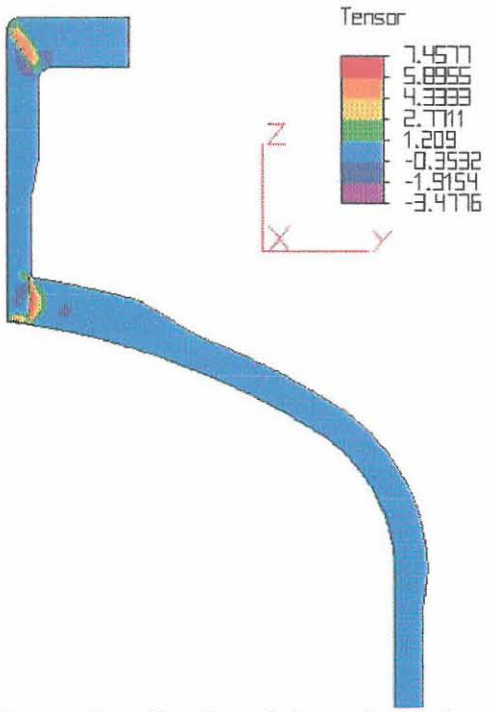

Figure D.6 Predicted through-thickness stress (σ_3) of model D_1

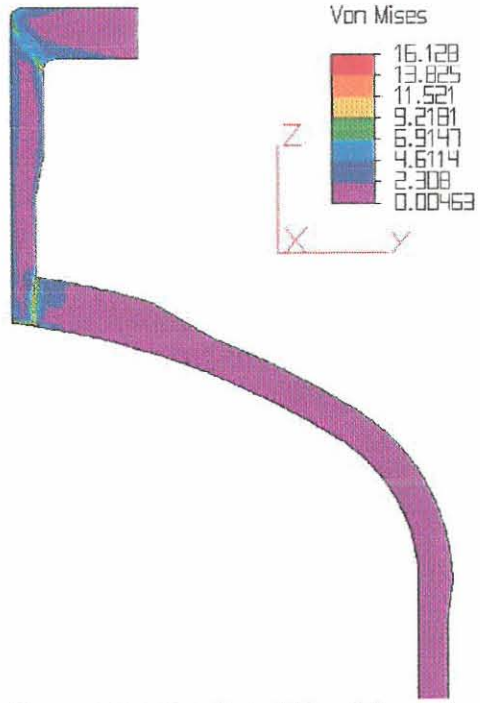

Figure D.7 Predicted Von Mises stress of model D_1

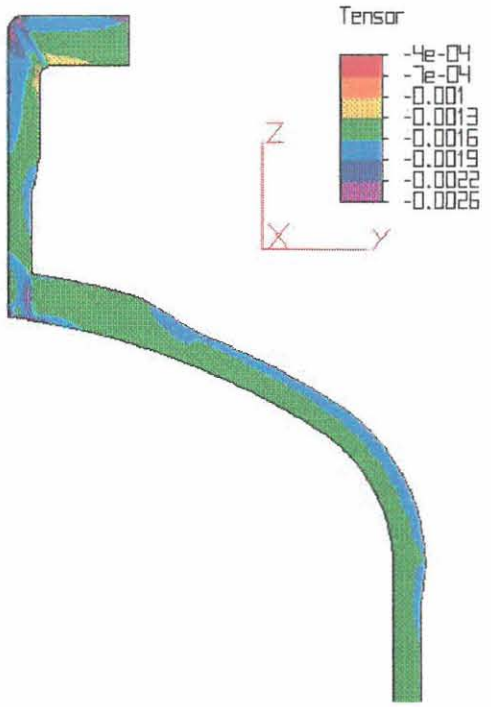

Figure D.8 Predicted in-plane strain (ε_1) of model D_2

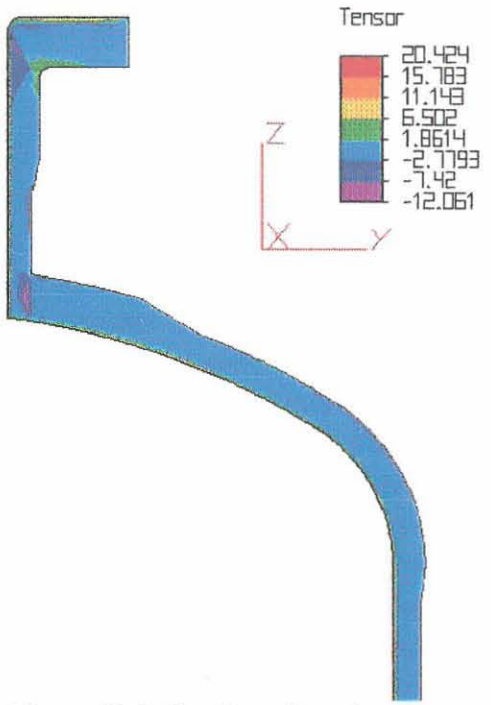

Figure D.9 Predicted in-plane stress (σ_1) of model D_2

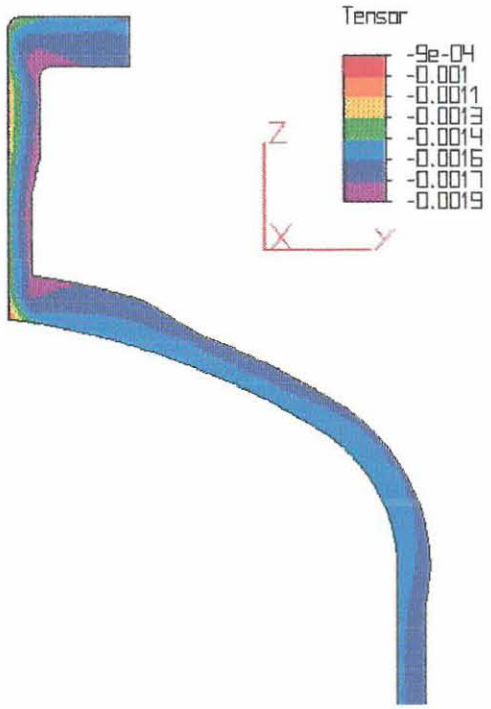

Figure D.10 Predicted in-plane strain (ε_2) of model D_2

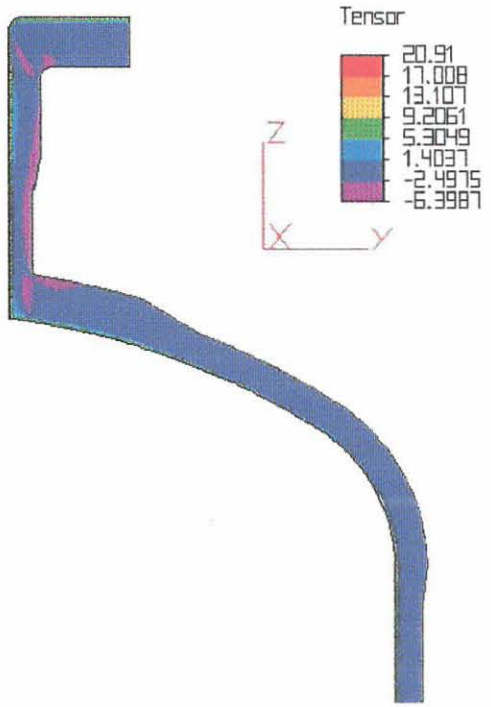

Figure D.11 Predicted in-plane stress (σ_2) of model D_2

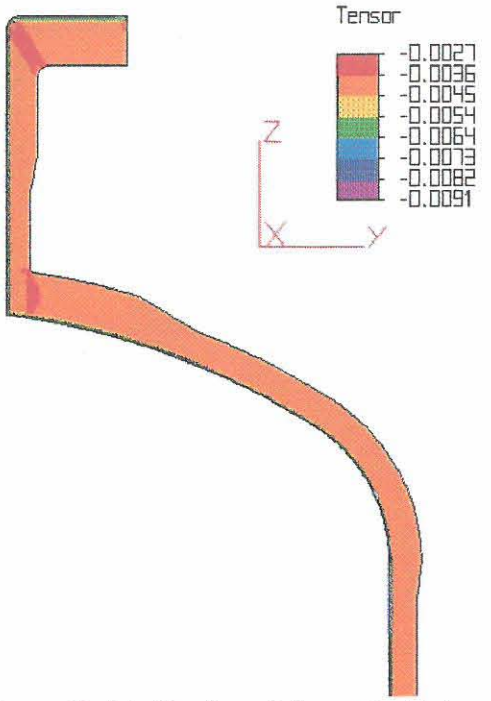

Figure D.12 Predicted through-thickness strain (ε_3) of model D_2

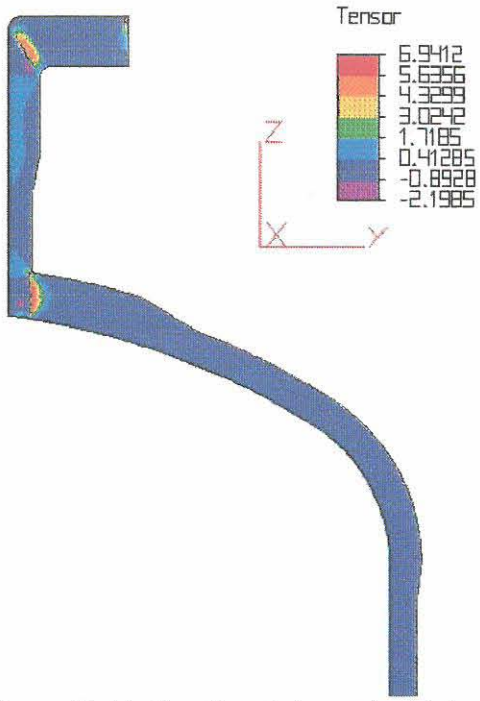

Figure D.13 Predicted through-thickness stress (σ_3) of model D_2

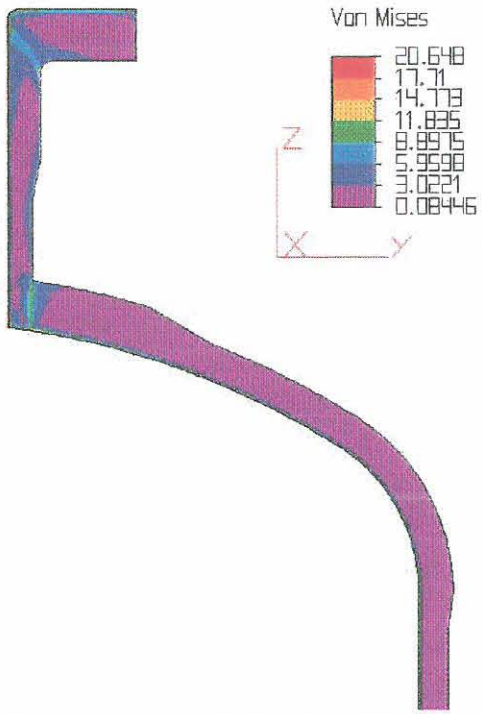

Figure D.14 Predicted Von Mises stress of model D_2

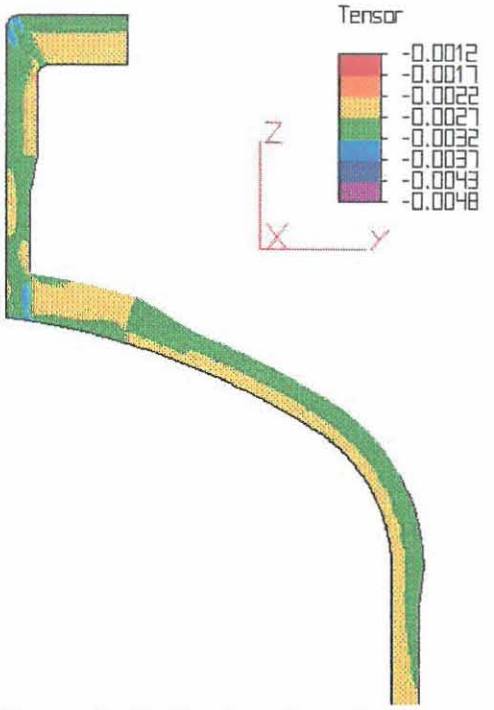

Figure D.15 Predicted in-plane strain (ε_1) of model D_3

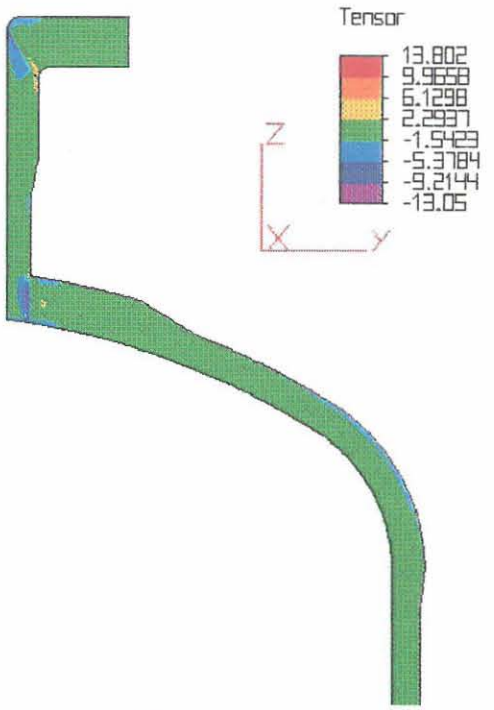

Figure D.16 Predicted in-plane stress (σ_1) of model D_3

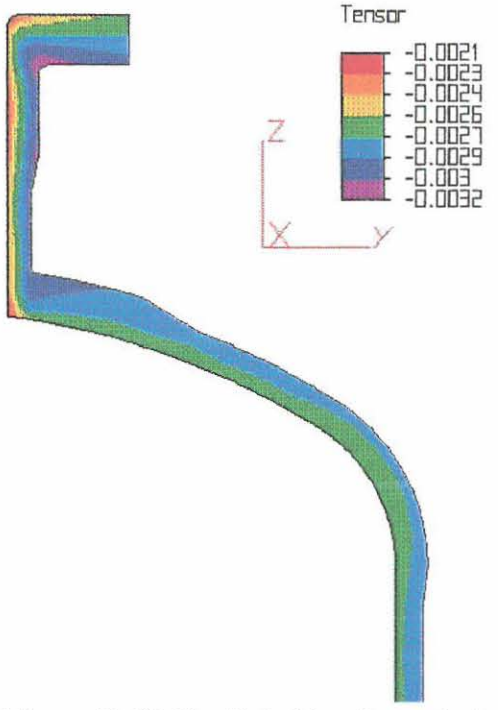

Figure D.17 Predicted in-plane strain (ε_2) of model D_3

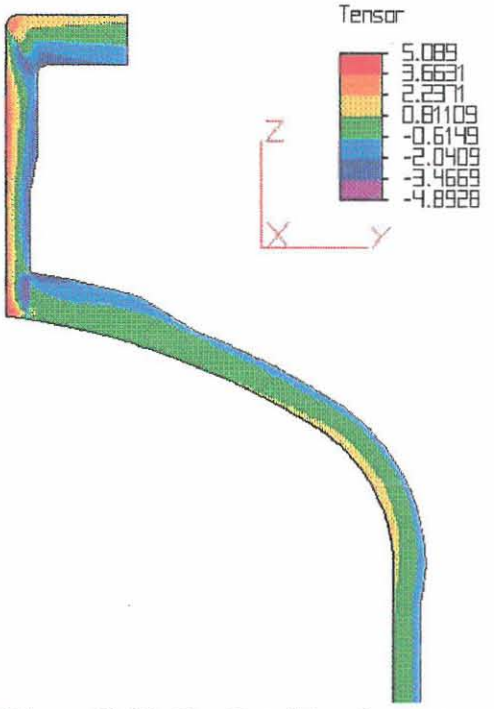

Figure D.18 Predicted in-plane stress (σ_2) of model D_3

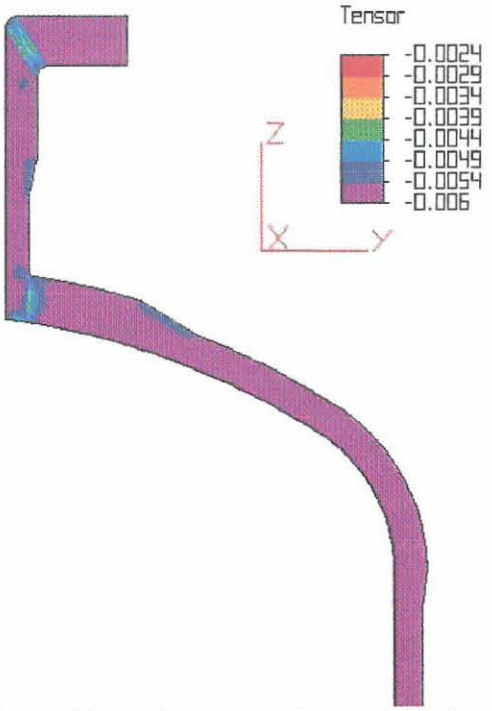

Figure D.19 Predicted through-thickness strain (ε_3) of model D_3

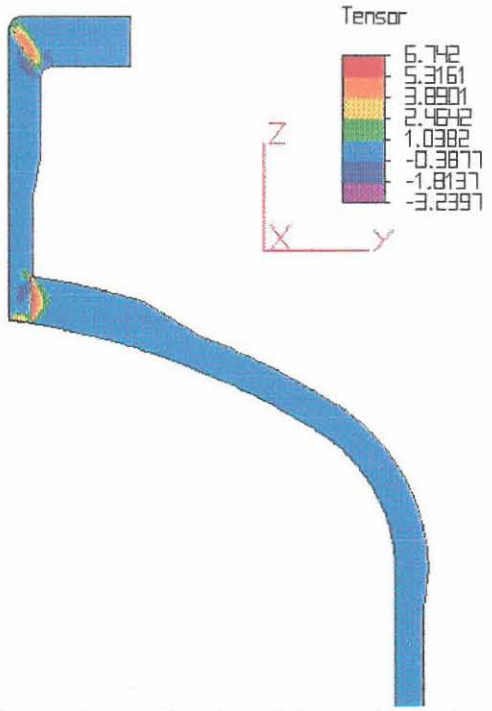

Figure D.20 Predicted through-thickness stress (σ_3) of model D_3

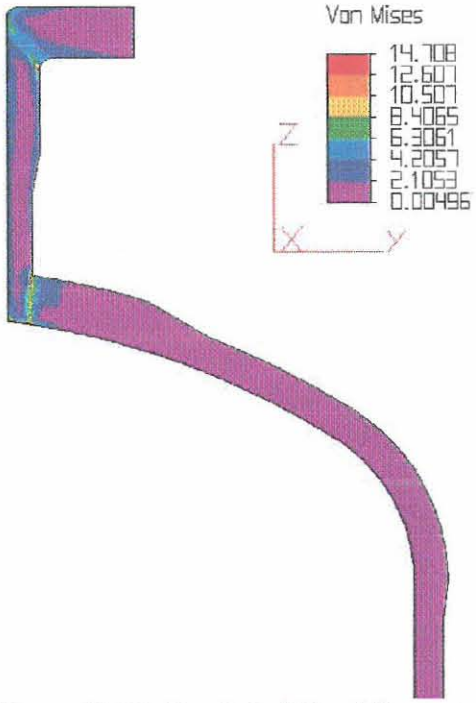

Figure D.21 Predicted Von Mises stress of model D_3

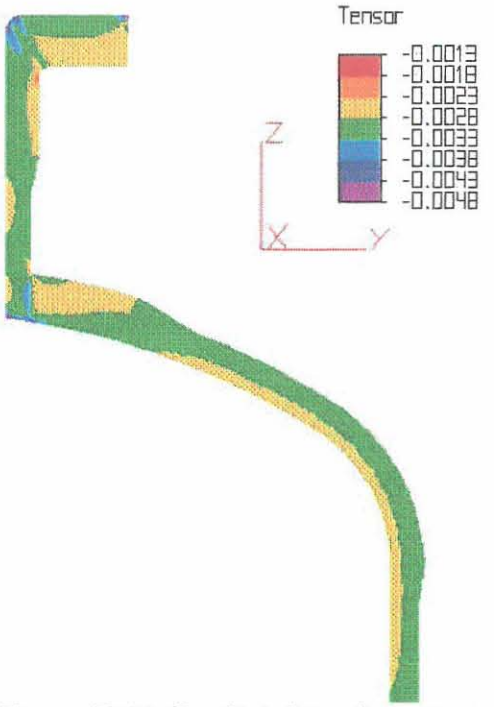

Figure D.22 Predicted in-plane strain (ε_1) of model D_4

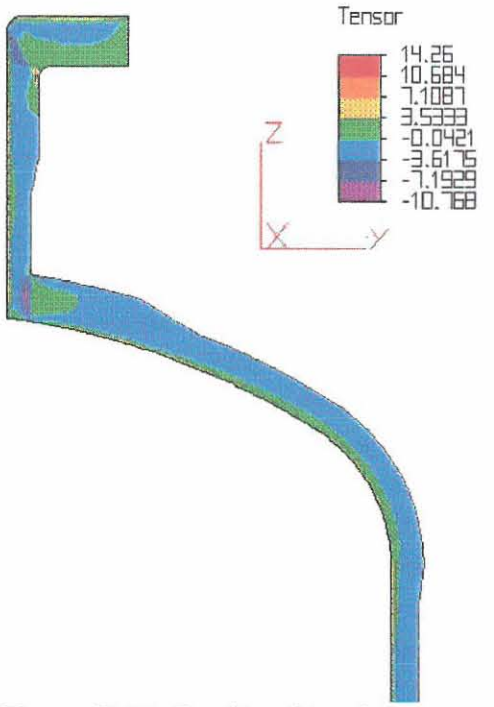

Figure D.23 Predicted in-plane stress (σ_1) of model D_4

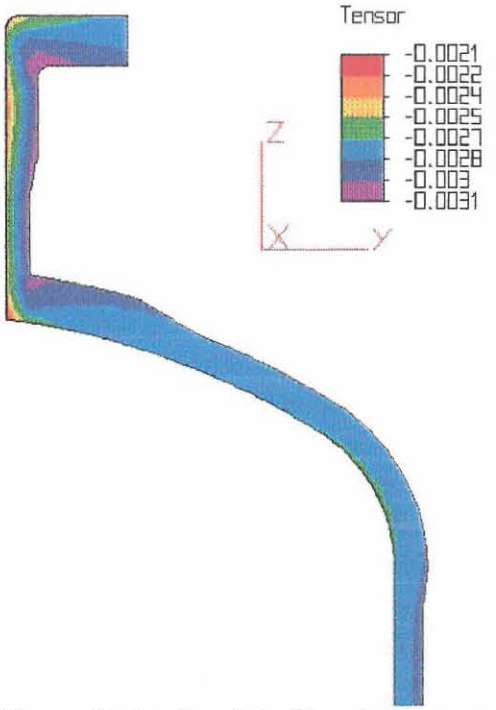

Figure D.24 Predicted in-plane strain (ε_2) of model D_4

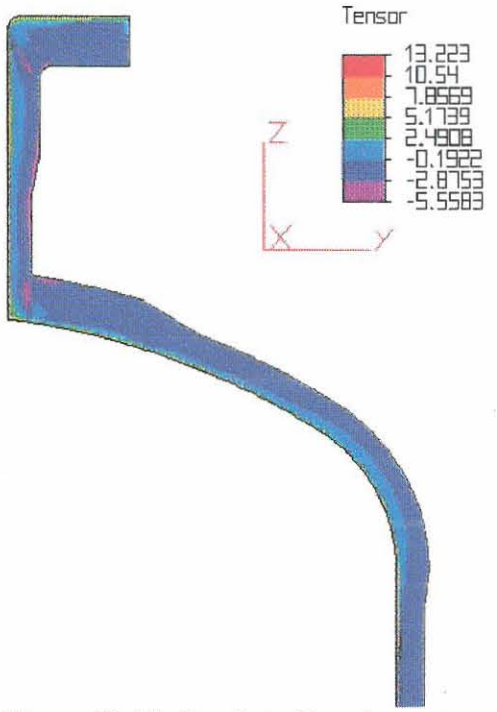

Figure D.25 Predicted in-plane stress (σ_2) of model D_4

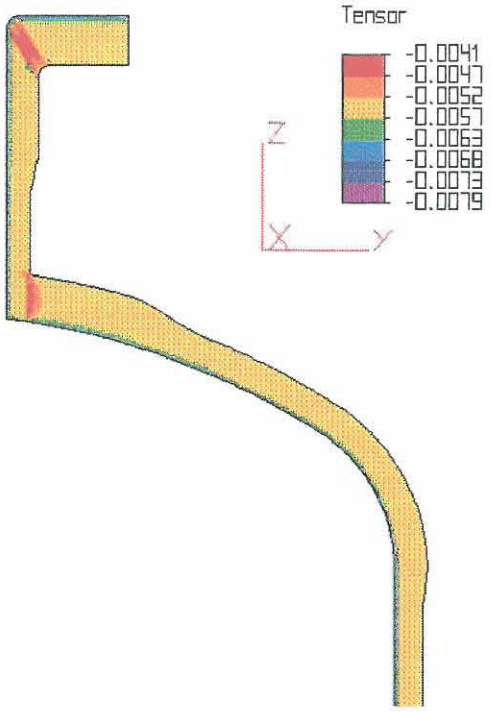

Figure D.26 Predicted through-thickness strain (ε_3) of model D_4

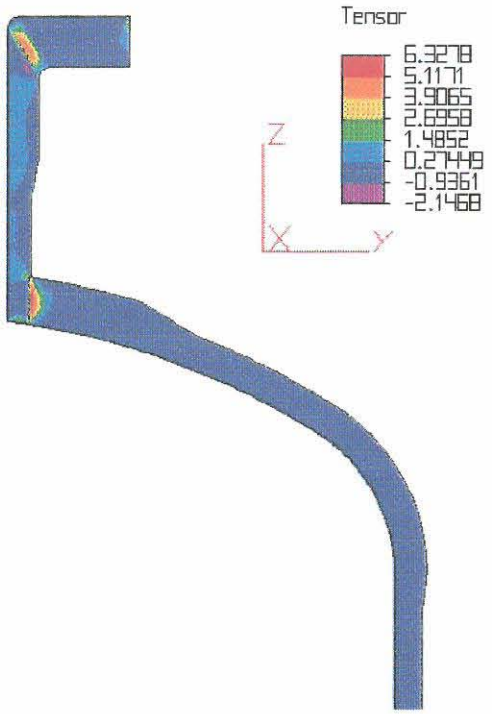

Figure D.27 Predicted through-thickness stress (σ_3) of model D_4

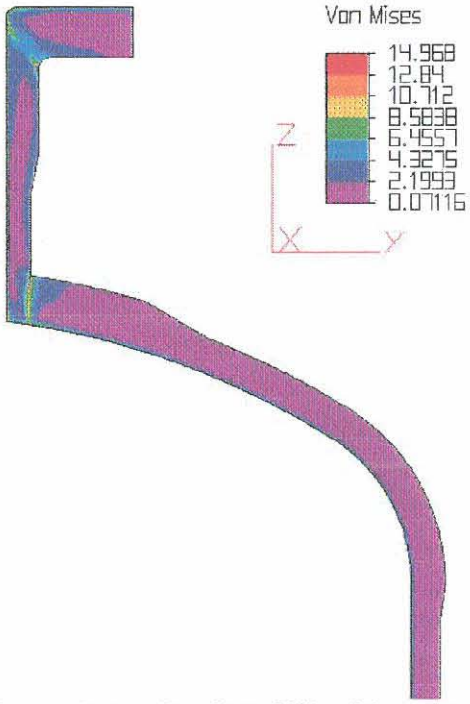

Figure D.28 Predicted Von Mises stress of model D_4

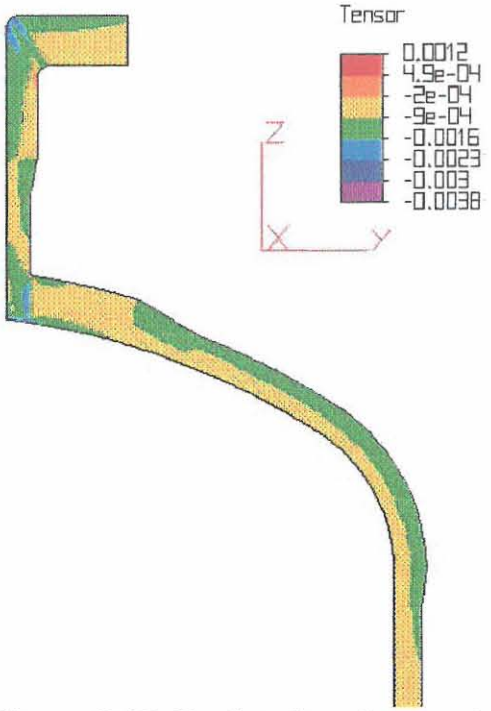

Figure D.29 Predicted in-plane strain (ε_1) of model D_5

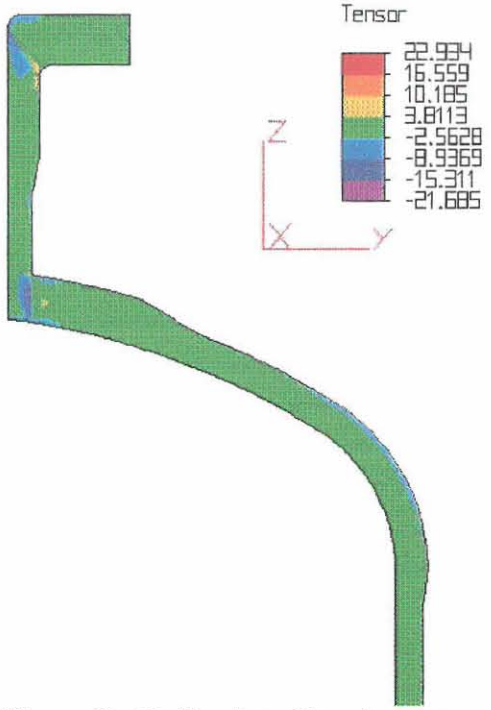

Figure D.30 Predicted in-plane stress (σ_1) of model D_5

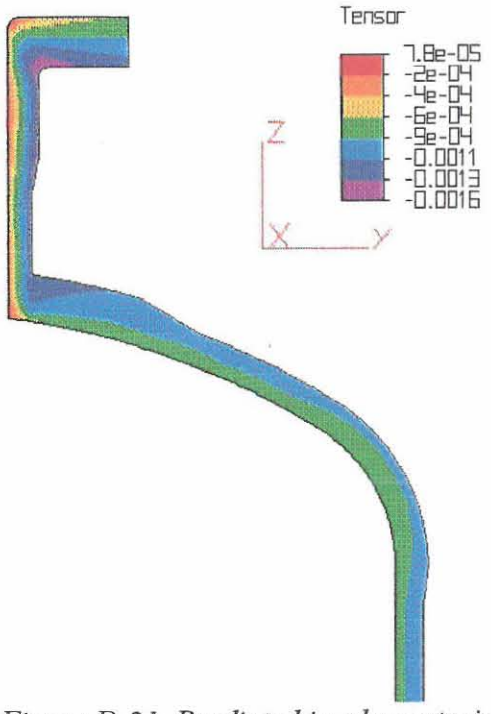

Figure D.31 Predicted in-plane strain (ε_2) of model D_5

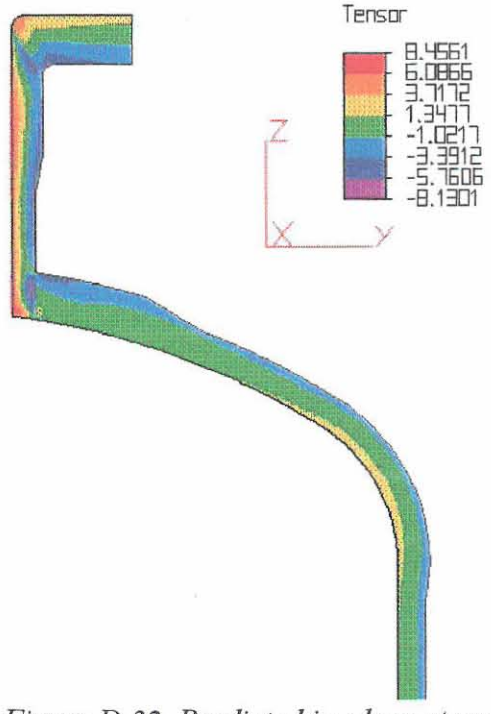

Figure D.32 Predicted in-plane stress (σ_2) of model D_5

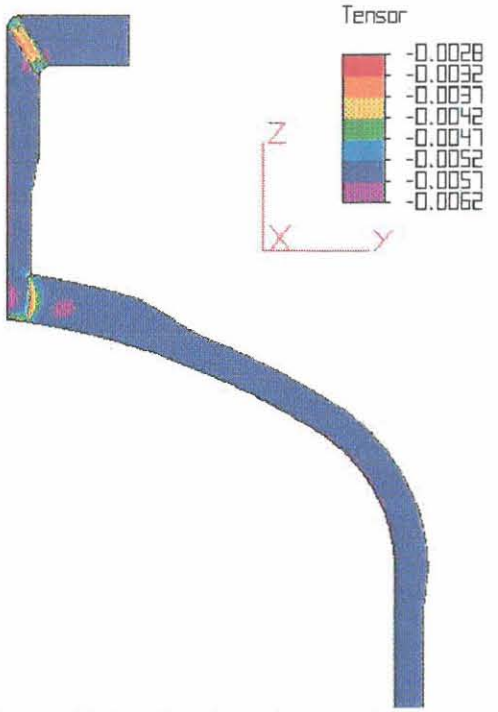

Figure D.33 Predicted through-thickness strain (ε_3) of model D_5

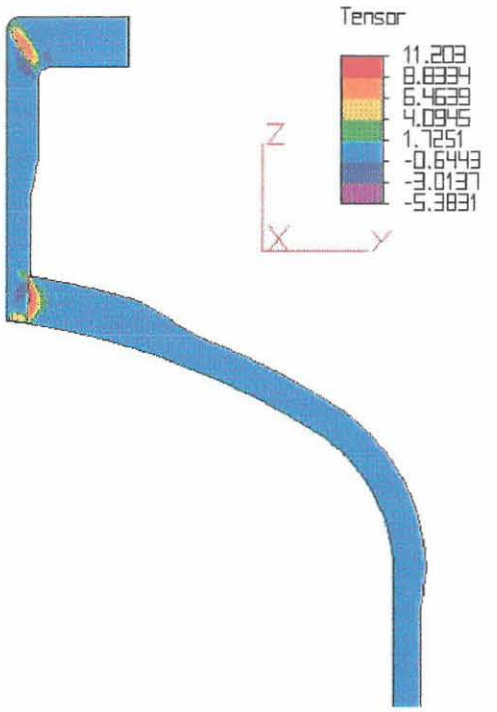

Figure D.34 Predicted through-thickness stress (σ_3) of model D_5

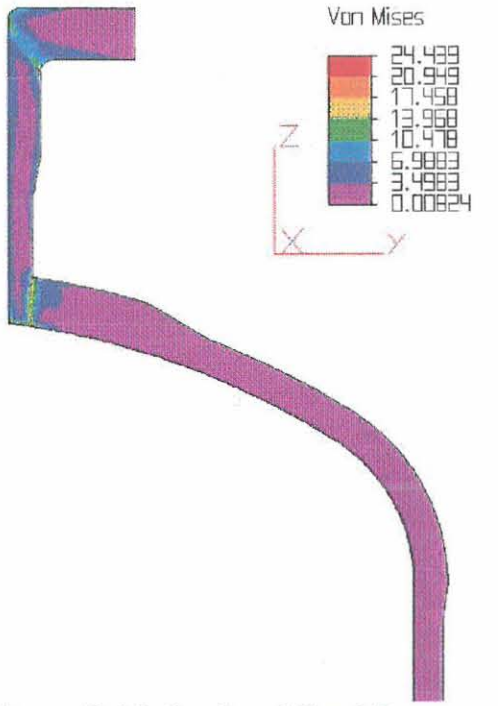

Figure D.35 Predicted Von Mises stress of model D_5

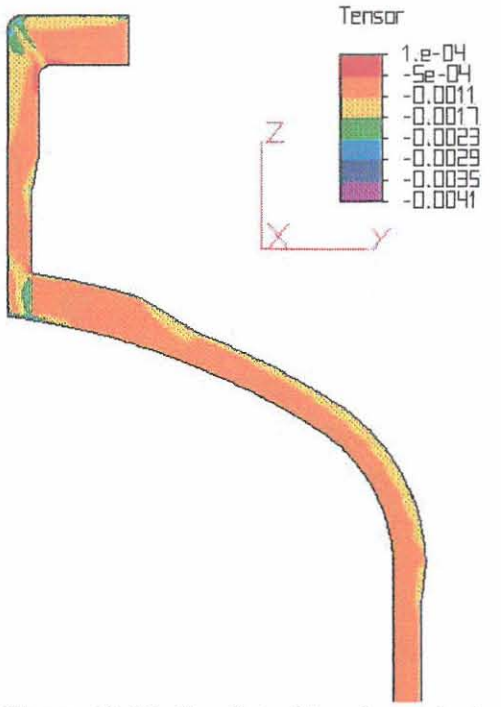

Figure D.36 Predicted in-plane strain (ε_1) of model D_6

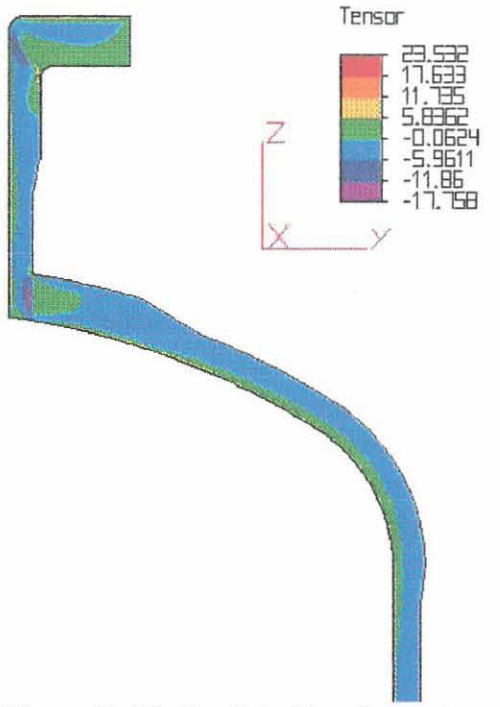

Figure D.37 Predicted in-plane stress (σ_1) of model D_6

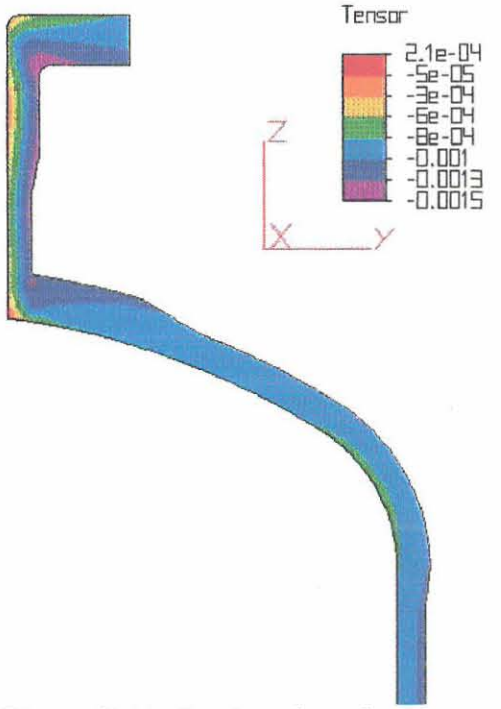

Figure D.38 Predicted in-plane strain (ε_2) of model D_6

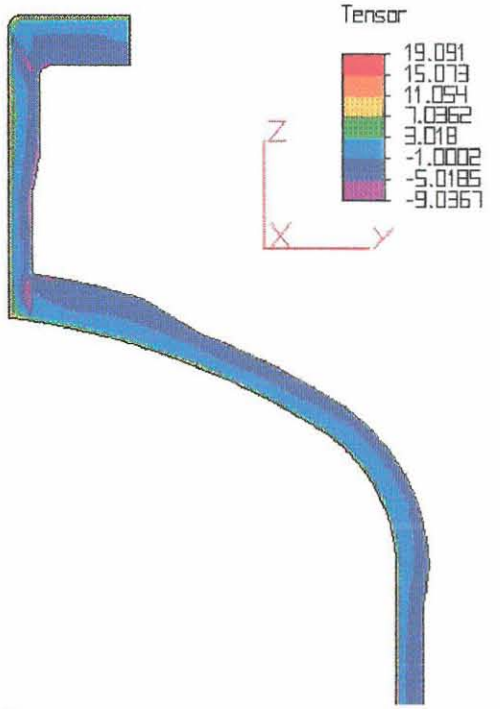

Figure D.39 Predicted in-plane stress (σ_2) of model D_6

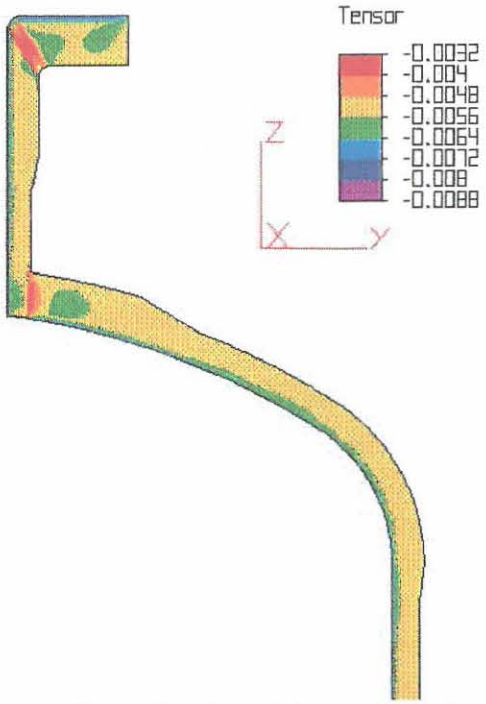

Figure D.40 Predicted through-thickness strain (ε_3) of model D_6

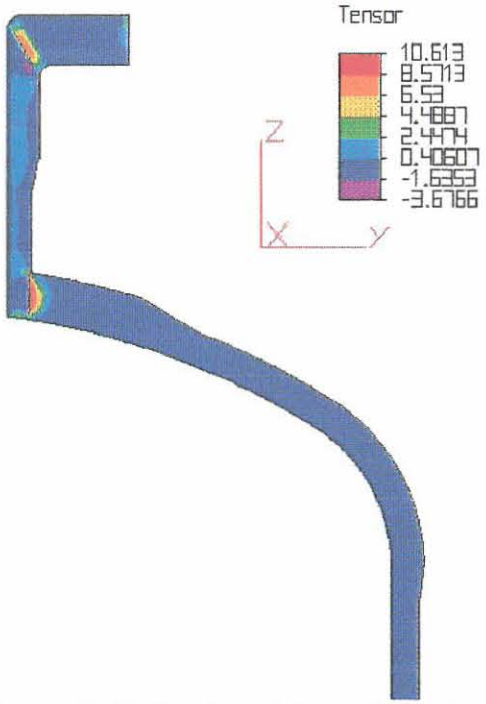

Figure D.41 Predicted through-thickness stress (σ_3) of model D_6

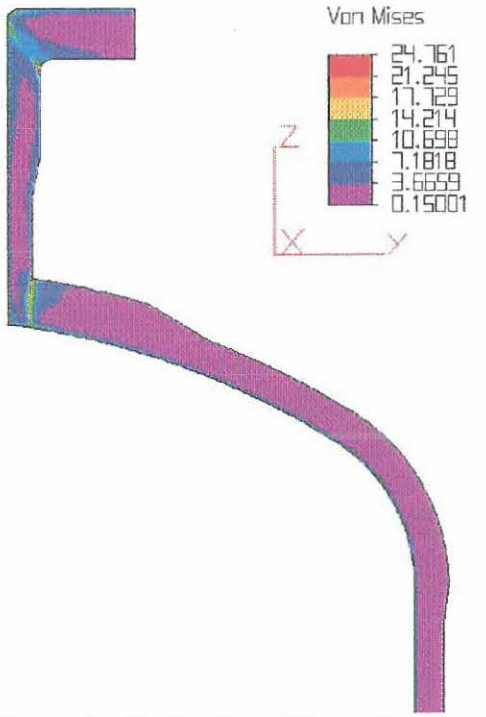

Figure D.42 Predicted Von Mises stress of model D_6

APPENDIX E. Papers presented at conferences and publications

- J F Oosthuizen & M A Stone, "RESIDUAL STRESSES IN CSM/VINYL ESTER RESIN LAMINATES DUE TO POST-CURE SHRINKAGE", Proceedings of the *1st International Conference on Composites Science and Technology*, 1996, pp. 365-370. Published in *Composite Structures*, Vol. 39 Nos 3-4, pp. 303-307, 1997.
- J F Oosthuizen, "POST-CURE SHRINKAGE STRESSES IN GRP TUBES", Paper presented at the *9th Wits RP/Composites Conference*, Midrand, South Africa, September 1996.
- J F Oosthuizen and W H Groenewald, "CURING STRAINS DEVELOPED DURING THE MANUFACTURE OF GRP TUBES", Paper presented at *11th International Conference on Composite Materials*, Gold Coast, Queensland, Australia, 1997. Published in the proceedings of the *11th International Conference on Composite Materials*, 1997, Vol. IV, pp. 324-332.
- J F Oosthuizen, "CURING "SHRINKAGE" OF GRP TUBES DURING HAND LAY-UP", Paper presented at the *10th Wits RP/Composites Conference*, Midrand, South Africa, October 1997.
- J F Oosthuizen & M A Stone, "POST CURE SHRINKAGE IN HUBBED FULL FACE FLANGE", Paper presented at the *13th Annual Technical Conference of the American Society for Composites*, Baltimore, Maryland, USA, 21-23 September 1998. Published in the proceedings of the *13th Annual Technical Conference of the American Society for Composites*, 1998, pp. 827-836.

REFERENCES

1. Shi-Chang Tseng and Osswald T.A., "Prediction of Shrinkage and Warpage of Fiber Reinforced Thermoset Composite Parts", *Journal of Reinforces Plastics and Composites*, **13**, August 1994, pp. 698-721.
2. Hancox N.L. and Mayer R.M., In *DESIGN DATA FOR REINFORCED PLASTICS, A guide for engineers and designers*, Chapman & Hall, 1994.
3. *BS 4994: 1987, "BRITISH STANDARD SPECIFICATION FOR DESIGN AND CONSTRUCTION OF VESSELS AND TANKS IN REINFORCED PLASTICS"*, British Standards Institution.
4. *ASME BOILER AND PRESSURE VESSEL CODE. AN AMERICAN NATIONAL STANDARD. SECTION X, FIBER REINFORCED PLASTIC PRESSURE VESSELS, 1989 EDITION, ADDENDA 1990*, American Society of Mechanical Engineers, 1990.
5. DERAKANE, "Vinyl Ester Resins, Product and Usage Guide", The Dow Chemical Company.
6. Dixon B.G., Longenecker D.M. and Ferrarini J., "Curing of Unsaturated Polyester Resins for Corrosion Resistant Structures", *31st Annual Technical Conference, Reinforced Plastics/Composites Institute*, The Society of the Plastics Industry, Inc., 1976, Section 15-D.
7. Bogetti T.A. and Gillespie J.W. Jr., "Process-Induced Stress and Deformation in Thick-Section Thermoset Composite Laminates", *Journal of Composite Materials*, **26**, No. 5, 1992, pp. 626-659.
8. Tutuncu, N. and Winkler, S. J., "Stresses and Deformations in Thick-Walled Cylinders Subjected to Combined Loading and a Temperature Gradient", *Journal of Reinforced Plastics and Composites*, **12**, February 1993, pp. 198-209.

9. Kardomateas, G.A., "Transient Thermal Stresses in Cylindrically Orthotropic Composite Tubes", *Journal of Applied Mechanics*, **56**, June 1989, pp. 411-417.

10. Yuan F.G., "Thermal Stresses in Thick Laminated Composite Shells", *Composite Structures*, **26**, 1993, pp. 63-75.

11. Tungikar, V.B. and Koganti, M.R., "Three Dimensional Exact Solution of Thermal Stresses in Rectangular Composite Laminate", *Composite Structures*, **27**, 1994, pp. 419-430.

12. Wu, C.H. and Tauchert, T.R., "Thermoelastic Analysis of Laminated Plates. 1: Symmetric Specially Orthotropic Laminates", *Journal of Thermal Stresses*, **13**, 1980, pp. 247-259.

13. Hyer, W.H., Cooper, D.E. and Cohen, D., "Stresses and Deformations in Cross-Ply Composite Tubes Subjected to a Uniform Temperature Change", *Journal of Thermal Stresses*, **9**, 1986, pp. 97-117.

14. Hyer, W.H. and Cooper, D.E., "Thermal Stresses in Composite Tubes Using Complementary Virtual Work", *Journal of Thermal Stresses*, **11**, 1988, pp. 97-117.

15. Guemes J.A., "Curing Residual Stresses and Failure Analysis in Composite Cylinders", *Journal of Reinforced Plastics and Composites*, **13**, May 1994, pp. 408-419.

16. Tzeng, J.T. and Pipes, R.B., "Thermal Residual Stress Analysis for *in situ* and Post-Consolidated Composite Rings", *Composites Manufacturing*, **3**, No.4, 1992, pp. 273-279.

17. Crasto, A.S. and Kim, R.Y., "On the Determination of Residual Stresses in Fiber-Reinforced Thermoset Composites", *Journal of Reinforced Plastics and Composites*, **12**, May 1993, pp. 545-558.

18. Eduljee, R.F. and Gillespie, J.W. Jr., "Elastic Response of Post- and *in situ* Consolidated Laminated Cylinders", *Composites: Part A*, **27A**, 1996, pp. 437-446.

19. Stone, M.A., Schwartz, I.F. and Chandler, H.D., "Residual Stresses associated with Post-Cure Shrinkage in GRP Tubes", *Composite Science and Technology*, **57**, 1997, pp. 47-54.

20. Hoa, S.V., In *Analysis for Design of Fiber Reinforced Plastic Vessels And Pipings*, Technomic Publishing Company, Inc., 1991, pp.33-35.

21. Halpin, J.C. And Tsai, S.W., "Effects of Environmental Factors on Composite Materials", *AFML-TR*, 1969, pp. 67-423.

22. Agarwal B.D. and Broutman, L.J., In *Analysis and Performance of Fiber Composites*, John Wiley & Sons, Inc., 1990.

23. Foye, R.L., "The Transverse Poisson's Ratio of Composites", *Journal of Composites*, **6**, 1972, pp. 293-295.

24. Matthews, F.L., and Rawlings, R.D., In *Composite Materials: Engineering and Science*, Chapman & Hall, 1994.

25. Cox, H.L., "The Elasticity and Strength of Paper and Other Fibrous Materials", *British Journal of Applied Physics*, **3**, 1952, pp. 72-79.

26. Tsai, S.W. and Pagano, N.J., "Invariant Properties in Composite Materials", In S. W. Tsai, J.C. Halpin and N.J. Pagano (eds.), Composite Materials Workshop, Technomic Publishing Co. Lancaster, PA (1968), pp. 233-252.

27. Christensen, R.M. and Waals, F.M., "Effective Stiffness of Randomly Oriented Fibre Composites", *Journal of Composite Materials*, **6**, 1972, pp. 518-532.

28. Hashin, Z., "On Elastic Behavior of Fibre Reinforced Materials of Arbitrary Transverse Phase Geometry", *Journal of the Mechanics and Physics of Solids*, **13**, 1965, pp.119-134.

29. Hashin, Z., "Viscoelastic Fiber Reinforced Materials", *AIAA Journal*, **4**, 1966, pp. 1411-1417.

30. Hill, R., "Theory of Mechanical Properties of Fiber-Strengthened Materials: I. Elastic Behavior", *Journal of the Mechanics and Physics of Solids*, **12**, 1964, pp.199-212.

31. Schapery, R.A., "Thermal Expansion Coefficients of Composite Materials Based on Energy Principles", *Journal of Composite Materials*, **2**, 1968, pp. 380-404.

32. Halpin, J.C. and Pagano, N.J., "The Laminate Approximation for Randomly Oriented Fibrous Composites", *Journal for Composite Materials*, **3**, 1969, pp. 720-724.

33. Daniel, I.M. and Ishai, O., In *Engineering Mechanics of Composite Materials*, Oxford University Press, Inc., 1994.

34. Gibson, R.F., In *Principles of Composite Material Mechanics*, McGraw-Hill, Inc., 1994.

35. Datoo, M.H., In *Mechanics of Fibrous Composites*, Elsevier Science Publishers Ltd., 1991.

36. DION® VER 9100 PA Data Sheet, *NCS Resins*.

37. Kitching, R., Tan, A.L. and Abu-Mansour T.M.N., "The Influence of Through Thickness Properties on Glass Reinforced Plastic Laminated Structures", *Composite Structures*, **2**, 1984, pp. 105-151.

38. Oosthuizen, J.F. and Stone, M.A., "Residual Stresses in CSM/Vinyl Ester Resin Laminates Due To Post-cure Shrinkage", *Composite Structures,* **39**, Nos 3-4, 1997, pp. 303-307.

39. Stone, M.A., Schwartz, I.F. and Chandler, H.D., "Residual Stresses arising from Partial In-service Post-cure of GRP Structures", *Composites*, **25**, 1994, pp. 177-181.

40. "CHEM-MAT" CHEMICAL GRADE SURFACE TISSUE, Product Data Sheet, Effective: 2 November 1987, Vivian Regiana Sales Ltd.

29. Hashin, Z., "Viscoelastic Fiber Reinforced Materials", *AIAA Journal*, **4**, 1966, pp. 1411-1417.

30. Hill, R., "Theory of Mechanical Properties of Fiber-Strengthened Materials: I. Elastic Behavior", *Journal of the Mechanics and Physics of Solids*, **12**, 1964, pp.199-212.

31. Schapery, R.A., "Thermal Expansion Coefficients of Composite Materials Based on Energy Principles", *Journal of Composite Materials*, **2**, 1968, pp. 380-404.

32. Halpin, J.C. and Pagano, N.J., "The Laminate Approximation for Randomly Oriented Fibrous Composites", *Journal for Composite Materials*, **3**, 1969, pp. 720-724.

33. Daniel, I.M. and Ishai, O., In *Engineering Mechanics of Composite Materials*, Oxford University Press, Inc., 1994.

34. Gibson, R.F., In *Principles of Composite Material Mechanics*, McGraw-Hill, Inc., 1994.

35. Datoo, M.H., In *Mechanics of Fibrous Composites*, Elsevier Science Publishers Ltd., 1991.

36. DION® VER 9100 PA Data Sheet, *NCS Resins*.

37. Kitching, R., Tan, A.L. and Abu-Mansour T.M.N., "The Influence of Through Thickness Properties on Glass Reinforced Plastic Laminated Structures", *Composite Structures*, **2**, 1984, pp. 105-151.

38. Oosthuizen, J.F. and Stone, M.A., "Residual Stresses in CSM/Vinyl Ester Resin Laminates Due To Post-cure Shrinkage", *Composite Structures,* **39**, Nos 3-4, 1997, pp. 303-307.

39. Stone, M.A., Schwartz, I.F. and Chandler, H.D., "Residual Stresses arising from Partial In-service Post-cure of GRP Structures", *Composites*, **25**, 1994, pp. 177-181.

40. "CHEM-MAT" CHEMICAL GRADE SURFACE TISSUE, Product Data Sheet, Effective: 2 November 1987, Vivian Regiana Sales Ltd.

41. SI3595 Series Isolated Measurement Pods and Cards, Solartron Instruments.

42. Blach, A.E. and Hoa, S.V., "The Effects on Pull-back on Stresses in FRP Flanges", *Experimental Techniques*, Supplement, November 1988, pp. 12-16.

43. ALGOR®, Finite Element Analysis and Event Simulation Software for the 21st Century, Algor Inc. 1998.

44. COSMOS/M 2.0, A Complete Finite Element Analysis System™, STRUCTURAL RESEARCH & ANALYSIS CORP., 1998.